

**Development of sustained release matrix
tablets of drugs based on the rheological
properties of *Albizia procera* gum**

Thesis submitted by

Sudipta Mukherjee

Doctor of Philosophy (Pharmacy)

**DEPARTMENT OF PHARMACEUTICAL TECHNOLOGY,
FACULTY COUNCIL OF ENGINEERING & TECHNOLOGY
JADAVPUR UNIVERSITY
KOLKATA-700032, INDIA**

2023

PROFORMA – 1

“Statement of Originality”

I Sudipta Mukherjee registered on 23rd August, 2017 do hereby declare that this thesis entitled “**Development of sustained release matrix tablets of drugs based on the rheological properties of *Albizia procera* gum**” contains literature survey and original research work done by the undersigned candidate as part of Doctoral studies.

All information in this thesis have been obtained and presented in accordance with existing academic rules and ethical conduct. I declare that, as required by these rules and conduct, I have fully cited and referred all materials and results that are not original to this work.

I also declare that I have checked this thesis as per the “Policy on Anti Plagiarism, Jadavpur University, 2019”, and the level of similarity as checked by iThenticate software is 4 %.

Jasmina Khanam
12.12.2023
PROF. JASMINA KHANAM
PROFESSOR
PHARMACEUTICAL TECHNOLOGY
JADAVPUR UNIVERSITY

Sudipta Mukherjee
Signature of Candidate

Date: 12.12.2023

Signature of the Supervisor
and date with Office Seal

Prof. Jasmina Khanam

Professor

Department of Pharmaceutical Technology

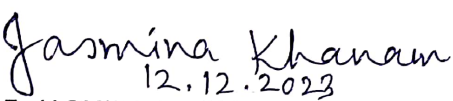
Jadavpur University,

Kolkata, India- 700032. India.

PROFORMA - 2

CERTIFICATE FROM THE SUPERVISOR

This is to certify that the thesis entitled “**Development of sustained release matrix tablets of drugs based on the rheological properties of *Albizia procera* gum**” submitted by Shri Sudipta Mukherjee, who got his name registered on 23rd August, 2017 for the award of Ph. D. (Pharmacy) degree of Jadavpur University is absolutely based upon his own work under the supervision of **Prof. Jasmina Khanam** and that neither his thesis nor any part of the thesis has been submitted for any degree/diploma or any other academic award anywhere before.


12.12.2023
PROF. JASMINA KHANAM
PROFESSOR
PHARMACEUTICAL TECHNOLOGY
JADAVPUR UNIVERSITY

Signature of the Supervisor
and date with Office Seal

Prof. Jasmina Khanam

Professor

Department of Pharmaceutical Technology

Jadavpur University,

Kolkata, India- 700032. India.

Development of sustained release matrix tablets of drugs based on the rheological properties of *Albizia procera* gum

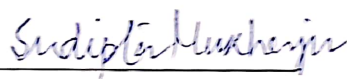


DECLARATION OF THE RESEARCH FELLOW

I do hereby declare that the work incorporated in thesis entitled "Development of sustained release matrix tablets of drugs based on the rheological properties of *Albizia procera* gum" has been carried out by me in the Department of Pharmaceutical Technology, Jadavpur University, Kolkata 700032 under the supervision of Prof. Jasmina Khanam. Neither the thesis nor any part of the thesis has been submitted for any degree/diploma or any other academic award anywhere before.

Date: 12.12.2023

Place: Kolkata, India


(Sudipta Mukherjee)

**Dedicated to Almighty, my family
and Science**

ACKNOWLEDGEMENT

With immense gratitude and the guidance of the Almighty, the completion of my dissertation journey and the subsequent Ph.D. represents a profound moment. This period has been an invaluable part of my life, offering immense learning in the realm of science. As I stand here, I find myself indebted to numerous individuals, and yet words might fall short to express my gratitude.

Firstly, I extend my sincere appreciation to Prof. (Dr.) Jasmina Khanam from the Department of Pharmaceutical Technology, Jadavpur University, whose support and encouragement in her laboratory were pivotal. Her commitment to science, dynamic approach, and innovative thinking significantly boosted my morale and fueled my research. Her support in the initial phases of my dissertation and throughout my research activities and thesis writing has been invaluable.

My deepest respect goes to Prof. Biswanath Sa, Late Prof. Tuhinadri Sen, and other Professors whose teachings and guidance have been instrumental in reaching this significant milestone.

I express my gratitude to Prof. Sanmay Karmakar and Prof. Amalesh Samanta from the Department of Pharmaceutical Technology, Jadavpur University, for their continuous support and cooperation throughout my research project.

Working under esteemed research programs supported by the University Grants Commission, New Delhi (DSA Phase-III and UPE-II programs of the UGC), has been a privilege.

I am indebted to my supportive lab mates Nancy, Rudranil Bhowmik, Adil da, Abhishek, Shubha, Arnab, Avik Majhi, and Sandip Baidya for their camaraderie and assistance.

My deepest gratitude goes to my grandparents, parents, sister, wife Srabani, and her parents, who have been an integral part of my journey, imparting invaluable teachings and forming the cornerstone of my vision and support. My hardworking parents have sacrificed their comforts for me and showered me with unconditional love and care.

My mother, a beacon of resilience and strength, has been an exemplary role model. I owe my deepest gratitude to my father for his blessings, guidance, and unwavering support. I also extend heartfelt thanks to my sister Sudeshna Mukherjee, her husband Mr. Apurba Pal, and their daughter little Binita (Puchu), as well as my soulmate and wife Srabani and her parents, for their invaluable support.

My apologies extend to all unnamed individuals whose contributions helped me complete my research work.

Sudipta Mukherjee

Jadavpur University, Kolkata

Preface

The research presented in this thesis, titled "Development of sustained release matrix tablets of drugs based on the rheological properties of *Albizia procera* gum," represents a meticulous exploration into the potential of *Albizia procera* gum in the realm of drug delivery systems. Conducted under the supervision of Prof. Jasmina Khanam, this study delves into the rheological intricacies of *A. procera* gum, a fast-growing species found in tropical forests across India and Vietnam. Renowned for its adaptability and root suckering ability, this gum holds promise for pharmaceutical applications.

The focal point of this work lies in unraveling the impact of the galactose and arabinose components of *A. procera* gum on its rheological properties and subsequently on drug delivery systems. Chemical modifications, particularly carboxymethylation and ionic crosslinking, are investigated to understand alterations in gum stability and drug diffusivity. The fundamental aim is to grasp the gum's rheological behavior to predict drug release patterns and evaluate polymer matrix strength—key elements for effective drug delivery systems.

This multifaceted study progresses through three phases. The initial phase concentrates on synthesizing carboxymethyl *Albizia procera* gum (CMAP) and formulating matrix tablets to explore drug release dynamics and rheology. The subsequent phase scrutinizes the effects of ionic crosslinking on the gum and its impact on matrix tablets. Finally, the study extends to assess stability and optimize formulations for long-term drug release and stability, ultimately aiming to identify the most efficient formulation among Native *Albizia procera* gum (NAP), CMAP, and crosslinked CMAP.

The preface provides an overview of the purification process for Native *Albizia procera* gum, the synthesis and characterization of CMAP, and the subsequent study of Crosslinked Carboxymethylated *Albizia procera* gum (CCMAP). The meticulous characterization studies through various analytical techniques offer critical insights into their chemical composition, thermal behavior, structural properties, and surface characteristics.

Additionally, the investigation delves into drug-polymer interactions and their influence on drug release kinetics, offering tailored drug delivery strategies. The exploration of Metformin (MET) and Diltiazem (DIL) as model drugs further enhances the understanding of drug-polymer interactions and their implications for sustained-release matrix tablets.

The preface encapsulates the essence of this comprehensive research, laying the foundation for a nuanced understanding of *Albizia procera* gum's potential in pharmaceutical formulations. This study bridges the gap between polymer rheology and drug release kinetics, promising advancements in specialized drug delivery systems and ensuring enhanced therapeutic efficacy across various medical domains.

TITLE.....	i
LIST OF PUBLICATIONS	ii –iii
CERTIFICATE	iv-vi
DEDICATION	vii
ACKNOWLEDGEMENT	viii
PREFACE.....	ix-x
LIST OF FIGURE.....	ix
LIST OF TABLES	xiv
ABBREVIATIONS.....	xvii
 CHAPTER 1. INTRODUCTION.....	 1
1.1 THE POLYMERS AND NATURAL POLYSACCHARIDES	3
1.2 ALBIZIA PROCERA.....	9
1.3 CARBOXYMETHYLATION	13
1.4 RHEOLOGY.....	15
1.5 MATRIX TABLET	18
1.6 METFORMIN AS A DRUG IN A SUSTAINED-RELEASE FORMULATION.....	22
1.7 DILTIAZEM AS A DRUG IN A SUSTAINED-RELEASE FORMULATION.....	23
 CHAPTER 2. LITERATURE REVIEW.....	 25
 CHAPTER 3. AIM AND OBJECTIVES.....	 41
 CHAPTER 4. MATERIALS	 53
4.1 SPECIFICATIONS OF DRUGS AND CHEMICALS.....	55
4.2 LIST OF INSTRUMENTS	56
 CHAPTER 5. METHODS	 59
5.1 ANALYTICAL METHODS	59
5.2 INSTRUMENTAL METHODS.....	64
5.3 PURIFICATION OF NATIVE ALBIZIA PROCERA GUM (NAP)	73
5.4 SYNTHESIS AND CHARACTERIZATION OF CARBOXYMETHYL ALBIZIA PROCERA (CMAP).....	75

5.5	PREPARATION OF CROSSLINKED CMAP (CCMAP)	79
5.6	RBC LYSIS TEST	81
5.7	PRE-FORMULATION STUDIES	83
5.8	FABRICATION OF SR MATRIX TABLETS	91
5.9	CHARACTERIZATION OF TABLETS AND DETERMINATION OF DRUG CONTENT.....	95
5.10	IN-VITRO DRUG RELEASE STUDY	97
5.11	STUDY OF RELEASE KINETICS AND MECHANISM OF DRUG RELEASE ON IN- VITRO RELEASE PROFILES.....	99
5.13	ACCELRATED STABILITY STUDY.....	103
5.14	STATISTICAL ANALYSIS	104
 CHAPTER 6. RESULTS AND DISCUSSION : ANALYTICAL ASSESSMENT OF DRUGS		105
 CHAPTER 7. RESULTS AND DISCUSSION : ALBIZIA PROCERA GUM MODIFICATION: SYNTHESIS AND CHARACTERIZATION		121
7.1	CHARACTERIZATION OF NAP	123
7.2	CHARACTERIZATION OF CMAP.....	131
7.3	CHARACTERIZATION OF CCMAP	143
7.4	RBC LYSIS TEST.....	150
 CHAPTER 8. RESULTS AND DISCUSSION : COMPARATIVE RHEOLOGICAL ASSESSMENT OF POLYMERIC MATRICES.....		153
8.1	COMPARATIVE RHEOLOGICAL ASSESSMENT OF POLYMERIC MATRICES.....	155
8.1.1	DYNAMIC ROTATIONAL STUDY (FLOW CURVE)	155
8.1.2	FLOW CURVE MODEL	157
8.1.3	DYNAMIC OSCILLATORY STUDIES.....	160
8.2	DAMPING FACTOR.....	172
 CHAPTER 9. PRE-FORMULATION EVALUATION		175
9.1	DRUG – POLYMERS INTERACTION STUDIES	177
9.2	EVALUATION OF MICROMERITIC PROPERTIES OF POLYMERIC GRANULES	185
9.3	EVALUATION OF PLACEBO MATRIX TABLETS.....	188
9.4	SWELLING AND EROSION STUDY	189
9.5	TOPOGRAPHY OF TABLETS BY SEM STUDIES.....	197

CHAPTER 10. EVALUATION OF MATRIX TABLETS FORMULATIONS AND DRUG RELEASE CHARACTERISTICS.....	199
10.1 PHYSICAL CHARACTERIZATION AND DRUG RELEASE FROM MET-LOADED MATRIX TABLET FORMULATIONS	202
10.2 PHYSICAL CHARACTERIZATION AND DRUG RELEASE FROM DIL-LOADED MATRIX TABLET FORMULATIONS	218
10.3 MECHANISM OF DRUG RELEASE FROM MET-LOADED MATRIX TABLET FORMULATIONS.....	236
10.4 MECHANISM OF DRUG RELEASE FROM DIL-LOADED MATRIX TABLET FORMULATIONS.....	241
10.5 CORRELATION BETWEEN POLYMER RHEOLOGY AND DRUG RELEASE	246
10.6 ACCELERATED STABILITY STUDY.....	248
CHAPTER 11. SUMMARY AND CONCLUSION.....	255
BIBLIOGRAPHY.....	275

List of Figures

FIGURES	PAGE NO.
<hr/>	
<i>Figure 1.1: Types of Natural polymers</i>	6
<i>Figure 1.2: (a) β-D-galactopyranose, (b) α-L-arabinofuranose</i>	12
<i>Figure 1.3: Structure of Albizia procera gum</i>	12
<i>Figure 1.4: (a) Traditional release (b) Controlled release</i>	21
<i>Figure 6.1: UV spectrum of MET in deionized water</i>	108
<i>Figure 6.2: Calibration curve of MET in deionized water</i>	109
<i>Figure 6.3: UV spectrum of MET in acidic solution of pH 1.2</i>	110
<i>Figure 6.4: Calibration curve of MET in acidic solution of pH of 1.2</i>	110
<i>Figure 6.5: UV spectrum of MET in PB solution of pH 6.8</i>	111
<i>Figure 6.6: Calibration curve of MET in PB solution of pH of 6.8</i>	112
<i>Figure 6.7: UV spectrum of DIL in Deionized water</i>	113
<i>Figure 6.8: Calibration curve of DIL in deionized water</i>	113
<i>Figure 6.9: UV spectrum of DIL in acidic solution of pH 1.2</i>	114
<i>Figure 6.10: Calibration curve of DIL in acidic solution of pH 1.2</i>	115
<i>Figure 6.11: UV spectrum of DIL in PB solution of pH 6.8</i>	116
<i>Figure 6.12: Calibration curve of DIL in PB solution of pH 6.8</i>	116
<i>Figure 7.1: FTIR spectra of NAP</i>	124
<i>Figure 7.2: DSC thermogram of NAP</i>	125
<i>Figure 7.3: Solid state ^{13}C NMR spectrum of NAP</i>	127
<i>Figure 7.4: XRD patterns of NAP</i>	128
<i>Figure 7.5: Zeta potential of NAP dispersion</i>	130
<i>Figure 7.6: Conversion of NAP to CMAP</i>	133
<i>Figure 7.7: FTIR spectra of CMAP</i>	135
<i>Figure 7.8: DSC thermogram of CMAP</i>	136
<i>Figure 7.9: Solid state ^{13}C NMR spectrum of CMAP</i>	138
<i>Figure 7.10: XRD patterns of CMAP</i>	139
<i>Figure 7.11: Zeta potential of CMAP dispersion</i>	141
<i>Figure 7.12: Crosslinking of CMAP</i>	143

List of Figures

FIGURES	PAGE NO.
<i>Figure 7.13: FTIR spectra of CCMAP</i>	145
<i>Figure 7.14: DSC thermogram of CCMAP</i>	146
<i>Figure 7.15: XRD patterns of CCMAP</i>	148
<i>Figure 7.16: Zeta potential of CCMAP dispersion</i>	149
<i>Figure 8.1: Flow curves of (a) NAP, (b) CMAP and CCMAP in water, acidic solution (pH 1.2) and PB solution of pH 6.8.</i>	158
<i>Figure 8.2: Comparative viscosity profiles of (a) NAP-W, CMAP-W and CCMAP-W matrices; (b) NAP-A, CMAP-A and CCMAP-A matrices; (c) NAP-B, CMAP-B and CCMAP-B matrices</i>	159
<i>Figure 8.3: Amplitude sweep of (a) NAP, (b) CMAP and (c) CCMAP in water, acidic solution (pH 1.2) and PB solution of pH 6.8.</i>	162
<i>Figure 8.4: Amplitude sweep between (a) NAP-W, CMAP-W and CCMAP-W matrices; (b) NAP-A, CMAP-A and CCMAP-A matrices; (c) NAP-B, CMAP-B and CCMAP-B matrices</i>	163
<i>Figure 8.5: Frequency sweep of (a) NAP, (b) CMAP and (c) CCMAP in water, acidic solution (pH 1.2) and PB solution of pH 6.8.</i>	169
<i>Figure 8.6: Frequency sweep between (a) NAP-W, CMAP-W and CCMAP-W matrices; (b) NAP-A, CMAP-A and CCMAP-A matrices; (c) NAP-B, CMAP-B and CCMAP-B matrices</i>	170
<i>Figure 8.7: Angular frequency-dependent relationship between G'' and G' in (a) NAP matrices: NAP (W), NAP (A), NAP (B); (b) CMAP matrices: CMAP (W), CMAP (A), CMAP (B); (c) CCMAP matrices: CCMAP (W), CCMAP (A), CCMAP (B)</i>	171
<i>Figure 8.8: Damping factor of NAP, CMAP and CCMAP</i>	173
<i>Figure 9.1: FTIR spectrum of (a) Metformin, (b) Metformin-polymer mixture</i>	178
<i>Figure 9.2: DSC thermogram of (a) MET and (d) MET with polymer mixtures</i>	180

List of Figures

FIGURES	PAGE NO.
<i>Figure 9.3: FT-IR spectrum of (a) DIL and (b) DIL with polymer mixtures</i>	182
<i>Figure 9.4: DSC thermogram of (a) DIL and (b) DIL with polymer mixtures</i>	184
<i>Figure 9.5: Swelling (%) of NAP, CMAP and CCMAP: (a) at pH 1.2, (b) at pH 6.8.....</i>	191
<i>Figure 9.6: Comprehensive representation of the dissolution of (a) NAP after 2 hrs., (b) NAP after 10 hrs., (c) CMAP after 2 hrs., (d) CMAP after 10 hrs., (e) CCMAP after 2 hrs., (f) CCMAP after 10 hrs.</i>	192
<i>Figure 9.7: Erosion (%) of NAP, CMAP, and CCMAP at (a) pH 1.2, (b) pH 6.8.....</i>	196
<i>Figure 9.8: SEM images of (a) NAP at 0 hr., (b) NAP at 2 hrs., (c) NAP at 6 hrs.; (d) CMAP at 0 hr., (e) CMAP at 2 hrs., (f) CMAP at 6 hrs.; (g) CCMAP at 0 hr., (h) CCMAP at 2 hrs., (i) CCMAP at 6 hrs.</i>	198
<i>Figure 10.1: Drug release profiles of MET from NAP matrix tablet formulations.....</i>	205
<i>Figure 10.2: Drug release profiles of MET from CMAP matrix tablet formulations.....</i>	209
<i>Figure 10.3: Drug release profiles of MET from CCMAP matrix tablet formulations.....</i>	213
<i>Figure 10.4: Drug release profiles of MET from NAP, CMAP and CCMAP matrix tablet formulations with marketed tablet</i>	216
<i>Figure 10.5: Drug release profiles of DIL from NAP matrix tablet formulations.....</i>	221

List of Figures

FIGURES	PAGE NO.
<i>Figure 10.6: Drug release profiles of DIL from CMAP matrix tablet formulations.....</i>	225
<i>Figure 10.7: Drug release profiles of DIL from CCMAP matrix tablet formulations.....</i>	230
<i>Figure 10.8: Drug release profiles of DIL from NAP, CMAP and CCMAP matrix tablet formulations with marketed tablets</i>	234
<i>Figure 10.9: Release kinetics Models of MET-loaded NAP matrix tablet formulations (F1, F5, F10) (a) Zero-order, (b) 1st-order, (c) Korsmeyer–Peppas model, (d) Higuchi's model</i>	238
<i>Figure 10.10: Release kinetics Models of MET-loaded CMAP matrix tablet formulations (F1, F5, F10) (a) Zero-order, (b) 1st-order, (c) Korsmeyer–Peppas model, (d) Higuchi's model.....</i>	239
<i>Figure 10.11: Release kinetics Models of MET-loaded CCMAP matrix tablet formulations (F1, F5, F10) (a) Zero-order, (b) 1st-order, (c) Korsmeyer–Peppas model, (d) Higuchi's model.....</i>	240
<i>Figure 10.12: Release kinetics Models of DIL-loaded NAP matrix tablet formulations (F1, F5 and F10) (a) Zero-order, (b) 1st-order, (c) Korsmeyer–Peppas model, (d) Higuchi's model.....</i>	242
<i>Figure 10.13: Figure 10.10: Release kinetics Models of DIL-loaded CMAP matrix tablet formulations (F1, F5 and F10) (a) Zero-order, (b) 1st-order, (c) Korsmeyer–Peppas model, (d) Higuchi's model.....</i>	243
<i>Figure 10.14: Figure 10.11: Release kinetics Models of DIL-loaded CCMAP matrix tablet formulations (F1, F5 and F10) (a) Zero-order, (b) 1st-order, (c) Korsmeyer–Peppas model, (d) Higuchi's model.....</i>	244
<i>Figure 10.15: Effect of storage on the release of MET-loaded (a) NAP formulations, (b) CMAP formulations, (c) CCMAP formulations.....</i>	250

List of Figures

FIGURES	PAGE NO.
<hr/>	
<i>Figure 10.16: Effect of storage on the release of DIL-loaded (a) NAP formulations, (b) CMAP formulations, (c) CCMAP formulations</i>	251

List of Tables

TABLES	PAGE NO.
<i>Table 5.1: Formulation of placebo matrix tablets.....</i>	87
<i>Table 5.2: Formulations of MET-loaded matrix tablets.....</i>	93
<i>Table 5.3: Formulations of DIL-loaded matrix tablets.....</i>	94
<i>Table 5.4: Diffusion exponent values and mechanisms of drug release</i>	102
<i>Table 6.1: % recovery of MET in various spiked drug solutions.....</i>	117
<i>Table 6.2: % recovery of DIL in various spiked drug solutions</i>	118
<i>Table 6.3: Solubility data of MET and DIL.....</i>	119
<i>Table 7.1: Different Batches of CMAP.....</i>	133
<i>Table 7.2: Elemental analysis of NAP and CMAP</i>	142
<i>Table 7.3: RBC Lysis Evaluation at 540 nm: 1 and 3 Hr Incubation</i>	150
<i>Table: 9.1: Micromeritic properties of granules</i>	186
<i>Table 9.2: Physical characteristics of placebo tablets</i>	188
<i>Table 9.3: Water penetration velocity of placebo matrix tablets.....</i>	194
<i>Table 10.1: Characteristics and active ingredient content of MET-loaded NAP matrix tablets</i>	203
<i>Table 10.2: AUC of MET release from NAP matrix.....</i>	206
<i>Table 10.3: ANOVA Table of cumulative release of MET from NAP matrix tablet formulations.....</i>	206
<i>Table 10.4: Characteristics and active ingredient content of MET-loaded CMAP matrix tablets.....</i>	207
<i>Table 10.5: AUC of MET release from CMAP matrix.....</i>	210
<i>Table 10.6: ANOVA Table of cumulative release of MET from CMAP matrix tablet formulations.....</i>	210
<i>Table 10.7: Characteristics and active ingredient content of MET-loaded CCMAP matrix tablets.....</i>	211
<i>Table 10.8: AUC of MET release from CCMAP matrix.....</i>	214
<i>Table 10.9: ANOVA Table of the cumulative release of MET from CCMAP matrix tablet formulations.....</i>	214
<i>Table 10.10: ANOVA Table of cumulative release of MET from NAP, CMAP and CCMAP matrix tablet formulations</i>	217
<i>Table 10.11: Characteristics and active ingredient content of DIL-loaded NAP matrix tablets</i>	219
<i>Table 10.12: AUC of DIL release from NAP matrix tablets.....</i>	222
<i>Table 10.13: ANOVA Table of cumulative release of DIL from NAP.....</i>	222

List of Tables

TABLES	PAGE NO.
<hr/>	
<i>Table 10.14: Characteristics and active ingredient content of DIL-loaded CMAP matrix tablets.....</i>	223
<i>Table 10.15: AUC of DIL release from CMAP matrix tablets.....</i>	226
<i>Table 10.16: ANOVA Table of cumulative release of DIL from CMAP</i>	226
<i>Table 10.17: Characteristics and active ingredient content of DIL-loaded CCMAP matrix tablets.....</i>	227
<i>Table 10.18: AUC of DIL release from CCMAP matrix tablets</i>	231
<i>Table 10.19: ANOVA Table of cumulative release of DIL from CCMAP.....</i>	231
<i>Table 10.20: ANOVA Table of cumulative release of DIL from NAP, CMAP and CCMAP matrix tablet formulations.....</i>	235
<i>Table 10.21: Coefficient of determination (R^2) from MET Release Kinetics Data of NAP matrix tablet formulations.....</i>	238
<i>Table 10.22: Coefficient of determination (R^2) from MET Release Kinetics Data of CMAP matrix tablet formulations.....</i>	239
<i>Table 10.23: Coefficient of determination (R^2) from MET Release Kinetics Data of CCMAP matrix tablet formulations.....</i>	240
<i>Table 10.24: Coefficient of determination (R^2) from DIL Release Kinetics Data of NAP formulations.....</i>	243
<i>Table 10.25: Coefficient of determination (R^2) from DIL Release Kinetics Data of CMAP formulations.....</i>	244
<i>Table 10.26: Coefficient of determination (R^2) from DIL Release Kinetics Data of CCMAP formulations</i>	245
<i>Table 10.27: Similarity factors (f_2) of corresponding to both MET and DIL formulations.....</i>	252
<i>Table 10.28: Accelerated stability study profile of MET-loaded formulations.....</i>	253
<i>Table 10.29: Accelerated stability study profile of DIL-loaded formulations.....</i>	253

ABBREVIATIONS

^{13}C NMR	Carbon-13 Nuclear Magnetic Resonance
Alpha	Level of significance
ANOVA	Analysis of variance
AP	Albizia procera
ATR	Attenuated Total Reflection
AUC	Area Under the Curve
CCMAP	Crosslinked Carboxymethylated Albizia procera
cm	Centimeter
cm/s	Centimeter per second
cm^{-1}	Wavenumber (Inverse centimeter)
CMAP	Carboxymethylated Albizia procera
CPR	Cumulative % release
CR	Controlled release
DF	Degrees of Freedom
DIL	Diltiazem hydrochloride
DS	Degree of substitution
DSC	Differential scanning calorimetry
F	F-statistic
f_2	Similarity factor
FTIR	Fourier Transform Infrared Spectroscopy
G'	Storage modulus
G''	Loss modulus
gm/ml	Grams per milliliter
Hrs or hrs	Hours
log CPR	Logarithm of Cumulative Percentage Release
log t	Logarithm of time
LVE	Linear Viscoelastic Region
MCAA	Monochloroacetic acid.
MCC	Microcrystalline Cellulose

mcg	Microgram
MET	Metformin hydrochloride
MS	Mean Square
mW	Milliwatt
NAP	Native Albizia procera
nm	Nanometer
O-carboxymethyl	Carboxymethyl group is attached to an oxygen atom
Pa	Pascal
Pa.S	Pascal- seconds
PB	Phosphate buffer
P-value	Probability value
QS	Quantity sufficient
R ²	Coefficient of determination
Rad	Radian
S ⁻¹	Second inverse
SD	Standard Deviation
sec	second
SEM	Scanning Electron Microscopy
SQRT	Square root
SR	Sustained release
SS	Sum of Squares
tanδ	Loss tangent
TSPD	Tri-sodium phosphate dodecahydrate
w/v	Weight per volume
XRD	X-ray Powder Diffraction
γ	Strain
λ _{max}	The wavelength of maximum absorbance
µg or, mcg	Microgram
ω	Angular frequency spectrum

CHAPTER 1

INTRODUCTION



Introduction

In present era natural and synthetic polymers have gained tremendous importance in both the pharmaceutical and biomedical industries because of their versatile uses. Polymers are used as ingredients in dosage form development in pharmaceutical industries to achieve better delivery of drugs in the physiological system [Gandhi et al., 2012]. Formulation scientists who are developing new formulations must have a thorough understanding of the role of polymers. This chapter discusses basic information on natural polymers, chemistry, properties and types of polymer, modification of polymers, rheological study, and pharmaceutical uses.

1.1. The polymers and natural polysaccharides

In essence, a polymer is a large molecule created by polymerization reaction of many small molecules, known as monomers. Polymers maintain the individuality of their repeating units and exhibit traits like toughness, high elasticity, viscoelasticity, and a preference for forming amorphous or semicrystalline structures rather than crystals [McCrum et al., 1997].

Nomenclature of polymer is based generally on the type of monomer residues comprising the polymer. A copolymer is a polymer that has two or more types of repeat units, whereas a homopolymer is a polymer that contains just one type of repeat unit. A terpolymer is a copolymer that has three different kinds of repetition units [Beines et al., 2007]. The spatial arrangement and microscale ordering of polymer chains determine polymer morphology. The interactions between the polymer chains affect a polymer's macroscopic physical characteristics.

Disordered polymers such as random copolymers and highly branched polymers result in the formation of glassy structures in the solid state [Carragher & Seymour, 2012]. Polymers typically form a dynamic "statistical cluster" in melt

and solution [Katzenberg et al., 2000]. The conformations of respective molecules' are frozen in the solid state. Chain molecules that are entangled or hooked together form a "mechanical bond" with one another. Intermolecular and intramolecular attractive forces become apparent only when molecule segments are in close proximity. The irregular structures of the molecules hinder a tighter arrangement.

Regarding linear polymers, When in the solid state, linear polymers featuring a periodic structure, minimal branching, and stereo regularity tend to exhibit a semi-crystalline structure. [Carraher & Seymour, 2012] Simple- polymers (like polyethylene) have chains that arrange in zigzags in the crystal. Crystallites or lamellae are dense chain packs made up of several zigzag conformations. The lamellae are ~ 10 nm thick, and are substantially thinner than the polymers' length [Kulkarni et al., 2012]. They form by one or more molecular chains folding in a more or less regular pattern. Between the lamellae, there are amorphous structures. Individual molecules can produce one or more lamellae (chains known as tie molecules) and become entangled with other lamellae. A spherulite superstructure made up by many lamellae typically has a diameter between 0.05 to 1 mm [Kulkarni et al., 2012].

The crystallinity and strength of the secondary valence bonds are affected by or determined by the kind and order of (functional) residues in the repeat units. When the residual of the repeating units permit the formation of hydrogen bonds, particular strong intermolecular interactions happen. Strong intramolecular interactions can result in a various folded states for single linear chains, each with its circuit architecture. Both the Superstructure and Crystallinity are influenced by the circumstances surrounding their formation. Semi-crystalline structures result in increased stiffness, density, melting temperature, and resistance of a polymer when compared to amorphous structure [Lin Y et al., 2020].

Cross-linked polymers emerge through the interconnection of lengthy polymer chains, resulting in the creation of a three-dimensional networked structure. Cross-linked polymers are utilized in making a large number of materials as they are mechanically robust [Fortman et al., 2018]. Either of addition polymerization or condensation polymerization is used to create these polymers.

In nature, polymers exist abundantly. Nucleic acids, proteins, and polysaccharides as natural polymers are components of our body as well. Another natural polymer that is essential to the structural integrity of plants, is cellulose. The majority of natural polymers are created by condensation polymers [Wilbon et al., 2013; Yuan et al., 2021].

Natural polymer as classified into three main types: polysaccharides, proteins, and nucleic acids. Polysaccharides, such as cellulose, starch, and chitin, are composed of repeating sugar units and are most abundant natural polymers on Earth [Bhatia 2016; Sam et al., 2014]. There are numerous examples of natural polymers (Figure 1.1) in the world. Following is a brief description of a few of them:

Cellulose is a polymer produced from the glucose monomers, a paramount component of plants [Narain 2020]. Carbohydrate polymers are formed by repeating monomer units of monosaccharides (simple sugars) and have many uses in food and pharmaceuticals. A polymer of the monosaccharide glucose is starch. Amylopectin and amylose are two different glucose polymers that produce up the molecules of starch by condensation [Mudgil & Barak 2013; Flieger et al., 2020].

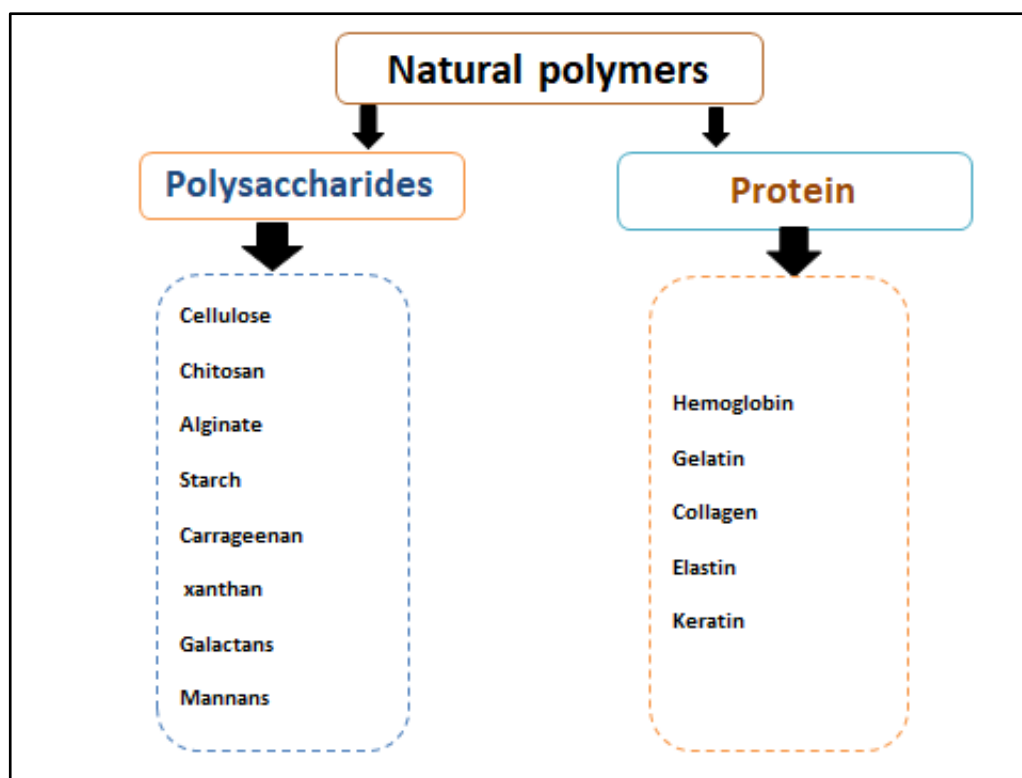


Figure 1.1: Types of Natural polymers

Carbohydrate- polymer is categorized into three main types based on the number of sugar units in the polymer chain. Oligosaccharides contain 2-10 sugar units, while polysaccharides have more than ten units. The monosaccharide units are linked jointly by glycosidic bonds, forming linear or branched structures.

Natural polysaccharides exhibit diverse properties depending on their structure and composition [García-González et al., 2011], such as gel forming, film-forming and emulsifying properties, and these are generally hydrophilic because of the presence of hydroxyl groups in their structure. Plant gums have uses as biopolymers and drug carriers to control drug release [Layek & Mandal 2020; Shokri & Adibkia 2013].

Some common carbohydrate polymers are:

1. Cellulose derivatives: Cellulose derivatives, notably hydroxypropyl cellulose (HPC), hydroxyethyl cellulose (HEC), and methylcellulose (MC), are widely applied as excipients within tablet formulations, effectively regulating the release of drugs [Gübitz & Paulo 2003].

2. Starch and its derivatives: Native starch can be modified by cross-linking or grafting with other polymers to make it suitable as drug carriers, providing controlled release and targeted delivery [Zhang et al., 2022].

3. Alginate: Alginate, extracted from brown seaweeds, is a widely used plant-based polymer in drug delivery systems [Elieh-Ali-Komi & Hamblin 2016]. It forms hydrogels in the presence of divalent cations, such as calcium ions, which can encapsulate drugs intending slow release of drugs for oral, transdermal, and injectable drug delivery applications.

4. Chitosan: Chitosan is a carbohydrate polymer derived from chitin found in the exoskeleton of crustaceans, and it has uses in drug delivery systems (oral, nasal, and topical) [Shirwaikar et al., 2008]. Its mucoadhesive and film-forming properties facilitate drug absorption and localized drug delivery.

5. Pectin: Pectin, derived from fruits and vegetables, is a natural polysaccharide that proved its suitability for making nanoparticles and microspheres intending targeted drug delivery and improved drug stability.

6. Gum Arabic: Gum arabic, obtained from the Acacia tree, is a water-soluble plant gum that can form stable emulsions, and this has utilization in the encapsulation of lipophilic drugs [Prasad et al., 2022].

7. Locust bean gum: It is derived from the seeds of the carob tree (*Ceratonia siliqua*), stands as a galactomannan gum, prized for its role as a thickening and gelling agent [Barak & Mudgil 2014].

The applications of plant gums as biopolymers and drug carriers:

Plant gums such as agar, alginate, carrageenan, and gellan gum have uses as gelling agents to enhance stability, and biocompatibility. Gums, such as chitosan, pectin, and gum arabic have film-forming agents to provide barrier properties against moisture, gases, and UV radiation. Plant gums have uses in incorporating drugs within their matrix to protect against degradation and providing stability [Jiang et al., 2023]. Plant gums are generally considered safe, biocompatible and non-toxic, and can be metabolized and eliminated from the body.

Chemically modified natural polysaccharides gained importance as it can enhance their properties, expand their applications, and improve their performance in various fields [Mohammed et al., 2021]. Here are some key reasons why chemical modification of carbohydrate polymers is significant. Chemically modified natural polysaccharides can exhibit enhanced solubility, stability against factors such as pH, temperature, and enzymatic degradation, making them more suitable for specific applications. To meet specific therapeutic needs rate and duration of release can be tailored by introducing functional groups or cross-linking agents into carbohydrate structure. Structurally- modified polymers interacts with living tissues, improving biocompatibility, reducing potential adverse reactions or toxicity. Chemical modification can introduce targeting ligands or functional groups onto carbohydrate polymers, enabling specific interactions with target cells or tissues and thus minimizing off-target effects. Modification of the polymer- backbone improves the mechanical and rheological properties allowing for the development of strong- films, coatings, or hydrogels , expanding the range of potential applications [Ali & Ahmed 2018]. Chemically converted polymer opens up opportunities for incorporating additional properties, such as antimicrobial activity, antioxidant capacity, or stimuli responsiveness.

Ionic-crosslinking of natural polysaccharides is a strategy for achieving sustained release in drug delivery systems [Alvarez-Lorenzo et al., 2013]. Additionally, 'crosslinking of polymer' is significant for drug delivery manipulation because of several advantages.

Ionic cross linking allows for the formation of hydrogels or gel-like networks [Zhang et al., 2018] facilitating entrapment of drugs and providing a barrier retarding the diffusion of drugs, and thus it controls release rate [Nahar et al., 2017]. It also enhances stability in storage/transport period, and protects against environmental factors, such as pH changes or enzymatic degradation. Ionic-crosslinking have uses to develop stimuli-responsive drug delivery systems allowing targeted drug release at the desired site. Easy processing makes it suitable for large-scale production and commercialization of drug delivery systems. Ionically modified polymers are biocompatible and biodegradable, non-toxic, and can be metabolized and eliminated from the body. Gums have

the ability to swell and form a hydrogel matrix facilitating absorption and retention of large amounts of water and thus slowing down the diffusion of drugs from the matrix. The rate of swelling and subsequent drug release is dependent on the degree of crosslinking and the nature of the crosslinking ions. The release rate of the drug is made tuned by introducing pH-sensitive or temperature-sensitive moieties within the hydrogel and enables triggered release under specific physiological conditions. Overall, ionic crosslinking of carbohydrate polymers offers a versatile and effective strategy for modifying drug delivery systems, providing controlled release, stability, targeted delivery, and improved bioavailability of drugs.

1. Controlled Drug Release: Ionic crosslinking allows for the formation of hydrogels or gel-like networks from carbohydrate polymers. These networks can entrap drugs within their structure and control their release. The crosslinked structure provides a barrier that hinders the diffusion of drugs, resulting in sustained and controlled release profiles. The release rate is made tuned by altering the crosslinking density or the concentration of crosslinking ions. The gel-like structure can protect drugs from premature degradation or metabolism, allowing for improved absorption and prolonged residence time at the site of action and thus enhancing bioavailability.

1.2. *Albizia procera*

Albizia Procera, known for its rapid growth, semi-deciduous nature, preference for light and relatively resilient nature against drought having the tendency to produce root suckers as subjected to damage. There exist numerous species within the *Albizia procera* genus, among which one variant is recognized locally in India under names like safed-siris, karanji, Dun-siris, and forest-siris. The *Albizia* genus, categorized under the Fabaceae family and falling within the subfamily Mimosoideae, encompasses these diverse species. About 150 species make up the *Albizia* genus, which are distributed throughout tropics of Asia, Africa, Madagascar, America, and Australia. *Albizia procera* thrives across an array of tropical forest types within its habitat, encompassing

tropical semi evergreen forests, tropical humid deciduous forests, lower alluvial Savannah woodlands, and northern sub-tropical deciduous-leaved forests [Meena & Gupta 2014]. In Vietnam, this particular species flourishes in various ecological niches, spanning from the lush expanse of tropical rainforests to the arid expanses of dry open forests and the wide-reaching savannas [Nguyễn NC 1996]. Many albizias are used as ornamentals because of their lovely flowers. Albizias are significant fodder, lumber, and medicinal plants.

Description: The typical height of the *A. Procera* tree ranges from 7 to 15 meters, although under favorable conditions, it can extend up to 30 meters. Its trunk, varying between straight and crooked, measures 35-60 cm in diameter, usually stretching up to 9 meters in length. Smooth, light grey-green, yellowish-green, or brown in color, the bark has horizontal ridges and is occasionally flaking with tiny, fine scales. The inner bark is pinkish or straw-colored, and the underside of the bark is green above and orange below the surface.

The leaves of *A. procera* are lopped off the tree in numerous states for use as fodder since they are thought to be suitable for most ruminants in India, including cattle, sheep, goats, elephants, and deer. The leaves exhibit sufficient levels of nitrogen (N), potassium (K), calcium (Ca), and magnesium (Mg) for animal production. However, their sodium (Na) and phosphorus (P) contents are inadequate, suggesting that this species should not be solely relied upon for fodder. Combining it with other fodder species is recommended. Moreover, the leaves contain high levels of lignin and crude fiber, making them challenging to digest. As albizia trees produce gums, they have been used in foods and pharmaceuticals as a natural emulsifier instead of arabic gum [De Paula et al., 2001; Avachat et al., 2011]. The mineral content of leaves is 6.2% ash, 19.9% protein, 3.3% fat, 39.7% carbs, 1.51% calcium, and 0.3% phosphorus.

A large amount of a reddish-brown gum is exuded from the injured stems that is chemically similar to gum arabic, and is a substitute for it. In food and pharmaceutical applications, procera gum has uses as a natural emulsifier in place of arabic gum. Besides that, its matrix forming ability, non-toxicity, biocompatibility and biodegradability can play great role on superior patient compliance, as well as great sustainability. Plant's entire composition has anti-

cancer properties, spermicidal action at a low dilution. The bark's decoction is administered for rheumatism and bleeding, in treating pregnancy-related issues and stomachaches. Indians apply leaves as a poultice to sores. Animal experiments, specifically on mice, have revealed the toxicity of the leaves. Additionally, the seeds contain procera A, a substance proven to be poisonous to mice and rats through both oral and parenteral (injected) administration [Randrianarivo et al., 2014]. The presence of hydrocyanic acid in the tree has been determined.

Several investigations have revealed the composition of *A. procera* gum, highlighting the presence of β -(1 \rightarrow 3)-D-galactopyranose units alongside a proportion of β -(1 \rightarrow 6)-D-galactopyranose units. Furthermore, these studies have identified the existence of α -(1 \rightarrow 3)-L-arabinofuranose units within the gum extracted from *A. procera* (Figure 1.2) [De Paula et al., 2001; Avachat et al., 2011; Pachuau et al., 2012; Zhang et al., 2018]. As per specific research, the predominant monosaccharides derived from the hydrolysis of *A. procera* gum are galactose and arabinose. It has been established that the arrangement of linkages and the monosaccharide constituents within the gum's structure play a pivotal role in shaping its rheological behavior and functional attributes [Izydorczyk et al., 2005]. The structure of *A. procera* gum is shown in Figure 1.3.

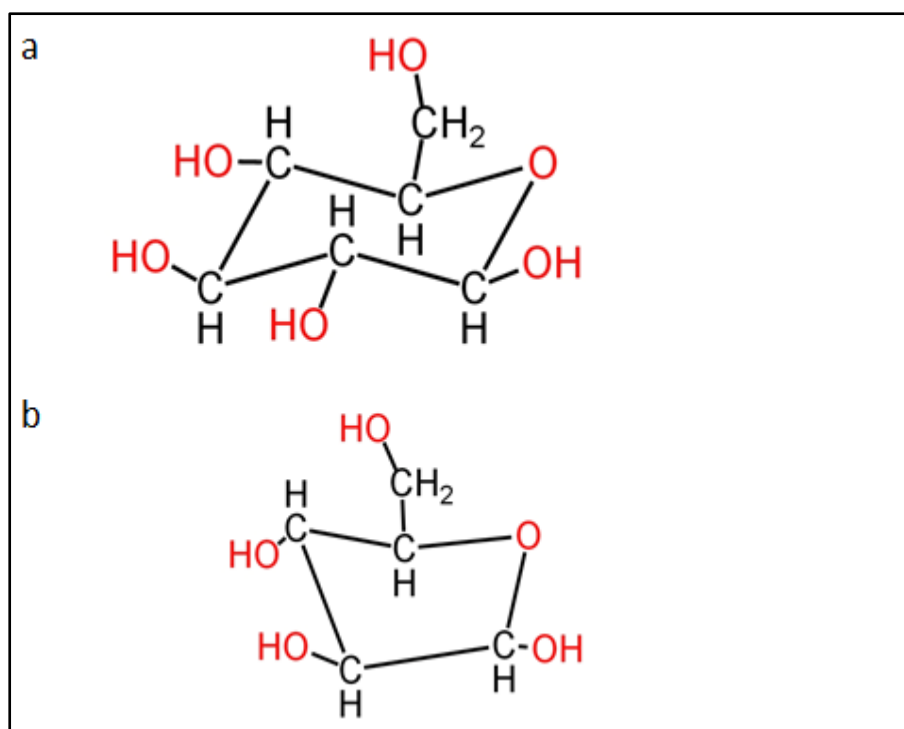


Figure 1.2: (a) β -D-galactopyranose, (b) α -L-arabinofuranose

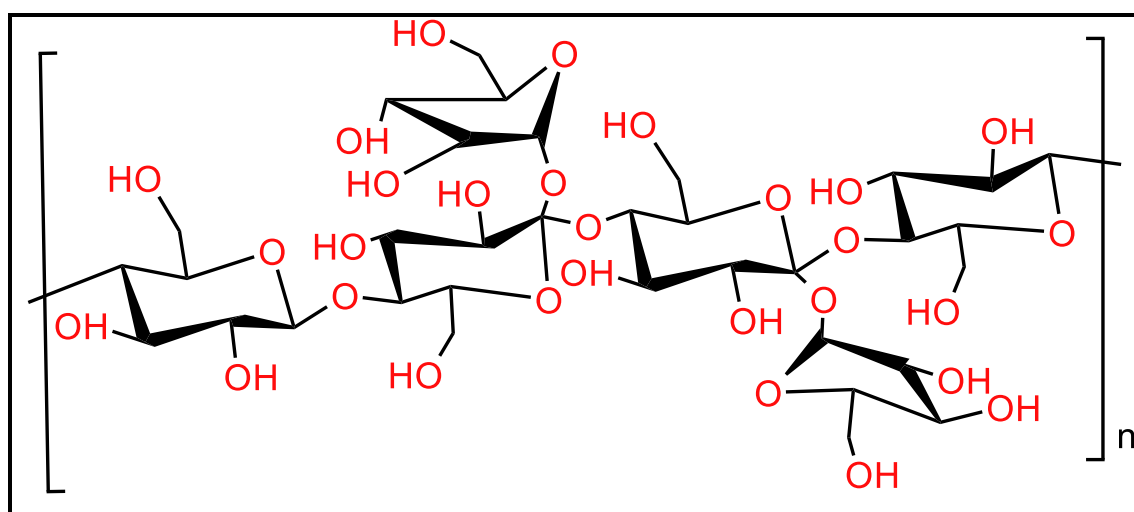


Figure 1.3: Structure of *Albizia procera* gum

1.3. Carboxymethylation

The carboxymethylation reaction on polymers involves attaching carboxymethyl groups (-CH₂COOH) onto the polymer backbone. This reaction typically happens by reacting the polymer with sodium chloroacetate (or its precursor, chloroacetic acid) in the presence of an alkali catalyst [Kazzaz et al., 2019; Sengupta & Datta 2021]. Here are the few steps involved in the carboxymethylation reaction on polymers: Activated chloroacetic acid by reacting chloroacetic acid with a base, such as sodium hydroxide or sodium carbonate, to form the reactive intermediate. The activated chloroacetic acid reacts with the polymer by heating in a suitable solvent, such as water, alcohol, or organic solvents. This reaction incorporates carboxymethyl groups on the polymer backbone because of nucleophilic attack of the polymer on the activated chloroacetic acid [Mourya et al., 2010].

The modified polymer is purified to remove if any un-reacted reagents or byproducts to prevent unwanted side reactions or contamination using techniques such as precipitation, dialysis, or column chromatography. Following the process, the resultant product undergoes characterization through diverse analytical methods like Fourier-transform infrared spectroscopy (FTIR) or nuclear magnetic resonance (NMR) spectroscopy. These techniques serve to validate the effective integration of carboxymethyl groups into the final product [Chakravorty et al., 2016].

The degree of carboxymethylation refers to the extent of substitution of carboxymethyl groups on the polymer backbone and is controlled by adjusting the ratio of chloroacetic acid to the polymer and the reaction time. Higher concentrations of chloroacetic acid or longer reaction times generally lead to higher degrees of carboxymethylation.

The distribution of carboxymethyl groups along the polymer chain can vary depending on the reactivity of different functional groups present in the polymer. Reactive functional groups, such as hydroxyl or amino groups, may preferentially react with chloroacetic acid, resulting in a more random distribution of carboxymethyl groups. However, certain polymers may have

specific sites or regions that are more reactive, leading to a more localized distribution of carboxymethyl groups [Kaity & Ghosh 2013].

The degree and distribution of carboxymethyl groups have influences on properties of the carboxymethylated polymer are influenced by. Introducing carboxymethyl groups can enhance the water solubility, biocompatibility, adhesive properties, and rheological behavior of carrier polymer. In addition, the carboxymethyl groups can provide ionizable functionality, allowing for pH responsiveness or complexation with other molecules or ions.

It is important to note that both the carboxymethylation reaction and the distribution of carboxymethyl groups along the polymer chain are affected by various factors, including the nature of the polymer, reaction conditions (time, temperature, reactant concentration, and catalyst type), and the presence of other functional groups or additives. Optimization of these parameters is necessary to achieve the desired degree of carboxymethylation, control the distribution of carboxymethyl groups, and obtain properties desired of the carboxymethylated polymer.

Coulombic repulsion in carboxymethylation [Davis 1991]:

Coulombic repulsion refers to the electrostatic force of repulsion between charged particles. In the case of polymer chains, coulombic repulsion can occur when charged groups or ions present within the polymer structure. These charged groups can be either naturally occurring or introduced by incorporating charged monomers or additives.

When polymer chains contain charged groups, such as ionizable functional groups or dissociated ions, they can experience electrostatic repulsion due to the like charges on adjacent chains. According to Coulomb's law, the Coulombic repulsion stems from the principle that the force exerted between two charged particles is directly related to the product of their charges and inversely related to the square of the distance between them.

The coulombic repulsion between polymer chains can have prominent effects on their behavior and properties. Coulombic repulsion causes chain expansion and an increase in the inter-chain distance, which affect the volume, dimensions, and mechanical properties of the polymer, and has an effect on the

solubility and swelling behavior of polymers in solvents or aqueous environments owing to loose packing of polymer chains. Coulombic repulsion between like-charged polymer chains can prevent their close association or aggregation, which improves colloidal stability or dispersion. The repulsive forces between charged polymer chains can hinder their flow which causes increased viscosity or resistance to deformation.

When carboxymethylated polymers are present, coulombic repulsion can occur due to the negatively charged carboxylate groups ($-\text{COO}^-$) on the polymer chains. Carboxymethyl groups ($-\text{CH}_2\text{COOH}$) onto the polymer backbone can ionize in aqueous environments to form carboxylate anions ($-\text{COO}^-$). Ionization and charge density of the carboxylate groups are controlled by adjusting the pH or ionic strength of the environment, thereby modulating the extent of coulombic repulsion. The degree of coulombic-repulsion in carboxymethylated polymers can be affected by factors such as the extent of carboxymethylation, pH, ionic strength, and the presence of counter ions. Understanding and manipulating the coulombic repulsion in carboxymethylated polymers is significant in the design of charged polymers for various applications, including drug delivery, tissue engineering, and controlled release systems.

1.4. Rheology

Rheology, stemming from the Greek "rheo" for "flow" and "logy" for "study," explores the dynamics of material movement. Its main domain involves observing how substances behave in liquid states, but it also covers the study of 'soft solids' or semi-solids that exhibit plastic flow rather than elastic deformation when exposed to external forces [Isaac et al., 2015; Kulawik-Pióro et al., 2019]. It delves into investigating how materials deform and flow when subjected to applied forces or stresses. It examines the relationship between the applied stress or force and the resulting deformation or flow behaviour of a material. It encompasses the behavior of substances with intricate microstructures, including hydrogels, suspensions, polymers, and various glass

formers like silicates. Additionally, it extends its application to numerous pharmaceutical forms such as ointments, creams, emulsions, and various additives. Rheological properties are important in various industries and fields, including materials science, chemistry, engineering, and biology.

Newtonian fluids are distinguished by a sole viscosity coefficient tied to temperature, remaining unaltered by the shear rate. This trait of constant viscosity is observed in a limited group of fluids. Conversely, non-Newtonian fluids display variations in viscosity in response to strain. Mathematical equation that defines the viscosity is:

$$\tau = \mu \left[\frac{\delta u}{\delta y} \right]^n \quad (1)$$

Where τ is the amount of shear stress (Pa), μ is the coefficient of viscosity (Pa.S), $\delta u/\delta y$ represents the rate of shear (S-1), and n is the consistency index.

$n = 1$ represents the Newtonian system. However, for non-Newtonian systems $n \neq 1$; $n < 1$ then the flow will be Pseudo plastic; $n > 1$ then the flow will be dilatant [Sochi 2010].

Studies in rheology often center on non-Newtonian fluids, seeking to establish the essential functions required to connect stress with the rate of strain or shear rates. An increase in relative flow velocity causes a reduction in the viscosity of the product as evident in the extrusion of semisolid (gel, ointment/paste) from its container and the force is applied either by pressing. Some shear-thinning substances are exhibiting thixotropy.

Rheological studies are categorized into two tests models: (i) rotational test models (change in viscosity against different shear rates) and (ii) oscillatory test models (change in storage modulus (G'), loss modulus (G'') against different angular frequencies (ω), or strains). The G' and G'' of a material signify the elastic part and the viscous part of the material respectively [Xu et al., 2016; Wang et al., 2021;]. If a material has $G' > G''$ then the material is considered elastic but in the case of $G' < G''$ then the material is considered viscous in nature.

Dynamic rotational study:

Flow curves were used to compare the flow behavior with the increasing shear rate of samples as well as the viscosity profiles.

Oscillatory tests [Sa B et al., 2019]:

(a) Amplitude sweep: It involves varying the amplitude of deformation or shear stress while maintaining a constant frequency. This amplitude represents the highest point of the oscillatory motion. The analysis plots the storage modulus (G') and the loss modulus (G'') against the deformation. During this sweep, these moduli are plotted concerning the deformation (% strain).

The linear viscoelastic region (LVE) characterizes the area where stress demonstrates a linear relationship with strain for the given sample. The storage modulus (G') (Pa) represents the material's elastic response, storing deformation energy under shear. Conversely, the loss modulus (G'') (Pa) quantifies the deformation energy utilized by the material during shear, signifying the viscous aspect of a viscoelastic material. [Li WH et al., 1999]. The mathematical expression that describes the relation between G' and G'' is:

$$G' + iG'' = G^* \quad (2)$$

$$\eta^* = G^*/\omega \quad (3)$$

Where G^* is the complex dynamic modulus, η^* is the complex viscosity and ω is the angular frequency.

(b) Frequency sweep: Once the Linear Viscoelastic Region (LVE) is identified, conducting a frequency sweep within this stress range enables a deeper understanding of the material's behavior and its distinct characteristics. The former shows some frequency independence and also the storage (or elastic) modulus, G' is dominant over the entire frequency range. Frequency-dependent and in this case, is dominated by the loss (or viscous) modulus, G'' . The system has little internal network and is easily disturbed. The frequency sweep stands as a crucial assessment evaluating a material's viscoelastic traits. It maintains a constant amplitude of deformation, as determined in the amplitude sweep, within the Linear Viscoelastic Region (LVE), while varying the angular frequency (ω).

1.5. Matrix tablet

A matrix tablet is a type of oral controlled-release solid dosage form that consists of the active pharmaceutical ingredient (API) dispersed or embedded within a matrix or a uniform solid. The matrix forms by various materials, such as polymers, sugars, or hydrophilic excipients. The drug releases from the matrix through different mechanisms, including diffusion, erosion, or a combination. The matrix acts as a reservoir for the drug, regulating its release rate and ensuring a sustained and controlled delivery [Varma et al., 2004].

Matrix tablets offer several advantages over immediate-release (IR) formulations because of their sustained action due to release retardant polymer, less frequent dosing, patient compliance, reduced side effects, improved stability during storage, lesser degradation, and reduced fluctuation in drug plasma level. Because of its compatibility with others, it can accommodate a wide range of drugs. Release rate of a drug is tailored by selecting appropriate polymers and adjusting the formulation parameters to achieve desired release profiles, such as zero-order, first-order, or pulsatile- release.

Matrix tablets are formulated with various techniques, such as direct compression, wet granulation, or hot melt extrusion. The choice of matrix material depends on factors such as drug properties, desired release profile, and compatibility with the manufacturing process [Patel et al., 2011]. Commonly used matrix materials include hydrophilic polymers like hydroxypropyl methylcellulose (HPMC), hydroxyethyl cellulose (HEC), or ethyl cellulose (EC).

The development of matrix tablets involves careful consideration of parameters such as desired drug release kinetics, matrix composition, drug-polymer compatibility, and manufacturing feasibility. Various *in vitro* and *in vivo* tests determine the release profiles, drug stability, and bioavailability of the drug.

The design of a controlled-release matrix tablet involves several steps and considerations. Here is a general outline of the process:

1. Formulation development initiates with (i) selection of drug considering drug solubility in physiological fluid, therapeutic dose, biological half-life,

bioavailability, and drug diffusion, (ii) selection of matrix materials (polymers and other ingredients) which are compatible with the drug, (iii) determination of drug loading based on requirement and drug's characteristics.

2. Matrix Tablet Design:

- Tablet design considers tablet size and shape and related outcomes like ease of swallowing, patient compliance, and manufacturing feasibility.
- Select the tablet excipients: Choose appropriate excipients like diluents, binders, lubricants, and disintegrants based on compatibility with the matrix material and drug.

3. Manufacturing Process:

- Granulation or direct compression: Decide on the manufacturing technique based on the properties of the matrix material and the drug. Granulation technique is appropriate for materials that do not compress well, while direct compression is suitable for compressible matrix materials.
- Mixing and blending: Thoroughly mix the drug, matrix material, and excipients to ensure uniform distribution and homogeneity.
- Compression: Use a tablet press to compress the mixture into tablet form, applying an appropriate compression force to achieve the desired tablet hardness.

4. Evaluation and Quality Control:

- In vitro release testing: Conduct dissolution studies to assess the drug release profile from the matrix tablet, ensuring it meets the desired release specifications.
- Tablet characterization: Perform tests such as tablet hardness, friability, weight variation, and disintegration time to ensure the tablets meet quality control standards.
- Stability studies: Conduct stability testing to evaluate the physical and chemical stability of the matrix tablets over time.

Concept of sustained release:

Since many past decades, patients got medicines via various pharmaceutical dosage forms such as tablets, capsules, ointments, liquids, and injections as carriers. These conventional dosage forms deliver the drug content at the site of application/absorption.

The notion of sustained release emerged during the early 1950s, with the pioneering patent attributed to Israel Lipowski, who focused on coated pellets as a method for sustained release [Chang & Robinson 1990]. Over the years, sustained-release research has remained a focal point for scientists and formulation experts, perpetually renewing their interest. Creating a successful sustained-release product is a challenging endeavor, entailing the careful consideration of various factors such as the drug's physicochemical properties, pharmacokinetics, the intended route of administration, targeted disease treatment, and crucially, the incorporation of the drug into a dosage form that ensures the desired temporal and spatial delivery pattern. Controlled release involves employing a delivery mechanism to administer the drug into the patient's system at a predetermined rate, specific intervals, or according to specific release profiles [Jantzen & Robinson 2002]. Modulated release involves employing a drug delivery mechanism capable of adjusting the drug release rate according to environmental cues, biofeedback, sensor input, or external control devices. Both the 'Prolonged release system' and 'Extended-release system' serve the common purpose of sustaining the drug's plasma concentration at a therapeutic level over an extended duration.

Controlled drug delivery involves the strategic combination of a natural or synthetic polymer with a drug or active agent, allowing the active agent to release from the material in a precisely planned manner. This release might be consistently spread over an extended period or prompted by environmental stimuli or external triggers. The ultimate aim of managing drug delivery is to enhance treatment effectiveness while mitigating the risks of both inadequate and excessive dosing. Although various modified-release products exist in prescription and over-the-counter medications, only a select few have demonstrated therapeutic advantages. Terms like sustained release, sustained

action, prolonged action, controlled release, extended-release, and 'depot dosage form' denote drug delivery systems engineered to maintain a prolonged therapeutic effect by continuously administering medication after a single dosage.

In a sustained-release system, the dosage form governs the drug molecule's release rate in the body rather than relying on the biological absorption process. Prolonged release dosage forms function by minimizing fluctuations in plasma drug levels through a slower drug release rate compared to its absorption rate, thus delaying absorption [Ankit et al., 2013]. Thus for sustained release formulation:

$$K_{\text{release}} \ll K_{\text{absorption}}$$

The sustained-release (SR) drug delivery system aims to link how the body processes drugs (pharmacokinetics) with how these drugs influence the body (pharmacodynamics) concerning active pharmaceutical components. This objective is pursued by employing innovative delivery methods or modifying the molecular makeup and physiological traits related to the selected administration route.

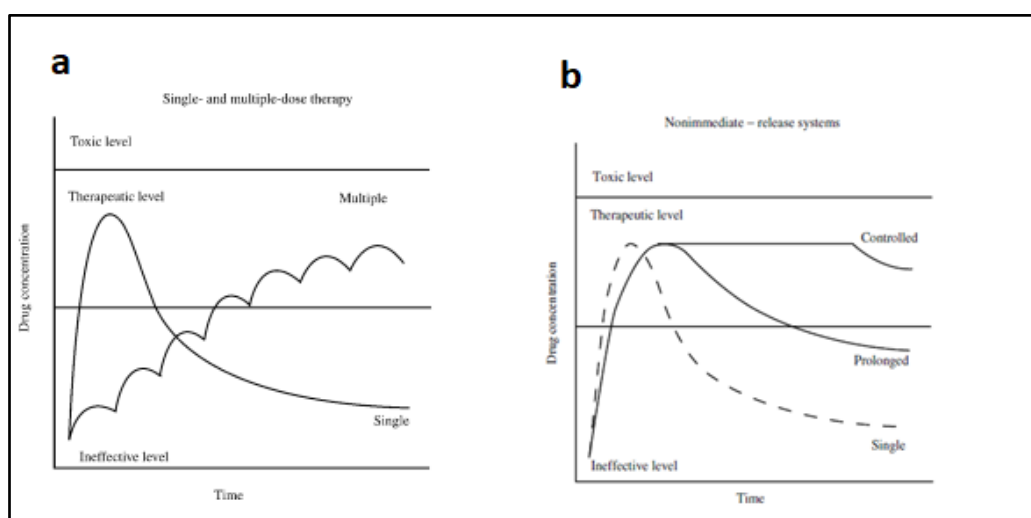


Figure 1.4: (a) Traditional release (b) Controlled release

Controlled drug delivery systems are designed for long-term administration. The release rate from sustained dosage form must be slower than the absorption and elimination of the drug that the release must be the rate-limiting step i.e. $K_r \ll K_a$. The rate of drug release generally depends on dissolution rate. So if, the dosage form needs to control absorption the rate of dissolution should be controlled.

1.6. Metformin as a drug in a sustained-release formulation

Metformin is a widely used medication that belongs to the class of drugs known as biguanides. Medical practitioners typically prescribe it for the treatment of type-II diabetes mellitus, a condition distinguished by increased blood sugar levels due to the body's resistance to insulin or insufficient insulin production.

Mechanism of Action: Metformin functions by curbing the liver's glucose production and enhancing insulin sensitivity in peripheral tissues like muscles and fat. Notably, it doesn't prompt the pancreas to release insulin. Metformin activates an enzyme called AMP-activated protein kinase (AMPK), which regulates various metabolic processes involved in glucose and lipid metabolism [Zhou et al., 2019]. It helps to decrease the absorption of glucose from the intestines also.

Effectiveness: Metformin is considered one of the first-line treatments for type-II diabetes. It is often prescribed in combination with other antidiabetic medications or as part of a comprehensive treatment plan that includes lifestyle modifications.

Some research suggests that metformin may have a positive impact on weight management, as it can help reduce appetite and promote weight loss in individuals with obesity or polycystic ovary syndrome (PCOS) [Jensterle Sever et al., 2014].

Side Effects: Metformin commonly induces gastrointestinal discomfort, marked by symptoms like nausea, diarrhea, and abdominal unease. Typically mild and

temporary, these side effects can occasionally trigger a severe condition known as lactic acidosis, marked by an accumulation of lactic acid in the blood. This is more likely to occur in individuals with kidney or liver impairment or in those taking high doses of the medication.

Dosage and Administration: Metformin comes in diverse forms like immediate-release tablets, extended-release tablets, and oral solutions, offering varied options for administration [Derosa et al., 2017]. It is important to note that metformin should only be used under medical supervision, and the dosage and frequency should be adjusted as necessary to ensure optimal glycemic control and minimize side effects. Regular monitoring of blood glucose levels is advised.

1.7. Diltiazem as a drug in a sustained-release formulation

Diltiazem is classified as a type of medication belonging to the pharmaceutical group known as calcium channel blockers [McDonagh et al., 2005]. Its primary application encompasses addressing diverse cardiovascular ailments such as hypertension (elevated blood pressure), angina (chest discomfort), and specific forms of arrhythmias (irregular heartbeats).

Mechanism of Action: Diltiazem functions by inhibiting calcium channels within the smooth muscle cells present in both blood vessels and the heart. This action inhibits the entry of calcium ions, leading to relaxation and dilation of the blood vessels and a reduction in peripheral resistance. It also has an inhibitory effect on the heart's electrical conduction system, which can help regulate heart rate and rhythm.

Indications: Diltiazem is commonly prescribed for the treatment of hypertension (both essential and secondary), chronic stable angina, and variant angina. It is also used to manage certain types of supraventricular tachycardia

(SVT), atrial fibrillation/flutter, and to prevent recurrent episodes of paroxysmal supraventricular tachycardia (PSVT).

Dosage and Administration: The appropriate form and dosage will be determined by the prescribing healthcare professional according to the specific condition being treated, the patient's response, and other individual factors. It is important to note that the dosage and duration of diltiazem should only be prescribed by a healthcare professional. Diltiazem comes in multiple forms, spanning immediate-release tablets, extended-release capsules, and intravenous (IV) formulations for varied administration and effect durations. Regular monitoring and follow-up visits with a healthcare professional are important.

Side Effects: As with any medication, diltiazem carries potential side effects. These often include dizziness, headaches, flushing, constipation, and occasional swelling in the ankles or feet. Rare but serious side effects may include low blood pressure, heart rhythm disturbances, liver problems, and allergic reactions. It's crucial to promptly notify a healthcare provider of any uncommon or severe side effects experienced while taking this medication.

Drug Interactions: Diltiazem has the potential to interact with various medications, such as specific antibiotics, antifungal treatments, and drugs that influence heart rhythm. It is important to inform the prescribing healthcare professional about all other medications, supplements, and herbal products being taken to avoid potential interactions.

Diltiazem is available in sustained-release formulations, which are designed to provide a controlled and prolonged release of the medication over an extended period [Frishman, 1993]. Sustained-release diltiazem tablets allow for once-daily dosing and help maintain consistent therapeutic levels in the body.

CHAPTER 2

LITERATURE REVIEW

Literature Review

In recent years, the applications of various natural polymers (hydrophilic & hydrophobic) have increased significantly as they are widely employed for the fabrication of Novel Drug Delivery Systems. Natural polymers are large molecules made up of repeating subunits found in nature, such as proteins, nucleic acids, and polysaccharides (synthetic or natural types). Tree exudate gums like gum arabic, gum tragacanth, guar gum, gum karaya, and albizia procera gum are all examples of naturally occurring polysaccharides obtained from natural sources. [Hamdani et al., 2019]. In the pharmaceutical industry, natural polymers play a crucial role in the drug delivery systems due to their versatile utilities; it aids in dosage form design, as a drug carrier. It ensures sustained and controlled drug delivery; reduces drug toxicity, increases drug bioavailability, and facilitates targeted drug delivery. Its most important property is that it is biocompatible and can be used in various medical devices and implants. Natural polysaccharides are manipulated structurally by modification/ crosslinking to alter rheological behavior, flow ability, surface charge, mechanical strength, and swelling/degradation of gum to achieve a stable product with desired drug release [Bajpai et al., 2008]. Mucoadhesive properties and surface charge of polysaccharides/gums facilitate the interaction of the polymer with biological membranes and cells. Overall, polymers have revolutionized the pharmaceutical industry and have led to the development of new and novel drug delivery systems, such as nanoparticles, controlled release (CR) tablets, sustained release (SR) tablets, hydrogels, and microspheres [Kaur et al., 2018].

K. Raghuram Reddy et al., 2003 in their research, they endeavored to create sustained-release tablets of nicorandil, intended for once-daily usage. The formulation involved the use of potential hydrophilic matrix materials, including hydroxypropyl methylcellulose (HPMC), sodium

carboxymethylcellulose (CMC), and sodium alginate. Moreover, they employed ethylcellulose (EC), Eudragit RL-100 (ERL), Eudragit RS-100 (ERS), and the hydrophilic polymer polyvinylpyrrolidone (PVP) as granulating agents. Their findings indicated that the hydrophilic matrix systems employing HPMC, CMC, and sodium alginate demonstrated efficacy in regulating the release of the highly soluble drug, nicorandil.

Al-Saidan et al., 2005 crafted controlled-release tablets using guar gum for the oral administration of water-soluble diltiazem hydrochloride. They experimented with different viscosity grades of guar gum (LM1-30%, MM2-40%, and HM2-50%) and conducted detailed assessments of drug release in lab settings mimicking the gastrointestinal and colonic environments. Their results revealed that HM2 tablets enabled controlled release through Fickian diffusion, similar to commercially available sustained-release diltiazem hydrochloride tablets (D-SR tablets). Notably, HM2 tablets showcased prolonged drug release in live subjects, outperforming the D-SR tablets. Additionally, stability tests demonstrated that HM2 guar gum matrix tablets remained sturdy under harsh conditions of 40°C and 75% relative humidity for duration of six months. This investigation concluded that guar gum matrix tablets hold significant promise as a means for controlling the oral release of diltiazem hydrochloride.

Wong et al., 2011 created an indomethacin matrix tablet for colonic administration and discovered that the presence of CaCl_2 in the pectin matrix slowed the release of the medication, even at high doses. In this investigation, drug release was characterized by a sigmoidal power law pattern, which had a correlation coefficient of roughly 0.99. The tablet's pectin matrix followed an erosion-controlled method for medication release. It was determined that a significant amount of Ca^{+2} ion causes in situ cross-linking of the pectin matrix, which causes indomethacin to release sigmoidally.

Nerurkar et al., 2005 examined carrageenans and cellulose ethers' impact on ibuprofen's release from controlled-release tablet matrices. Polymer blends were tested for their influence on drug release at different concentrations. Cryogenic

scanning electron microscopy visualized hydration-induced surface changes. Multiple regression analysis predicted the 50% release time (t_{50}) based on polymer concentration. Most formulations showed consistent, prolonged ibuprofen release (12–16 hours) with linear profiles ($r^2 \geq 0.96$ –0.99). The blend with Viscarin and HPMC in a 1:2 ratio had the longest t_{50} (9.3 hours); the 2:1 methylcellulose and Gelcarin blend had the shortest (3 hours). Tablets with 10% polymer often disintegrated prematurely. Viscarin and HPMC combinations yielded consistent linear release, contrasting with less effective methylcellulose and HPMC blends. Most formulations followed anomalous release patterns, except for methylcellulose and Gelcarin at 1:1 and 1:2 ratios, displaying zero-order release.

Wu B et al., 2008 a biphasic release matrix tablet involving pectin/calcium interactions for indomethacin delivery. This study scrutinized how various factors affected this system, stability, and pharmacokinetics. pH variation from 1.2 to 7.4 correlated with an increased overall release rate. pH elevation heightened power law correlation (n) and reduced release lag time ($T_{0.1}$) at pH 6.8 and 7.4. Elevated sodium chloride levels above 0.5% notably impacted biphasic release, with a significant rise at 0.9%. Pectin and calcium interaction was disrupted by sodium chloride levels surpassing 2%, leading to an accelerated release of the drug. The addition of pectinase (Pectinex Ultra SP-L) initiated drug release at a concentration of 22.2 pg/ml. Stress testing at extreme humidity increased release, but stability tests over 6 and 12 months affirmed reliable release characteristics. Pharmacokinetic dog studies revealed delayed absorption and colon-specific potential for the HPMC/pectin/calcium tablet compared to the HPMC/pectin tablet and indomethacin crude drug. The tablet exhibited a lower AUC, signifying incomplete absorption and potential for colon-specific drug delivery.

In 2006, M. Harris Shoaib et al. designed a sustained-release ibuprofen tablet meant for once-daily use. They employed hydroxypropyl methylcellulose (HPMC) to regulate drug release, alongside Avicel pH 101 and Magnesium stearate to analyze various drug release parameters following distinct release

kinetic models. Comprehensive characterization encompassing physical and chemical aspects of the formulated tablets revealed results that fell within acceptable ranges. The drug release profile was well-aligned with the Higuchi model expression. Moreover, the mechanism governing drug release was identified as a multifaceted combination involving diffusion, swelling, and erosion.

In 2007, Gafourian et al. delved into the release mechanisms within compressed tablets, analyzing two distinct HPMC substitution types (K4M & E4M) and investigating how the chemical structure of drugs impacted these mechanisms through the QSPR (Quantitative-Structure-Property Relationship) technique. This method aimed to establish significant statistical connections between release parameters and various structural descriptors, encompassing molecular mechanical, quantum mechanical aspects, graph-theoretical parameters, as well as the drug's partition coefficient and aqueous solubility. Interestingly, they found that dipole moment and the size of the drug molecules effectively substituted the latter. The data comparison using the similarity factor distinctly differentiated the effects induced by the two diverse grades of HPMC.

Giovanna Corti et al., 2008 developed a sustained-release matrix tablet of metformin hydrochloride (MH) using hydrophobic tri acetyl- β -cyclodextrin (TA β CD), dispersed in polymeric materials such as hydroxyl-propyl methyl-cellulose, xanthan gum, chitosan, ethyl-cellulose, Eudragit®L100-55, and Precirol® in which compatibility was checked by DSC analysis. The investigation of drug release in simulated gastric and jejunal fluids demonstrated that the management of release control was notably improved by using blends of a hydrophobic swelling polymers in combination with a pH-dependent polymer (like Eudragit®L100-55), as opposed to employing a single polymer alone.

In 2008, Emami et al. delved into the development of sustained-release matrix tablets of flutamide using the direct compression method. They explored the impact of various polymers- cellulose ethers (HPMC and NaCMC), natural gums (guar and xanthan gums), and compressible Eudragit (RSPO and RLPO) in different ratios on both tablet characteristics and the drug release profile. Across nearly all formulations, an increase in polymer percentage corresponded to a decrease in the release rate, yet the specific pattern of drug release primarily relied on the type of polymer employed. Notably, formulations H2F4 (25% HPMC) and S3F4 (40% RSPO) exhibited satisfactory sustained-release patterns following first-order kinetics.

In 2009, Tako et al. conducted a comparative analysis of the rheological attributes—including flow curve and elastic moduli—between native gellan gum and de-acylated gellan gum in the presence of CaCl_2 . The findings demonstrated that native gellan gum flow curves showed plastic behavior above 0.2%. Up until a temperature of 40 °C, the elastic modulus increased slowly before abruptly decreasing. The elastic modulus increased with the addition of CaCl_2 (6.8 mM), remained steady with temperature increase up to 65 °C, and then rapidly declined. With the addition of CaCl_2 , the deacylated gellan gum's elastic modulus was shown to be stronger. When introduced to a urea solution (4.0 M), the elastic modulus of native gellan gum exhibited a notably higher value compared to its value in a standard aqueous solution. Native gellan gum molecules were postulated to form intra- and intermolecular interactions in the presence of Ca^{+2} .

Barakat NS et al. in 2009 conducted an investigation into the impact of both lipophilic (Compritrol 888 ATO) and hydrophilic components (a blend of HPMC and Avicel) on carbamazepine release from granules and compressed tablets. They compared dissolution profiles of each formulation with those of Tegretol CR tablets, assessing mean dissolution time (MDT), dissolution efficiency (DE%), and the similarity factor ($f(2)$ factor). The release mechanism observed in the matrix tablet formulations for CBZ moved from non-Fickian diffusion to

Case II, attributed to increased HPMC content, highlighting erosion as a significant contributing factor. Moreover, augmenting drug loading accelerated drug release and led to an anomalous controlled-release mechanism due to delayed tablet hydration.

Shah SN, et al., 2009 optimized the release of a water-insoluble drug, flurbiprofen by response surface methodology from the sustained release matrix tablets formed by natural gums as the matrix polymers (xanthan and acacia). A central composite design employing two factors, Xanthan and acacia, each at five different levels, was utilized to methodically optimize the drug release pattern. The products underwent characterization via instrumental analysis, specifically Fourier transform infrared spectroscopy. The percentage of drug release within 2 hours and 8 hours served as response variables (termed Y1 and Y2, respectively). Mathematical models, derived through polynomial equations via multiple linear regression analysis for these response variables, demonstrated statistical significance ($P < 0.05$). Visual representation through contour plots effectively depicted the interrelation between the response and independent variables. Notably, drug release in an alkaline medium adhered to zero-order kinetics, ensuring minimal drug release in 0.1 N HCl at pH 1.2.

In 2010, Moin & Shivakumar formulated sustained-release matrix tablets of diltiazem hydrochloride (DTZ) employing karaya gum (K) either alone or in conjunction with locust bean gum (LB) and HPMC across various ratios of drug to gum. Their findings strongly indicate that karaya gum, whether used independently or in a compatible blend with LB and HPMC, proves to be well-suited for the formulation of sustained-release matrix tablets for diltiazem.

Wilson et al., 2011 developed and tested levofloxacin sustained-release matrix tablets for the efficient treatment of colonic microbial infections. Using different hydrophilic polymers that influence release rate, such as hydroxypropyl methylcellulose (HPMC), guar gum, xanthan gum, locust bean gum, and starch, different formulations were made. Result of in vitro drug release from formulations in a medium of pH 1.2 and pH 6.8 PBS was

satisfactory which is under the control of diffusion, and the process was non-Fickian and it indicates its effectiveness for treating colon infections.

Tang Hongbo et al., 2011 modified guar gum using epichlorohydrin as a crosslinking agent, ethanol as a solvent, and sodium hydroxide as a catalyst, and studied the characteristics of crosslinked guar gum as compared to guar gum. The study revealed that the degree of crosslinking was undoubtedly influenced by the crosslinking agent, reaction temperature, and pH. Crosslinking enhanced alkali and acid performance.

Lalduhsanga Pachuau et al., 2012 investigated the monosaccharide composition and physicochemical properties of *Albizia procera* gum. The gum powder was characterized by flow property, moisture content, FTIR spectrum analysis, viscosity measurement, and scanning electron microscopy. Following acid hydrolysis, the individual monosaccharides underwent isolation and assessment using high-performance anion-exchange chromatography-PAD. The findings distinctly identified arabinose and galactose as the primary constituents among the monosaccharides within the exudate gum.

In 2012, Pachuau et al. devised controlled-release matrix tablets of paracetamol incorporating *Albizia procera* gum. The tablets were formulated through the wet granulation method, employing varying concentrations of *procera* gum and hydroxyl-propyl methylcellulose (HPMC), followed by comprehensive evaluations. The findings revealed an anomalous drug release pattern from the matrix tablets. The collective results from diverse assessments strongly advocated the potential of *A. procera* gum as an effective agent for retarding drug release in controlled-release formulations.

In 2012, Ali Rafe et al. explored the influence of temperature and concentration on the viscoelastic and gelling characteristics of basil seed gum (BSG) through oscillatory rheological assessments. Their investigation encompassed strain sweep, stress sweep, and frequency sweep analyses to understand these properties comprehensively. The gum was subjected to heating (20–90 °C) and

cooling (90–20 °C) and characterized as a thermo-reversible gel. The findings highlighted that within the linear viscoelastic range observed at a 0.5% strain, the storage modulus (G') consistently surpassed the loss modulus (G'') across all concentrations, and both moduli escalated with higher BSG concentration. Additionally, the frequency sweep analysis indicated that the BSG solution exhibited characteristics akin to a typical weak gel. Moreover, there existed a linear correlation between the complex viscosity (η^*) and the frequency of the solution. In conclusion, BSG is a suitable synergistic gel for application in food systems.

In 2013, S. Kaity et al. synthesized sodium carboxymethyl ether of locust bean gum using Williamson synthesis, employing monochloroacetic acid as the etherifying agent to modify its hydrophilic properties. They incorporated this modified gum in crafting interpenetrating polymer network microspheres intended for controlling the release of buflomedil hydrochloride for up to 12 hours. The formulation underwent detailed characterization employing FTIR, ^{13}C NMR, and XRD techniques to evaluate its structural properties.

In 2014, Maity S & Sa B conducted modifications on carboxymethyl xanthan gum, transforming it into cross-linked carboxymethyl xanthan gum via a calcium chloride solution. The alteration in the quantity of Ca^{2+} ions significantly affected the viscosity of the gel layer, impacting the swelling and erosion dynamics of the matrix, thereby resulting in diverse drug release profiles. Additionally, they noted a reduction in water penetration into the swollen layer. Their observations highlighted that the degree of cross-linking played a crucial role in governing the mechanism behind drug release.

R. Singh et al., 2014 formulated tablets using partially converted carboxymethylated guar gum in which calcium gluconate acts as a crosslinking agent. The results demonstrated that an increase in Ca^{2+} ion concentration up to a level that raised the gel layer's viscosity and decreased the entry of water into the matrix which retards drug release. Beyond a certain level of Ca^{2+} ion concentration, the matrix was eroded, which resulted in a decrease in gel

viscosity and an increase in drug release rate following a non-Fickian or anomalous transport mechanism.

In 2016, Bao H et al. conducted an investigation into the chemical and rheological characteristics of polysaccharides extracted from the fruit body of *Auricularia auricular-judge*. Their analysis revealed the composition of proteins at 8%, carbohydrates at 72%, with glucose accounting for 62%, mannose for 33%, and galactose comprising 5% of the polysaccharides. In this study, Polysaccharide was extracted from *Auricularia auricular-judge* (AP) with hot water, and the viscosity curves of AP were analyzed using the Power-law model for evaluation. Viscosity and consistency are affected by its concentration, presence of salt and extreme pH values. The extracellular polysaccharide dispersions exhibited shear-thinning (pseudo-plastic) behavior. The robustness of the gel is exhibited at its higher concentrations (e.g., 2%). The gel strength of AP is decreased by adding 1 M CaCl₂ at acidic or alkaline pH. Rheology and DSC test results indicate that the material might be employed in food systems that require heat tolerance.

Chakravorty A et al., 2016 formulated matrix tablets of natural and carboxymethylated locust bean gum (LBG) using metronidazole and ibuprofen as model drugs. The rheological changes upon carboxymethylation promoted the drug release because electrostatic repulsion between the chains of carboxymethylated LBG creates a more porous structure facilitating faster diffusion of the drug molecules into the surrounding medium from the matrix.

In 2011, Palmer D et al. explored the impact of anionic sodium carboxymethylcellulose, specifically CELLOGEN® HP-HS and/or HP-12HS, on the release dynamics of propranolol hydrochloride, theophylline, and ibuprofen from hydrophilic matrices composed of polyethylene oxide, namely POLYOX™ WSR 1105 and/or Coagulant. While ibuprofen and theophylline showed expected release patterns, propranolol HCl displayed notably slower release when combined with sodium carboxymethyl-cellulose (NaCMC) compared to single-polymer matrices. This interaction indicates the potential for

designing extended-release drug forms lasting over 12 hours, using less polymer. This approach may benefit water-soluble drugs, allowing once-daily dosing. Fourier transform infrared absorption spectroscopy was employed to explain altered release profiles, suggesting a sustained-release mechanism possibly formed as a salt due to an ionic interaction between propranolol HCl's amine group and NaCMC's carboxyl group.

In 2019, Sa B et al. delved into the examination of factors affecting the stability of the polysaccharide coat within the initial lag period, approximately spanning six hours. Their research involved the compression of core tablets containing two model drugs, subsequently coated with varying quantities of carboxymethyl locust bean gum (CMLBG). They observed that the integrity of the coat was eroded during the lag time due to the viscosity of CMLBG, which was predominantly dependent on CMLBG concentration and partially on solution pH.

In 2018, Quanquan Miao and his team conducted research focusing on the rheological properties of solutions derived from five different gums: Gum Tragacanth, Gum Shiraz, Karaya Gum, Ghatti Gum, and Arabic Gum. They reported that mucilage solutions of these gums showed non-Newtonian (flow behavior index (n) <1), shear-thinning with thixotropic nature. Karaya gum is sensitive to temperature as E_a (2.683 kcal) is high, whereas other gums are temperature stable. Shiraz gum is acid-stable and arabic gum is alkali stable. The addition of salt ions causes a reduction of viscosity. According to the Power-law model, the ghatti gum solution has the highest k value (13.217) indicating its higher viscosity, and gum karaya with the highest n value (0.437) suggests greater shear thinning property. Except for karaya gum, where the storage modulus G' is lower than the loss modulus G'' , the other four gums exhibit a higher storage modulus, signifying superior elastic properties in these gums. This information is useful in designing any viscous product.

In their 2019 study, Jana S & his co-authors emphasized the promising prospects of Interpenetrating Networks (IPNs) in the realm of controlled drug delivery applications. These IPN hydrogels involve a combination of two or more polymers forming a network, wherein at least one polymer undergoes polymerization and/or crosslinking in the presence of the others. Compared to individual polymers, IPNs exhibit superior qualities. Their discussion centered on IPNs composed of various natural polysaccharides, such as alginate, chitosan, carrageenan, xanthan gum, and locust bean gum, specifically for oral drug delivery purposes.

In the year 2021, Sankula K.R. and other co-authors analyzed various properties of Bhara, Grewia, and Mucuna gums to explore their suitability as release-retardant polymers. These gums showcase non-Newtonian plastic flow, alongside low moisture content, significant swellability, and remarkable water retention capabilities. These characteristics not only hint at their gelling behavior but also affirm their aptness for crafting controlled-release delivery systems. The bacterial and fungal counts were within limits and pathogenic microorganisms were absent and acute toxicity studies indicated that these gums were safe to use.

In 2022, Manabendra Dhua and fellow researchers explored the potential application of a highly carboxylated xanthan (CX) gum, possessing increased viscosity, as an excipient in crafting IPN hydrogel beads along with carboxylated guar (CG) gum. Their investigation involved evaluating the control of glimepiride release from these hydrogels within simulated gastrointestinal fluids. The drug-loaded IPN matrix exhibited pH-dependent swelling, allowing for controlled drug release in simulated in vivo pH environments. Their findings suggested that incorporating at least 25% CX as an additive was advantageous in developing pH-sensitive IPN hydrogel beads with CG, thereby extending the drug release duration within simulated gastrointestinal fluids.

Veronika Mikušová & researchers in 2022 conducted a comparative investigation into the rheological and textural characteristics, along with the in vitro release of ibuprofen (IBU), using various polysaccharide-based hydrogels categorized as neutral, anionic, and cationic. Their research included combinations of cationic hydrogels with neutral or anionic ones to explore how these combinations could alter IBU release profiles. They compared hardness, adhesiveness, and structural viscosity at a shear rate of 6.45 s⁻¹ and minimal retracting force among selected hydrogels, both with and without IBU. The rheological findings aided in identifying suitable hydrogels for potential dermal application. The study concluded that chitosan effectively modified diffusion profiles for negatively charged drugs within combined polymeric systems, thus enabling prolonged drug release.

Jana S & researchers in 2022 formulated and assessed microbeads of diclofenac sodium (DFS) loaded within an Interpenetrating Polymer Network (IPN) of carboxymethyl tamarind gum and gellan gum. The process involved the use of ionic gelation (Al⁺³ ions) technique for fabrication. In vitro, the study showed sustained activity till 8 hr following the Korsmeyer-Peppas model. Upon oral administration of these microbeads containing DFS, in vivo studies demonstrated sustained anti-inflammatory effects in rats induced with carrageenan, indicating prolonged activity against inflammation.

In 2023, Madiha Melha Yahoum and a team of researchers developed a mathematical framework aimed at predicting the rheological flow patterns of modified xanthan gum. To achieve this, they created six distinct derivatives of xanthan gum through etherification processes, utilizing hydrophobic benzylation with benzyl chloride and carboxymethylation using monochloroacetic acid at three distinct ratios labeled as R, with values set at 2.4 and 6. They observed that carboxymethyl xanthan gum derivatives showed a higher degree of substitution (DS) than that of hydrophobically modified benzyl xanthan gum, and viscosity was found to decrease with increasing DS. The molecular weight of benzyl xanthan gum is higher than that of carboxymethyl xanthan gum. An Artificial Neural Networks (ANN) model was formulated

specifically to anticipate the apparent viscosity of both native XG and its derivatives. This predictive model holds the potential to significantly reduce the need for numerous costly and time-consuming experimental investigations.

Thus, the review of literature on polysaccharides, carboxymethylation, cross-linking, rheology, and drug release from sustained-release tablet formulations revealed the following information:

Polysaccharides, such as locust bean gum (LBG), xanthan gum, and chitosan, have been widely used in native or modified form to prepare sustained-release tablet formulations owing to their biocompatibility, biodegradability, and low toxicity. Carboxymethylation can modify solubility, swelling, mucoadhesive properties of polysaccharides, and drug release from the matrix by improving the mechanical strength and stability of the matrix, which can prolong drug release.

Rheological properties of gums and their viscosity play an important role in the formulation of sustained-release tablets which depends on various factors, including the type and amount of polysaccharide used, the degree of carboxymethylation, the degree of cross-linking, and these parameters can affect the swelling and drug release from gum matrix. Higher viscosity can result in slower drug release due to increased resistance to diffusion. Rheological study reveals the gel strength and elasticity of the matrix influencing drug release. A more elastic matrix can result in slower drug release due to increased resistance to swelling and diffusion.

The review suggests that the use of carboxymethylated polysaccharides, cross-linking agents, and careful control of rheological properties can be effective strategies for developing sustained-release tablet formulations with controlled drug release.

,

CHAPTER 3

AIM AND OBJECTIVES

Aim and Objectives

The objective of this work is to investigate the impact of carboxymethylation and ionic crosslinking on the rheological properties and drug release behavior of native *Albizia procera* gum (NAP). Specifically, the study aims to understand how these modifications affect the gelation behavior, viscosity, and drug release kinetics of the resulting carboxymethylated and crosslinked *A. procera* matrices.

Aims:

- Carboxymethylation of Albizia procera Gum: The first aim is to chemically modify the native Albizia procera gum by carboxymethylation, introducing carboxymethyl groups onto the polysaccharide chain. This aims to enhance the water solubility and modify the rheological properties of the gum.
- Characterization of Carboxymethylated Albizia procera: The study aims to characterize the carboxymethylated Albizia procera gum in terms of the degree of substitution and rheological properties, including viscosity and gelation behavior.
- Drug Release from Carboxymethylated Procera Gum Matrix Tablets: To study the drug release kinetics from the matrix tablets containing carboxymethylated procera gum and evaluate how the decreased viscosity and weak gel affect the drug release, resulting in faster drug release profiles.
- Impact of Carboxymethylation on Drug Release: To investigate the influence of carboxymethylation on drug release kinetics from the matrix tablets prepared using carboxymethylated Albizia procera gum.

This aims to understand how the modification affects drug entrapment and release mechanisms.

- **Ionic Crosslinking of Carboxymethylated Albizia procera:** The study aims to further modify the carboxymethylated Albizia procera gum through ionic crosslinking by calcium ions, forming a crosslinked matrix. This process aims to manipulate the gelation behavior and mechanical properties of the gum.
- **Characterization of Crosslinked Albizia procera:** To comprehensively characterize the crosslinked Albizia procera gum, including the extent of crosslinking, changes in rheological properties, and swelling behavior.
- **Impact of Ionic Crosslinking on Drug Release:** The study aims to compare the drug release profiles from the matrix tablets prepared using the crosslinked Albizia procera gum with those from carboxymethylated and native gum matrices. This aims to shed light on how ionic crosslinking impacts drug release kinetics. It seeks to compare the drug release kinetics between matrix tablets containing crosslinked procera gum and those made of carboxymethylated and native gum matrices, aiming to comprehend the sustained drug release attributes attained through crosslinking.
- **Mechanical Properties Assessment:** To evaluate the mechanical properties, including gel strength and viscoelastic behavior, of the crosslinked Albizia procera gum matrices, and compare them with the carboxymethylated and native gum matrices.
- **Understanding the Gelation Behavior:** The study aims to investigate the mechanism behind the gelation behavior of both carboxymethylated and crosslinked Albizia procera gum matrices, focusing on the impact of coulombic repulsion and ionic interactions and its correlation with drug release rates.
- **Comparison of Rheological Parameters:** To compare the rheological parameters (G' , G'' , viscosity) of carboxymethylated and crosslinked Albizia procera gum matrices with the native gum matrices, providing insights into how these modifications affect the gelation and viscoelastic

behavior. The rheological properties, particularly the gel strength, of the polymer matrix influence its structural integrity during swelling and erosion. Polymers with higher gel strength can maintain their structure for a longer duration, providing sustained drug release. On the other hand, lower gel strength may lead to matrix disintegration and faster drug release.

- **Assess pH-Responsive Drug Release:** To investigate whether the carboxymethylated and crosslinked Albizia procera gum exhibit pH-responsive drug release behavior, allowing for controlled release of drugs based on the environmental pH at the target site.
- **Polymer Swelling:** The swelling behavior of the polymer matrix affects the extent of drug entrapment during the formulation process. Polymers that swell more can encapsulate a higher amount of drug, resulting in a higher drug loading capacity in the matrix tablets.
- **Potential Drug Delivery Applications:** To discuss the potential applications of the carboxymethylated and crosslinked Albizia procera gum matrices as drug delivery systems based on their rheological properties and drug release characteristics.
- **Correlate Rheological Changes with Drug Release:** To establish correlations between the rheological properties of carboxymethylated polysaccharides and their drug release profiles, providing insights into the mechanisms governing drug release.
- **Kinetic Modeling of Drug Release:** In order to comprehend the release mechanism and kinetics from the ionic crosslinked matrix tablets, the drug release data was fitted to diverse kinetic models such as zero-order, first-order, Higuchi, and Korsmeyer-Peppas models.
- **Stability Studies:** To assess the stability of the crosslinked polymer matrix tablets over an extended period, evaluating the drug release behavior and physical characteristics under different storage conditions.
- **Stability and Longevity of Drug Release:** The rheological properties of the polymer matrix impact the stability and longevity of drug release over time. Polymers with stable and well-defined rheological

characteristics provide consistent drug release profiles, enhancing the predictability and reliability of the drug delivery system.

- **Implications for Drug Delivery Applications:** To discuss the implications of the findings for potential drug delivery applications, considering the suitability of carboxymethylated and crosslinked procera gum matrices for various pharmaceutical formulations.
- **Comparative Analysis:** To compare the rheological and drug release properties of carboxymethylated and crosslinked Albizia procera gum with the native gum assessing its suitability for specific drug delivery applications.
- **Formulation Development:** To explore and develop pharmaceutical formulations (e.g., tablets, hydrogels) using carboxymethylated Albizia procera gum as an excipient, considering its modified properties for improved drug delivery.
- **Optimization of Formulation Rheology:** To optimize the rheological properties of the carboxymethylated and crosslinked gum matrices for desired drug release kinetics, achieving controlled and sustained drug release.
- **Establishment of correlation between rheological changes and drug release:**

Overall, the study aims to provide valuable insights into the rheological behavior and drug release capabilities of carboxymethylated and crosslinked *Albizia procera* gum matrices. The findings could contribute to the development of novel drug delivery systems using natural polysaccharides as excipients with tunable properties for various pharmaceutical applications. The study is also aimed to investigate the potential of carboxymethylated Albizia procera gum as a versatile and biocompatible excipient with tailored properties for drug delivery applications. The objectives focus on characterizing the modified gum, assessing its drug delivery capabilities, and optimizing its use in pharmaceutical formulations.

This study also aims to clarify the spectral characteristics and solubility behaviors of Metformin (MET) and Diltiazem (DIL) in different solvent systems. These drugs were selected due to their crucial roles in matrix tablet formulations.

1st phase of work and objective

The 1st phase of work involved the synthesis of carboxymethyl *Albizia procera* gum (CMAP) from NAP and characterization using several instrumental methods. Subsequently, NAP and CMAP were used to prepare matrix tablets with a view to examine the suitability of the polysaccharides as matrix materials for NDDS. Rheological studies of the polymers were performed to explain the release of the drugs from the matrix tablets.

Brief description of work done

1. Derivatization of NAP to CMAP via a twostep base catalyzed reaction.
2. Determination of degree of substitution via classical titrimetric method and characterization of CMAP using different instrumental analyses include Fourier transform infrared (FTIR), Differential scanning calorimetry (DSC), X-ray powdered diffraction (XRD), Zeta potential analysis, and Solid-state ¹³C NMR Spectroscopy.
3. Investigation of drug-excipients interaction using various instrumental methods such as FTIR spectroscopy, Differential scanning calorimetry (DSC) studies.
4. Preparation of matrix tablets of Metformin HCl (MET) and Diltiazem HCl (DIL) using NAP or CMAP via classical wet granulation technique.
5. Determination of physical properties of developed matrix tablets such as weight variation, crushing strength, thickness and friability, and drug content.
6. In-vitro drug release from MET and DIL matrix tablets in deionized water, acid solution (pH 1.2), and phosphate buffer (PB) solution (pH 6.8).

7. Investigation into the swelling behavior of drug-free NAP and CMAP matrix tablets was conducted in water, acid solution (pH 1.2), and MPB solution (pH 6.8).
8. Rheological study of NAP and CMAP and establishment of correlation between matrix swelling, drug release and rheological properties of NAP and CMAP.

2nd phase of work and objective

The second phase of the study aims to explore the impact of ionic crosslinking on the carboxymethylated *Albizia procera* gum and its influence on the rheological properties, drug release behavior, kinetics, and swelling erosion characteristics of sustained-release matrix tablets containing MET and DIL drugs. The objectives focus on characterizing the crosslinked gum, formulating the matrix tablets, and studying the drug release mechanisms to gain a comprehensive understanding of the sustained release system.

The second phase of the study also includes the formulation of immediate release tablet using CMAP and sustained release matrix tablet using crosslinked CMAP.

Brief description of work done

1. Modification of Carboxymethylated *Albizia procera* Gum through Ionic Crosslinking: The primary objective is to modify the carboxymethylated *Albizia procera* gum by ionic crosslinking using calcium ions. This aims to enhance the rheological properties and gelation behavior of the gum, potentially impacting drug release characteristics.
2. Characterization of Crosslinked *Albizia procera* Gum: To comprehensively characterize the crosslinked *Albizia procera* gum (CCMAP) in terms of its physicochemical properties, such as chemical structure and degree of crosslinking. The characterization of CCMAP involved employing various

- instrumental analyses; including Fourier transform infrared (FTIR), Differential scanning calorimetry (DSC), X-ray powdered diffraction (XRD), and Zeta potential analysis.
3. Comparative Rheological Study: comparative rheological study between CMAP, CCMAP, and NAP. This study aims to understand the influence of carboxymethylation and ionic crosslinking on the rheological properties of the gums.
 4. Matrix Tablet Formulation with MET and DIL Drugs: To formulate sustained-release matrix tablets containing Metformin (MET) and Diltiazem hydrochloride (DIL) drugs using CCMAP. The goal is to achieve controlled drug release of both drugs over an extended period. A similar approach is used in the formulation of immediate release tablets containing the drugs Metformin (MET) and Diltiazem hydrochloride (DIL).
 5. Drug Release Profile: evaluation of the drug release profiles of MET and DIL drugs from the immediate release and the sustained-release matrix tablets. This study includes the assessment of cumulative drug release over time to understand the sustained release behavior.
 6. Release Kinetics Modeling: application of mathematical models (e.g., Higuchi, Korsmeyer-Peppas) to fit the dissolution data of both MET and DIL drugs and characterize their release kinetics from the matrix tablets. This can help to determine the release mechanism (e.g., Fickian diffusion, non-Fickian release) and understand how the modifications in the gum affect drug release.
 7. Swelling Erosion Study: To investigate the swelling and erosion behavior of the placebo matrix tablets over time. This study aims to understand how the gum modifications influence the matrix integrity and drug release mechanism, particularly in the context of swelling-controlled or erosion-controlled release.
 8. Comparative Evaluation of Drug Release: comparison of the drug release profiles and kinetics of MET and DIL drugs from the matrix tablets containing CMAP and CCMAP gums with those containing native gum.

This comparison will reveal the impact of gum modifications on drug release behavior.

9. **Mechanistic Insights:** correlation of the rheological properties of the modified gums with the drug release kinetics and swelling erosion characteristics of the matrix tablets. This will provide mechanistic insights into how gum modifications influence drug release behavior.

3rd phase of work and objective

The third phase of the work aims to evaluate the stability of the sustained-release matrix tablets under accelerated conditions and perform statistical optimization to identify the most stable and efficient formulation. This phase is critical in determining the long-term stability of the developed formulations, ensuring that they can maintain their drug release characteristics and remain suitable for pharmaceutical use over an extended period.

Brief description of work done

1. **Accelerated Stability Studies:** conduct accelerated stability studies on the sustained-release matrix tablets containing Metformin (MET) and Diltiazem hydrochloride (DIL) drugs formulated with NAP, CMAP, and CCMAP. The aim is to evaluate the long-term stability of the formulations under stressed conditions, such as high temperature and humidity, and assess any potential degradation or changes in drug release behavior.
2. **Characterization of Formulations under Stress Conditions:** To comprehensively characterize the NAP, CMAP, and CCMAP formulations after subjecting them to accelerated stability studies. This includes analyzing

changes in physical appearance, drug content, drug release profiles, and any other relevant parameters.

3. Identification of Critical Stability Indicators: To identify critical stability indicators that can predict the stability and shelf life of the sustained-release matrix tablets. These indicators may include drug degradation products, changes in release kinetics, and other markers of formulation stability.
4. Statistical Optimization of Formulations: To perform statistical optimization of the NAP, CMAP, and CCMAP formulations using statistical approaches. This aims to identify the optimal formulation parameters (e.g., polymer concentration, drug-to-polymer ratio) that result in the most stable and efficient sustained-release matrix tablets.
5. Selection of Best Formulation: Based on the statistical optimization, the objective is to select the best formulation among NAP, CMAP, and CCMAP that exhibits the most desirable stability profile, drug release behavior, and drug content uniformity.
6. Comparison of Stability Profiles: To compare the stability profiles of the NAP, CMAP, and CCMAP formulations and identify the formulation with the highest stability and the least susceptibility to degradation.
7. Influence of Gum Modifications on Stability: To evaluate the impact of gum modifications (carboxymethylation and crosslinking) on the stability of the sustained-release matrix tablets containing MET and DIL drugs. This includes assessing if the modifications provide any advantages in terms of stability.
8. Potential Formulation Improvements: Based on the stability and statistical optimization results, to propose potential formulation improvements for NAP, CMAP, and CCMAP formulations to enhance their stability and drug release characteristics further.

CHAPTER 4 & 5

MATERIALS AND METHODS



MATERIALS

4. MATERIALS

4. 1. Specifications of Drugs and Chemicals

4.1.1. Metformin hydrochloride (MET) (Indian Pharmacopoeia) and **Diltiazem hydrochloride** (DIL) (Indian Pharmacopoeia) was obtained as gift sample from Stadmed Pvt. Ltd., Kolkata, India.

4.1.2. *Albizia procera* gum Pulverized native *Albizia procera* (NAP) gum was obtained from Mizoram, India).

4.1.3. Following are the chemicals procured from Merk Specialties Pvt. Ltd., Mumbai, India:

Hydrochloric Acid (HCl, 35-38%), sodium hydroxide (NaOH, LR grade), Magnesium stearate (MS), calcium chloride dehydrate, methanol, ethanol 95%, isopropyl alcohol and phenolphthalein.

Following are the chemicals purchased from Loba Chemie Pvt. Ltd. Mumbai, India:

Tri-sodium phosphate dodecahydrate (TSPD), tri-sodium citrate (TSC), and monochloroacetic acid.

Glacial acetic acid was procured from Thermo Fisher Scientific India Pvt. Ltd., Mumbai, India. Lactoseanhydrous was supplied by Oxford Lab Fine Chem LLP, Mumbai, Maharashtra. NaCl (0.9% w/v) solution was obtained from Pharma Impex Laboratories Pvt. Ltd., Kolkata, India

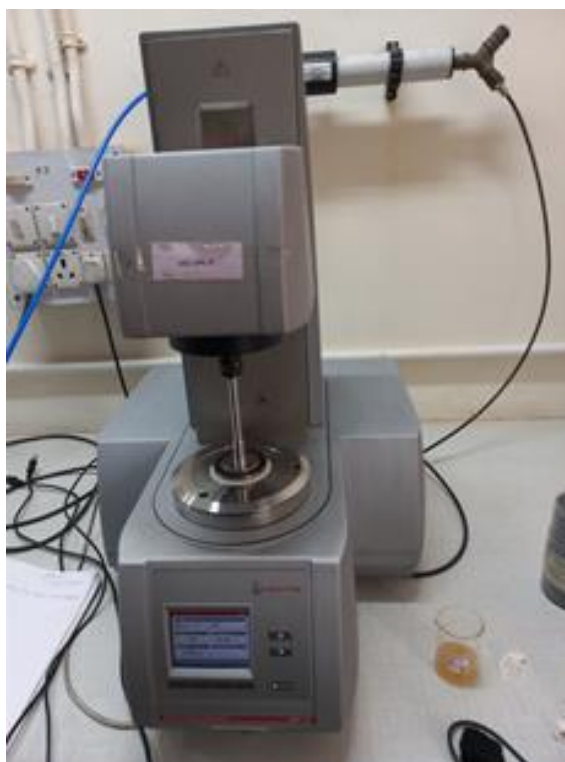
Colloidal anhydrous silicon dioxide (Aerosil) and microcrystalline cellulose (MCC, PH 102) were gift samples by Stadmed Pvt. Ltd., Kolkata, India.

During the entirety of the study, analytical-grade reagents and solvents were consistently employed without additional purification. In-house double-distilled water was consistently used, while Mili-Q water (Millipore, specific resistivity of 18.2 mΩ) was specifically utilized for the rheological study.

4.2. List of Instruments

1. **Electronic pan balance:** Precisa, XB600 M-C, (Switzerland).
2. **Magnetic stirrer:** 2 MLH, (Remi, Mumbai, India).
3. **Mechanical stirrer with axial turbine:** RQ-121/D, Remi, (Mumbai, India).
4. **pH meter :** Orion 2 star, (Thermo Scientific, Singapore).
5. **Fourier transform infrared (FTIR) spectrophotometer:** RX-1 (Perkin Elmer, UK), Alpha II (Bruker, U.K).
6. **Microplate Spectrophotometer:** Spectra-Max-M5 Multi-Mode Microplate Reader (Molecular Devices, USA).
7. **Double-beam spectrophotometer:** UV, 2450 (Shimadzu, Japan).
8. **Differential scanning calorimeter:** DSC-4000 (Perkin-Elmer, United States).
9. **X-ray diffractometer:** Ultima III (Rigaku, Japan).
10. **Elemental Analyzer:** 2400 series II (Perkin-Elmer Inc. U.S.A).
11. **NMR Spectrometer:** ECX400 - 400 MHz High Resolution Multinuclear ¹³C FT-NMR Spectrometer (Jeol, Japan).
12. **Zetasizer:** Nano ZS90 (Malvern Instruments Ltd., UK).
13. **Modular Compact Rheometer:** MCR 102 (Anton Parr, Austria).
14. **Tray Dryer:** Lambda (Orionis, Kolkata, India).
15. **Tablet compression machine:** RIMEK (Karanavati Engineering Ltd., Gujarat, India).

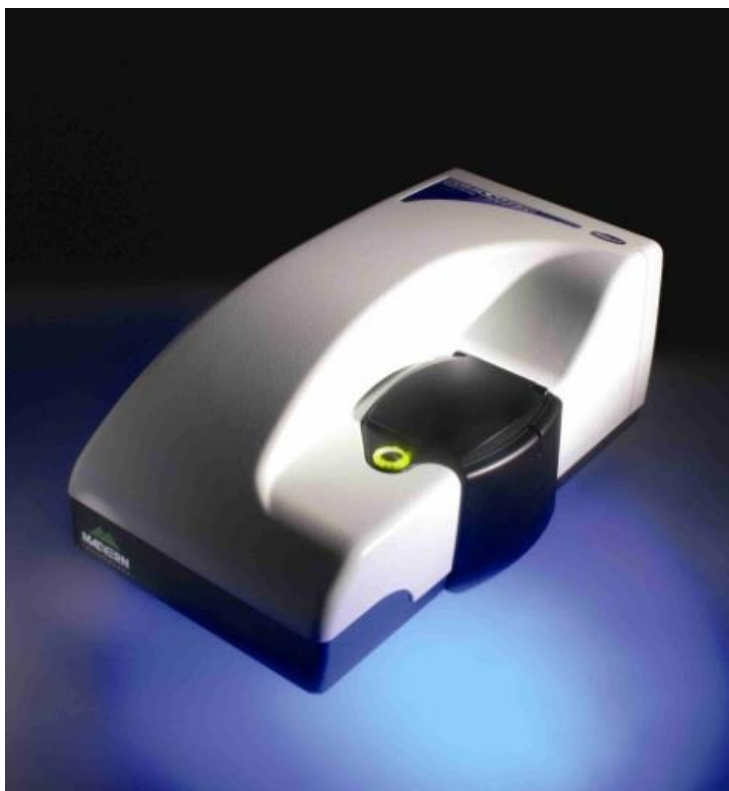
- 16. Monsanto type tablet hardness tester:** (Cadmach, Ahmedabad, India).
- 17. Friabilator:** (Campbell Electronics, Mumbai, India).
- 18. Digimatic Caliper:** CD-6"CS (Mitutoyo Corporation, Japan).
- 19. USP II tablet dissolution test apparatus:** TDP-06P (Electro-lab, India).
- 20. Scanning electron microscope (SEM):** S-3400 N, E-1010 (Hitachi, Japan).
- 21. Centrifuge:** 5804 R (Eppendorf, Chennai, India).
- 22. Stability Chamber** (Thermo Lab, Mumbai, India).



Rheometer: MCR 102



Microplate Spectrophotometer: Spectra-Max-M5



Zetasizer: Nano ZS90

METHODS

5. METHODS

5.1. Analytical methods

5.1.1. Preparation of 0.1 (N) HCl solution (acid solution of pH 1.2)

Concentrated hydrochloric acid (HCl) measuring 8.5 ml was mixed with 200 ml of distilled water within a volumetric flask, eventually reaching a total volume of 1000 ml by adding more distilled water. The pH of the resulting solution was meticulously adjusted to 1.2 and confirmed using a pH meter.

5.1.2. Preparation of 0.2 (M) Tri-sodium phosphate dodecahydrate (TSPD)

Within a volumetric flask, 76 grams of Trisodium Phosphate (TSP) were combined with 500 ml of distilled water, then further adjusted to reach a final volume of 1000 ml by adding more distilled water.

5.1.3. Preparation of phosphate buffer (PB) solutions of pH 6.8 and 7.4

A volume of 250 ml of a 0.2 M solution of tri-sodium phosphate dodecahydrate was introduced into a volumetric flask containing 750 ml acid solution of pH 1.2. Before adding, the solution was ensured to be warmed to a temperature between 36.5° to 37.5° C. Subsequently, any necessary adjustments to the pH were made using 2M hydrochloric acid or 2M sodium hydroxide until the target values of pH 6.8 \pm 0.05 and pH 7.4 were reached. The resulting solution's pH was then verified using a pH meter [Indian Pharmacopoeia 2010, vol-1].

5.1.4. Determination of λ_{max} of Metformin hydrochloride (MET) in deionized water

A solution was prepared by dissolving 10 milligrams of MET in 50 milliliters of deionized water, reaching a final volume of 100 milliliters with additional deionized water. After filtration through Whatman filter paper no.41, different volumes (ranging between 1ml to 5ml) were extracted from this initial stock solution and diluted to 100 milliliters using deionized water. Subsequently, the solution underwent scanning across a wavelength range of 200 to 400 nanometers using a multimode microplate spectrophotometer (Spectra-max M5).

The same procedural approach was utilized to ascertain the λ_{max} value of MET in an acidic solution with a pH of 1.2 as well as in a phosphate buffer (PB) solution with a pH of 6.8 and 7.4.

5.1.5. Determination of λ_{max} of Diltiazem hydrochloride (DIL) in deionized water

A solution was created by dissolving 10 milligrams of DIL in 50 milliliters of deionized water, followed by adjusting it to a final volume of 100 milliliters using more deionized water. After filtration through Whatman filter paper no.41, several aliquots ranging from 1 ml to 5 ml were withdrawn from this initial solution and further diluted to a total volume of 100 ml using deionized water. Subsequently, these diluted solutions underwent spectrophotometric analysis within the wavelength range of 200-400 nanometers, conducted with a multimode microplate spectrophotometer (Spectra-max M5).

The same methodology was applied to ascertain the λ_{max} value of DIL in both an acidic solution with a pH of 1.2 and in PB solutions at pH levels of 6.8 and 7.4.

5.1.6. Calibration curve of MET in deionized

A spectrophotometric calibration curve was established for MET in deionized water, centered at 232 nm. Initially, 10 milligrams of MET were precisely weighed and dissolved in 50 milliliters, later adjusted to a final volume of 100 milliliters using deionized water within a 100 milliliter volumetric flask. This prepared solution was marked as the stock solution, holding a concentration of 0.1 milligrams per milliliter (mg/ml). Subsequently, aliquots of 2, 4, 6, 8, and 10 milliliters were withdrawn from the stock solution and diluted to a final volume of 100 milliliters using deionized water, achieving a concentration range of 2-10 micrograms per milliliter (mcg/ml).

The absorbance of these resultant solutions was measured at 232 nm. To ensure precision, the experiment was repeated thrice across two consecutive days, and the average values were utilized for subsequent calculations. By plotting the Absorbances against the respective drug concentrations, the calibration curve was generated.

Applying a similar approach, a spectrophotometric calibration curve for MET was constructed within an acidic medium of pH 1.2 and phosphate buffer (PB) solutions with pH values of 6.8 and 7.4, employing a common wavelength of 233 nm.

5.1.7. Method development for the estimation of DIL in deionized water

The standard stock solution of Diltiazem Hydrochloride was meticulously prepared in the following sequence: Initially, 10 milligrams of DIL were precisely weighed and transferred into a 100 milliliter volumetric flask. The drug was dissolved in 50 milliliters of deionized water using sonication, following which the volume was adjusted to the mark (100 milliliters) using additional deionized water. This resulting solution was labeled as the stock solution with a concentration of 100 mcg/ml. To obtain various concentrations,

appropriate dilutions were made from the stock solution, resulting in concentrations of 6, 8, 10, 12, 14, and 16 mcg/ml respectively. The absorbance values of these diluted solutions were recorded at 236 nm.

The relationship between absorbance and concentrations was established using the simple regression equation method. The obtained regression equation represents the relationship presented in the calibration curve.

The analogous approach was adopted to establish a spectrophotometric calibration curve for DIL, encompassing both an acidic solution at pH 1.2 and a phosphate buffer (PB) solution across pH values of 6.8 and 7.4.

5.1.8. Analysis for the recovery of MET in various spiked drug solutions

The recovery analysis for MET was conducted across three successive days, encompassing four distinct stages of spiked drug solutions. These analyses were performed both in the presence and absence of the polymers utilized in the formulation process.. Known quantities (1g) of NAP (native *Albizia procera* gum powder), carboxymethylated *Albizia procera* gum (CMAP), and crosslinked carboxymethylated *Albizia procera* gum (CCMAP) were dissolved in 250 ml of PB solution (pH 7.4) and distributed among five conical flasks. Flask No.1 served as the control and did not contain any drug solution. For drug content of 0.1% w/v, MET was dissolved in PB solution of pH 7.4. Known volumes of this drug solution (0.1% w/v) were added to flasks No. 2, 3, 4, and 5, and the volumes were adjusted to 25 ml to achieve drug concentrations of 5 mcg /ml, 10 mcg /ml, 15 mcg /ml, and 20 mcg /ml, respectively. The resulting solutions were then filtered and analyzed using spectrophotometry at 233 nm. The same experiment was repeated using an acidic solution with a pH of 1.2 and a PB solution with a pH of 6.8. The percentage recovery was calculated using the following relationship:

$$\text{recovery (\%)} = \frac{\text{Experimental value}}{\text{Theoretical value}} \times 100 \quad (5.1)$$

The recovery analysis for DIL, The resulting solutions was analyzed using spectrophotometry at 236 nm followed by same procedure.

5.1.9. Measuring the solubility of MET and DIL

5.1.9.1. Study of the solubility of MET in deionized water

To determine the solubility of MET; approximately 1 gram of the compound was added in 100 ml of deionized water contained within a 250 ml stoppered conical flask. The mixture was shaken at 31°C for 72 hours. Later, the solution underwent filtration through a Whatman filter paper featuring a pore diameter of 11 µm. Following filtration, 4 ml of the filtrate were diluted to 25 ml using deionized water. Subsequently, the absorbance of this solution was measured at 232 nm using a spectrophotometer. The solubility of the drug was then calculated using the calibration curve previously prepared in deionized water.

The analogous approach was adopted to determine the solubility of MET, encompassing both an acidic solution at pH 1.2 and a phosphate buffer (PB) solution across pH values of 6.8.

5.1.9.2. Solubility study of DIL in deionized water

In a 250 ml stoppered conical flask, approximately 1 gram of DIL was added in excess to 50 ml of deionized water. The flask was then shaken at 31°C for a period of 72 hours to ensure complete dissolution. Afterward, the solution was filtered through a whatman filter paper with a pore diameter of 11 µm. From the filtered solution, 1 ml was taken and diluted to 100 ml using deionized water, creating a stock solution. Following this, 2 ml of the initial stock solution were

extracted and subsequently diluted to a total volume of 25 ml using deionized water. The absorbance of this diluted solution was measured at 236 nm using a spectrophotometer. The solubility of the drug was determined using the calibration curve previously constructed in deionized water.

The methodological similarity was extended to the evaluation of DIL solubility, encompassing assessments in both an acidic medium at pH 1.2 and a phosphate buffer (PB) solution with a range of pH values, notably 6.8.

5.2. Instrumental methods

5.2.1. Fourier Transform Infrared (FTIR) spectroscopic analysis

After meticulously grinding the specimens into fine powder, each sample was meticulously combined with desiccated potassium bromide in a meticulous 1:100 ratio. These meticulously prepared mixtures were then adroitly pelletized under the controlled pressure of a specialized hydraulic press, applying a force of 400 kg cm^{-2} . Following this meticulous preparation, the resulting pellets were subjected to thorough FTIR spectral analysis utilizing an advanced FTIR spectrophotometer (Perkin Elmer, RX-1, UK), with the meticulous scanning of the spectral range spanning from 4000 to 400 cm^{-1} .

However, it is of considerable importance to note that the utilization of ATR-FTIR (Attenuated Total Reflection Fourier Transform Infrared) method skillfully eliminates the requisite potassium bromide (KBr) sample pelletization process. ATR represents an ingenious sampling technique meticulously designed to circumvent the conventional necessity of KBr pelletization, a preparatory step deeply ingrained in traditional transmission FTIR spectroscopy. In the case of solid samples, this methodology involved the precise application of gentle pressure, pressing the sample onto the crystal surface, ingeniously avoiding the need for pelletization altogether.

5.2.2. Differential Scanning Calorimetry (DSC) study

The specimen's DSC thermograms were recorded using a differential scanning calorimeter (DSC-4000, Perkin-Elmer, United States). To secure airtight conditions, aluminum pans were utilized to contain the samples. The controlled heating process ranged from 30 to 300°C, escalating at a rate of 10°C per minute, maintained by a constant flow of nitrogen gas.

5.2.3. X-ray Powder Diffraction (XRD) study

The finely powdered polymer samples underwent analysis using an advanced X-ray diffractometer (ULTIMAIII, Rigaku, Japan) to obtain their X-ray diffraction (XRD) patterns. This equipment, operating at 40 kV voltage and 30 mA current, employed K- β filtered Cu radiation with a wavelength of 1.54056 Å as its primary radiation source, ensuring accurate and detailed readings. The process entailed a meticulous scanning of the powdered specimens at a deliberately chosen speed of 3°/min, spanning a comprehensive range from 5 to 80° diffraction angle (2 θ).

5.2.4. Solid state ¹³C NMR Spectroscopy

The exploration of solid-state ¹³C-NMR spectra was undertaken by subjecting precisely weighed quantities of powdered polymer samples, each weighing 300 mg, to the scrutiny of an NMR spectrometer operating at impressively high field strength of 400 MHz. This investigation was conducted with acute precision, utilizing a cross-polarization method that facilitated the elucidation of structural insights within the samples.

5.2.5. Elemental analysis

The sample underwent elemental analysis using a CHNS/O Elemental Analyzer to determine its carbon, hydrogen, nitrogen, and sulfur content. Additionally, the sodium content of the sample was measured using a Flame Atomic Absorption Spectrophotometer.

5.2.6. Zeta potential measurements

The analysis of zeta potential measurements was carried out using a Zetasizer (Nano ZS-90, Malvern Instruments Ltd., UK). A 1% (w/v) dispersion of the polymers was prepared at a precisely maintained neutral pH for these measurements. The experimental setup ingeniously employed deionized water as the dispersion medium and incorporated the utilization of disposable zeta cells (DTS 1070), a technological feat that enhanced the precision of each sample's assessment at a controlled temperature of 25°C. Remarkably, the experiments were meticulously repeated three times, generating a comprehensive dataset that was further analyzed with the utmost precision and sophistication using the advanced "Zetasizer" software version 7.03 PSS0012 - 34 EN-JP (Malvern Instruments Ltd., UK).

5.2.7. Rheological Study

The comprehensive suite of rheological investigations was executed utilizing the Modular Compact Rheometer (Anton Parr, MCR 102, Austria), a remarkable instrument chosen for its precision and reliability. Consistent use of the standard geometry of 1° cone (CP-40) with a diameter of 40 mm persisted across the diverse range of studies conducted. Each planned experiment was conducted at varying pH levels, carefully maintaining a 5% (w/v) matrix of polymers at a controlled temperature of 25°C, all while closely managing the air pressure at 6.8646 bar within a compressor unit, ensuring the integrity of the experimental conditions.

The methodical approach encompassed the implementation of two distinct test methodologies: the dynamic rotational mode, primarily a flow curve study, and the oscillatory mode, which included both amplitude sweep and frequency sweep studies, providing a comprehensive insight into the material's viscoelastic properties. In the dynamic rotational mode, the focus was on discerning the shear viscosity profiles under varying shear rates while simultaneously

exploring the pH-dependent alterations in the shear viscosity of the polymeric matrices.

The oscillatory mode, on the other hand, was strategically employed to delve into the intricate interplay of the storage and loss moduli (G' and G'') of the polymers. This was conducted through a meticulous amplitude sweep study, artfully performed at a constant angular frequency ($\omega=6.2831853$ rad/sec) and the deliberate manipulation of strain ($\gamma=0.01$ – 10%) was employed to induce controlled structural deformations within the interlaced polymer matrix.

Furthermore, a comprehensive analysis of the fluctuations in both G' and G'' across the angular frequency spectrum ($\omega=0.1$ – 10 rad/sec) was astutely conducted using a frequency sweep study, making judicious use of the pre-determined strain (%) data acquired during the linear viscoelastic (LVE) regime, as established through the earlier amplitude sweep experimentation. This comprehensive approach contributed to a comprehensive understanding of the complex rheological behaviors exhibited by the polymer matrices under different conditions.

5.2.7.1. pH adjustment of the polymeric matrices:

The pH levels of the polymeric matrices underwent adjustments by incorporating varied amounts of deionized water (to achieve neutrality), an acidic solution of pH 1.2 (for an acidic environment), and a buffer solution with a pH of 6.8, creating a diverse range of pH levels.

5.2.7.2. Post data Analysis:

The collected data from the rheological studies were analyzed to identify correlations between pH and the observed changes in properties, damping factor

and established the flow curve model. The data was processed and analyzed utilizing the "Rheoplus" software (US 200, version 3.62).

The following flow curve models were employed as the function of viscosity to the above study:

Carreau -Yasuda model:

The Carreau-Yasuda model was used to describe the flow behavior of viscoelasticity of polymer matrix. It incorporates both shear-thinning and viscoelastic properties. The model includes parameters such as the consistency index, flow behavior index, and relaxation time, which provide information about the material's resistance to flow, degree of shear thinning, and the time it takes for the material to relax after deformation.

$$\eta - \eta_{\infty} / \eta_0 - \eta_{\infty} = [1 + (\lambda\dot{\gamma})^a]^{(n-1)/a} \quad (5.2)$$

Where, η_0 is the zero shear viscosity (Pa.s) while η_{∞} infinite viscosity closer to solvent viscosity, λ is the constant with unit time, $\dot{\gamma}$ is the strain (%), a is the width of the transition region between η_0 and power-law and $n-1$ is the power-law slope in the Carreau -Yasuda model [Bush & Phan-Thien 1984].

Ostwald-de- waele model:

The Ostwald de Waele model, commonly referred to as the power-law model serves to depict the flow characteristics of non-Newtonian substances [Shapovalov 2017]. This model is particularly adept at characterizing materials that display shear-thinning attributes, showcasing a reduction in viscosity with escalating shear rates. It establishes a power-law correlation between shear stress (τ) and shear rate ($\dot{\gamma}$). Essentially, this model offers insights into the behavior of the flow curve:

$$\tau = K\dot{\gamma}^n \quad (5.3)$$

Bingham model:

The Bingham model was used to describe whether the matrix exhibited a yield stress and behave as a viscous fluid once the yield stress is exceeded. Above the yield stress, it postulates a direct association between shear stress and shear rate, assuming a linear relationship [Hong et al., 2008]. The model parameters, including the yield stress and plastic viscosity, provide information about the material's resistance to flow and its flow behavior once flow is initiated. τ is the shear stress as the function of strain, while τ_0 is the yield stress.

$$\tau - \tau_0 = \eta_{pl}\dot{\gamma} \quad (5.4)$$

Casson model:

The Casson model was used to describe the matrices if exhibit a yield stress and have a significant structural component. It presumes the material acts akin to a Bingham plastic, characterized by a yield stress (τ_y) and a plastic viscosity (η_{pl}).

$$\tau^{0.5} = \tau_y^{0.5} + \eta_{pl}^{0.5} \dot{\gamma}^{0.5} \quad (5.5)$$

Herschel-Bulkley model:

The Herschel-Bulkley model is an extension of the Bingham plastic model and it was used to describe materials that exhibit both a yield stress and shear thinning behavior. It assumes a nonlinear correlation between shear stress (τ) and strain ($\dot{\gamma}$) beyond the yield stress, where τ_y symbolizes the threshold stress to trigger material flow. The parameters K and n denote the consistency index and the flow behavior index, respectively. Below the yield stress, the substance behaves as a solid, impeding flow. The flow index (n), a dimensionless value, characterizes the material's behavior: $n = 1$ signifies Newtonian flow, $n < 1$ denotes shear thinning (pseudo-plastic), and $n > 1$ implies shear thickening (dilatant) behavior [Huang & Garcia 1998].

$$\tau - \tau_y = K\dot{\gamma}^n \quad (5.6)$$

Cross model:

The Cross model is an extension of the Ostwald de Waele (power-law) model that includes a yield stress component. It was used to describe the polymer matrices that exhibit both shear-thinning and yield stress behavior. The model parameters, including the yield stress, consistency index, and flow behavior index, provide information about the polymer's ability to resist flow until a certain stress threshold is reached and its shear-thinning behavior once flow is initiated [Osswald T & Rudolph 2015]. In the Cross model m is the shear thinning index (dimensionless constant) ranges from 0 (Newtonian) to 1 (infinite shear thinning) and λc as cross constant.

$$\eta - \eta_{\infty} / \eta_0 - \eta_{\infty} = \left[\frac{1}{1 + \lambda c \dot{\gamma}^m} \right] \quad (5.7)$$

Ellis model:

The Ellis model, also known as the Ellis fluid model or the Ellis equation, was used to describe the flow behavior of complex fluids that exhibit both shear-thinning and viscoelastic properties. The Ellis model combines both the power-law behavior and the viscoelastic behavior to describe the flow behavior of complex fluids. It provides a more comprehensive description of the material's behavior compared to simpler models that consider only one aspect, such as shear-thinning or viscoelasticity.

$$\eta = \left[\frac{\eta_0}{1 + [\tau / \tau_2]^{\alpha-1}} \right] \quad (5.8)$$

In the Ellis model, τ_2 is the shear stress roughly identified when η has fallen to half of its final asymptotic value [Al-Behadili A et al., 2019].

Damping factor

The damping factor implemented in the modeling of polymer matrix to understanding of nonlinear viscoelasticity phenomena [Rolón-Garrido VH & Wagner 2009]. The dumping factor, determined by the loss tangent ($\tan \delta =$

G''/G'), gauges the internal frictions within matrices [Wang et al., 2022]. Its values align with distinct viscoelastic functions:

$\tan\delta=0$: Represents material ideal elasticity.

$\tan\delta=100$: Indicates material ideal viscosity.

$\tan\delta>1$: Reflects material with higher viscosity than elasticity.

$\tan\delta<1$: Signifies material having more elasticity than viscosity.

$\tan\delta=1$: Indicates a material displaying viscoelastic characteristics.

The physical interpretation of the damping function from different types of deformation on the experimental results was investigated for NAP, CMAP and CCMAP matrices at different pH.

5.2.7.3. Polymeric Matrix Preparation:

In this study, polymeric matrices were characterized under different pH conditions to investigate the impact of pH on their structural, rheological, and mechanical properties. The variation in pH was chosen as it can significantly influence polymer chain conformation, interactions, and gelation behavior. The experimental methods utilized encompass dynamic rheology, mechanical strength testing, and the assessment of entanglement and gel network formation.

Three distinct categories of polymeric matrices were prepared at a concentration of 5% (w/v). The polymers used in the experiment were denoted as Polymer-A, Polymer-B, and Polymer-W, respectively. The preparation of each category of polymeric matrix was carried out as follows:

Polymer-A:

Polymer-A polymeric matrices were formulated by dissolving the necessary polymer quantity in an acid solution under consistent stirring at 50°C temperature. At room temperature, the solution was carefully adjusted to pH 1.2

with a 0.2 (M) HCl solution. The concentration of Polymer-A was maintained at 5% (w/v) throughout the preparation (eg: NAP-A, CMAP-A, CCMAP-A).

Polymer-B:

In the case of Polymeric matrices containing Polymer-B, each polymer was added to a Phosphate buffer solution at a concentration of 5% (w/v). Following this, the solution's pH was meticulously tuned to 6.8 by cautiously introducing a 0.2 M NaOH solution.

Polymer-W:

Polymeric matrices under Polymer-W category were prepared using deionized water to achieve a neutral pH condition. The deionized water served as the solvent for the polymer, and each polymer was dissolved in deionized water at 5% (w/v) concentration to produce the desired polymeric matrix.

The concentrations mentioned in this study refer to the weight/volume (w/v) percentage, which indicates the weight of the polymer in grams per 100 mL of the solvent or medium used for each preparation.

The variation in pH will enable a comprehensive understanding of the pH-dependent responses of these polymeric systems, providing valuable insights for diverse applications in matrix tablet dissolution and drug release where pH sensitivity plays a crucial role.

5.2.8. Scanning electron microscopic (SEM) study

The placebo matrix tablets were collected from dissolution chamber to study the morphological changes during dissolution study. The surface morphology of polymer layer was examined under SEM. The samples underwent gold-palladium-alloy coating through fine coat ion-sputter (Hitachi, E-1010). They were observed under different conditions: 10.0 Kv X 100 SE, 10.0 Kv X 1.00k SE, and 10.0 Kv X 500 SE, all with a tilt angle of 45°. The

coated samples were subsequently analyzed under field emission Scanning Electron Microscope (Hitachi, S-3400 N).

The tablets underwent SEM analysis to study their Surface Topography. Both the outer and inner surfaces of the tablet were coated with a gold-palladium-alloy using a fine coat ion-sputter (Hitachi, E-1010). The examination was conducted at different accelerating voltages: 10.0 kV X 100 SE, 10.0 kV X 1.00k SE, and 10.0 kV X 500 SE, with a tilt angle of 45 degrees. Subsequently, the coated samples were analyzed using a field emission Scanning Electron Microscope (Hitachi, S-3400 N).

5.3. Purification of Native *Albizia procera* gum (NAP)

The purification process for the initial crude gum powder followed a devised procedure, characterized by a series of systematic steps. Commencing with a preliminary phase, the crude gum powder was subjected to a controlled boiling treatment in 80% (v/v) ethanol, orchestrated to effectively inactivate enzymes and facilitate the extraction of low molecular weight carbohydrates and any extraneous colorant constituents. Subsequent to the boiling phase, the resultant gum powder was adeptly dispersed in deionized water, and a judicious period of gentle stirring was administered throughout the span of a night, employing the resourceful aid of a magnetic stirrer. This strategic step paved the way for an optimum dissolution process, while concurrently fostering the necessary conditions for the separation of any residual undissolved particles.

Continuing this process towards refining the gum solution, the subsequent phase involved the patient allowing of the gum solution to rest undisturbed for a span of 12 hours at ambient room temperature. This strategic interval enabled the deliberate settling and eventual separation of any residual particles that might have escaped the initial dissolution phase.

Progressing further along this carefully purification sequence, the gum solution, now attuned to a higher level of refinement, was subjected to an exacting filtration procedure. This involved the methodical passage of the solution through a medium, specifically Whatman No.1 filter paper, employed to eliminate any vestiges of solid impurities that might have persisted.

Elevating the purification process to its final stages, the filtered solution was primed for a transformative phase of precipitation, characterized by the precise addition of threefold volumes of propanol. This strategic incorporation of propanol triggered the formation of a distinct precipitate, deftly and selectively capturing the purified gum material. The gathered precipitated gum was subsequently entrusted to a period of deliberate air drying, thus culminating in the attainment of a refined gum material, now poised for its next phase of evaluation [Brummer and Cui 2005; Vinod et al. 2008].

The concluding touch of refinement involved subjecting the dried gum material to a judicious sieving process, proficiently carried out through a No. 85 sieve. This sieving process was orchestrated to attain a harmonious consistency in particle size, a prerequisite for ensuring uniformity within the ensuing analysis. The culmination of this meticulous purification journey found its epilogue in the careful storage of the resulting gum material within desiccators, a protective measure ensuring the integrity of the material's purity and quality until further analysis ensued.

5.4. Synthesis and characterization of carboxymethyl Albizia procera (CMAP)

5.4.1. Carboxymethylation of *A. procera*

The carboxymethylation of NAP was executed through a base-catalyzed reaction mechanism [Dodi G et al., 2011]. Initially, the powdered NAP underwent sieving using a 45 mesh sieve, followed by precise weighing. To initiate the reaction, a creamy dispersion was meticulously formulated by gradually introducing the powdered NAP (10 g) into an aqueous solution of sodium hydroxide (with a concentration range of 40-48% w/v). This amalgam was carefully maintained within a dual walled stainless steel isothermal chamber, regulated at a temperature spanning from 0 to 8°C. The process was further enhanced by vigorous stirring, fostering optimal hydration of the mixture. Subsequently, within a temperature range of 15 to 18°C, the gradual addition of mono chloroacetic acid (MCAA) (45% w/v) was meticulously carried out over a period of one hour. Throughout this phase, consistent stirring was maintained, and the mixture was allowed to undergo a controlled reaction.

The subsequent phase of the procedure involved elevating the temperature to 65°C using a water bath, with continuous stirring, and maintaining this state for one hour. After this, the mixture was left to rest at room temperature for duration of 24 hours, ensuring the completion of the reaction. The produced mass was precipitated using an 80% v/v aqueous methanol solution and carefully filtered using 8 mm filters. The gathered filtered residue underwent a meticulous air-drying procedure, along with several washes using 80% v/v aqueous methanol. Afterward, the pH of the resulting substance, CMAP, was finely adjusted to neutral using glacial acetic acid, followed by a wash with pure methanol. The semi-crystalline CMAP was then meticulously air-dried and subsequently subjected to a drying process within a hot oven maintained at a temperature of 60°C for a period of 24 hours.

The carboxymethylation process, detailed above, was systematically applied across six distinct batches of CMAP, denoted as P1, P2, P3, P4, P5, and P6. The overarching objective of this investigation was to scrutinize and optimize the influence of temperature, spanning a range of 45-75°C, as well as varying quantities of MCAA (within the range of 40-50% w/v), on the intricate carboxymethylation process.

5.4.2. Characterization of CMAP

5.4.2.1. Determination of degree of substitution (DS)

About 500 mg of CMAP was carefully added to a solution containing 5 ml of aqueous methanol (80% v/v), forming a well-dispersed mixture. A concentrated HCl solution was methodically introduced into this dispersion, and the amalgam was stirred continuously for duration of 3 hours. Following this, the mixture underwent meticulous filtration, and the residue obtained was subjected to repeated washing using aqueous methanol (80% v/v) until the point of neutrality was reached, as confirmed by litmus paper testing [Toğrul & Arslan 2003]. A final washing phase, utilizing pure methanol, was executed before the sample was subjected to a drying process.

A precisely measured quantity of 200 mg of the dried CMAP was then introduced into 1.5 ml of an aqueous methanol solution (70% v/v). Within a matter of minutes, the mixture underwent further modification through the addition of 20 ml of distilled water, followed by the introduction of 5 ml of a 0.5 N NaOH solution. A dedicated shaker was employed to facilitate agitation of the mixture over a period of 3 hours, thereby ensuring complete dissolution of the sample. Subsequently, the resulting solution was subjected to titration using 0.4 N HCl, with phenolphthalein serving as an indicator throughout the process. The degree of substitution for the O-carboxymethyl group was calculated using the following equation [Barai et al., 1997]:

$$Ds = \left[\frac{0.162 A_{NaOH}}{1 - 0.058 A_{NaOH}} \right] \quad (5.9)$$

Where, A_{NaOH} represents the milli-equivalents of NaOH required per gram of sample.

5.4.2.2. Fourier Transform Infrared (FTIR) analysis

The pulverized specimens of NAP and CMAP were individually combined with desiccated potassium bromide in a precise ratio of 1:100 within a mortar. Following the blending phase, the resultant mixture was pelletized using a hydraulic press under a precisely controlled pressure of 400 kg cm⁻². These formed pellets underwent comprehensive analysis using an advanced FT-IR spectrophotometer (Perkin Elmer, RX-1, UK). This comprehensive analysis was carried out across a spectral range spanning from 4000 cm⁻¹ to 400 cm⁻¹.

5.4.2.3. X-ray Powder Diffraction (XRD) study

The powdered samples of NAP and CMAP were subjected to X-ray diffractometry using an ULTIMAIII X-ray diffractometer (Rigaku, Japan). Operating at 40 kV and 30 mA, the X-ray generator utilized K- β filtered Cu radiation at 1.54056 Å. Scanning the powdered specimens from 5 to 80° diffraction angle (2 θ) at a rate of 3°/min facilitated the diffractogram acquisition.

5.4.2.4. Solid state ¹³C NMR Spectroscopy

The Solid State ¹³C NMR analysis involved using 300 mg of powdered NAP and CMAP samples on a JEOL NMR Spectrometer (Japan) operating at a field strength of 400 MHz. The study employed the cross-polarization method for analysis.

5.4.2.5. Elemental analysis

Powdered samples of NAP and CMAP underwent elemental analysis using a CHNS/O Elemental Analyzer, following the procedure outlined in section 5.2.5.

5.4.2.6. Zeta potential comparison

Powdered samples of NAP and CMAP were separately dispersed in deionized water at a concentration of 1% (w/v) to prepare the test samples and comparative analysis of the Zeta potential was performed using a zetasizer.

The Zeta potential values of NAP and CMAP dispersions in deionized water were recorded and compared. The data obtained from the zetasizer were analyzed to evaluate any significant differences between the two samples. The methodology employed for this analysis has been previously discussed in section 5.2.6.

5.4.2.7. Comparative rheological studies

Rheological assessments were carried out on the polymer matrices (5% w/v) of NAP and CMAP, formulated with varied media. Each polymer had three types of matrices formulated at different pH levels. The obtained data from the rheological study were analyzed to evaluate the significant differences between the two samples. The methodology for these rheological analyses has been previously described in section 5.2.7.

5.5. Preparation of crosslinked CMAP (CCMAP)

Approximately 10g of semi-crystalline CMAP powder on a dry basis was meticulously weighed and subsequently sifted through a BS screen #45 to ensure a uniform particle size. The sieved powder was gradually introduced into de-ionized water while undergoing continuous stirring over the course of one hour, resulting in the formation of coherent slurry. Following this, a freshly prepared solution of NaOH (2% w/v, 10 ml) was gradually introduced to the slurry in a deliberate manner, facilitating the complete solubilization of the components. The resultant amalgamation was then carefully transferred into an aqueous solution of CaCl_2 (5% w/w, 50 ml) and subjected to thorough agitation. This mixture was allowed to stand undisturbed throughout the night. Subsequently, on the ensuing day, the formed mass underwent a process of vacuum filtration, leading to the retrieval of a filtered cake that was subsequently rinsed with methanol [Huang et al., 2006]. The resulting cake was then subjected to a drying process within a hot air oven set to 60°C for a duration of four hours. Upon obtaining the dried crosslinked CMAP (CCMAP), the material underwent a subsequent stage of grinding and screening to facilitate its comprehensive characterization, as per previously reported methods. The aforementioned protocol was applied to six distinct batches of CMAP, designated as C1, C2, C3, C4, C5, and C6. The central aim of this investigation revolved around the examination of the varying effects of different quantities of CaCl_2 on the crosslinking process.

5.5.1. Characterization of CCMAP

5.5.1.1. FTIR spectrum analysis

The FTIR spectra of CCMAP powdered sample was analyzed using a FTIR spectrophotometer (Perkin Elmer, RX-1, UK). The purpose of this analysis was to compare the FTIR spectra of CCMAP and CMAP and identify any changes

or shifts in the characteristic peaks. The methodology is already discussed in section 5.2.1.

5.5.1.2. Differential Scanning Calorimetry (DSC) study

The thermal analysis of CCMAP was performed using a differential scanning calorimeter (DSC-4000, Perkin-Elmer, USA). The DSC thermogram of CCMAP was then compared to the thermogram of CMAP to identify any changes in their thermal behavior. The methodology is already discussed in section 5.2.2.

5.5.1.3. Zeta potential analysis and comparison

The powdered sample of CCMAP was dispersed in deionized water at a concentration of 1% (w/v) to make the test samples. The Zeta potential of CCMAP was then analyzed using a zetasizer. The resulting Zeta potential value was compared with that of CMAP to identify any changes in their surface charge properties. The methodology is already discussed in section 5.2.6.

5.5.1.4. X-ray Powder Diffraction (XRD) study

The same methodological approach was employed to ascertain the XRD pattern of CCMAP, mirroring the procedure outlined earlier in the section 5.2.3.

5.5.1.5. Comparative Rheological studies

The rheological experiments involved using 5% (w/v) matrices of CCMAP in various media at a temperature of 25°C. A Modular compact rheometer was utilized for these experiments. The obtained rheological data was then compared with that of CMAP to discern the differences in flow behavior, gel

strength, low-viscosity extrapolation (LVE), and viscoelastic properties between the two samples. The methodology is already discussed in section 5.2.7.

5.6. RBC lysis test

Fresh goat blood was procured from a slaughterhouse, and 80 ml of this blood was skillfully preserved using a prepared 10% (w/v) solution of Tri-sodium citrate within a 0.9% (w/v) NaCl solution. This preservation technique serves the purpose of preventing the coagulation of blood while simultaneously safeguarding the inherent integrity of the blood sample [Fischer et al., 2003]. After preservation, the fresh blood was moved to 1.5 ml Eppendorf tubes and then precisely centrifuged at 2000 rpm for 10 minutes. This centrifugation process is pivotal as it effectively segregates the constituents of the blood based on their distinct densities, culminating in the formation of a dark red-hued pellet predominantly consisting of red blood cells (RBCs). The liquid fraction, known as the supernatant, housing plasma and other components, was subsequently discarded [Phuong et al., 2020].

The isolated RBC pellets underwent a triple washing procedure using freshly prepared phosphate buffer (pH 7.4). This thorough washing sequence serves the vital purpose of eliminating any residual impurities or undesired substances, ensuring the attainment of a pristine and refined RBC pellet. Once adequately cleansed, these RBC pellets were then judiciously utilized to create a well-defined 1% RBC suspension by suspending them in a formulated phosphate buffer (PB) solution.

In the experimental setup, each well of an arranged 96-well plate was filled with a precisely measured 30 μ l volume of the 1% RBC suspension. To this, another 30 μ l of the phosphate buffer (PB) solution was added, and carefully determined volumes of the respective sample solutions (NAP, CMAP and CCMAP) were introduced, ultimately leading to the final volume of each well being maintained within the range of 150 to 200 μ l. The assembled plate was subsequently

positioned within an incubator set at a temperature of 37°C, where it remained for duration of 1 hour and 3 hours. This designated incubation period facilitated the interaction between the sample solutions and the RBCs.

Upon the conclusion of the incubation phase, the optical density of the distinct samples was meticulously assessed at a specific wavelength of 540 nm using a Multimode plate spectrophotometer. This measurement process serves as a critical tool to gauge any discernible modifications in the inherent properties of the RBCs, as variations in optical density can often serve as indicative markers of diverse biological responses.

In order to effectively validate the results, two separate control samples were conscientiously incorporated into the experimental design. A positively oriented control was established utilizing marketed water for injection, thus enabling a comparative assessment with anticipated RBC behavior. In parallel, a negatively oriented control was fashioned utilizing a 0.9% (w/v) NaCl solution, strategically implemented to evaluate and quantify any background effects. This designed experimental framework facilitates the evaluation of the impact exerted by the distinct sample solutions upon the RBCs. Such evaluation had undertaken through the lens of optical density alterations, thereby offering a valuable insight into the potential influence of these solutions on the intrinsic properties of the cells.

5.7. Pre-formulation studies

5.7.1. Drug – Polymers Interaction Studies

5.7.1.1. Drug-polymer FTIR compatibility study

FTIR spectra of the standalone drugs (MET and DIL) and their mixtures with the powdered polymers (NAP, CMAP, and CCMAP) were captured utilizing an FTIR spectrophotometer. A comparative analysis of the obtained spectra for the drugs and the drug-polymer mixtures was carried out to assess the compatibility between the drugs and polymers, as elaborated in Section 5.2.1.

5.7.1.2. Drug-polymer thermal compatibility study

Thermal analyses encompassing both the individual drugs and their amalgamation with polymers were carried out via a differential scanning calorimeter (DSC-4000, Perkin-Elmer, USA). By capturing DSC thermograms of the drugs as well as their combinations with polymers, the aim was to probe for potential interactions between these components. The details of this methodology have been expounded upon in Section 5.2.2.

5.7.2. Characterization of the powder flow

The granules physical characteristics, including flow-ability, compressibility, and cohesiveness, were assessed through the determination of various micromeritic parameters: angle of repose, Carr's index, bulk density, tapped density, and Hausner ratio. To carry out this analysis, a granulation process was employed, incorporating drugs (MET, DIL), polymers (NAP, CMAP, CCMAP), as well as additional components such as lactose, MCC (Microcrystalline Cellulose), and water as binder.

5.7.2.1. Angle of Repose

The angle of repose for granules containing the drug-polymer was determined using the fixed funnel standing method. Accurately weighed granules were placed in a funnel adjusted to touch the apex of the granule heap. The granules flowed freely onto the surface, forming a cone, and its diameter was measured. The angle of repose was calculated utilizing an equation based on these measurements. [Cooper and Gunn 1986]:

$$\theta = \tan^{-1} \frac{h}{r} \quad (5.10)$$

Where, θ represents the angle of repose, r stands for the radius of the base of the pile, and h signifies the height of the pile.

5.7.2.2. Bulk Density & Tapped Density

The bulk density and tapped density were determined using a 10 ml graduated cylinder. The granule sample was carefully placed into the cylinder, and then 100 mechanical taps were applied to aid in the settling of the granules [Cooper and Gunn 1986]. The resultant tapped volume was recorded, allowing for the subsequent calculation of both bulk density and tapped density. To ensure precision and consistency, each experiment related to micromeritics properties was repeated in triplicate.

$$\text{Bulk density } (\rho_b) = \frac{\text{wt.of the powder}(w)}{\text{Bulk volume of the packing}(v_b)} \quad (5.11)$$

$$\text{Tapped density } (\rho_T) = \frac{\text{wt.of the powder}(w)}{\text{Tapped volume of the packing}(v_T)} \quad (5.12)$$

5.7.2.3. Carr's Index

A precise amount of granules was gathered and their volume ascertained through the employment of either a graduated cylinder or a container of known volume. Subsequently, the mass of the collected granules was divided by the earlier determined volume to derive the granules' bulk density. For tapped density measurement, the identical quantity of granules used in the bulk density assessment was deposited into a graduated cylinder. A consistent mechanical tapping, comprising 100 taps, was then applied to compact and settle the granules within the cylinder. Following the tapping procedure, the volume of the granules was re-evaluated, leading to the determination of the tapped density.

The equation used to determine the compressibility index involves dividing the difference between the tapped density and the bulk density by the tapped density, multiplied by 100. This calculation offers a quantitative representation of the granules' compactibility and flow characteristics, aiding in the assessment and optimization of the formulation for tablet production [Wells & Aulton 1988]:

$$Carr's\ Index\ (\%) = \left[\frac{Tapped\ Density(\rho_T) - Bulk\ Density(\rho_b)}{Tapped\ Density(\rho_T)} \right] \times 100 \quad (5.13)$$

5.7.2.4. Hausner Ratio

The Hausner ratio is a pivotal parameter used in pharmaceutical formulation, specifically in assessing the flowability characteristics of granular materials. It's a measure that provides insight into the packing and flow properties of these granules. Calculated from the relationship between the tapped density and the bulk density, the Hausner ratio serves as an indicator of the granules' flow behavior.

The bulk density of granules refers to their density when loosely packed or poured into a measuring container without any external forces applied. It

represents the initial volume occupied by the granules. In contrast, the tapped density reflects the volume of the same granules after they have undergone a standardized mechanical tapping process. This tapping simulates handling and compaction, replicating the effects of transportation or tablet compression during manufacturing.

The Hausner ratio is computed using the formula::

$$\text{Hausner Ratio} = \frac{\text{Tapped density}(\rho_T)}{\text{Bulk Density}(\rho_b)} \quad (5.14)$$

5.7.3. Formulation of placebo matrix tablets

To delve into the attributes of matrix swelling and erosion, placebo matrix tablets were meticulously formulated. Within the scope of this investigation, the active drug was omitted, and instead, a precise combination of inert constituents and a consistent polymer quantity (NAP, CMAP, and CCMAP) were employed to fabricate the placebo tablets.

For the diverse formulations, careful adherence was maintained to the weight ratios specified in Table 5.1. Section 5.8.1 will cover the procedure for preparing the placebo matrix tablet.

Table 5.1: Formulation of placebo matrix tablets

<i>Sl no.</i>	<i>Ingredients per tablet (mg)</i>	<i>X1</i>	<i>X2</i>	<i>X3</i>
1	NAP	600	-	-
2	CMAP	-	600	-
3	CCMAP	-	-	600
4	Lactose anhydrous	380	380	380
5	MCC	100	100	100
6	Purified water	Qs*	Qs*	Qs*
7	Magnesium stearate	18	18	18
7	Aerosil	2	2	2

***Qs indicate quantity sufficient**

5.7.4. Swelling study

5.7.4.1. Swelling study in deionized water

The investigation into the swelling behavior of placebo matrix tablets (designated as X1, X2, and X3) was systematically conducted in deionized water. The investigation involved employing a USP-II tablet dissolution test setup from *Electrolab*, India (specifically, model *TDP 06P*), meticulously maintained at a constant temperature of $37 \pm 0.5^{\circ}\text{C}$. Each tablet, positioned within a stainless steel wire mesh basket, was subjected to an initial weighing, followed by immersion in a 900 ml volume of the test medium [Maity & Sa 2014]. Subsequent to immersion, the basket was set into motion at a constant stirring speed of 75 rpm. Following a predefined time interval, the basket enclosing the hydrated matrix tablet was meticulously retrieved, surplus water was carefully blotted, and a fresh weight measurement was taken. The quantification of tablet swelling percentage was determined employing the following equation:

$$\% \text{ Swelling} = \left[\frac{(W_2 - W_1)}{W_1} \times 100 \right] \quad (5.15)$$

In the equation, W_1 signifies the tablet's initial weight measured at the starting time (0), while W_2 denotes the tablet's weight measured at a specific time 't' subsequent to its immersion in the test medium.

5.7.4.2. Swelling study in pH 1.2 acid solution

Conducting a swelling investigation in an acid solution of pH 1.2, the placebo matrix tablets denoted as X1, X2, and X3 underwent examination. The experimental protocol involved the use of a USP-II tablet dissolution test

apparatus (model *TDP 06P*, *Electrolab*, India), meticulously regulated at a consistent temperature of $37 \pm 0.5^{\circ}\text{C}$ to ensure precision and accuracy throughout the procedure. The approach employed for this study mirrored the methodology previously utilized for the swelling study conducted in deionized water.

Furthermore, within the aforementioned protocol, an additional swelling analysis was carried out, this time in a phosphate buffer solution with a pH of 6.8.

5.7.4.3. Determination of water penetration velocity in placebo matrix tablets

The determination of water penetration velocity in a tablet through a swelling study provides insights into the rate at which water permeates the tablet structure, which can have implications for the tablet's disintegration, dissolution, drug release, and overall performance. Water penetration velocity data can be used in mathematical models to predict drug release behavior under different conditions, aiding in formulation design.

Water penetration velocities were ascertained utilizing the following equation [Quintana et al. in 1999]:

$$V = \left(\frac{1}{2\rho A} \right) \times \frac{dw}{dt} \quad (5.16)$$

Here, V stands for the velocity of water penetration, dw/dt denotes the gradient of the curve illustrating the relationship between percentage swelling and the square root of time ($\sqrt{\text{Time}}$), ρ symbolizes the density of the water, acid solution, and PB solution at a temperature of 310 K, and A represents the tablet's surface area .

The surface area of the caplet-shaped convex tablet can be calculated by considering its curved top curved surface, bottom surface, and the lateral

surface connecting those [Ford et al., 1987]. The determination of the surface area was accomplished using the subsequent formula:

$$A = 2\pi r(h + 2r) \quad (5.17)$$

In this context, h signifies the thickness of the tablet, while r represents its radius, both of which were ascertained through the utilization of calipers. The radius (r) of the cylindrical shape was calculated as half of the length (length/2).

5.7.4.4. Erosion study

The erosion investigation was executed using a methodology akin to the swelling study, with the sole distinction being the retrieval of the basket containing the placebo matrix tablet from the test medium (water, acid solution, and PB solution) at predetermined time intervals. Subsequently, the basket was subjected to drying in a hot air oven set at 70°C until a consistent weight was achieved [Singh R et al., 2014]. The percentage of erosion at various time points was computed utilizing the following equation:

$$\% \text{ Erosion} = \left[\frac{(W_1 - W_3)}{W_1} \times 100 \right] \quad (5.18)$$

In this context, W_1 denotes the tablet's initial weight at the commencement of the experiment, while W_3 signifies the tablet's weight after complete drying at time t subsequent to immersion in the test medium.

5.8. Fabrication of SR Matrix tablets

5.8.1. Preparation of matrix tablets

To formulate the matrix tablets wet-granulation method was employed for all formulations [Bandelin 1989]. By the following systematic procedure, tablets containing the desired drug and polymer combinations were successfully prepared, ensuring proper mixing, granulation, and compression to meet the specified hardness range:

Weighing of ingredients: All ingredients, including the drugs and polymer were accurately weighed according to the specified batch size.

Sieving: The drug, powdered polymer, microcrystalline cellulose and lactose were sieved individually through a mesh #40 sieve to achieve consistent particle size distribution for each component.

Dry Mixing: The drug was thoroughly mixed with the polymer and other ingredients using a dry mixing process for 15 minutes.

Moistening and Granulation: The dry powder blend was adequately moistened with purified water until it formed a cohesive mass. Subsequently, this cohesive mass underwent screening through a mesh #16 sieve to yield moist granules.

Drying: The damp granules were subjected to drying in a tray dryer set at 65°C until the moisture content was reduced to 2% w/v.

Sieving and Lubrication: The granules, once dried, underwent sieving through a mesh size 20 conforming to the British Standard (BS). Subsequently, the granules were lubricated with magnesium stearate at a concentration of 0.25% to 5% (w/w) and aerosol 0.1% to 0.5% (w/w) of the total tablet weight.

Tablet Compression: The lubricated granules were compressed into tablets using a tablet compression machine (RIMEK, Karanavati Engineering Ltd., Gujarat, India) equipped with a 19.5 mm oval concave surface punch.

Adjustment of Compression Force: The compression force was meticulously fine-tuned to yield tablets with hardness falling within the range of 49.05 to 68.67 Newton.

Preparation of NAP, CMAP and CCMAP Tablets: The procedure outlined above was replicated for the formulation of tablets incorporating NAP, CMAP and CCMAP.

5.8.2. Formulation of MET-loaded matrix tablets

The process of formulating MET-loaded matrix tablets entailed the integration of MET as the active ingredient, along with diverse polymer quantities. These MET-loaded matrix tablet formulations were categorized into three groups (Group-I, Group-II, Group-III), utilizing the individual polymer like NAP, CMAP, and CCMAP. Within each category, a comprehensive set of 10 formulations was meticulously crafted, involving alterations in the polymer quantities. The specific proportions were determined based on Table 5.2, with distinct formulations assigned to each weight ratio. Elaborations on this procedure are provided in section 5.8.1.

Table 5.2: Formulations of MET-loaded matrix tablets

<i>Sl no.</i>	<i>Ingredients per tablet (mg)</i>	<i>F1</i>	<i>F2</i>	<i>F3</i>	<i>F4</i>	<i>F5</i>	<i>F6</i>	<i>F7</i>	<i>F8</i>	<i>F9</i>	<i>F10</i>
1	MET	250	250	250	250	250	250	250	250	250	250
2	Polymer***	250	300	350	400	450	500	550	600	700	800
3	Lactose anhydrous	500	450	400	350	300	250	250	200	130	30
4	MCC	80	80	80	80	30	80	30	30	-	-
5	Purified water	<i>QS*</i>	<i>QS*</i>	<i>QS*</i>	<i>QS*</i>	<i>QS*</i>	<i>QS*</i>	<i>QS*</i>	<i>QS*</i>	<i>QS*</i>	<i>QS*</i>
6	Magnesium stearate	18	18	18	18	18	18	18	18	18	18
7	Aerosil	2	2	2	2	2	2	2	2	2	2
	***Polymer: Group-I: NAP; Group-II: CMAP; Group-III: CCMAP										

**QS indicate quantity sufficient*

5.8.3. Formulation of DIL-loaded matrix tablets

The process of formulating DIL-loaded matrix tablets encompassed the incorporation of DIL as the active component, accompanied by varying quantities of polymers. These DIL-loaded matrix tablet formulations were further categorized into three additional groups (Group-IV, Group-V, Group-VI), employing distinct polymers such as NAP, CMAP, and CCMAP. Within each category, an elaborate set of 10 formulations was meticulously developed, entailing adjustments in the polymer quantities. These specific proportions were determined according to Table 5.3, with each distinct formulation assigned to its respective weight ratio. A detailed account of this procedure can be found in section 5.8.1.

Table 5.3: Formulations of DIL-loaded matrix tablets

<i>Sl no.</i>	<i>Ingredients per tablet (mg)</i>	<i>F1</i>	<i>F2</i>	<i>F3</i>	<i>F4</i>	<i>F5</i>	<i>F6</i>	<i>F7</i>	<i>F8</i>	<i>F9</i>	<i>F10</i>
1	DIL	120	120	120	120	120	120	120	120	120	120
2	Polymer***	120	240	360	480	540	600	720	780	840	900
3	Lactose anhydrous	680	600	500	400	340	320	200	160	120	60
4	MCC	160	120	100	80	80	40	40	20	-	-
5	Purified water	<i>QS*</i>	<i>QS*</i>	<i>QS*</i>	<i>QS*</i>	<i>QS*</i>	<i>QS*</i>	<i>QS*</i>	<i>QS*</i>	<i>QS*</i>	<i>QS*</i>
6	Magnesium stearate	18	18	18	18	18	18	18	18	18	18
7	Aerosil	2	2	2	2	2	2	2	2	2	2
***Polymer: Group-I: NAP; Group-II: CMAP; Group-III: CCMAP											

**QS indicate quantity sufficient*

5.9. Characterization of Tablets and Determination of Drug Content

5.9.1. Uniformity of weight

The methodology adhered strictly to the established guidelines [Pharmacopoeia Vol-I 2010]. Twenty tablets from each formulation underwent weight variation analysis utilizing an electronic balance (model XB600 M-C, Switzerland). Randomly selected tablets were individually weighed, and their weights (m_1 , m_2 , ..., m_{20}) were compared against the average tablet weight.

$$\text{Average weight (m)} = \left[\frac{m_1 + m_2 + m_3 + \dots + m_{20}}{20} \right] \quad (5.19)$$

5.9.2. Hardness

The determination of hardness involved testing 10 tablets per formulation using a pre-calibrated Monsanto hardness tester (Cadmach, Ahmedabad, India). The tablet under examination was positioned between the spindle and anvil. By turning the screw knob clockwise, the necessary pressure to secure the tablet in place was applied. The scale was then adjusted to zero using the indicator. Pressure was progressively increased until the tablet fractured.

5.9.3. Physical dimensions of tablet

Utilizing a calibrated digital caliper, the physical dimensions of the tablets including length, breadth, and thickness were measured. A total of ten tablets were assessed for their physical dimensions in each formulation.

5.9.4. Friability test

The friability evaluation of each formulation involved testing 20 tablets using the Roche friabilator manufactured by Campbell Electronics, Mumbai, India. To determine the weight loss percentage, the friabilator was set to rotate at a consistent speed of 25 ± 1 rpm for 4 minutes (equivalent to 100 revolutions). After this, the tablets were carefully de-dusted and subjected to reweighing. The friability percentage was calculated using the subsequent equation:

$$\text{Friability (\%)} = \left[\frac{(W_1 - W_2)}{W_1} \times 100 \right] \quad (5.20)$$

The equation defines W_1 as the initial weight of the tablets before tumbling, while W_2 signifies the weight of the matrix tablets after the tumbling process.

5.9.5. Content uniformity test

5.9.5.1. Content uniformity for tablets containing MET

A fine powder was generated by grinding and weighing 20 tablets, yielding approximately 0.1g of metformin hydrochloride. This powder was precisely measured and shaken for 15 minutes in a mixture with 70ml of water. Afterward, it was diluted to a total volume of 100 ml and then filtered. From this filtrate, a 10 ml portion was further diluted to 100 ml using water. Another 10 ml from this second dilution underwent a similar dilution process to reach a final volume of 100 ml with water. The resulting solution (0.01 mg/ml) was then analyzed for absorbance at 232 nm using a double-beam spectrophotometer (Shimadzu, UV, 2450, Japan). The quantity of $C_4H_{11}N_5$, HCl was determined utilizing a specific absorbance value of 798 at 232 nm.

5.9.5.2. Content uniformity for tablets containing DIL

A batch of 10 tablets was weighed and subsequently pulverized using a mortar and pestle. The resulting finely ground powder was precisely weighed to acquire 100 mg (equivalent to 120 mg of Diltiazem HCl) and subsequently placed into a 250 ml conical flask, pre-filled with 100 ml of a phosphate buffer at pH 6.8. The mixture underwent stirring for a duration of 45 minutes utilizing an ultrasonic bath (sonicator). Following this, the solution was subjected to filtration, and the drug content was ascertained by analyzing it through UV spectrophotometry, specifically at a wavelength of 236 nm (λ_{max}). The content of $\text{C}_{22}\text{H}_{26}\text{N}_2\text{O}_4\text{S}$, HCl (diltiazem hydrochloride) was subsequently determined by calculating the specific absorbance at 236 nm of the reference solution (RS). This reference solution contained 0.0012% w/v of diltiazem hydrochloride and was dissolved in a phosphate buffer solution of pH 6.8.

5.10. *In-vitro* drug release study

5.10.1. Study of *in-vitro* drug release from MET-loaded matrix tablets

The assessment of *in-vitro* drug release from the matrix tablets was conducted using a USP-II tablet dissolution tester (*Electro-lab, TDP 06P*, India) in solutions simulating acidic (pH 1.2) and phosphate buffer environments (pH 6.8) as per the guidelines outlined in Pharmacopoeia I, 2010. In a cylindrical dissolution vessel with a capacity of 1000 ml, a stirring rate of 100 rpm was maintained while immersing the tablets in a solution comprising 750 ml at a temperature of $37 \pm 0.5^\circ\text{C}$. Subsequently, a tablet chosen at random from each formulation was introduced into the vessel. During the experimental process, samples were drawn hourly and promptly replaced with an equivalent volume of fresh medium, also held at a temperature of $37 \pm 0.5^\circ\text{C}$. Following a 2-hour dissolution period in the acidic medium, an additional 250 ml of preheated 0.2M tri-sodium phosphate dodecahydrate solution (maintained at $37 \pm 0.5^\circ\text{C}$) was introduced. The pH of the medium was finely adjusted to 6.8 ± 0.05 using a 2M

sodium hydroxide solution. The dissolution procedure extended for a duration of 12 hours. The obtained samples were subjected to filtration, followed by appropriate dilution, and subsequently analyzed using spectrophotometry. The drug release quantity was determined by measuring its absorbance at the wavelength where it showed maximum absorption (λ_{max}) according to the respective medium. In the acidic solution, MET displayed its peak absorbance at 232 nm, while in the buffer solution, the highest absorbance was observed at 233 nm.

The procedure mentioned above was meticulously applied to every formulation within all categories of MET-loaded matrix tablets, where the polymers NAP, CMAP, and CCMAP were employed. This ensured that the process was consistently executed across each formulation, encompassing the entire spectrum of polymer variations.

5.10.2. Study of *In-vitro* drug release from DIL-loaded matrix tablets

Matrix tablets containing DIL were rigorously evaluated for in-vitro drug release using a USP-II tablet dissolution tester (*Electro-lab, TDP 06P*, India) mimicking both acidic (pH 1.2) and phosphate buffer (pH 6.8) environments. The experiment utilized a cylindrical dissolution vessel with a 1000 ml capacity, maintaining a constant stirring rate of 100 rpm under controlled conditions. Within this setup, 750 ml of 0.1M hydrochloric acid solution was maintained at a steady temperature of $37 \pm 0.5^\circ\text{C}$. For each formulation, a tablet was randomly selected and placed into the dissolution vessel.

Throughout the experiment's duration, hourly samples were withdrawn and promptly substituted with an equal volume of fresh medium, maintaining a temperature of $37 \pm 0.5^\circ\text{C}$. After the initial 2-hour dissolution in the acidic

medium, an additional 250 ml of 0.2M trisodium phosphate dodecahydrate solution (also kept at $37 \pm 0.5^{\circ}\text{C}$) was introduced. This was followed by precise pH adjustment to 6.8 ± 0.05 using a 2M sodium hydroxide solution. The dissolution process was continued for a total of 12 hours.

The collected aliquots underwent filtration and appropriate dilution before being subjected to spectrophotometric analysis. The assessment of drug release was conducted at the wavelength corresponding to the maximum absorbance (λ_{max}), revealing 236 nm as the optimal wavelength for DIL in both the acidic and buffer solutions. This comprehensive procedure facilitated the evaluation of DIL release profiles from matrix tablets across various formulations and polymer categories.

The aforementioned procedure was systematically implemented for every formulation spanning all categories of DIL-loaded matrix tablets, employing the polymers NAP, CMAP, and CCMAP. This rigorous approach ensured the uniform application of the method across the entirety of formulations, covering the diverse range of polymer compositions.

5.11. Study of release kinetics and mechanism of drug release on In-vitro release profiles

The drug release data was thoroughly scrutinized using multiple kinetic models, including but not limited to the zero-order, first-order, Higuchi, and Korsmeyer-Peppas models. Based on the resulting findings, the release mechanisms across different formulations were discerned by opting for the model that most precisely correlated with the collected data. The exploration of drug transport mechanisms was facilitated through examination of the coefficient of determination values and diffusion exponent values obtained from linear regression analysis. To delve into the intricacies of drug release mechanisms, the drug release data were fitted to the following exponential equations:

Zero – order release kinetics:

$$\frac{dq}{dt} = K_0 \quad (5.21)$$

Where, q = cumulative % release, K_0 = zero order release rate constant, t = time.

A graph showing the relationship between the cumulative % drug release (q) and time (t) was plotted, and the coefficient of determination (R^2) was calculated.

First order release kinetics:

$$\ln Q_t = \ln Q_0 + K_1 t \quad (5.22)$$

In this context, the symbol Q_t represents the quantity of drug released per unit surface area at a given time t, K_1 stands for the first-order release rate constant, and Q_0 represents the initial amount of the drug. A graphical representation depicting the correlation between the logarithm of cumulative percentage release and time was created, followed by the computation of the coefficient of determination (R^2).

For 1st order release kinetics two approaches are commonly used in pharmaceutical research. The choice between plotting the graph against log cumulative % release vs. time or log cumulative % of drug remaining vs. time depends on the perspective and convenience for analysis.

1. Log Cumulative % Release vs. Time:

This approach is often used when focusing on the release of the drug from the tablet. It provides a clearer view of how the drug is being released over time, especially in controlled release systems where the release is gradual.

2. Log Cumulative % of Drug Remaining vs. Time:

This approach is useful for emphasizing the amount of drug still retained in the system. It is a complementary perspective that can be valuable in understanding how much of the drug is left to be released over time.

Ultimately, the choice depends on the specific objectives of the study and the information researchers want to extract from the data. Both methods can yield valuable insights into the release kinetics of controlled release tablets.

Higuchi square root equation [Higuchi et al., 1963]:

$$\frac{M_t}{M_\infty} = K_{HG} t^{1/2} \quad (5.23)$$

In this context, M_t stands for the cumulative drug amount released at a specific time ' t ', while M_∞ denotes the total drug released over an infinite period. Additionally, K_{HG} signifies the Higuchi release rate constant. A graphical representation was crafted, illustrating the cumulative percentage release graphed against the square root of time, thereby portraying Higuchi release kinetics. Subsequently, the coefficient of determination (R^2) was computed to assess the fitting of the data.

Korsmeyer-Peppas model [Korsmeyer et al., 1983]:

$$\log[M_t/M_\infty] = \log K + n \log t \quad (5.24)$$

The variables M_t and M_∞ represent the cumulative drug amounts released at time ' t ' and at infinite time, respectively. The constant ' K ' and the diffusional

release exponent ' n ' are parameters characterizing the mechanism of drug release during dissolution.

A graph was plotted with $\log [M_t / M_\infty]$ on the y-axis and $\log t$ on the x-axis. The slope of the graph was used to calculate the " n " value. Table 5.4 presents various values of " n " that correspond to different release mechanisms:

Table 5.4: Diffusion exponent values and mechanisms of drug release

	<i>Diffusion exponent (n)</i>	<i>Drug Diffusion Dynamics and Its Overall Mechanism</i>
1	0.45	<i>Fickian diffusion</i>
2	$0.45 < n < 0.89$	<i>Anomalous(non fickian) diffusion</i>
3	0.89	<i>Case-II transport</i>
4	$n > 0.89$	<i>Super case-II transport</i>

5.12. SEM study of placebo NAP, CMAP and CCMAP matrix tablets

To visually observe the evolving characteristics of NAP, CMAP, and CCMAP matrix tablets during the dissolution process, SEM images were captured at various time intervals. The methodology for this study has been elaborated in the preceding section 5.2.8.

5.13. Accelerated stability study

For a span of 6 months, accelerated stability investigations were undertaken on matrix tablets laden with MET and DIL, encompassing each formulation involving NAP, CMAP, and CCMAP. The primary aim was to evaluate the enduring stability of MET and DIL within their respective formulations. To achieve this objective, ten tablets were randomly chosen from four batches of each formulation (F1, F4, F7, and F10) for both MET-loaded and DIL-loaded matrix tablets (NAP, CMAP, CCMAP). These selected tablets were individually placed in glass vials, meticulously sealed with bakelite caps, appropriately labeled for identification, and subsequently stored within a stability chamber. The environment was upheld at a steady 40°C temperature and a relative humidity of 75±5% for the entire six-month period.

Upon the culmination of this designated period, the samples were subjected to a comparative analysis alongside freshly prepared tablets. This examination encompassed assessments of drug content and dissolution profiles. To evaluate the likeness between the dissolution rates of the newly prepared and stored tablets, the similarity factor (f_2) was computed, employing the subsequent equation. (5.6) [Costa & Lobo, 2001]:

$$f_2 = 50 \log\{[1 + (1/n) \sum_{i=1}^n (R_t - T_t)^2]^{-0.5} \times 100\} \quad (5.25)$$

The equation comprises certain parameters: ' n ' signifies the number of dissolution time points, R_t represents the average percentage of drug released at each time point for the reference at time ' t ', and T_t denotes the average percentage of drug released at each time point for the test product at time ' t '. The comparison through the f_2 metric is widely embraced within multiple FDA and EMEA guidelines to gauge the likeness of in vitro dissolution profiles (Costa, 2001). An f_2 value of 100 signifies an identical match between profiles,

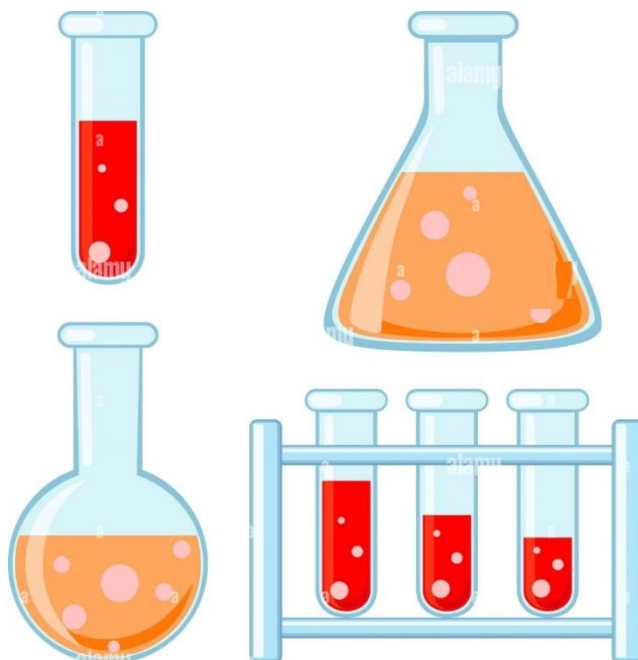
An f_2 value of 50 correlates with an average deviation of 10% across all time points. To ensure equivalence of the two dissolution profiles, the FDA and EMEA have established a recommended range of f_2 values between 50 and 100.

5.14. Statistical analysis

Statistical analyses were carried out using software such as Microsoft Excel 2010, Origin Pro 8.5, Graph-Pad Prism 7, and Design Expert 13. The influence of distinct formulation parameters on drug release was evaluated through analysis of variance (Two-way ANOVA) at a significance threshold of $p < 0.05$. A significant distinction was considered when the p-value fell below 0.05.

CHAPTER 6

RESULTS AND DISCUSSIONS



ANALYTICAL ASSESSMENT OF DRUGS

Analytical Assessment of Drugs

6.1. Analytical Assessment of Drugs

The analysis of drugs is a pivotal process that ensures the safety, efficacy, and quality of pharmaceutical products. Drug analysis is fundamental in maintaining quality standards throughout the drug manufacturing process [Panzitta et al., 2017]. It involves rigorous testing and validation procedures to guarantee consistency in formulation and performance, and to identify active pharmaceutical ingredients (APIs). This is essential to prevent counterfeiting and ensure patients receive the correct medication. The analysis also helps determine the purity of drugs.

The quantitative analysis employs various analytical techniques to quantitatively measure the concentration of drugs in formulations. This is vital for dosing accuracy and efficacy.

Analytical techniques are a range of advanced techniques, including spectroscopy, microscopy, and chromatography, to analyze drugs at molecular levels [Rouessac F & Rouessac A 2022]. Drug analysis is a requirement of regulatory bodies like the FDA and EMA in the pharmaceutical industry to ensure safety of patient.

In the present study, MET and DIL were designated as the model drugs. Owing to the presence of chromophores in both substances, they were found to yield well-defined spectra within the UV range. Consequently, the UV spectrophotometric method was deemed suitable for the straight forward analysis of these model drugs.

6.1.2. Calibration curve of Metformin hydrochloride (MET) in deionized water

The determination of the wavelength of maximum absorption of MET in deionized water was conducted in accordance with the procedure outlined in section 5.1.4 of chapter 5. As illustrated in Figure 6.1, the spectrum was presented, revealing that the λ_{\max} was ascertained to be 232 nm. The result of this investigation is graphically represents the spectrum of MET in deionized water. At the wavelength of 232 nm, the calibration curve ($Y=0.0166x + 0.0136$, $R^2= 0.9993$) for MET in deionized water was constructed. The outcomes of this endeavor have been thoughtfully depicted in Figure 6.2. The calibration curve demonstrated its linearity effectively upto 50 mcg/ml, providing strong validation for the method's precision in quantifying MET within that specific concentration range. The method is found robust, reliable and precise.

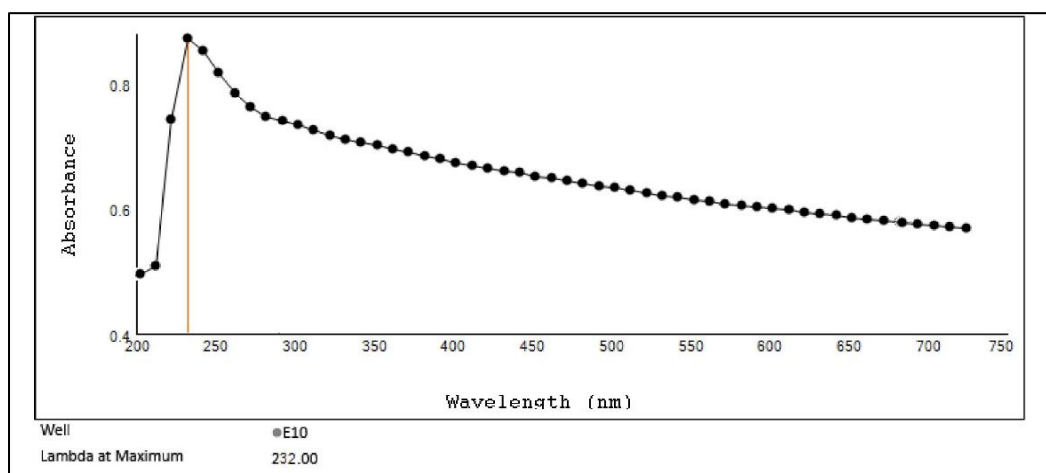


Figure 6.1: UV spectrum of MET in deionized water

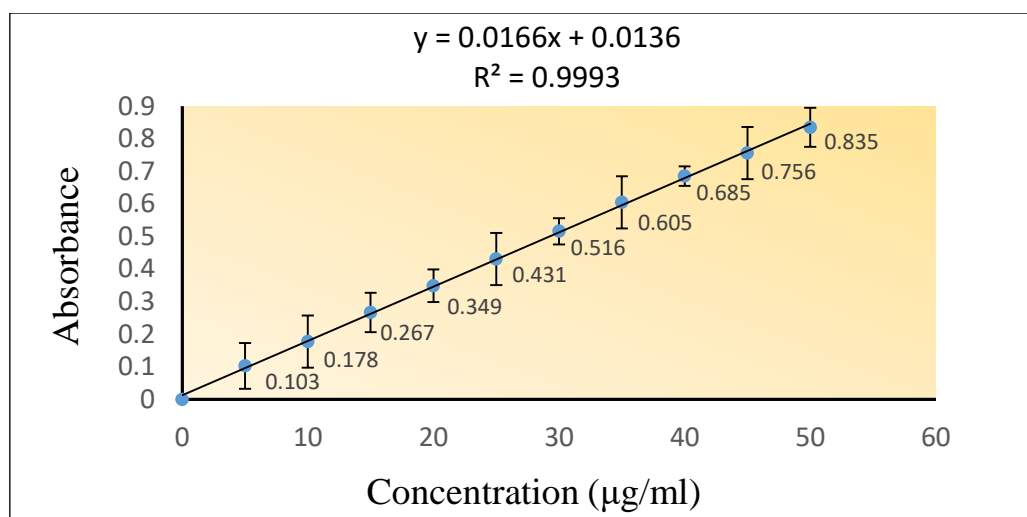


Figure 6.2: Calibration curve of MET in deionized water

6.1.3. Calibration curve of MET in acidic solution of pH of 1.2

The wavelength of maximum absorption (λ_{max}) of MET in an acidic solution was determined at a pH of 1.2 as mentioned in section 5.1.4 of chapter 5 and the results are vividly portrayed in Figure 6.3. At the precise wavelength of 233 nm, the construction of the calibration curve for MET in an acidic solution with a pH of 1.2 was executed with the utmost precision. The results stemming from this endeavor have been thoughtfully presented in Figure 6.4, providing a visual representation of the outcomes. The calibration curve ($Y=0.0162+0.024x$, $R^2=0.9983$), is elegantly illustrated in Fig. 6.4. which exhibits linearity across the concentration range of up to 50 µg/ml. Furthermore, it serves as compelling and concrete evidence of the method's suitability, reliability and preciseness for the accurate quantification of MET within the defined concentration range.

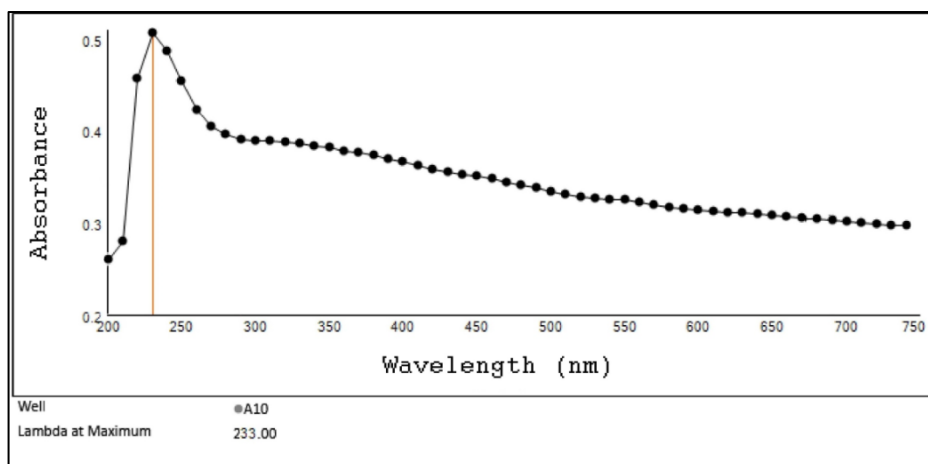


Figure 6.3: UV spectrum of MET in acidic solution of pH 1.2

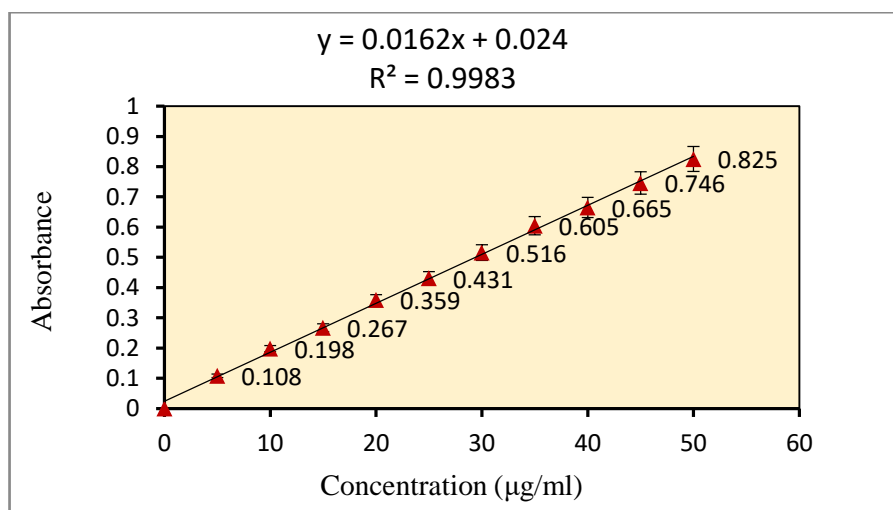


Figure 6.4: Calibration curve of MET in acidic solution of pH of 1.2

6.1.4. Calibration curve of MET in PB solution of pH of 6.8

The procedure to determine the wavelength of maximum absorption (λ_{max}) of MET in a PB solution with a pH of 6.8 was meticulously executed. The outcomes of this investigation were thoughtfully presented in Figure 6.5.

A precise calibration curve ($Y=0.0572x+0.0307$, correlation coefficient, $R^2=0.9992$) for MET in a PB solution at 233 nm was thoughtfully presented in Figure 6.6, demonstrating excellent linearity up to 40 $\mu\text{g/ml}$. This impressive linearity underscores the method's precision and reliability, making it suitable for accurate MET quantification within this concentration range.

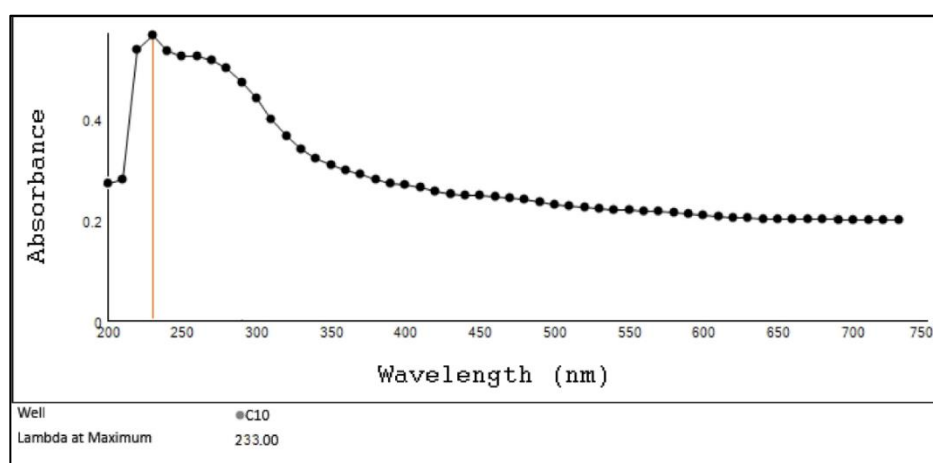


Figure 6.5: UV spectrum of MET in PB solution of pH 6.8

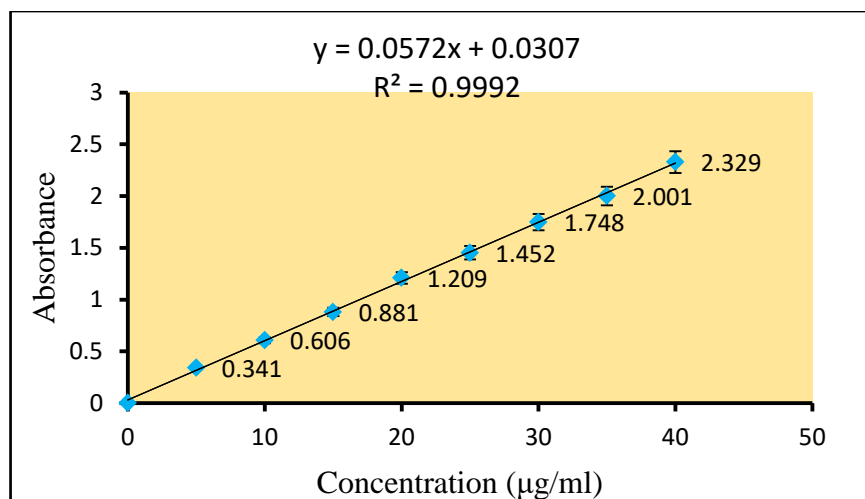


Figure 6.6: Calibration curve of MET in PB solution of pH of 6.8

6.2.1. Calibration curve of DIL in deionized water

The wavelength corresponding to the maximum absorption (λ_{max}) of DIL in deionized water was determined following the protocol outlined in section 5.1.5 of chapter 5. As depicted in Figure 6.7, the spectrum was presented, unequivocally revealing that the λ_{max} had been ascertained to be 236 nm.

In Figure 6.8, a meticulously constructed calibration curve ($Y=0.0398x+0.001, R^2 =0.9996$) for DIL in deionized water at 236 nm was presented, revealing exceptional linearity up to 16µg/ml affirming its suitability for the accurate quantification of DIL within this concentration range.

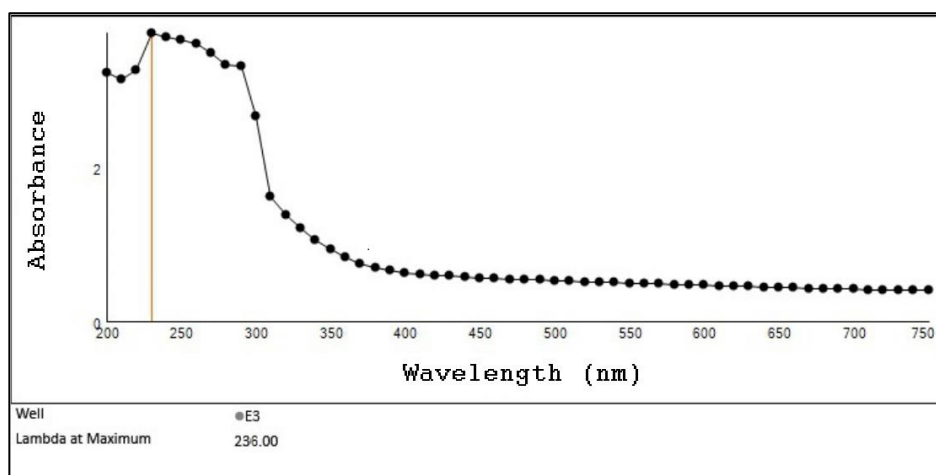


Figure 6.7: UV spectrum of DIL in Deionized water

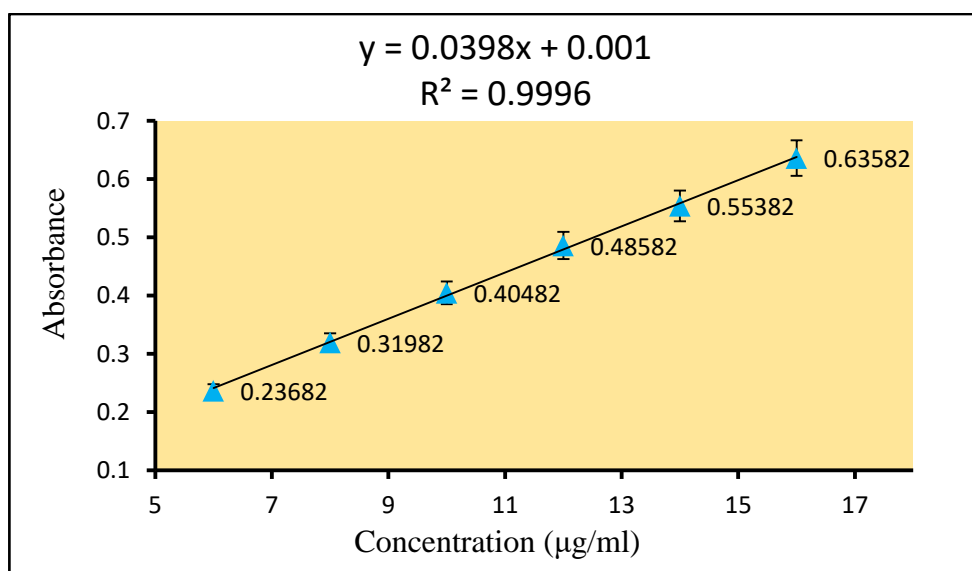


Figure 6.8: Calibration curve of DIL in deionized water

6.2.2. Calibration curve of DIL in acidic solution of pH 1.2

In Figure 6.9, the spectrum was presented, clearly indicating that the λ_{max} had been determined to be 236 nm. This inquiry visually represented the spectrum of DIL in an acidic solution with a pH of 1.2.

In Figure 6.10, a carefully crafted calibration curve ($Y=0.031x-0.0134$, $R^2=0.9998$) for DIL in an acidic solution with a pH of 1.2 at 236 nm was exhibited, demonstrating outstanding linearity. This exceptional linearity attests to the precision and reliability that characterize the analytical method employed in this study, confirming its appropriateness for the precise quantification of DIL within this concentration range.

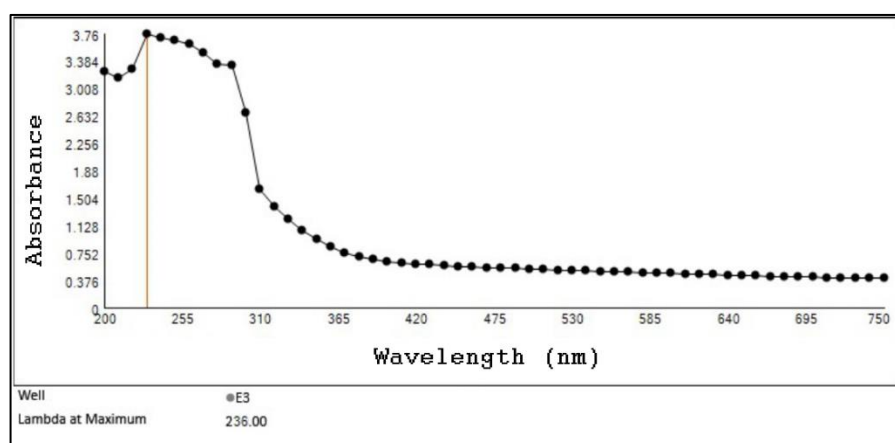


Figure 6.9: UV spectrum of DIL in acidic solution of pH 1.2

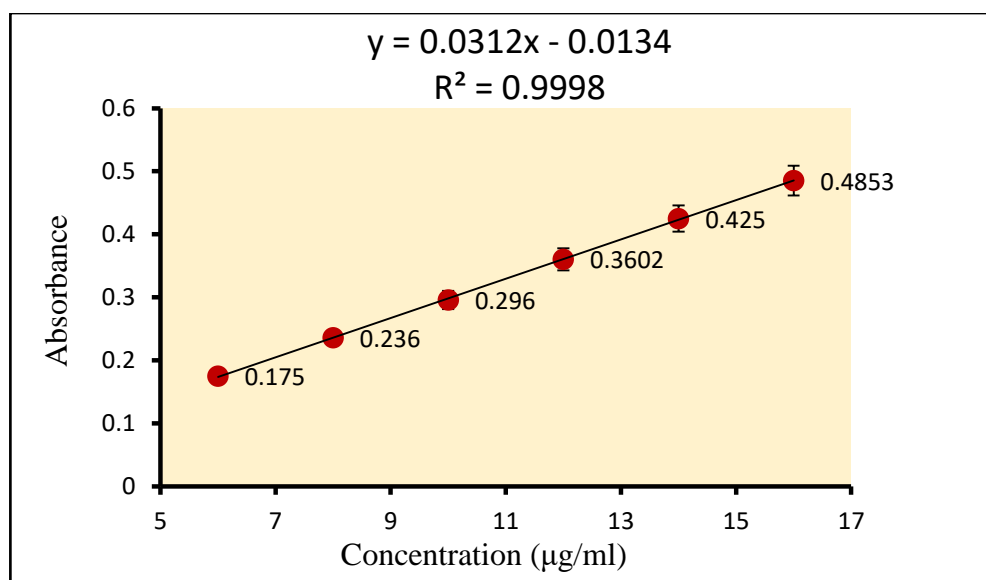


Figure 6.10: Calibration curve of DIL in acidic solution of pH 1.2

6.2.3. Calibration curve of DIL in PB solution of pH 6.8

The procedure for determining the wavelength of maximum absorption (λ_{max}) of DIL in a PB solution with a pH of 6.8 was executed and the results of this investigation were presented in Figure 6.11, providing a clear visualization of the λ_{max} at 236 nm.

In Figure 6.12, a calibration curve ($R^2=0.999$) for DIL in a PB solution at 236 nm was presented, showcasing exceptional linearity up to 16 µg/ml. This remarkable linearity highlights the precision and reliability of the method, rendering it suitable for precise DIL quantification within this concentration range.

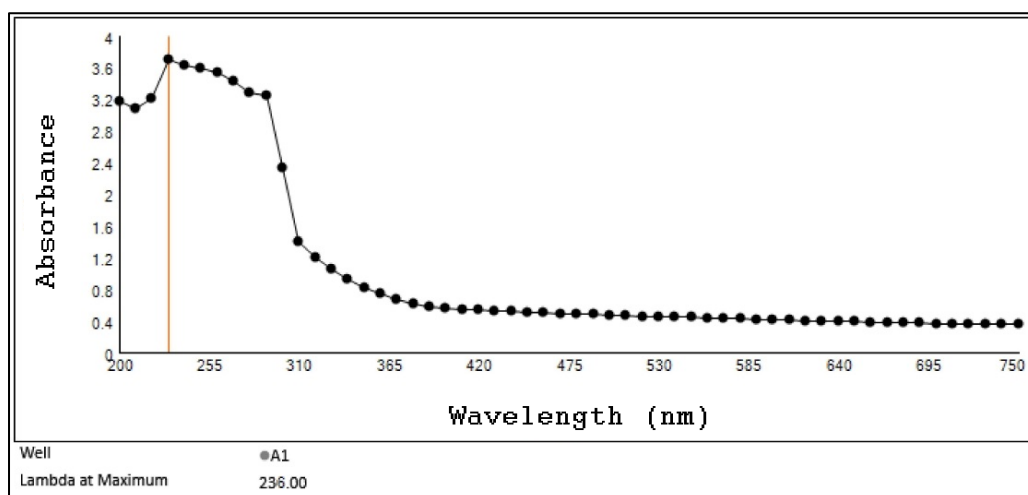


Figure 6.11: UV spectrum of DIL in PB solution of pH 6.8

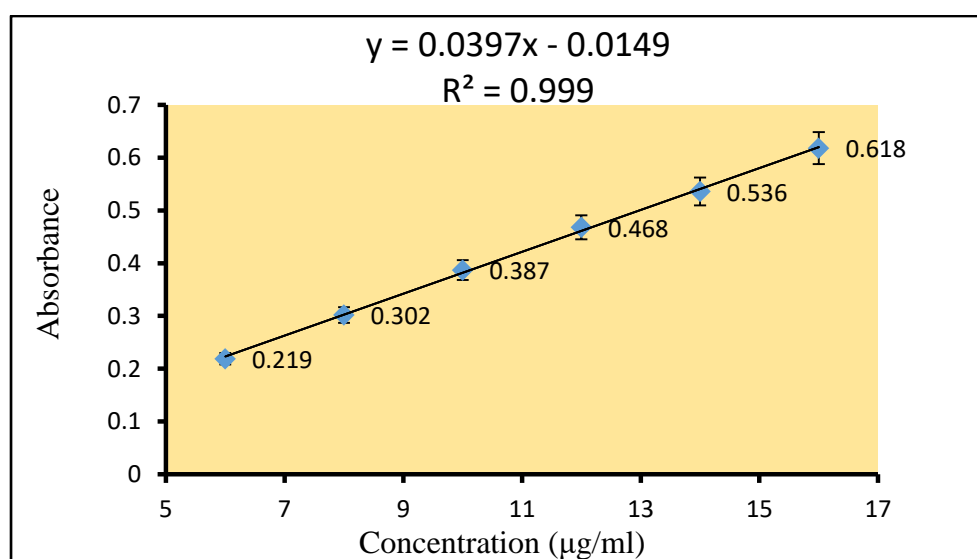


Figure 6.12: Calibration curve of DIL in PB solution of pH 6.8

6.3. Analysis for the recovery of drugs

6.3.1. Analysis for the recovery of MET in various spiked drug solutions

To confirm the absence of interference from the polymers in the analysis of MET, recovery analysis was rigorously carried out in duplicate across three successive days. This entailed evaluating four different levels of spiked drug solutions, both in the presence and absence of the polymers, following the detailed procedure outlined in section 5.1.8 of chapter 5. The results of the percentage recovery in different solutions are shown in Table 6.1. The results indicate that the polymer did not interfere in the analysis of the drug.

Table 6.1: % recovery of MET in various spiked drug solutions

Concentration (mcg/ml)	% recovery (Mean \pm SD, n=3) at pH 1.2	% recovery (Mean \pm SD, n=3) at pH 6.8	% recovery (Mean \pm SD, n=3) at pH 7.4
0	0	0	0
5	98.67 \pm 1.37	97.47 \pm 1.12	98.16 \pm 1.07
10	99.07 \pm 1.26	97.27 \pm 1.31	98.27 \pm 1.41
15	99.64 \pm 1.47	98.33 \pm 2.03	97.66 \pm 1.87
20	99.68 \pm 1.08	98.67 \pm 1.57	98.51 \pm 1.73

6.3.2. Analysis for the recovery of DIL in various spiked drug solutions

To ensure that the analysis of DIL was not affected by the polymers utilized in the formulations, recovery experiments were carried out over three consecutive days. These experiments were conducted in two times and involved four different levels of spiked drug solutions, both with and without the presence of the polymers. The procedure detailed in section 5.1.8 of chapter 5 was meticulously followed.

The outcomes, summarized in Table 6.2, display the percentage recovery of DIL in various solutions. These results unequivocally demonstrate that the presence of the polymers had no discernible impact on the drug analysis process.

Table 6.2: % recovery of DIL in various spiked drug solutions

Concentration (mcg/ml)	% recovery (Mean \pm SD, n=3) in acid solution of pH 1.2	% recovery (Mean \pm SD, n=3) in PB solution of pH 6.8	% recovery (Mean \pm SD, n=3) in PB solution of pH 7.4
0	0	0	0
6	98.23 \pm 1.08	96.79 \pm 1.38	97.33 \pm 1.11
8	98.67 \pm 1.67	98.54 \pm 1.35	98.43 \pm 1.28
10	99.47 \pm 1.23	99.33 \pm 1.64	98.87 \pm 1.31
12	99.89 \pm 1.22	99.08 \pm 1.25	98.69 \pm 1.17

6.4. Determination of solubility of MET and DIL

Table 6.3 presents the solubility of two drugs, Metformin and Diltiazem, at a temperature of 30°C in three different solvent systems: water, an acidic solution with a pH of 1.2, and a phosphate buffer solution with a pH of 7.4. These solubility values are reported in grams per milliliter (g/ml) and provide crucial information regarding the drugs' behavior in these different environments.

The solubility of Metformin appears to be influenced by the pH of the solvent. It is more soluble in the phosphate buffer solution with a pH of 7.4 compared to water and the acidic solution with a pH of 1.2. This suggests that Metformin is a weak base that becomes more soluble as the pH of the solution becomes more alkaline.

Similar to Metformin, Diltiazem also exhibits pH-dependent solubility. It is more soluble in water than in the acidic solution, and its solubility is only slightly higher in the phosphate buffer solution with a pH of 7.4.

Overall, these results indicate that both Metformin and Diltiazem have varying solubility depending on the pH of the solvent. This pH sensitivity is essential to consider when formulating these drugs into pharmaceutical products, as it can impact their dissolution and bioavailability in the body.

Table 6.3: Solubility data of MET and DIL

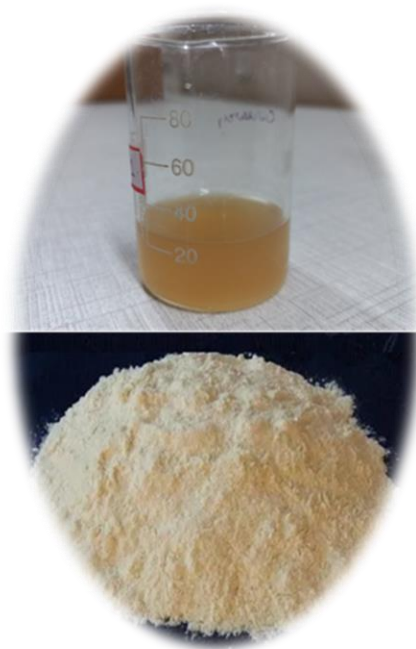
Drugs	Solubility (g/ml) at 34°C in		
	Water	Acid solution (pH 1.2)	MPB solution (pH 7.4)
Metformin	0.26	0.18	0.28
Diltiazem	0.068	0.054	0.065

6.5. Conclusion

In conclusion, this study has systematically explored the spectral properties and solubility behavior of Metformin (MET) and Diltiazem (DIL) across various solvent systems. Through this comprehensive investigation enrich the understanding of MET and DIL's spectral properties, calibration curves, and solubility behaviors across diverse solvent systems. These findings hold significant implications for pharmaceutical analysis and drug formulation, ensuring accurate and dependable drug quantification in various applications.

CHAPTER 7

***ALBIZIA PROCERA* GUM MODIFICATION: SYNTHESIS AND CHARACTERIZATION**



***ALBIZIA PROCERA* GUM MODIFICATION: SYNTHESIS AND CHARACTERIZATION**

7.1. Characterization of NAP

7.1.1. FT-IR spectrum analysis

The FTIR spectra (Fourier Transform Infrared spectra) of NAP, as depicted in Figure 7.1, provide valuable insights into the chemical composition and functional groups present in this substance. The spectrum covers a broad range of wavelengths from 4000 to 400 cm^{-1} , allowing for the identification of characteristic absorption bands that can be attributed to specific molecular vibrations. In this particular FTIR spectrum, several prominent absorption bands are observed. Notably, there are distinct peaks at 3449, 2921, 1634, 1502, and 1057 cm^{-1} . These specific wavenumbers are indicative of the vibrational frequencies associated with various chemical bonds and functional groups within NAP. The absorption band at around 3449 cm^{-1} is particularly prominent. This intense peak corresponds to the stretching vibrations of O-H bonds [Sadalage & Pawar 2021], specifically the hydroxyl (OH) groups within NAP. Such a strong absorption in this region suggests the presence of hydrogen bonds involving these hydroxyl groups. Hydrogen bonds are a type of intermolecular force that forms between the hydrogen atom of one molecule and a highly electronegative atom, such as oxygen or nitrogen, of another molecule. In the case of NAP, the hydroxyl groups are likely forming hydrogen bonds with neighboring molecules or groups, leading to the observed peak at 3449 cm^{-1} . Additionally, the presence of absorption bands at 3449, 2921, 1634, 1502, and 1057 cm^{-1} is consistent with typical bands associated with carbohydrates [Yuen et al., 2009]. These bands represent specific molecular vibrations related to the structural elements found in carbohydrates.

The FTIR spectrum of NAP provides valuable information about its chemical composition and functional groups. The presence of strong absorption bands at 3449 cm^{-1} , indicative of hydrogen bonding involving hydroxyl groups, along with other characteristic carbohydrate-related bands, suggests the presence of carbohydrates in NAP and provides important insights into its molecular structure and properties.

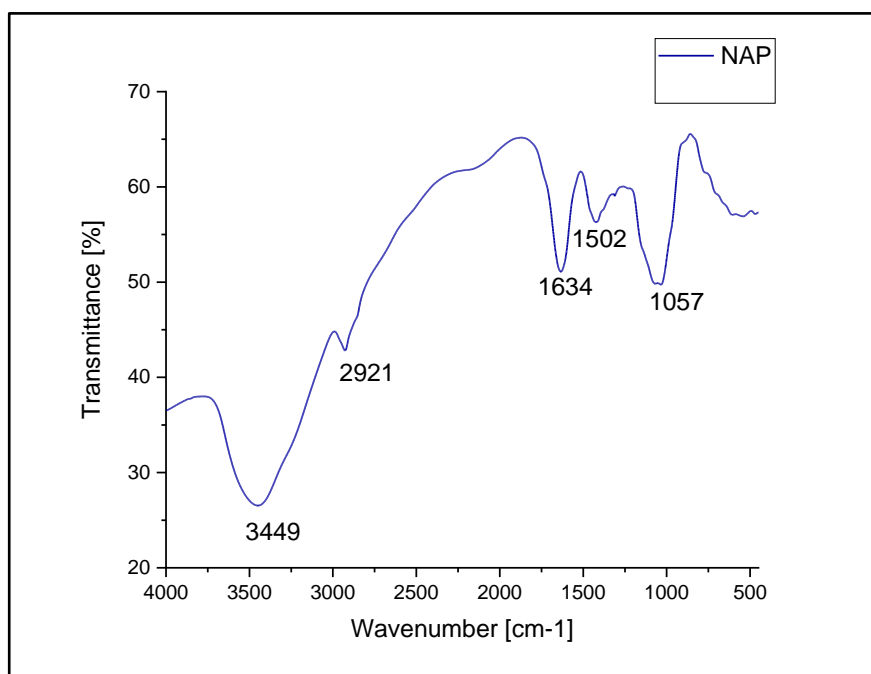


Figure 7.1: FTIR spectra of NAP

7.1.2. Differential Scanning Calorimetry (DSC) study

The DSC (Differential Scanning Calorimetry) thermograms presented in Figure 7.2 provide valuable information about the thermal behavior of NAP (presumably a substance or material). DSC is a powerful analytical technique used to investigate the changes in heat flow associated with temperature changes in a sample. In Figure 7.2, the DSC thermogram of NAP is depicted, and it reveals several significant thermal events. The first notable event is an exothermic peak occurring at $73.99\text{ }^{\circ}\text{C}$, characterized by a heat flow of 22.38

mW. This exothermic event indicates that NAP is releasing heat energy to its surroundings at this specific temperature. Such exothermic peaks in DSC thermograms often suggest processes like crystallization or chemical reactions occurring within the sample. Further along the thermogram, at approximately 239 °C, another distinct feature is observed. This feature corresponds to an intense melting peak with a heat flow of 14.15968 mW. This melting peak signifies that NAP is undergoing a phase transition from a solid to a liquid state at this temperature. The intense nature of this peak suggests that this phase transition is a well-defined and significant process within the material.

Despite the exothermic and melting events observed, it's important to note that the DSC thermograms of NAP overall indicate good thermal stability. This means that NAP can withstand changes in temperature without undergoing extensive decomposition or degradation. The absence of large endothermic peaks (indicative of degradation or decomposition) in the thermogram suggests that NAP can maintain its structural integrity within the studied temperature range [Gong et al., 2012].

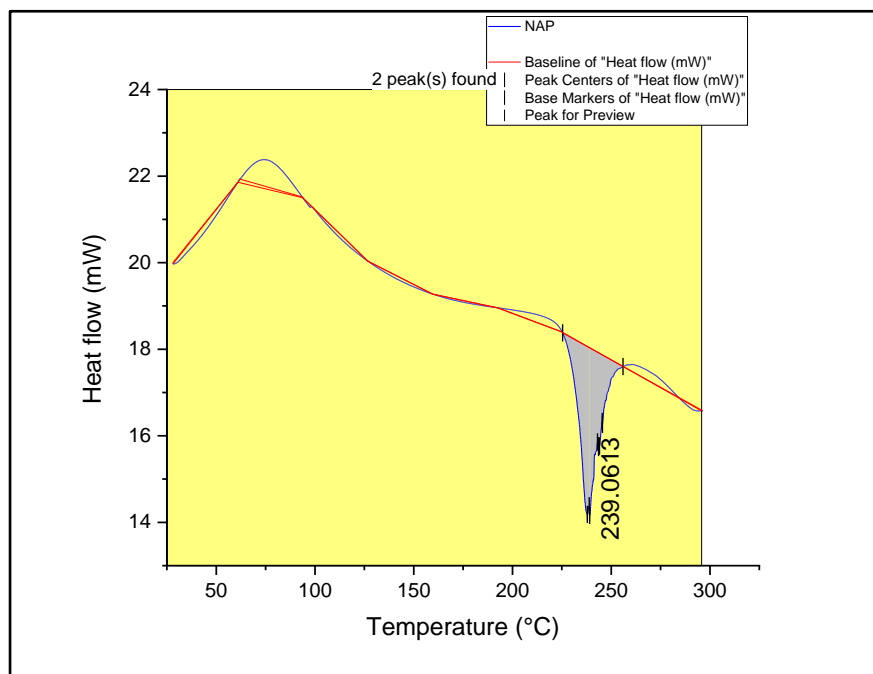


Figure 7.2: DSC thermogram of NAP

7.1.3. Solid State ^{13}C NMR Spectroscopy

The ^{13}C NMR spectra of NAP are presented in Figure 7.3, illustrating the distinctive signals that emerged within the spectrum. Notably, the NMR spectrum of NAP (Figure 7.3) exhibited specific signals at chemical shifts (δ) of 62.229 ppm, 72.740 ppm, and 103.760 ppm. The prominent peak at 62.229 ppm was attributed to the C-6 carbon of the galactose moiety, denoting the presence of the sugar ring carbon along with a hydroxyl group functionality characterized by sp^3 hybridization. Conversely, the signal at $\delta = 72.740$ ppm appeared as an inflation at 82 ppm due to the signals of the C-2, C-3, and C-4 β -carbon atoms [Yazdani et al.; 2019].

Furthermore, the appearance of the peak at $\delta = 76.671$ ppm indicated the presence of the β -carbon at pyranose ring closure. Simultaneously, the signal corresponding to the C-3 carbon atom of galactose manifested as a small bulge at 82.738 ppm. It is worth noting that this peak at 82.738 ppm was also associated with the presence of carbon at the furanose ring closure of α -anomers [Agrawal PK et al., 1985]. Moreover, the detection of a peak at $\delta = 99.316$ ppm was attributable to the signal from the β -anomeric carbon (C-1). Another noteworthy observation was the intense peak observed at $\delta = 103.760$ ppm, arising from the carbon (C-1) of arabinose, adding an important feature to the structural characterization of the compound [Chauhan D & Chauhan JS 2002].

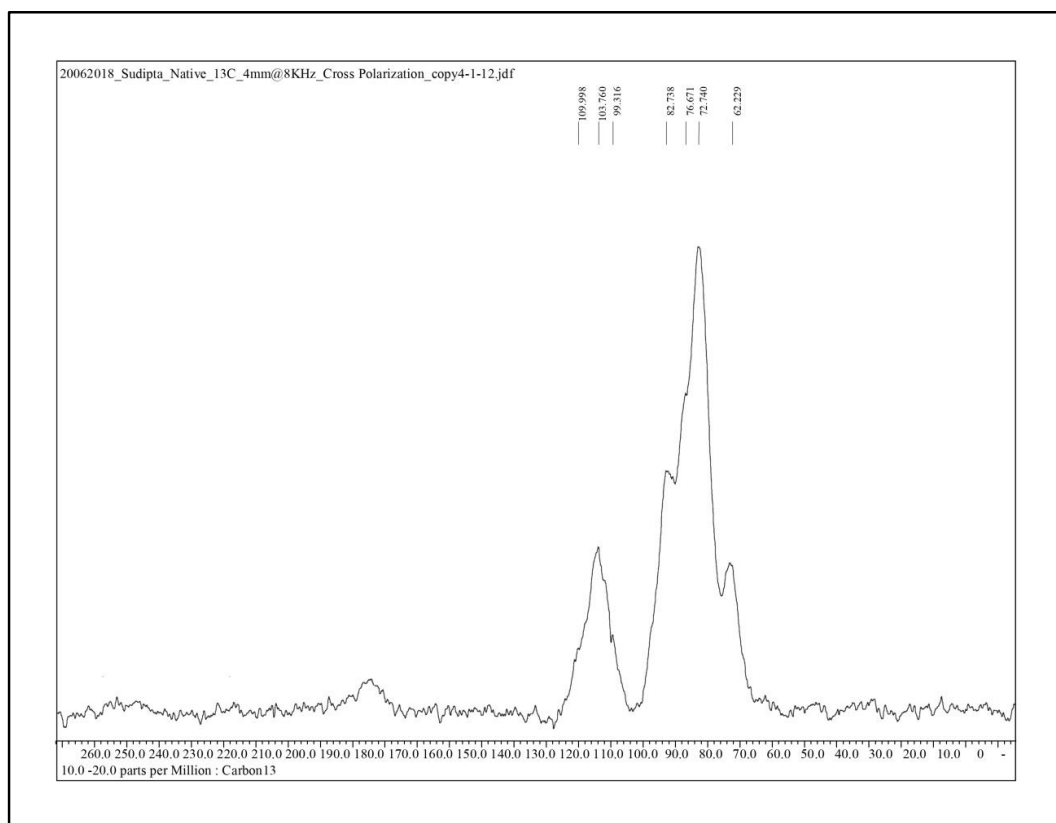


Figure 7.3: Solid state ^{13}C NMR spectrum of NAP

7.1.4. X-ray Diffractometry

The X-ray diffractogram of NAP, as depicted in Figure 7.4, showcases the material's amorphous nature. The diffractogram exhibits a broad, featureless pattern without distinct peaks, indicative of an amorphous solid lacking a regular lattice structure. The Two-Theta (θ) values ranging from 5 to 80 degrees and the corresponding intensities (CPS) exhibit a relatively uniform and smooth distribution, further supporting the amorphous nature of the material. The absence of sharp diffraction peaks in the diffractogram implies a disordered atomic arrangement within the material. This lack of long-range order suggests that NAP does not possess a well-defined crystalline structure, consistent with an amorphous solid. The amorphous nature of NAP is crucial in the context of its application, as it often leads to distinct material properties, including enhanced solubility, improved bioavailability, and modified dissolution kinetics.

Additionally, the relatively constant intensity values across the entire range of Two-Theta values indicate a uniform amorphous structure throughout the material [Kumar & Nair 1994]. This uniformity suggests that the NAP sample used for the X-ray diffraction analysis does not contain any crystalline domains or long-range periodicity.

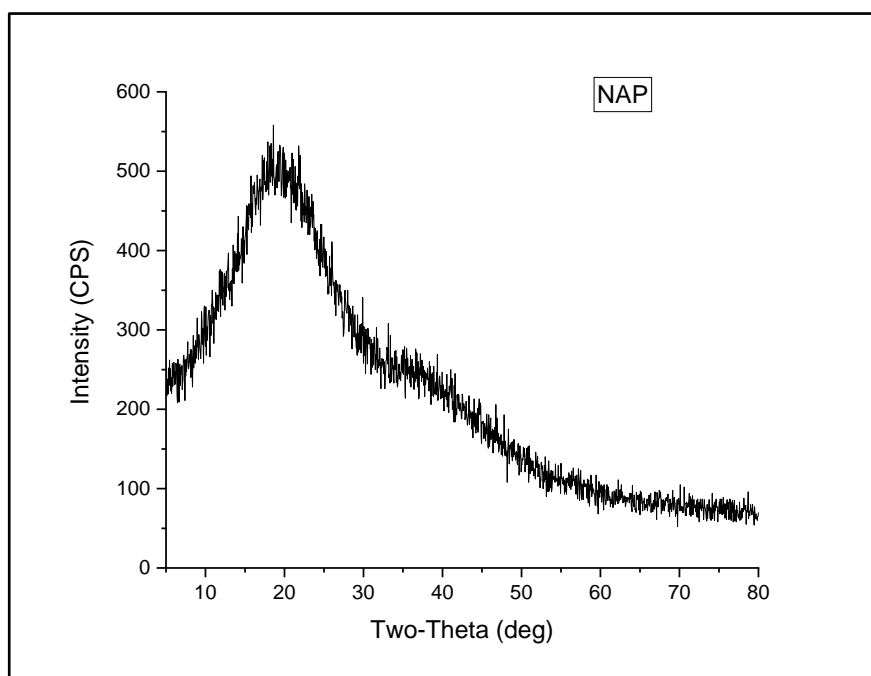


Figure 7.4: XRD patterns of NAP

7.1.5. Zeta potential measurements

The zeta potential, a critical parameter in colloidal chemistry and surface science, characterizes the electrokinetic potential present at the interfacial bilayer, precisely at the slip plane that divides the mobile fluid phase from the fluid phase adhering to the surface [Liu Y et al., 2020; Ye F et al., 2017]. This property is instrumental in understanding the stability and behavior of colloidal suspensions and interfaces. In the specific case of NAP (as shown in Figure 7.5), the measured zeta potential was recorded as -0.944. The presence of a

negative zeta potential can lead to improved physical stability, preventing flocculation and sedimentation of particles within the suspension.

Furthermore, understanding the zeta potential of NAP is crucial in comprehending its interactions with biological systems, particularly in the context of drug delivery and bioavailability. The negative charge on the NAP surface can influence its interaction with biological membranes and proteins, impacting its absorption, distribution, and cellular uptake. The zeta potential of NAP plays a pivotal role in determining its surface reactivity and its susceptibility to chemical and biological transformations. The magnitude of the zeta potential can influence the rate of surface reactions, such as adsorption, desorption, and chemical degradation, ultimately affecting the material's stability and performance under various environmental and biological conditions.

Overall, the determination of the zeta potential of NAP provides valuable insights into its colloidal stability, surface reactivity, and interactions with biological systems, laying the groundwork for the rational design and optimization of NAP-based formulations for targeted drug delivery and other biomedical applications. Further investigations into the correlation between the zeta potential and the physicochemical properties of NAP can offer deeper insights into its behavior and pave the way for the development of more effective and tailored applications in pharmaceutical fields.

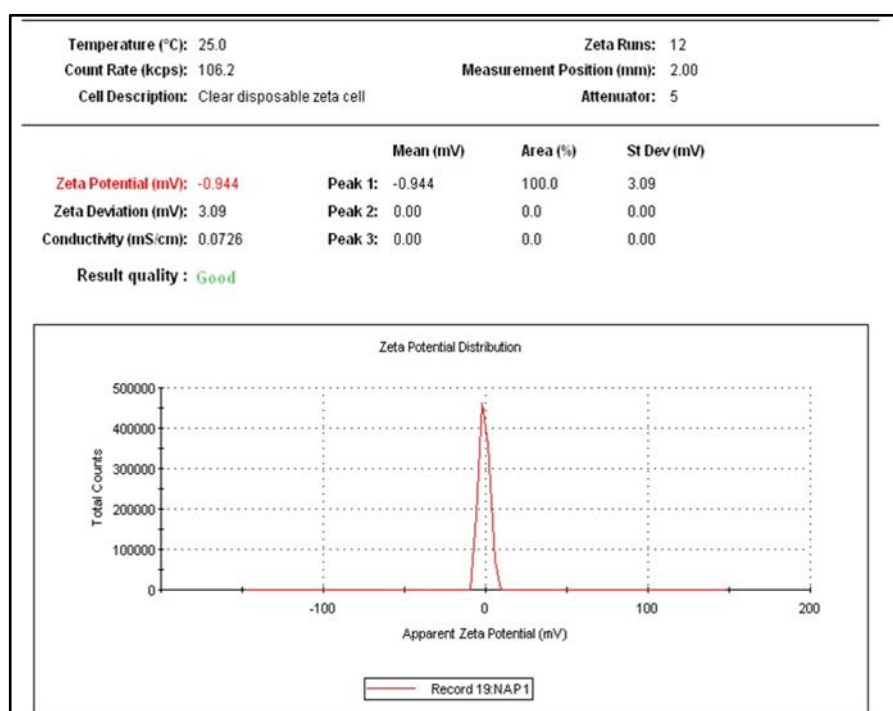


Figure 7.5: Zeta potential of NAP dispersion

7.2. Characterization of CMAP

7.2.1. Extent of carboxymethylation

The native gum derived from *A. procera*, known as NAP (Native *A. procera* gum), has been found to be predominantly composed of galactose and arabinose. Structurally, NAP is characterized by a linear chain consisting of (1→3)- β -D-galactopyranose units, along with some (1→6)- β -D-galactopyranose units and (1→3)-L-arabinofuranose units [Pachau L et al., 2012]. These structural features, essential for understanding its properties and behavior, form the backbone of NAP's macromolecular architecture.

The transformation of NAP to CMAP (Figure 7.6) involved the substitution of multiple hydroxyl groups with carboxymethyl groups, leading to a significant modification in its chemical composition. The conversion process began with the deprotonation of the hydroxyl groups in NAP by sodium hydroxide, resulting in the formation of alkoxides [Kaity & Ghosh 2013], as described in equation (1). Subsequently, the alkoxides of NAP underwent a reaction with monochloroacetic acid, giving rise to the introduction of carboxymethyl groups [Chakravorty A et al., 2016] as outlined in equation (2).

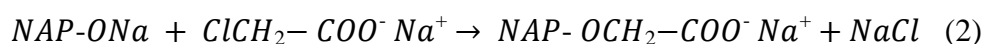
The chemical reactions involved in the synthesis of CMAP were not limited to the primary process but extended to the bulk liquid phase, leading to the concurrent formation of sodium glycolate through the interaction of monochloroacetic acid and sodium hydroxide, as depicted in equation (3). These side chain reactions further underscore the complexity of the chemical modifications occurring during the carboxymethylation of NAP.

The degree of substitution (DS) is a crucial parameter used to quantify the level of carboxymethylation within a compound. In the context of CMAP synthesis, the DS reflects the average count of substituted carboxymethyl groups per anhydroglucose unit. Based on the data presented in Table 2, the DS values for different batches of CMAP were observed to fall within the range of 0.38 to 0.51. These values indicate the extent to which the carboxymethylation reaction proceeded and provide insights into the degree of modification and

functionalization achieved during the chemical transformation of NAP into CMAP.

Understanding the degree of substitution is pivotal in evaluating the changes in the chemical structure and properties of the resultant CMAP. The degree of substitution not only influences the physicochemical characteristics of the modified gum but also has a significant impact on its solubility, viscosity, and compatibility with other compounds in various applications [Sara H et al., 2020]. It serves as a critical parameter for tailoring the properties of CMAP to meet specific requirements in diverse industrial applications.

Moreover, the elucidation of the chemical processes involved in the conversion of NAP to CMAP, along with the determination of the degree of substitution, provides valuable insights into the structural modifications and functionalization of *A. procera* gum, paving the way for the development of tailored applications in areas such as drug delivery, and other industrial sectors. Further investigations into the relationship between the degree of substitution and the properties of CMAP can offer deeper insights into its potential applications and facilitate its utilization in various pharmaceutical formulations.



At the bulk liquid phase, a side chain reaction occurred simultaneously with the formation of sodium-glycolate from monochloroacetic acid and sodium hydroxide.



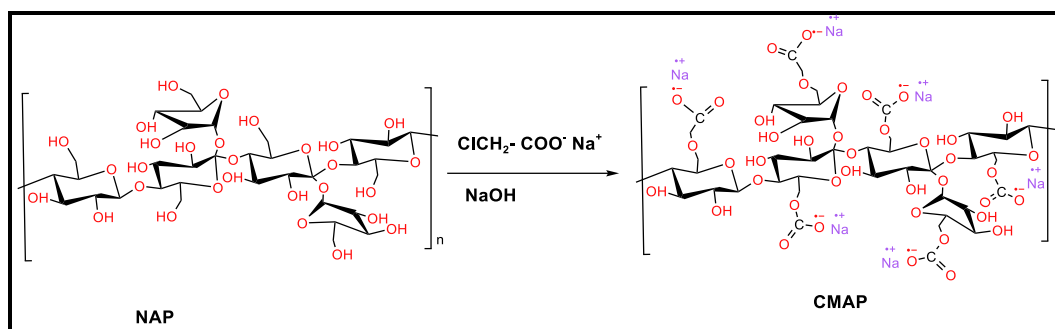


Figure 7.6: Conversion of NAP to CMAP

Table 7.1: Different Batches of CMAP

Batch no.	A*	D _S **	SEM*** (statistical significance of 5%) (n = 3)
P1	2.2069	0.41	±0.0492
P2	2.7	0.51	±0.0491
P3	2.045	0.38	±0.0484
P4	2.2069	0.41	±0.0469
P5	2.2068	0.41	±0.0298
P6	2.045	0.38	±0.0343

* Milliequivalents of NaOH required per gram of sample; ** Degree of substitution; *** Standard error of mean.

7.2.1. FT-IR spectrum analysis

The FT-IR spectra of CMAP as illustrated in Figure 7.7, reveal significant absorption bands at various wavenumbers, each representing distinct functional groups and structural components within the CMAP molecule. CMAP exhibited significant absorption bands at 3292.383, 2880.317, 2360.537, 1585.374, 1459.616, 1416.322, 1321.489, and 1020.494 cm^{-1} . The spectrum analysis

indicates the presence of characteristic carbohydrate bands, reinforcing the composition of CMAP as a modified gum with notable structural features aligned with its polysaccharide nature [Khondkar 2009].

CMAP exhibited a broadened absorption band within the range of 3600-3200 cm^{-1} , attributed to the stretching vibrations of hydroxyl groups (O—H). The distinct bands appearing in the spectral region of 1610-1370 cm^{-1} provided clear evidence of the presence of carboxyl groups (—COO), suggesting successful carboxymethylation as well as the modification of the chemical structure during the synthesis process. The C=O stretching of acids was represented by the band at 1420-1418 cm^{-1} . Furthermore, bands at 1318 and 1322 cm^{-1} corresponded to the scissoring of methyl groups (—CH_2). The spectra showed characteristic vibrations of C—H stretching at 2880.317 cm^{-1} and 2880.062 cm^{-1} [Aguir C & M'Henni MF 2006].

The appearance of bands corresponding to the stretching vibrations of $>\text{CH—O—CH}$ at approximately 1020 cm^{-1} highlighted the presence of specific linkages within the CMAP molecular structure, providing insights into the configuration of the glycosidic linkages and the modification pattern resulting from the carboxymethylation process. These findings emphasize the successful introduction of carboxymethyl groups onto the native *A. procera* gum, leading to the formation of CMAP with altered chemical properties and functionalities. Interestingly, the spectral shifts and changes in intensity observed in the O—H stretching bands suggested potential disruptions in hydrogen bonding within the CMAP structure, indicating the occurrence of structural modifications during the carboxymethylation reaction [Aguir C & M'Henni MF 2006]. This spectral analysis provides crucial evidence of the chemical changes induced by the modification process, shedding light on the structural transformations and the impact on the intermolecular interactions within the CMAP matrix.

Moreover, the characteristic peaks in the 950-1100 cm^{-1} range, signifying the presence of —C—O—C— groups, further underscore the intricate molecular architecture of CMAP, possibly denoting the existence of both β - and α -linkages within the modified gum. These observations contribute to a comprehensive understanding of the modifications induced during the

carboxymethylation process, offering valuable insights into the structural intricacies and chemical characteristics of CMAP.

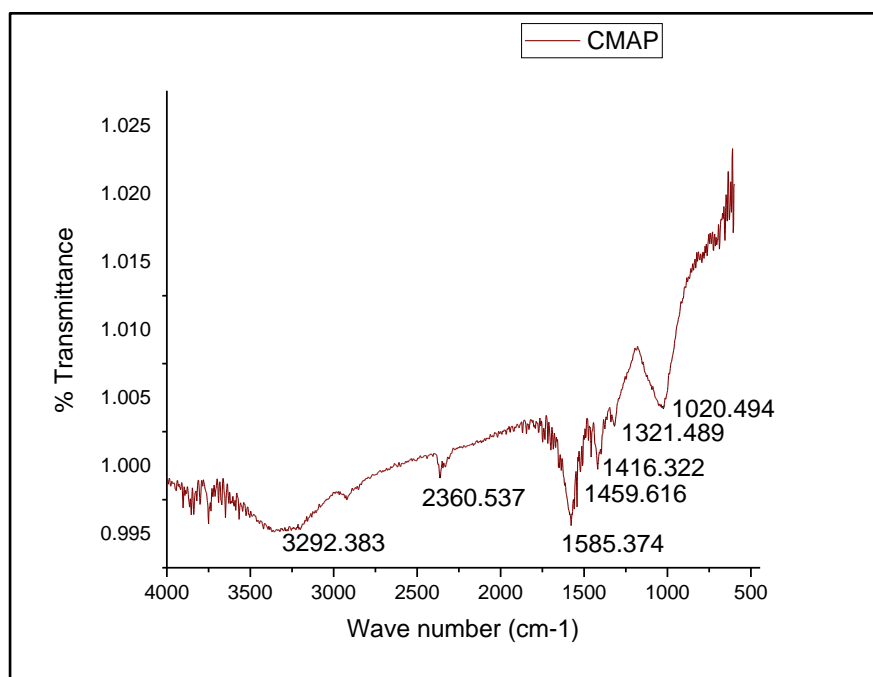


Figure 7.7: FTIR spectra of CMAP

7.2.2. DSC thermogram analysis

The DSC analysis of CMAP unveiled a distinct and prominent melting peak at 261.5 °C, accompanied by a notable heat flux of 9.899 mW, as demonstrated in Figure 7.8. These findings suggest that the carboxymethylation process has instigated notable modifications in the thermal properties of the material. The observed variations in the endothermic and exothermic behavior, alongside alterations in heat flow characteristics, can be attributed to the replacement of hydroxyl group protons during the carboxymethylation process. This process may have induced structural rearrangements within the polysaccharide, leading to the observed changes in the melting behavior.

It is widely recognized that the extent of carboxymethylation in polysaccharides can lead to the disruption of both intermolecular and intramolecular hydrogen bonds. Consequently, these structural changes can influence the vibrancy and configuration of chain segments within the material. The resulting alterations in

the polymer's molecular structure often lead to significant variations in the thermal degradation behavior. This aligns with the existing body of research, which highlights the impact of chemical modifications on the thermal properties of polymers and the role of structural changes in influencing their behavior during heating processes.

Despite these changes induced by the carboxymethylation process, the DSC thermograms of both NAP and CMAP indicated an overall retention of good thermal stability. This suggests that while the carboxymethylation process has brought about notable alterations in the material's melting behavior, the fundamental thermal stability of the polysaccharide has been largely preserved [Ojogbo et al., 2020]. These observations underscore the robust nature of the native material and its resilience in the face of chemical modifications introduced during the carboxymethylation process.

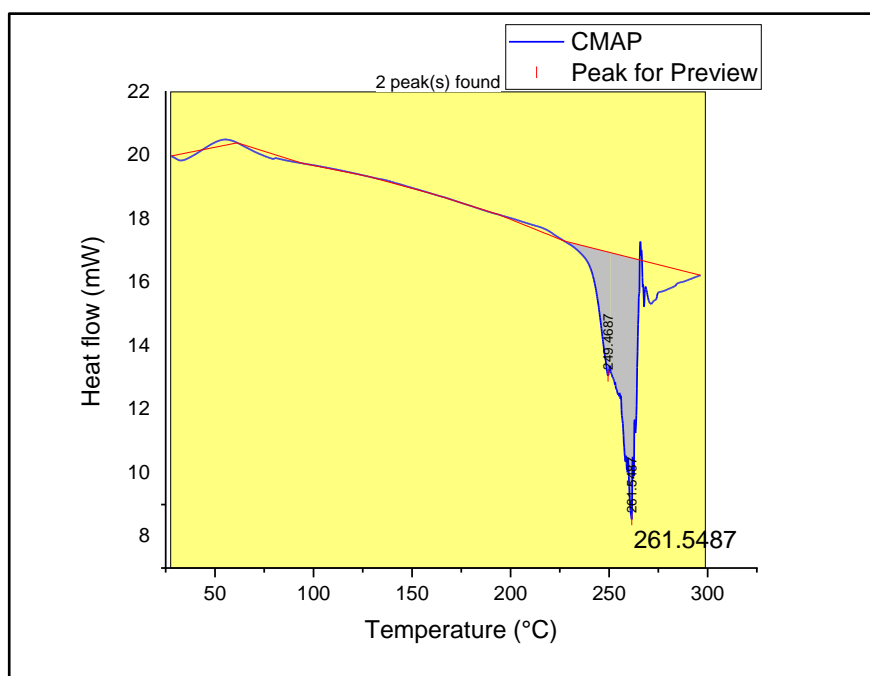


Figure 7.8: DSC thermogram of CMAP

7.2.3. Solid State ^{13}C NMR Spectroscopy

The detailed analysis of the ^{13}C NMR spectrum for the CMAP sample revealed several distinct signals corresponding to specific carbon atoms within the molecular structure (Figure 7.9). The signal observed at 62.570 ppm was attributed to the sp^3 hybridization of the C-6 carbon in the galactose moiety, serving as a clear indicator of the presence of the sugar ring carbon along with the functional hydroxyl group. Furthermore, the inflated signal ranging from 72.056 ppm to 82 ppm was associated with the signals from the C-2, C-3, and C-4 β -carbon atoms, elucidating the structural characteristics of the molecule. The presence of the β -carbon at pyranose ring closure was indicated by the distinctive signal observed at $\delta=73.081$ ppm, providing additional insights into the structural configuration of the polysaccharide [Baccile et al., 2009].

Additionally, the small bulge signal observed at 81.883 ppm corresponded to the signal from the C-3 carbon atom of galactose. The detection of a peak at 96.924 ppm was attributed to the β -anomeric carbon (C-1), further contributing to the comprehensive understanding of the structural composition of the sample. Notably, the intense signal identified at 103.418 ppm was attributed to the carbon (C-1) of arabinose, providing crucial information about the presence of this particular constituent in the molecular framework. The particular significance was the appearance of an additional sharp signal at 177.252 ppm in the CMAP sample, which was absent in the NAP spectrum (Figure 7.3). This signal was attributed to the carbon of the carboxymethyl group at the 3-O-position, underscoring the success of the carboxymethylation process on the NAP molecule. The positioning of this peak within the downfield region (170-220 ppm) is characteristic of the sp^2 hybridization of the carbonyl carbon, consistent with the expected chemical changes resulting from the carboxymethylation process. The presence of exocyclic carboxyl groups was also indicated by the signal at 177.252 ppm, providing further confirmation of the successful introduction of the carboxymethyl groups [Scholze B et al., 2001]. Consequently, the comparative analysis of the NAP and CMAP spectra highlighted the discernible differences between the two compounds,

underscoring the effectiveness of the carboxymethylation process and its impact on the molecular structure of the polysaccharide.

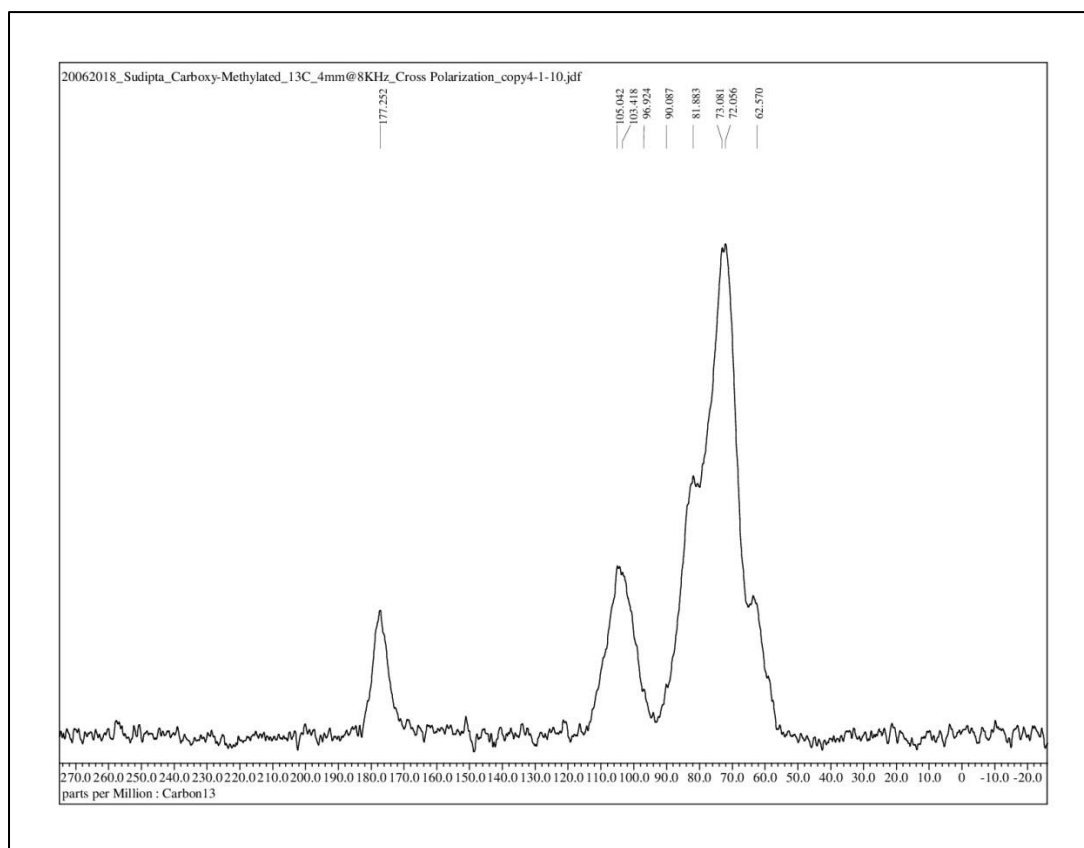


Figure 7.9: Solid state ^{13}C NMR spectrum of CMAP

7.2.4. X-ray Diffractometry

The X-ray diffractograms of the CMAP sample, illustrated in Figure 7.10, serve as crucial indicators of the material's crystalline nature, providing profound insights into its structural characteristics. Notably, the distinct patterns observed within the diffractogram, spanning 2θ values from 15.250° to 56.500° , shed light on the crystalline properties embedded within the CMAP structure. Of particular significance are the prominent, sharp, and intense patterns that emerge at approximately 2θ values of 31.700° (756 cps), 45.450° (409 cps), and

56.5° (182 cps), strongly suggesting the presence of crystallinity within the CMAP sample.

The manifestation of these characteristic patterns can be attributed to the intricate process of carboxymethylation, which induces structural modifications in the polymer, ultimately leading to the formation of distinct crystalline regions [Bhatia & Ahuja 2015]. This transformation can be understood as a consequence of the alterations in the molecular arrangement, resulting from the introduction of carboxymethyl groups. As such, the discernible crystalline patterns in the X-ray diffractograms of CMAP reflect the structural changes brought about by the carboxymethylation process, underscoring the significance of this chemical modification in shaping the crystalline nature of the polysaccharide.

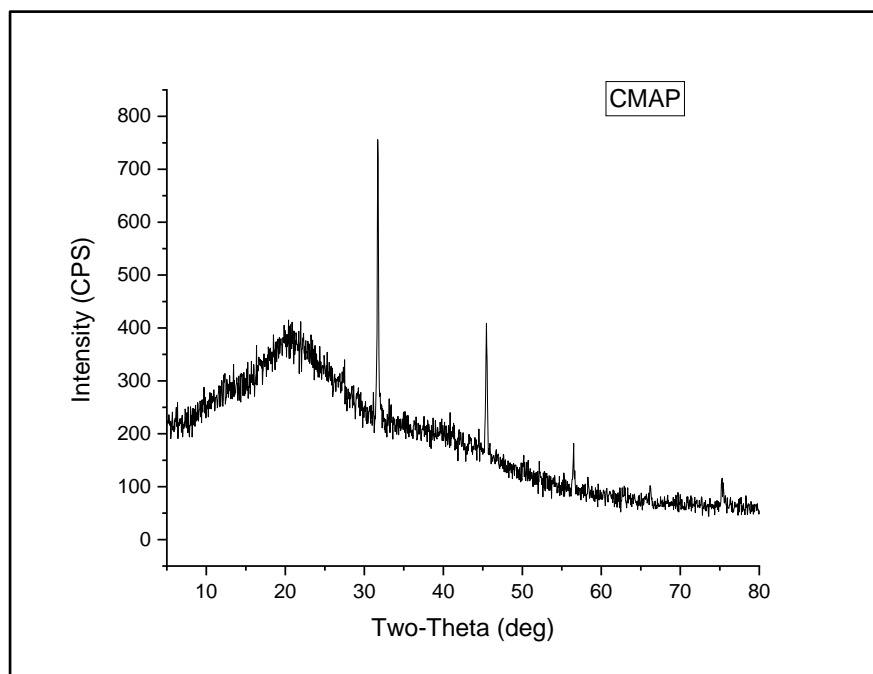


Figure 7.10: XRD patterns of CMAP

7.2.5. Zeta potential measurements

The zeta potential analysis, represented in Figure 7.11, has provided crucial insights into the surface charge properties of the CMAP samples, offering a deeper understanding of their electrochemical characteristics. Notably, the zeta potential evaluation unveiled a specific zeta potential value of -15.4 mV for the CMAP samples, highlighting a distinctly negative charge on the surface of these particles. This negative zeta potential of -15.4 mV signifies the prevalence of negatively charged sites on the CMAP particle surfaces, indicating a net negative charge on the overall CMAP structure. The origin of this negative zeta potential can be traced back to the presence of anions associated with the carboxymethyl groups ($-\text{OCH}_2\text{-COO}-$) [Borsagli et al., 2015; Prathapan et al., 2016] integrated into the polymer chains of CMAP. The presence of these anions significantly contributes to the overall negative charge observed on the surface of the CMAP samples. It is worth noting that a higher negative zeta potential, as observed in the case of CMAP, implies a stronger electrostatic repulsion among the CMAP particles. This phenomenon can facilitate enhanced dispersion and stability, a critical characteristic in various applications such as colloidal stability and suspension stability. The pronounced negative zeta potential of CMAP, thus, plays a vital role in dictating the interparticle interactions and overall stability of the polysaccharide, underscoring its significance in numerous practical and industrial contexts.

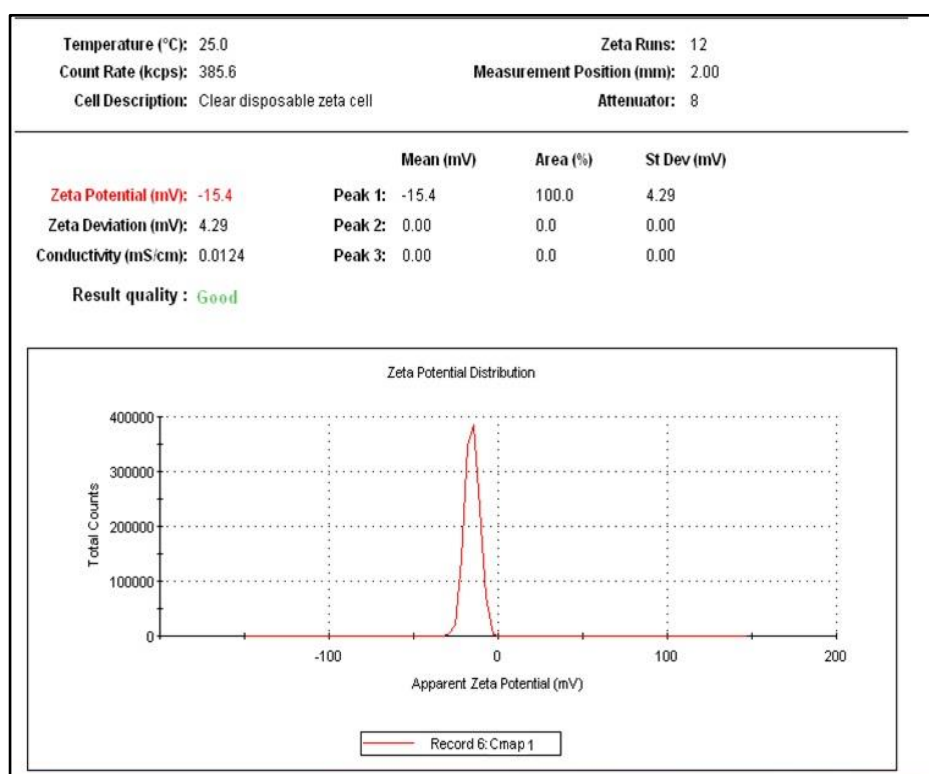


Figure 7.11: Zeta potential of CMAP dispersion

7.2.6. Elemental analysis

The elemental analysis conducted using the CHNS/O Elemental Analyzer on the powdered samples of NAP and CMAP provided valuable insights into the elemental composition of these substances. Table 7.2 presents the comprehensive results, showcasing the contents of various key elements within the two samples.

In the case of the NAP sample, the analysis revealed a carbon (C) content of 37.49%, a hydrogen (H) content of 7.137%, an oxygen (O) content of 0.0%, and a sulfur (S) content of 0.555%. Conversely, the CMAP sample exhibited a carbon content of 39.74%, a hydrogen content of 5.827%, an oxygen content of 0.0%, and a sulfur content of 0.250%. Notably, both the NAP and CMAP samples showed no detectable nitrogen (N) content.

The findings suggest subtle differences in the elemental composition between NAP and CMAP. Particularly, the higher carbon content in CMAP compared to NAP indicates a greater degree of carbonization resulting from the carboxymethylation process. Furthermore, the reduced hydrogen content in CMAP implies a decreased number of hydroxyl groups as a consequence of the carboxymethylation reaction.

Moreover, the absence of oxygen in both samples aligns with the expectations of the carboxymethylation process, where hydroxyl groups are substituted by carboxymethyl groups, thereby decreasing the oxygen content. The presence of sulfur in both NAP and CMAP could signify the inclusion of sulfur-containing compounds during the synthesis process.

Overall, the elemental analysis data provides a comprehensive understanding of the elemental composition of NAP and CMAP, offering valuable insights into their chemical makeup and shedding light on the structural modifications brought about by the carboxymethylation process.

Table 7.2: Elemental analysis of NAP and CMAP

050718_Soni varioEL CHNS serial number: 11064047							
06.07.18 15:55							
No.	Name	Wght. [mg]	Date Time	Info	O2	C/N Ratio	Content [%]
13	NAP	5.4700	--:--:--		Index 1	190.0	N: 0.000 C: 37.49 S: 0.555 H: 7.137
							3046 52230 390 22176
14	CMAP	5.6400	--:--:--	Su	Index 1	0.000	N: 0.000 C: 39.74 S: 0.250 H: 5.827
							2287 53672 197 17111

7.3. Characterization of CCMAP

7.3.1. Formation of CCMAP

Carboxymethylated Albizia procera gum (CMAP) with a degree of substitution of 0.51 was successfully synthesized from the native Albizia procera gum. The carboxymethylation process introduced COO^- groups onto the gum's chains rendering them reactive with divalent cations. This property was exploited in the subsequent crosslinking step using CaCl_2 to create crosslinked carboxymethylated Albizia procera gum (CCMAP). The successful conversion of CCMAP through the cross-linking of carboxymethylated gum with calcium chloride was achieved. The interaction between COO^- groups on CMAP chains and divalent calcium ions resulted in the formation of CCMAP (Figure 7.12).

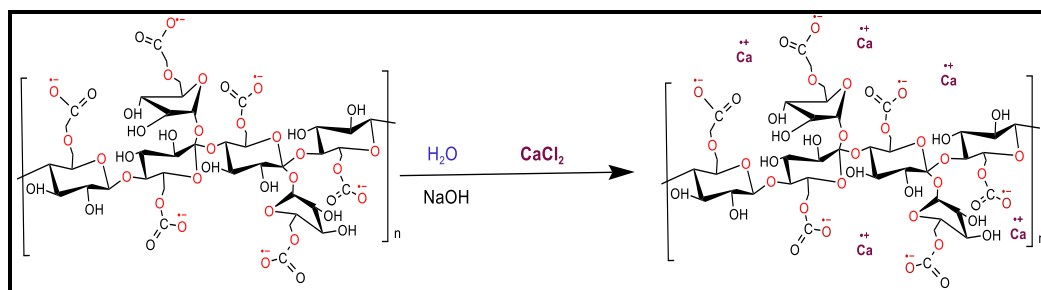


Figure 7.12: Crosslinking of CMAP

7.3.2. FT-IR spectrum analysis

The Figure 7.13 presentation of the FT-IR spectroscopy findings for CCMAP provides essential understandings of the material's structural alterations and interactions. Particularly, the widened band, observed within the $3600\text{--}3200\text{ cm}^{-1}$ range, is attributed to the O-H stretching of hydroxyl groups. This variance in the peak's intensity and position, especially compared to the FTIR spectrum of CMAP (Figure 7.7), potentially signifies changes in the interplay between the polymer and calcium ions, a critical aspect in examining CCMAP's behavior.

The specific manifestation of this shift in the O-H stretching band is closely linked to the particular polymer under examination and the nature of its interaction with calcium ions [Dagar et al., 2022]. Consequently, any discernible adjustments in the O-H stretching band impart vital information regarding the binding affinity of calcium ions in CCMAP. The heightened intensity of the O—H stretching band in CCMAP's FT-IR spectrum hints at potential crosslinking interactions with Ca^{+2} ions, a pivotal feature defining the material's behavior and properties [Coluccia S et al., 1987].

Besides the O-H stretching band, the CCMAP's spectrum showcased distinctive vibrations, including the C—H stretches at 2880.308 cm^{-1} and 2356.414 cm^{-1} , indicating the presence of specific chemical groups within the compound. Moreover, the identification of carboxyl groups (—COO) was facilitated by the appearance of bands within the $1610\text{-}1370\text{ cm}^{-1}$ range. The band at $1420\text{-}1410\text{ cm}^{-1}$ was attributed to the C=O stretching of acids, while the bands at 1318 and 1322 cm^{-1} were correlated with the scissoring of methyl groups (—CH₂). Furthermore, the band at 1016.371 cm^{-1} reflected the stretching frequency of >CH—O—CH [Lu R et al., 2005].

Overall, the insights from the FT-IR spectroscopy outcomes shed light on the structural transformations and interactions within CCMAP, illuminating the vital role of calcium ions and their consequent impact on the material's chemical and physical characteristics.

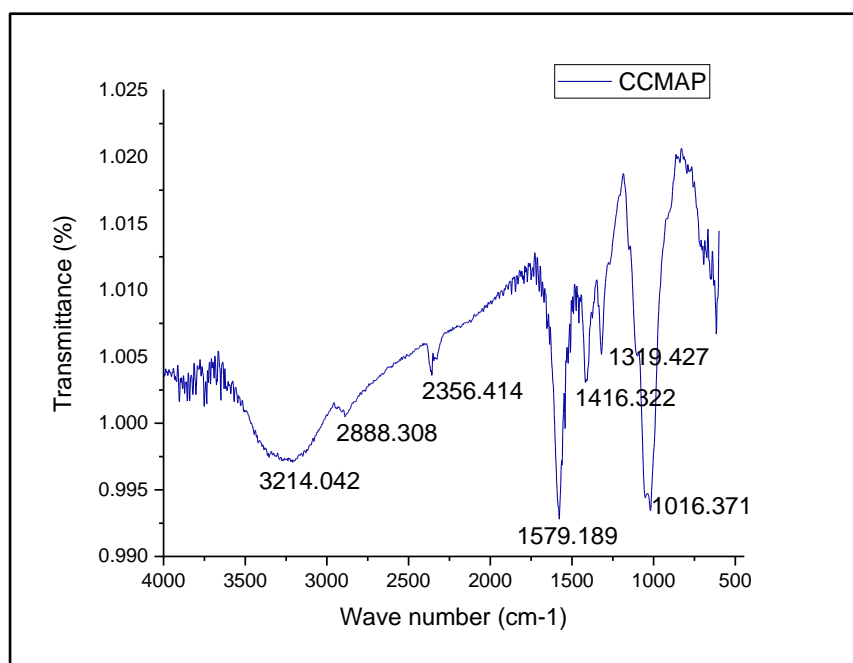


Figure 7.13: FTIR spectra of CCMAP

7.3.3. DSC thermogram analysis

The comprehensive insight provided by Figure 7.14, displaying the DSC thermograms for CCMAP, underscores the distinct thermal behavior of these polymers. A comparative analysis with the DSC thermogram of CMAP reveals an intriguing shift in the exothermic event for CCMAP, occurring at 55.15 °C with a heat flow of 21.08 mW. Additionally, both polymers exhibited endothermic peaks, while CCMAP presented a distinctive melting peak at approximately 263.97 °C, accompanied by a heat flow of 8.84 mW. This shift in the melting peaks from CMAP strongly suggests a significant alteration in the thermal properties of CCMAP, indicative of notable modifications brought about by the ionic crosslinking process.

The slightly shifted exothermic event and the altered melting peak in CCMAP in comparison to CMAP signify the complex interplay of structural modifications induced by the ionic crosslinking process. Such modifications likely contribute to the observed changes in the thermal behavior, underscoring

the role of the intermolecular interactions and crosslinking in enhancing the thermal stability of CCMAP [Hongbo et al., 2012]. This enhanced thermal stability is a crucial feature in various applications, particularly where materials are subjected to varying temperature conditions. The DSC thermograms, therefore, provide critical insights into the thermal characteristics of CCMAP, highlighting the importance of the ionic crosslinking process in influencing its thermal behavior and stability.

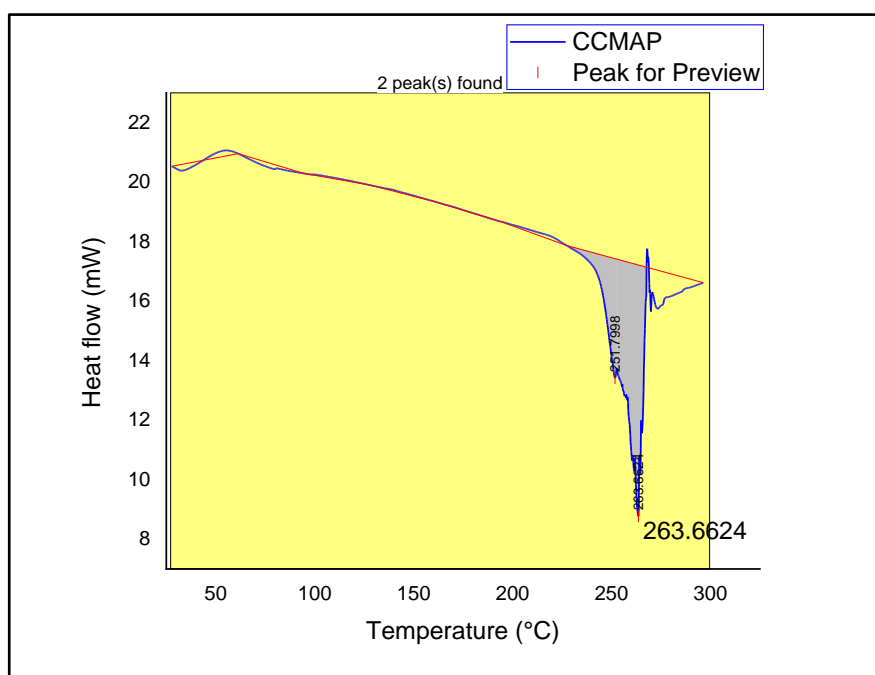


Figure 7.14: DSC thermogram of CCMAP

7.3.4. X-ray Diffractometry

Figure 7.15, showcasing the X-ray diffractograms of CCMAP, serves as a crucial tool in unraveling the crystalline nature of these materials. The distinctive patterns observed within the 2θ range of 17.35° to 47.1° in the X-ray diffractogram of CCMAP shed light on its structural characteristics. Notably, the discernible, well-defined peaks at specific 2θ values, including 17.35° ,

18.25°, 19.55°, 24.7°, 25.5°, 28.1°, 27.5°, 29.4°, 29.85°, 33.45°, and 47.1°, underscore the heightened degree of crystallinity within CCMAP, as compared to the diffractograms of CMAP. This elevated level of crystallinity is a direct consequence of the incorporation of calcium crosslinking, which induces more structured and orderly regions within the polymer matrix [Bhatia & Ahuja 2015].

The profound influence of the chemical modifications, particularly the carboxymethylation and calcium crosslinking processes, on the crystalline properties of the polymers is confirmed by the X-ray diffractogram analysis. While CMAP exhibits partial crystallinity resulting from carboxymethylation, CCMAP demonstrates a notably enhanced degree of crystallinity primarily attributed to the presence of calcium crosslinking. These discrepancies in the crystalline characteristics have far-reaching implications for the physical and chemical properties of both CMAP and CCMAP.

Understanding the structural modifications induced by the crosslinking process is crucial in tailoring the properties of these materials for various applications, including controlled drug delivery, tissue engineering, and biomedical devices. The X-ray diffractogram analysis, therefore, provides key insights into the underlying changes in the crystalline nature of CCMAP, emphasizing the pivotal role played by the intermolecular interactions and crosslinking in shaping its structural and functional properties.

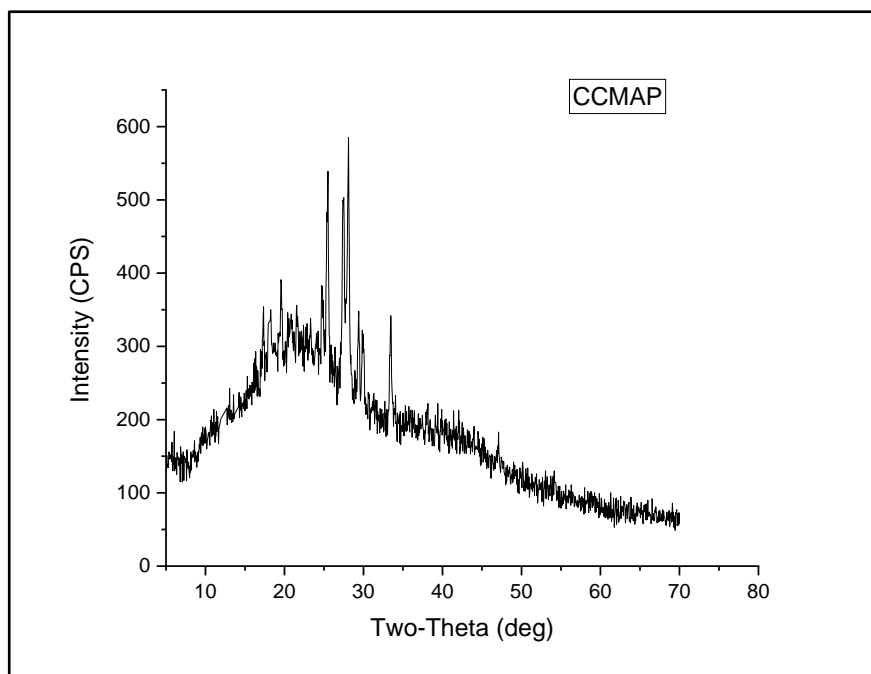


Figure 7.15: XRD patterns of CCMAP

7.3.4. Zeta potential measurements

Illustrated in Figure 7.16, the zeta potential analysis provides crucial insights into the surface charge characteristics of CCMAP samples. The measured zeta potential value for the CCMAP samples was found to be -4.57 mV . This result signifies a negative surface charge, indicating the presence of anionic sites on the carboxymethyl groups ($-\text{OCH}_2\text{-COO}^-$) along the polymer chains of CCMAP. The negative zeta potential observed in CMAP (-15.4 mV) is primarily attributed to the abundance of these anionic sites, contributing to the overall negative charge on the surface of CMAP. The higher negative zeta potential value is indicative of stronger electrostatic repulsion among CMAP particles, thereby promoting enhanced dispersion and stability of the material. However, in the case of CCMAP, despite the inherent negative charge due to the presence of carboxymethyl groups, the interactions between the positively charged calcium ions (Ca^{2+}) and the carboxymethyl groups ($-\text{OCH}_2\text{-COO}^-$)

along the chains of CCMAP led to a less negative zeta potential of -4.57 mV. The introduction of calcium ions altered the zeta potential towards the positive side, thereby reducing the overall negative charge. This shift in the zeta potential, while preserving the overall negative charge, reflects the intricate interplay between the chemical functionalities and the ionic crosslinking process within the CCMAP structure. Understanding the intermolecular interactions that influence the zeta potential is critical in comprehending the stability and behavior of CCMAP, particularly in the context of its potential applications in various fields, including biomedicine and pharmaceuticals.

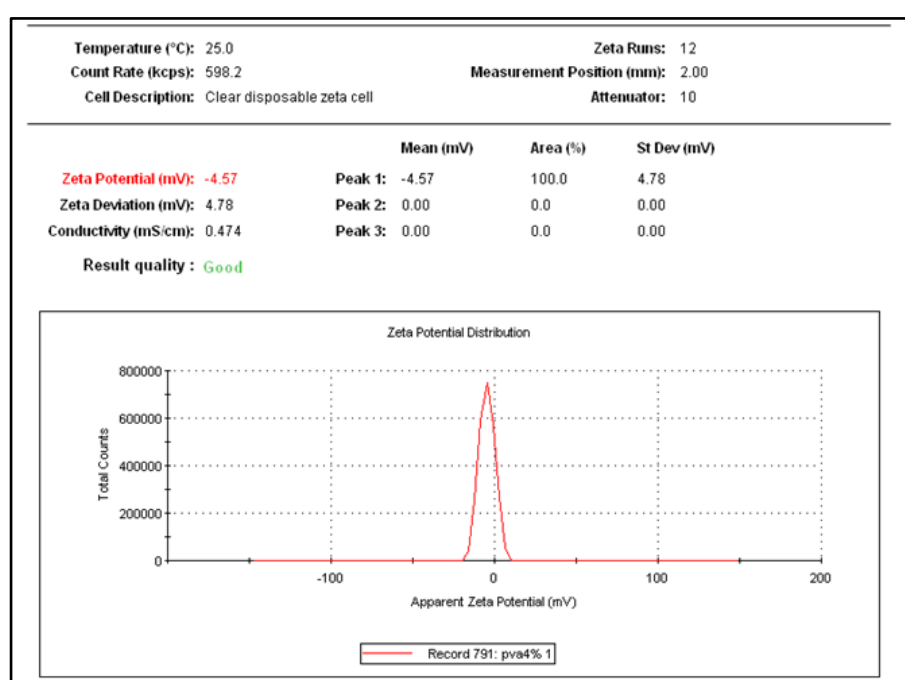


Figure 7.16: Zeta potential of CCMAP dispersion

7.4. RBC lysis test

The investigation conducted in this study aimed to assess the effects of NAP, CMAP, and CCMAP on red blood cell (RBC) properties, employing optical density (OD) measurements at 29.8°C after 1 and 3 hours of incubation. The data presented in Table 7.3 provided valuable insights into the interactions between the sample solutions and RBCs.

Initial analysis of the optical density for NAP and CMAP-treated samples indicated minimal fluctuations after 1 hour, suggesting a lack of substantial influence on RBC properties. This observation persisted even after the 3-hour incubation period, signifying that NAP maintained a consistent impact, leaving RBCs relatively unaffected. Similarly, CCMAP-treated samples exhibited optical densities that remained stable over the experimental duration, further supporting the notion that CCMAP did not significantly affect RBC properties.

In contrast, the positive control, represented by Water for Injection (WFI), demonstrated notably higher optical densities, indicating a substantial influence, potentially linked to osmotic effects. This discrepancy underscored the relatively milder impact of NAP, CMAP, and CCMAP on RBC properties compared to the potent effects of the positive control (WFI). This finding implies that the sample solutions of NAP, CMAP, and CCMAP can be deemed suitable for various applications concerning RBCs, as they do not significantly disrupt the inherent properties of these vital blood components.

Table 7.3: RBC Lysis Evaluation at 540 nm: 1 and 3 Hr Incubation

<i>Samples</i>	<i>Optical density at 540 nm</i>									
	After 1 hr					After 3 hrs				
NAP+RBC+PBS	0.0736	0.0749	0.0737	0.0761	0.0726	0.0737	0.0752	0.0739	0.0762	0.0728
CMAP+RBC+PBS	0.0728	0.0751	0.0731	0.0751	0.0714	0.0734	0.0753	0.0763	0.0756	0.0716
CCMAP+RBC+PBS	0.0719	0.0763	0.0733	0.0755	0.0758	0.0723	0.0765	0.0738	0.0758	0.0762
WFI (Positive control)	0.787	0.892	0.726			0.791	0.897	0.743		
Normal saline (Negative control)	0.0752	0.0769	0.0755			0.0752	0.0769	0.0755		
only RBC			0.1687					0.1687		

Conclusion:

The thorough characterization of Native Albizia procera Gum (NAP) through diverse analytical techniques provides deep insights into its chemical composition, thermal behavior, and surface characteristics. The investigations involving Carboxymethylated Albizia procera Gum (CMAP) and Crosslinked Carboxymethylated Albizia procera gum (CCMAP) illuminate the chemical transformations, structural modifications, and interactions shaping these materials. The analyses collectively unveil tailored properties in CMAP and CCMAP, crucial for applications in drug delivery, biomedical fields, and diverse industries. Moreover, the minimal impact of NAP, CMAP, and CCMAP on red blood cell properties suggests their suitability for various RBC-related applications without significant disruption, promising versatile uses across biomedical and pharmaceutical domains.

CHAPTER 8

COMPARATIVE RHEOLOGICAL ASSESSMENT OF POLYMERIC MATRICES

COMPARATIVE RHEOLOGICAL ASSESSMENT OF POLYMERIC MATRICES

8.1. Comparative rheological assessment of polymeric matrices

8.1.1. Dynamic rotational study (Flow curve)

The viscosity profiles of NAP, CMAP, and CCMAP matrices were thoroughly examined at various pH levels, revealing crucial insights into their flow behavior. Figure 8.1 (a, b, and c) vividly illustrated the flow curves of these matrices at different shear rates, highlighting their distinct viscosities and response to changes in shear rate. On the other hand, Figure 8.2(a, b and c) depicts the comparative viscosity profiles among NAP, CMAP and CCMAP matrices.

Particularly, the viscosity of the NAP matrix exhibited a declining trend with increasing shear rate, as illustrated in Figure 8.1a. Notably, the NAP matrices demonstrated non-Newtonian behavior, characterized by a pseudo-plastic flow pattern. This phenomenon is indicative of the disentanglement of polymeric chains occurring at a slower rate than the formation of new entanglements, as postulated by prior research. This intricate behavior was further underscored by the distinct viscosity values observed for NAP-W (in water), NAP-A (at pH 1.2), and NAP-B (at pH 6.8) at a low shear rate of 0.01290 s^{-1} (1420 Pa.s for NAP-W, 559 Pa.s for NAP-A, and 115 Pa.s for NAP-B). Remarkably, the rheogram depicted that NAP-W at neutral pH exhibited a notably higher viscosity than NAP-A at pH 1.2, while NAP-A displayed higher viscosity compared to NAP-B at pH 6.8. These findings emphasize the significant impact of pH levels on the viscosity of NAP matrices, suggesting that variations in the acidic or alkaline environment could lead to notable changes in the polymeric structure and subsequent viscosity. These results lay the groundwork for understanding the complex flow behavior of NAP matrices under varying pH conditions, facilitating potential applications in a diverse array of industries.

Flow curves of CMAP matrices also indicated shear-thinning behaviour however; they exhibited much lower viscosities than NAP matrices (Figure. 8.2). There has been an explanation for the increased degree of molecular chain entanglement with concentration attributed to an increase in the viscosity of polymers. Since, carboxymethyl groups ($-\text{OCH}_2\text{-COO}^-$) in CMAP contain anions, the chain segments are electrostatically repellent, preventing entanglements. Due to lack of entanglement, the viscosity of CMAP became lower than NAP matrices. The viscosity of CMAP-A (at pH 1.2) matrix was found to be higher than CMAP-W (at pH 7) and significantly higher than CMAP-B (Figure 8.1b). The functional groups get ionized at pH 6.8, and the repulsive force becomes strong, which leads to disentanglement and a decrease in viscosity [Wang CS et al., 2021; Sa B et al., 2019]. A shift in the molecular arrangements of the polysaccharide chains in buffer solution has been connected to the decreased viscosity of some ionic polymers with rising solution pH [Kaboarani & Blanchet 2014].

The comparative analysis of CCMAP-W with CMAP-A (at pH 1.2) and CMAP-B revealed a distinct trend, with the viscosity of CCMAP-W exceeding that of both CMAP-A and CMAP-B matrices, as highlighted in Figure 8.1c. This observation emphasizes the significant impact of the crosslinking process involving calcium ions (Ca^{+2}) and carboxylic groups in CCMAP formation. The resulting crosslinked structure ($-\text{OCH}_2\text{COO}^- \text{Ca}^{2+} -\text{OCH}_2\text{CO}-$) fundamentally alters the rheological behavior of the matrix, contributing to the notable increase in viscosity [Huang Y et al., 2006].

The process of crosslinking induced by the interaction between calcium ions and carboxylic groups has far-reaching consequences on the mobility of polymer chains within the CCMAP matrix. This phenomenon leads to the confinement and restriction of chain movement, thereby impeding the coulombic repulsion forces between them. As a consequence, the polymer chains within the CCMAP matrix become intricately entangled, thereby giving rise to a significant surge in viscosity.

This heightened viscosity in CCMAP-W facilitates the formation of viscoelastic gels, underscoring the complex interplay between the crosslinking mechanism and the resultant rheological characteristics. The intricate network formed due to the

intermolecular interactions in CCMAP-W signifies its potential utility in various applications requiring viscoelastic materials with tailored rheological properties.

8.1.2. Flow curve model

The flow curve model analysis revealed significant insights into the rheological behavior of NAP and CMAP matrices, shedding light on the most appropriate models for describing their flow properties. Notably, the Carreau-Yasuda model emerged as the most suitable model for capturing the flow characteristics of NAP-W, as evidenced by its distinct short Newtonian plateau observed at low shear rates ranging from 0.022 to 0.045 s⁻¹. This finding underscores the unique flow pattern exhibited by NAP-W, highlighting the prevalence of a specific flow regime in this matrix [Talens et al., 2021].

Contrastingly, the analysis indicated that the Cross model provided the most accurate fit for NAP-A, while the Ellis model effectively captured the pseudo-plastic flow exhibited by NAP-B. These diverse model fittings for NAP-W, NAP-A, and NAP-B underscore the nuanced rheological behavior of NAP matrices, elucidating the underlying mechanisms governing their flow patterns in distinct pH environments.

Furthermore, for CMAP matrices, the Ellis model [Al-Behadili A et al., 2019] emerged as the most suitable fit across all pH values, effectively capturing the shear stress aligning with half of the final asymptotic viscosity. This result implies a consistent flow behavior exhibited by CMAP, highlighting the robustness and uniformity of its flow properties under varying pH conditions.

Conversely, for the matrices CCMAP-W and CCMAP-A, the Carreau-Yasuda model was identified as the most appropriate match [Bush & Phan-Thien 1984].

These findings offer critical insights into the complex rheological characteristics of NAP, CMAP and CCMAP matrices, paving the way for a deeper understanding of their flow dynamics and potential applications in various industrial and scientific domains.

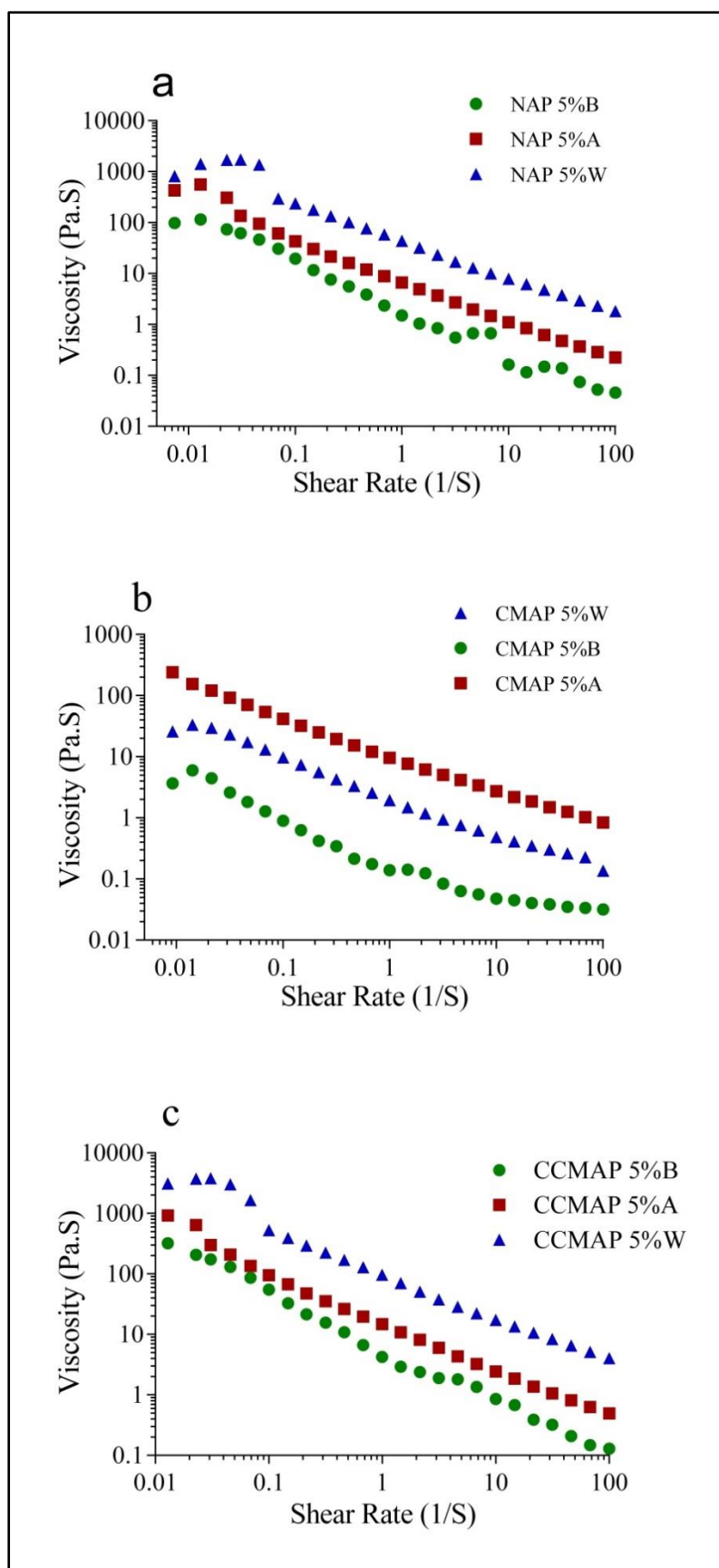


Figure 8.1: Flow curves of (a) NAP, (b) CMAP and CCMAP in water, acidic solution (pH 1.2) and PB solution of pH 6.8.

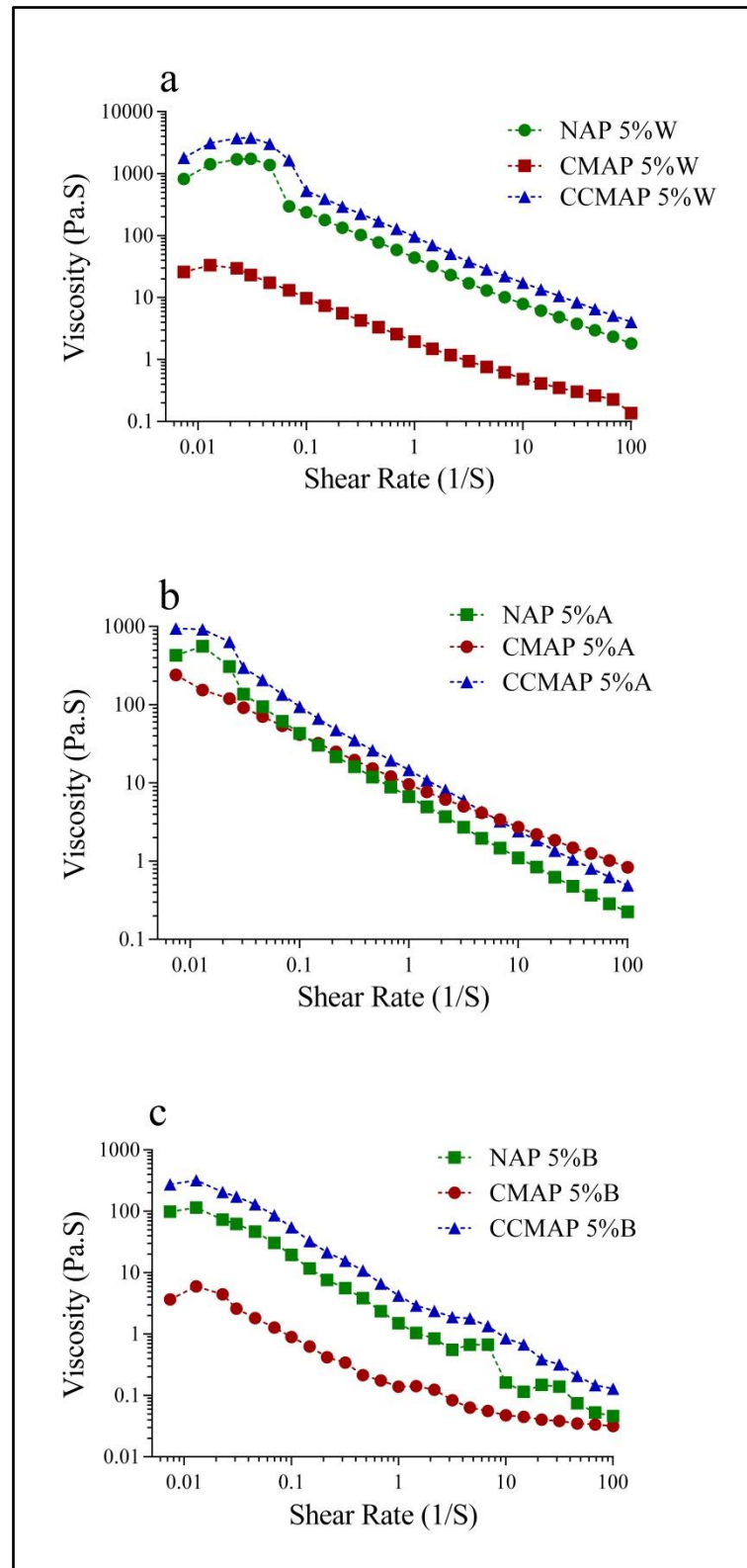


Figure 8.2: Comparative viscosity profiles of (a) NAP-W, CMAP-W and CCMAP-W matrices; (b) NAP-A, CMAP-A and CCMAP-A matrices; (c) NAP-B, CMAP-B and CCMAP-B matrices

8.1.3. Dynamic oscillatory studies

8.1.3.1. Amplitude sweep

In the context of linear viscoelasticity, it is crucial to establish the linear viscoelastic region (LVE), which denotes the range where stress exhibits a linear relationship with strain for the material under examination [Li C et al., 2011]. In this regard, two critical parameters are monitored: the storage modulus G' (expressed in pascals, Pa), which signifies the elastic response[39] and the loss modulus G'' (also expressed in Pa), which represents the viscous response. These parameters are observed as strain (%) is systematically varied during the course of amplitude deformation. Initially, within the LVE, polymers maintain their structural integrity. However, beyond a specific critical strain (%), structural deformations commence, marked by a decline in G' that surpasses the confines of the LVE. During the amplitude sweep, the amplitude of the deformation is varied with strain (%) at a constant frequency (Rad/sec) [Xiao F et al., 2013].

An illustration of the strain sweep results for each matrix of different pH (NAP, CMAP and CCMAP) is presented in Figure 8.3 (a, b, and c). Moreover, Figure 8.4 (a, b, and c) illustrates the comparative strain sweep analysis conducted across NAP, CMAP, and CCMAP at various pH levels.

G' and G'' in the amplitude curves were dependent on strain amplitude, and the LVE range was derived from these curves. Upon reaching a critical strain of 10%, LVE had been achieved, and G' values were found to be linear up to that point. Beyond the LVE the declination of G' indicated the occurrence of structural deformation. The critical strain refers to the mechanical strength of polymer and the amount of stress at which NAP and CMAP withstand before structural breakdown.

As indicated by the data presented in Figure 8.3 (a, b and c), the NAP-W matrices achieved a higher linear viscoelastic (LVE) region compared to both NAP-A and NAP-B. Similarly, the trend observed in the case of CMAP matrices followed the sequence of LVE as CMAP-A > CMAP-W > CMAP-B.

The LVE range and G' values of NAP were greater than CMAP in all cases (Figure 8.4 a, b and c). The overall critical strain of NAP (1-1.5%) was also found to be

higher than CMAP (0.01-0.03%). The electrostatic repulsion between the chains of CMAP disrupted entanglements results in low mechanical strength and shorter LVE. It's also worth mentioning that CMAP's LVE shows irregular patterns and increased instability.

In the case of CCMAP, interestingly, the results reveal distinctive behavior patterns for CCMAP. CCMAP demonstrates a critical strain of 2%, while CMAP exhibits a markedly lower critical strain of 0.03% (Figure 8.4 a, b and c). The amplitude sweep analysis conducted in this study revealed noteworthy differences in the mechanical behavior between NAP, CMAP and CCMAP. Notably, CCMAP exhibited a critical strain of 2%, representing the threshold at which this polymer can withstand stress before initiating deformation. In contrast, CMAP displayed a markedly lower critical strain of 0.3%, denoting its limited capacity to endure stress before deformation begins. The critical strain signifies the maximum stress threshold a material can endure without undergoing significant deformation. Beyond this point, the material experiences structural changes, initiating deformation or irreversible alterations in its form [Chakraborty A et al., 2016].

This divergence can be attributed to the effect of crosslinking, which effectively prevents CCMAP from undergoing ionization. Consequently, CCMAP manifests superior mechanical strength compared to NAP and CMAP. Furthermore, a noteworthy observation is the difference in the linear viscoelastic region (LVE) between these polymers. CMAP experiences a relatively shorter LVE, indicating a more limited range where its linear viscoelastic properties hold. In contrast, CCMAP exhibits a broader and more stable LVE, further highlighting the impact of crosslinking on the rheological behavior of the polymer.

Moreover, in accordance with the data illustrated in Figure 8.1c, the CCMAP matrices demonstrated the order of linear viscoelastic (LVE) as CCMAP-W > CCMAP-A > CCMAP-B.

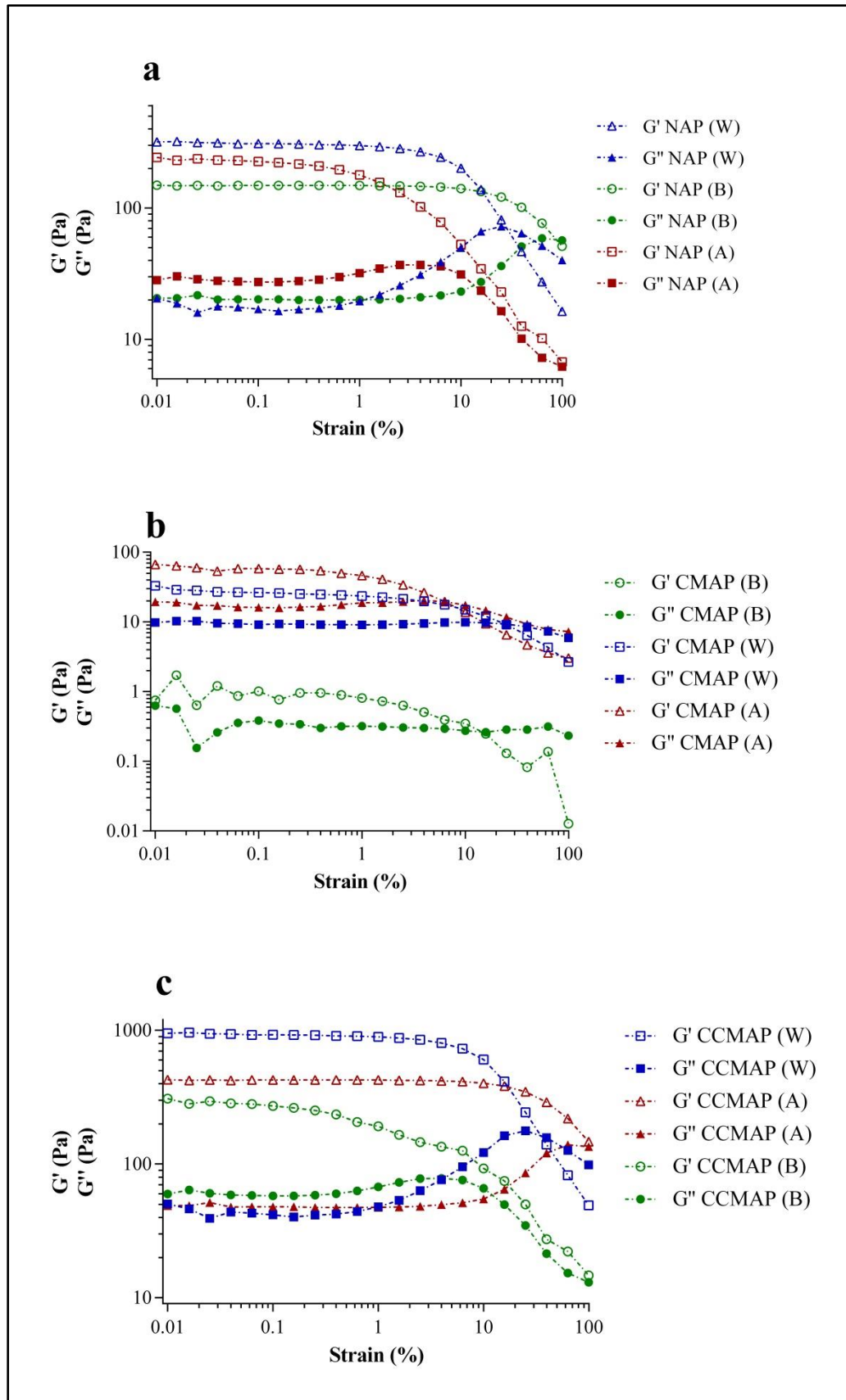


Figure 8.3: Amplitude sweep of (a) NAP, (b) CMAP and (c) CCMAP in water, acidic solution (pH 1.2) and PB solution of pH 6.8.

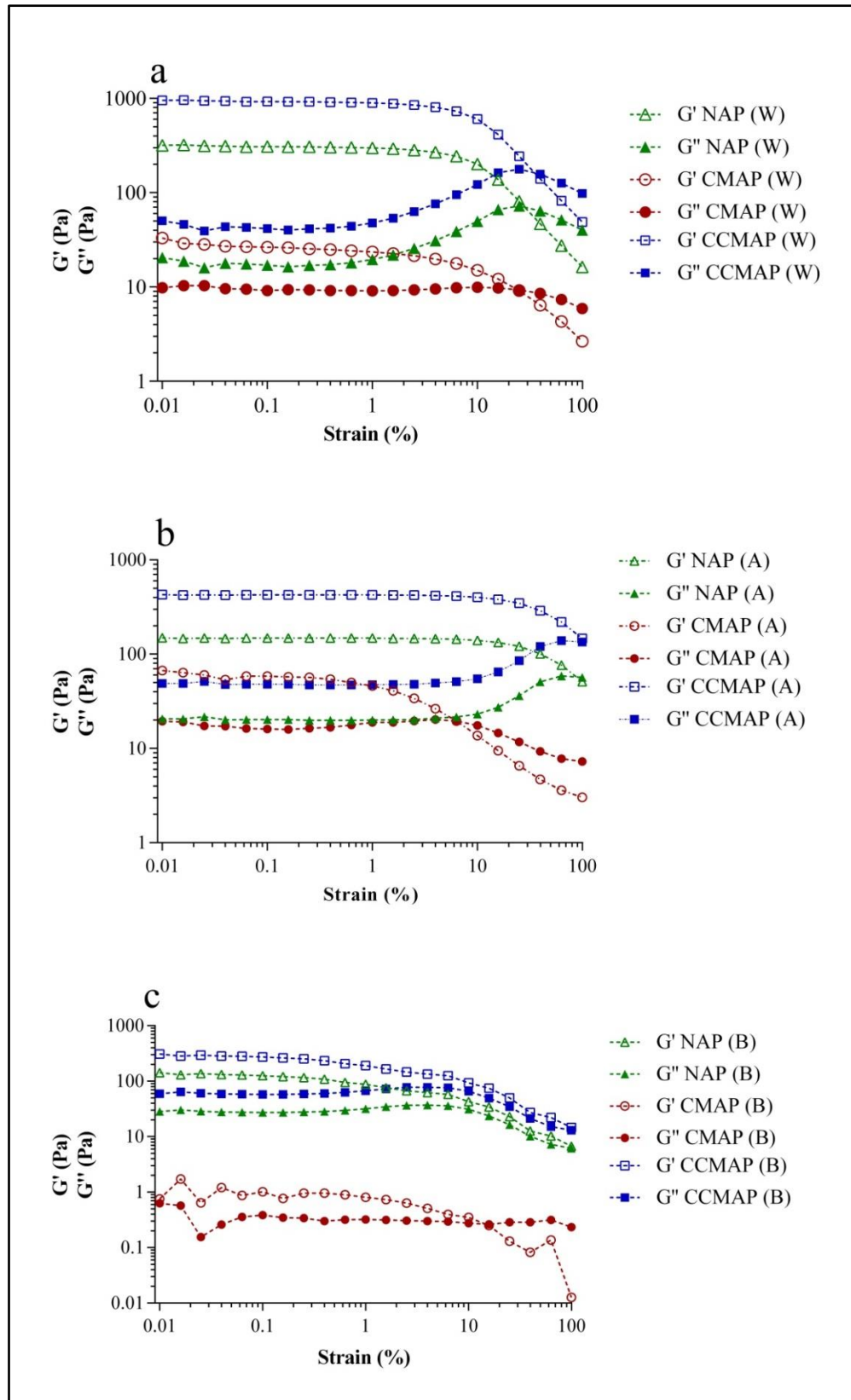


Figure 8.4: Amplitude sweep between (a) NAP-W, CMAP-W and CCMAP-W matrices; (b) NAP-A, CMAP-A and CCMAP-A matrices; (c) NAP-B, CMAP-B and CCMAP-B matrices

8.1.3.2. Frequency sweep

During the frequency sweep, the amplitude of the deformation is retained within the LVE, while the angular frequency (ω) is varied [Medina-Torres et al., 2000]. Variable oscillation frequencies make it possible to determine with greater precision the structural integrity, deformity, and rheological stability of a material. The higher values of G' over the G'' ($G' > G''$) indicate an elastic structure of material could be said to have a viscoelastic solid nature [Wang et al., 2021; Chakravorty A et al., 2016], while $G'' > G'$ impart the viscous behavior of the material could be said to have a viscoelastic [Kaboarani & Blanchet 2014]. The crossover point refers to the transition point at which the value of G' and G'' remains the same. For a material, before the crossover, if G' is higher than G'' , the crossover point could be considered as a deformation point. On the other hand, $G'' > G'$ remains before the crossover then it corresponds to a gel point [Rasid et al., 2021]. The higher differences between G' and G'' without crossing each other indicate the more rheological stability of a material.

The frequency sweep analysis was conducted on NAP, CMAP and CCMAP matrices as shown in Figure 8.5(a, b and c) and Figure 8.6(a, b and c). Based on the frequency sweep curve, it was observed that G' for NAP is much higher than G'' ($G' > G''$) in water and is also rheologically stable (Figure 8.5a). The values of G' for CMAP in water were also higher than G'' but in comparison to NAP, it was much less. At pH 1.2, NAP and CMAP were found to be stable and remain gel-like consistency, although G' values of NAP-A were lower than NAP-W (Figure. 8.5a). In case of CMAP at pH 1.2, the G' values were drastically higher than CMAP in water. However, both polymers were structurally deformed at pH 6.8 (Figure. 9c), as they have shown crossover points (NAP at 15.8 Rad/sec, CMAP at 25 Rad/sec). The appearance of any crossover region indicated the transformation of gel to sol. Moreover, the frequency sweep results indicated that NAP in water formed high entanglements and behaved as a strong viscoelastic gel than acidic pH. While at pH 6.8, the entanglements became weak. In contrast, CMAP at acidic pH has shown gel-like behavior, and ultimately, at pH 6.8, it lost its elastic energy and exhibited a weak gel with a disentangled structure. As the pH of the solution increased, there is a possibility that the functional groups ($-\text{COOH}-$) of CMAP would be ionized, leading to electrostatic repulsion and thus an increase in molecular dimension and a decrease

in entanglements [Medina-Torres et al., 2000]. However, there is also the possibility that the polymer chains would be de-polymerized as the pH advances [Achi & Okolo 2004]. Moreover, throughout the frequency sweep study it has been also noted that in all cases, G' values of NAP were always higher than CMAP (Figure 8.6).

The frequency sweep analysis of CCMAP revealed significantly higher G' (storage modulus) values compared to those of NAP and CMAP, as depicted in Figure 8.6 a, b, and c. Notably, the G' values consistently exceeded G'' (loss modulus) for the CCMAP matrices ($G' > G''$). The substantial disparity between G' and G'' in the frequency sweep curves, without any crossover between the two, indicated a heightened level of rheological stability for the CCMAP matrices when compared to NAP and CMAP matrices. This disparity underscored the presence of a robust viscoelastic structure in CCMAP.

The pronounced elevation of G' over G'' ($G' > G''$) in CCMAP matrices is a strong indicator of the viscoelastic nature of the material. This enhanced structural integrity can be attributed to the extensive entanglement within the CCMAP matrices, resulting from the cross-linking process.

8.1.3.3. Viscoelastic Behavior Analysis of Polymers via Frequency Sweep Data

The plotted data of G'' (Pa) against G' (Pa) at different angular frequencies for NAP, CMAP, and CCMAP polymer matrices across various pH levels showcased distinctive trends (Figure 8.7). The R-square values obtained from these plots serve as indicators of the goodness of fit for the linear relationship between G' and G'' within each matrix at different pH levels.

For the NAP polymer matrix, the R-square values were 0.893 for NAP W, 0.939 for NAP A, and 0.823 for NAP B. These values suggest a reasonably strong linear correlation between the storage and loss moduli for NAP at different pHs. Similarly, within the CMAP polymer matrix, the R-square values were 0.994 for CMAP W, 0.985 for CMAP A, and 0.857 for CMAP B, indicating robust linear relationships between G' and G'' across varying pH conditions.

In contrast, the CCMAP polymer matrix exhibited R-square values of 0.848 for CCMAP W, 0.913 for CCMAP A, and 0.784 for CCMAP B. These slightly lower R-square values, especially for CCMAP B, imply a comparatively weaker linear association between G' and G'' within the CCMAP matrix at pH 6.8.

The variations in R-square values across pH conditions within each polymer matrix indicate potential alterations in the linear relationship between the storage and loss moduli concerning changes in pH. It's notable that while NAP and CMAP matrices demonstrated relatively higher R-square values, indicating a stronger linear relationship, the CCMAP matrix, especially at pH 6.8 (CCMAP B), displayed a slightly diminished linear correlation between G' and G'' .

These findings suggest that the viscoelastic behavior within the CCMAP matrix might be more sensitive to pH changes compared to the NAP and CMAP matrices. The slight decrease in the goodness of fit at higher pH for CCMAP could signify alterations in the viscoelastic properties concerning pH variations.

The strong linear correlations implies that NAP and CMAP exhibited less disparity between its elastic and viscous properties across the tested angular frequencies, resulting in a more balanced and less viscoelastic behavior.

On the other hand, the lower R^2 values for CCMAP indicates a less perfect linear relationship between G' and G'' , signifying a larger disparity between its storage and loss moduli. This suggests that CCMAP showcased more significant differences between its elastic and viscous properties at various angular frequencies, demonstrating higher viscoelasticity.

The lower R^2 values for NAP B, CMAP B, and CCMAP B compared to their counterparts at other pH levels indicate a departure from the expected linear relationship between G' and G'' . These lower R-square values signify a reduced goodness of fit in describing the linear correlation between the storage and loss moduli for these polymers at pH 6.8.

Despite showing non-linearity at pH 6.8, with crossover between G' and G'' , these polymers also exhibited notably lower values of G' compared to other pH levels. This deviation from a strong linear relationship and the substantially lower values of G' could imply a deviation from typical viscoelastic behavior.

In the frequency sweep analysis, the observation of deformation in NAP B, CMAP B, and CCMAP B at pH 6.8 further supports the inference drawn from the R-square values. This deformation, along with the lowered R-square values, suggests that at pH 6.8, these polymers display behaviors that deviate from traditional viscoelastic properties observed at other pH levels.

The presence of crossover between G' and G'' in these polymers at pH 6.8 indicates a change in their response but doesn't necessarily confirm their viscoelastic nature, especially considering the notably low values of G' . Therefore, despite exhibiting non-linear behavior, the reduced R-square values and lower G' values suggest that NAP B, CMAP B, and CCMAP B at pH 6.8 may not conform to typical viscoelastic characteristics observed at other pH levels.

The R^2 values from G' versus G'' plots give insights into how NAP, CMAP, and CCMAP polymers behave at different pH levels. NAP and CMAP show stronger linear relationships between their elastic and viscous properties across pH conditions. However, CCMAP, especially at pH 6.8, displays weaker linear associations between G' and G'' . This suggests pH sensitivity in its viscoelastic behavior. At pH 6.8, NAP B, CMAP B, and CCMAP B have lower R-square values, showing less typical viscoelastic behavior, despite non-linear trends and reduced G' values. This challenges their viscoelastic nature at pH 6.8, indicating changes in how they respond to that specific pH condition.

For NAP, the best fit slope values were 0.2884 for NAP W (water), 0.1293 for NAP A (pH 1.2), and 0.0963 for NAP B (pH 6.8). Interestingly, these values indicate varying degrees of slope, suggesting differing viscoelastic properties across pH conditions. Similarly, in the case of CMAP, the best fit slopes for CMAP W, CMAP A, and CMAP B were 0.662, 1.083, and 0.1024, respectively, highlighting notable differences in viscoelasticity across different pH environments.

Furthermore, for CCMAP, the best fit slopes for CCMAP W, CCMAP A, and CCMAP B were 0.254, 0.0744, and 0.1047, respectively. These values showcase intriguing contrasts, especially noting the markedly low slope for CCMAP A,

suggesting a distinct viscoelastic behavior compared to the other pH levels within the same matrix.

The phase angle (δ) is defined as $\tan\delta = G''/G'$, providing an indication of the balance between the elastic and viscous components of a material. While the relationship between the best fit slope values and the phase angle can provide insights, directly determining the phase angle solely from the slope values might be challenging due to the non-linear nature of the relationship between G' and G'' (Ramli et al., 2022).

The observed differences in best fit slope values across pH conditions for each matrix suggest alterations in their viscoelastic characteristics concerning pH variations. It's notable that certain pH environments appear to influence the viscoelastic behavior of these matrices differently, as evidenced by the varying slopes.

In summary, the plotted data and best fit slope values highlight distinct viscoelastic behaviors among the NAP, CMAP, and CCMAP polymer matrices at different pH levels. The variations in slope values across pH conditions hint at the pH-sensitive nature of their viscoelastic properties, underscoring the complex interplay between pH environments and the viscoelastic behavior of these polymer matrices.

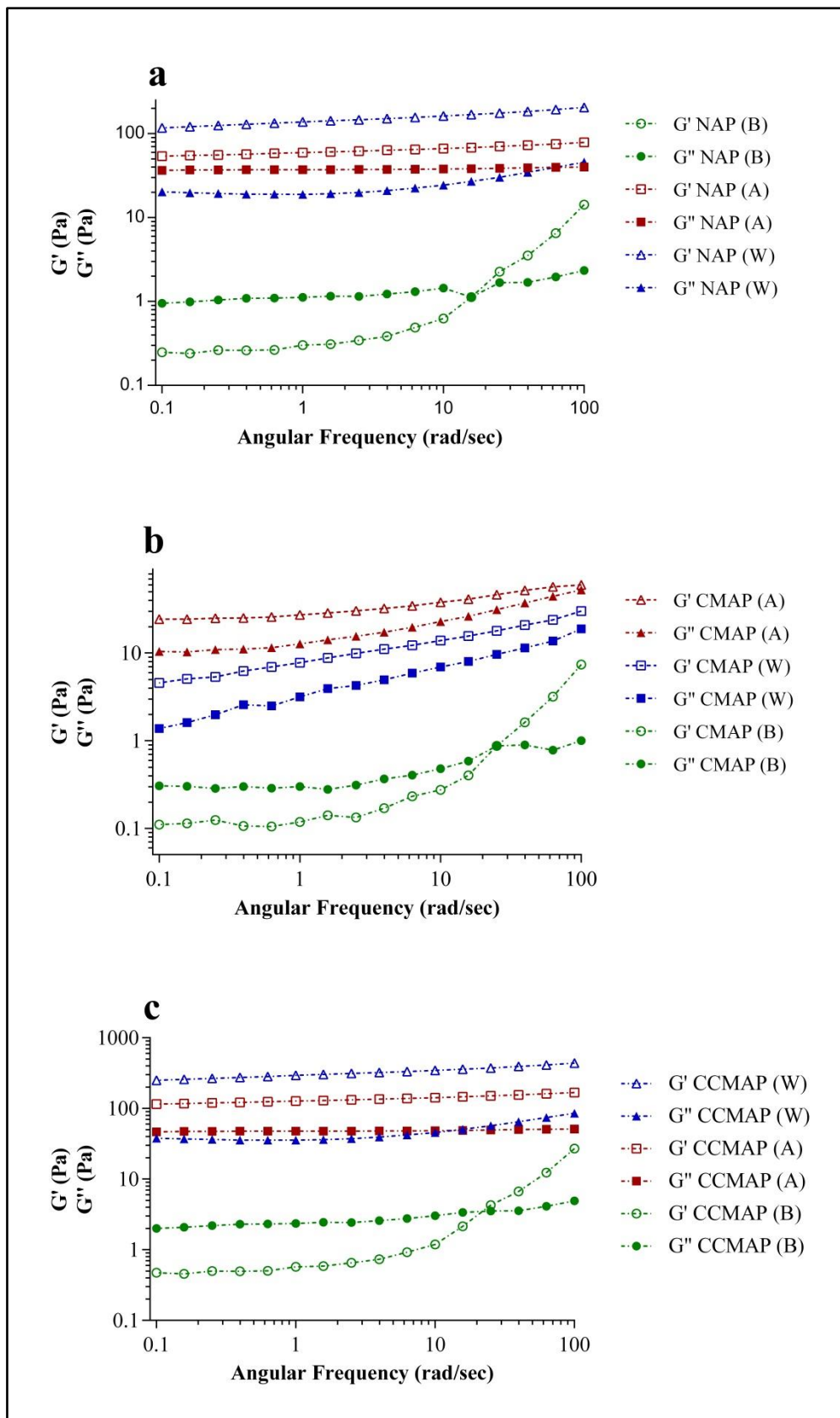


Figure 8.5: Frequency sweep of (a) NAP, (b) CMAP and (c) CCMAP in water, acidic solution (pH 1.2) and PB solution of pH 6.8.

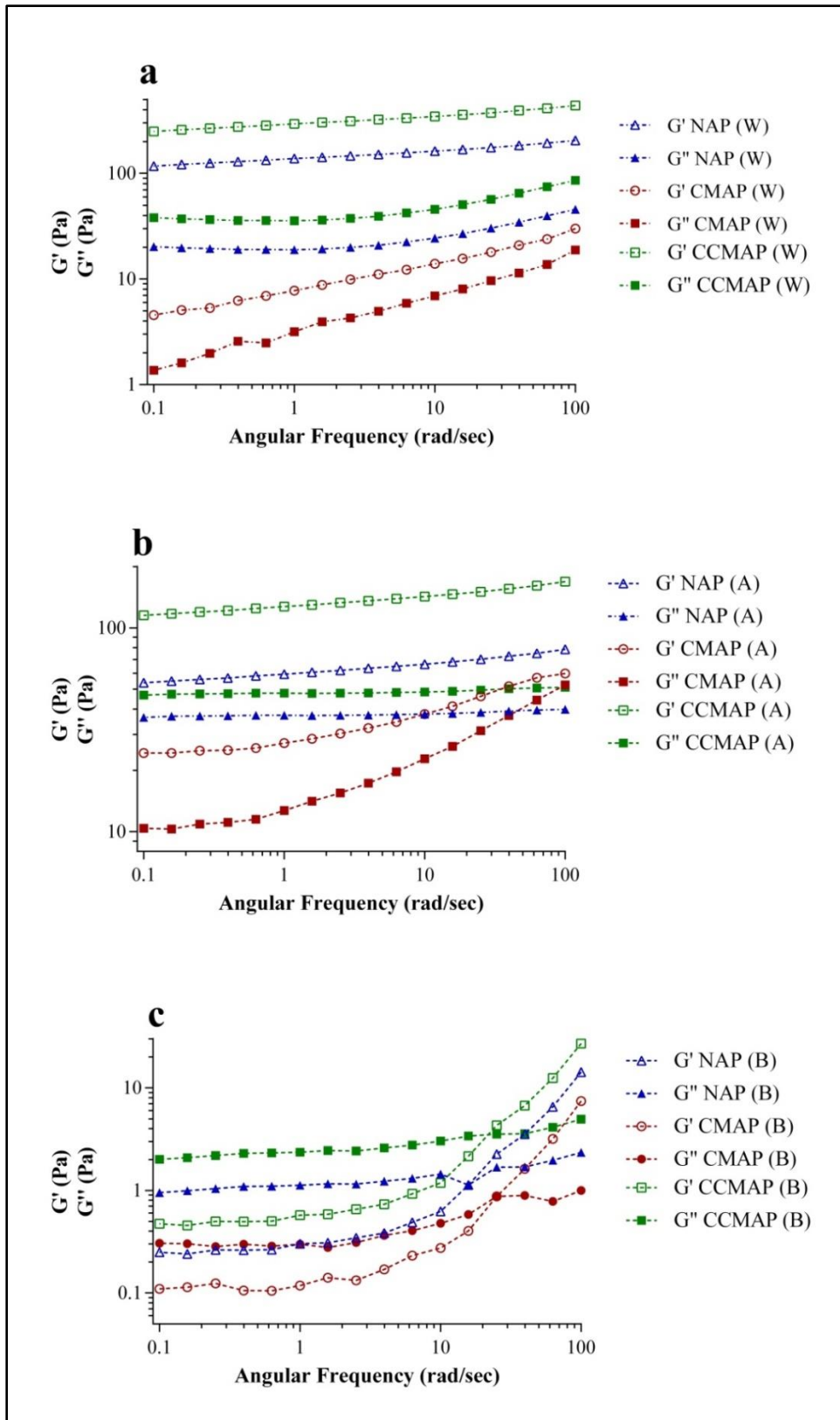


Figure 8.6: Frequency sweep between (a) NAP-W, CMAP-W and CCMAP-W matrices; (b) NAP-A, CMAP-A and CCMAP-A matrices; (c) NAP-B, CMAP-B and CCMAP-B matrices

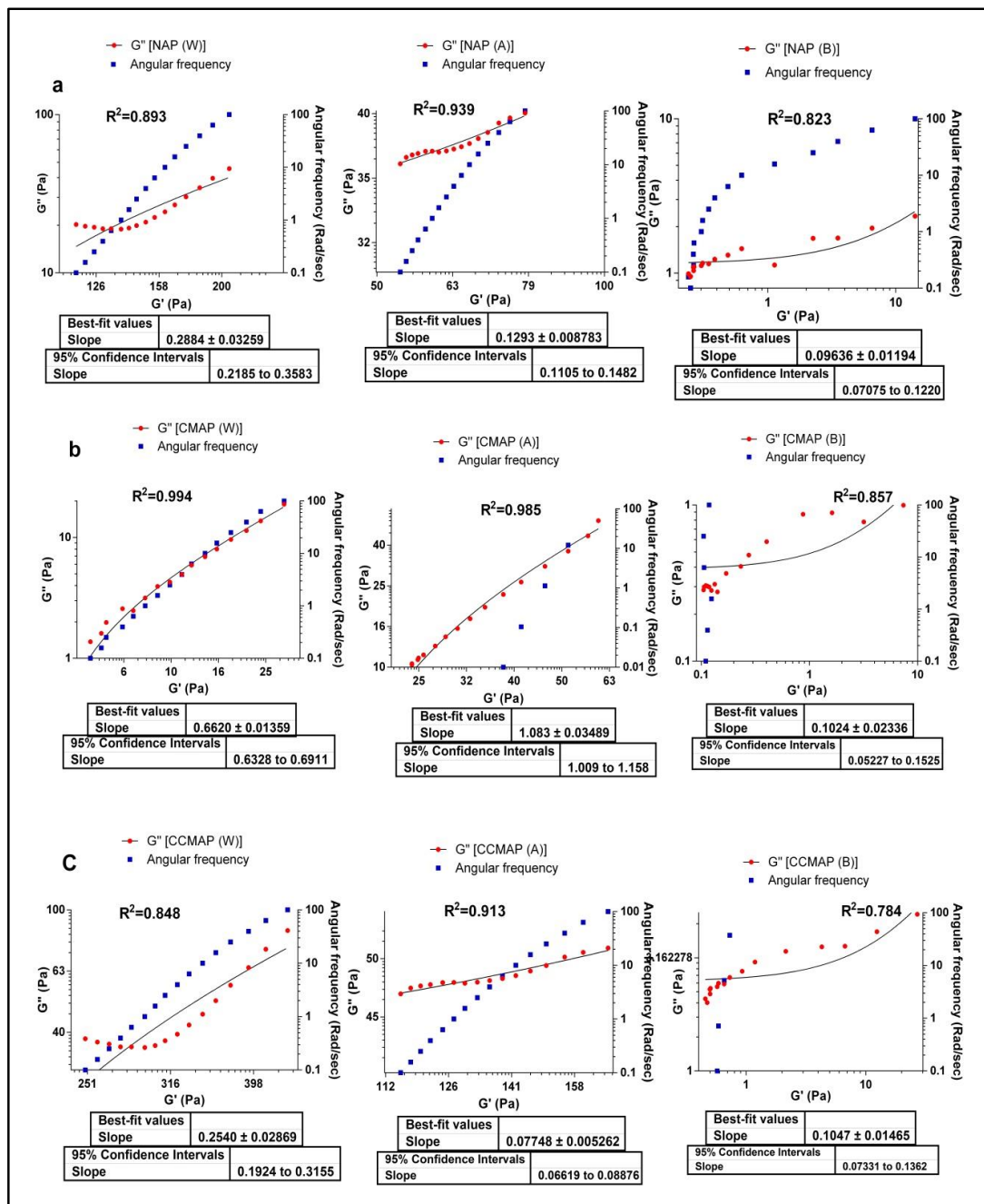


Figure 8.7: Angular frequency-dependent relationship between G'' and G' in (a) NAP matrices: NAP (W), NAP (A), NAP (B); (b) CMAP matrices: CMAP (W), CMAP (A), CMAP (B); (c) CCMAP matrices: CCMAP (W), CCMAP (A), CCMAP (B)

8.2. Damping factor

In the study of polymer melts, incorporating a damping function is crucial for comprehending the complexities of nonlinear viscoelasticity. This function, known as the loss tangent ($\tan\delta = G''/G'$), serves as a key parameter for evaluating internal frictions within materials [Rolón-Garrido & Wagner 2009]. Understanding the value of the loss tangent is vital as it provides valuable insights into the elasticity and viscosity of the materials under investigation. Specifically, certain values of $\tan\delta$ hold specific implications: when $\tan\delta=0$, the material is ideally elastic; when $\tan\delta =100$, the material is ideally viscous; when $\tan\delta>1$, the material is more viscous than elastic; when $\tan\delta<1$, the material is more elastic than viscous; and when $\tan\delta=1$, the material is considered viscoelastic [Wang et al., 2022].

Through an in-depth analysis of the damping function across different pH levels for NAP, CMAP, and CCMAP, insights were gleaned from the experimental results. Figure 8.8 illustrates that the loss tangents ($\tan\delta$) for CCMAP-W, NAP-W, and CMAP-W were all less than 1. Notably, the mean $\tan\delta$ value for CMAP-W (0.56) was higher than that of CCMAP-W (0.14) and NAP-W (0.16), indicating that CCMAP and NAP were more elastic in water compared to CMAP. A similar trend was observed at pH 1.2, where all polymers displayed elastic deformation. At this pH, CMAP ($\tan\delta=0.45$) exhibited slightly more elasticity than CMAP-W, while CCMAP at pH 1.2 ($\tan\delta=0.35$) and NAP at pH 1.2 ($\tan\delta=0.59$) remained less elastic compared to CCMAP-W and NAP-W. Moreover, all polymers demonstrated viscous behavior at pH 6.8, with the loss tangents exceeding 1.

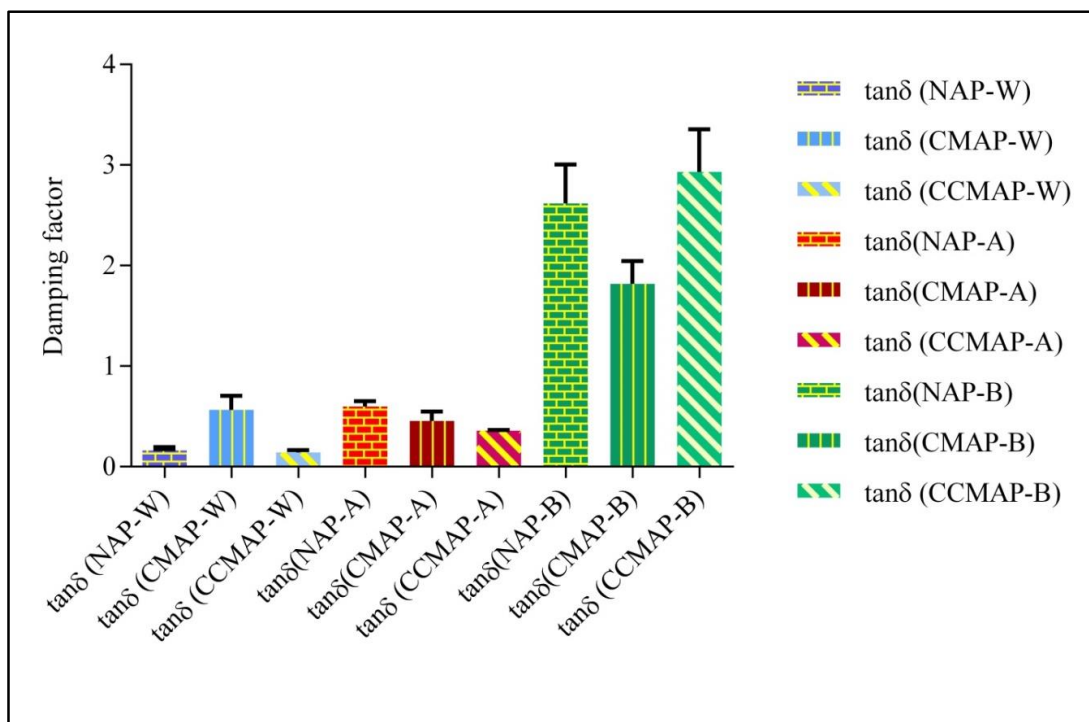


Figure 8.8: Damping factor of NAP, CMAP and CCMAP

Conclusion:

Based on the comprehensive analysis of various rheological parameters for NAP, CMAP, and CCMAP matrices, several important findings have been discerned. Notably, NAP and CCMAP exhibited robust viscoelastic gels characterized by high viscosity levels owing to their extensive entanglements. The presence of a stronger gel structure in CCMAP, surpassing that of NAP, can be attributed to the crosslinking facilitated by calcium ions. These crosslinking interactions effectively limit the mobility of the polymer chains, leading to a substantial increase in viscosity and the formation of viscoelastic gels.

In contrast, CMAP matrices demonstrated a weaker gel formation with lower viscosity and a shorter linear viscoelastic (LVE) region. The observed weak gel structure can be linked to the coulombic repulsion between the chains containing -COO^- groups. This repulsion leads to faster disentanglement, resulting in reduced viscosity levels. Furthermore, CMAP matrices were found to be rheologically

unstable, indicating a comparatively lower structural integrity when compared to CCMAP and NAP matrices.

An intriguing observation emerged during the evaluation of viscosity levels across different pH conditions. CCMAP and NAP matrices displayed higher viscosities at neutral pH than in acidic and buffer environments. In contrast, CMAP matrices exhibited slightly higher viscosities at pH 1.2 than in water and buffer solutions. This observation indicates the varying rheological responses of the matrices to changes in pH levels, with CMAP matrices showcasing a nuanced and relatively unstable behavior.

Considering the implications of these findings, it is predicted that the rheological characteristics and structural integrity of the matrices, particularly CCMAP, could significantly influence the drug release profiles when utilized in pharmaceutical formulations. The high mechanical strength and robust gel formation in CCMAP matrices, driven by the presence of calcium ions, suggest the potential for controlled and sustained drug release applications. Additionally, the contrasting rheological behaviors of CMAP matrices underscore the necessity for careful consideration of their application in drug delivery systems, particularly with regard to the stability and efficacy of the immediate drug release profile. Further investigations into the interaction between these matrices and specific drug compounds are warranted to fully comprehend and harness their potential in pharmaceutical formulations.

CHAPTER 9

PRE-FORMULATION EVALUATION

PRE-FORMULATION EVALUATION

9.1. Drug – Polymers Interaction Studies

9.1.1. Metformin-polymer FTIR compatibility study

The FTIR spectroscopy analysis conducted on the drug, Metformin (MET), and the drug-polymer mixtures offers valuable insights into the molecular interactions and structural changes within the composite materials. Figure 9.1a and b exhibit the FTIR spectra of the drug and the drug-polymer blend, respectively, providing a comprehensive view of the characteristic absorption bands and their corresponding wavenumbers.

In the FTIR spectrum of Metformin (Figure 9.1a), the distinctive absorption bands observed at 3374, 3309, and 3172 cm^{-1} were attributed to the amine N—H stretching vibrations. Notably, the absorption bands for N—H bonds in amines were relatively less intense compared to those of O—H bonds, reflecting the lower polarity of the former. Metformin displayed characteristic bands at 1626 and 1570 cm^{-1} , corresponding to C—N and C=N functional groups, respectively. It is important to note that the absorption bands within the 1626-1570 cm^{-1} range were also associated with N—H bending vibrations [Moradi et al., 2021]. Additionally, the absorption bands at 1170 and 1064 cm^{-1} were indicative of C—N stretching, while the band at 1476 cm^{-1} denoted C—H bending.

Remarkably, the FTIR spectrum obtained from the MET-polymer mixtures (Figure 9.1b) showcased the presence of all the characteristic bands of the drug at nearly the same wavelengths as in the pure MET spectrum [Smaeel & Al-Bayati 2021]. This observation suggests the absence of significant chemical interactions or structural modifications between Metformin and the polymer components. The

retention of the characteristic bands in the composite material highlights the maintenance of the inherent molecular structure of Metformin in the presence of the polymers, signifying a lack of substantial chemical bonding or alterations in the functional groups of the drug. These findings provide crucial insights into the compatibility and potential suitability of the selected polymers for drug delivery applications involving Metformin.

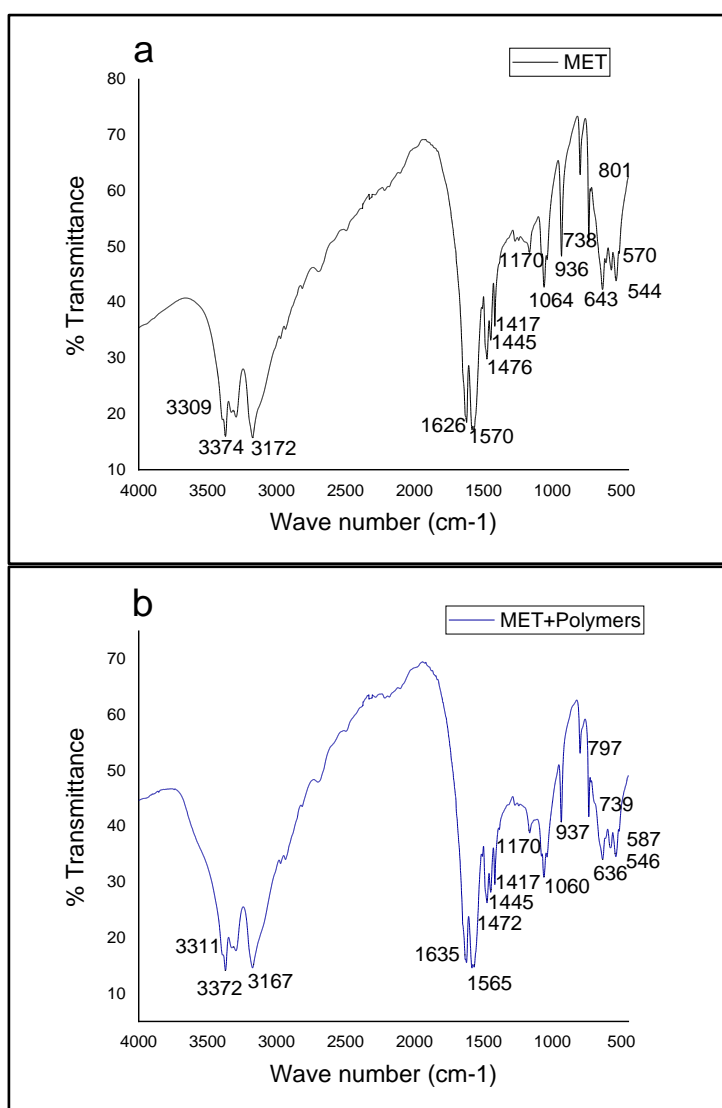


Figure 9.1: FTIR spectrum of (a) Metformin, (b) Metformin-polymer mixture

9.1.2. Metformin-polymer thermal compatibility study

The use of differential scanning calorimetry (DSC) studies serves as a valuable method for understanding the potential interactions between a drug and various excipients. Figure 9.2a and b depict the melting points of Metformin (MET) and its physical mixtures with NAP, CMAP, and CCMAP, offering critical insights into the thermal behavior and compatibility of the drug with the respective polymers.

The data analysis revealed that the melting point of MET, recorded at 222.37°C, was consistent across all of the polymer mixtures, closely resembling its reported value of 221.63°C [Rostamkalaei et al., 2019], as indicated in previous studies. Although there were minor reductions observed in the endothermic peak intensity, the melting point of MET in the presence of each of the examined polymers remained relatively unchanged. These results suggest the absence of any significant thermal interactions between the drug and the polymer components.

The unaltered melting point of MET in the presence of NAP, CMAP, and CCMAP, alongside the similarity in the observed values to the reported melting point of the drug, underscores the compatibility and inert nature of the chosen excipients with Metformin. The findings suggest that the polymers, namely NAP, CMAP, and CCMAP, do not exert any notable impact on the thermal characteristics of Metformin, further indicating their potential suitability for use as excipients in drug delivery systems without compromising the thermal stability or properties of the active pharmaceutical ingredient.

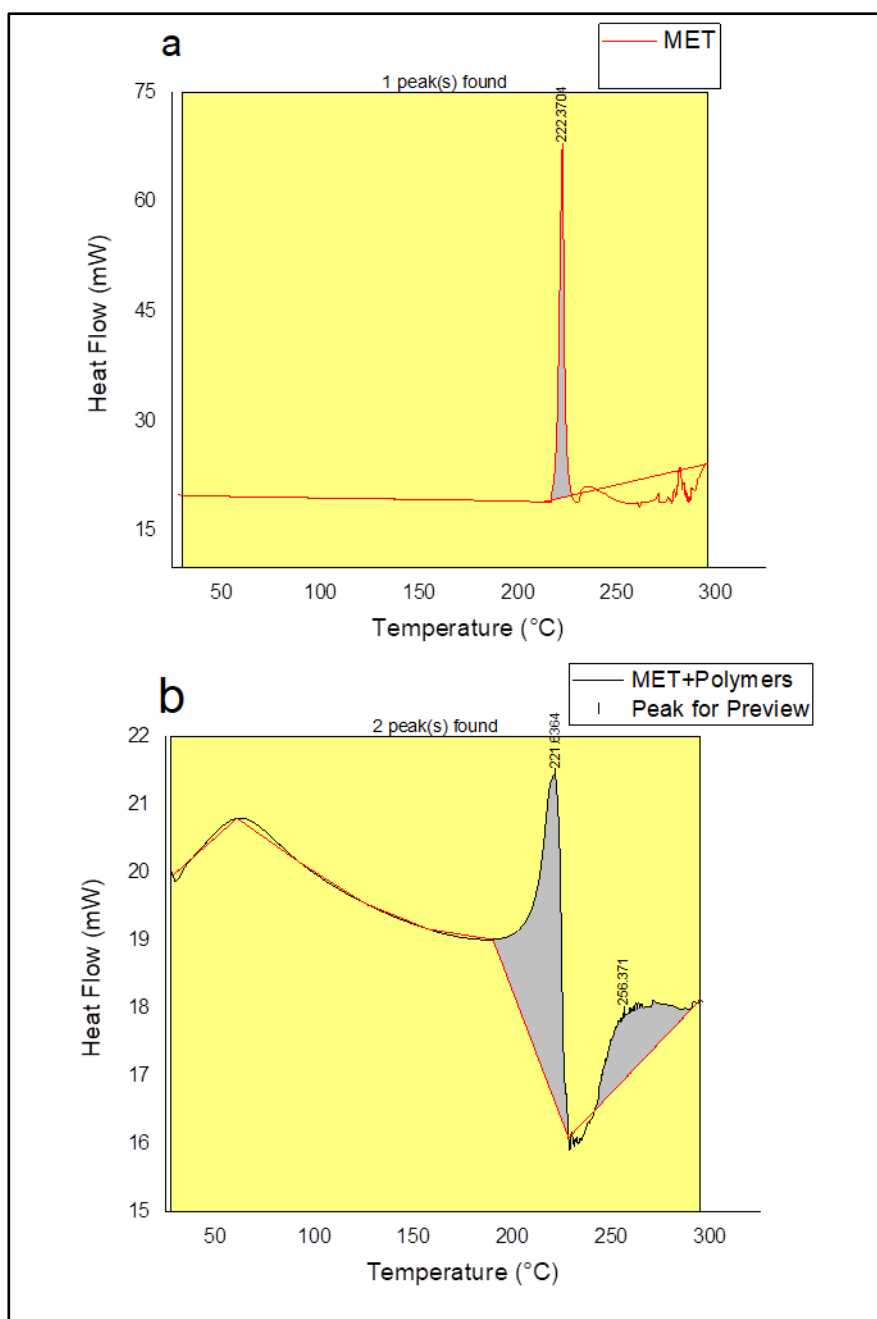


Figure 9.2: DSC thermogram of (a) MET and (d) MET with polymer mixtures

9.1.3. DIL-polymer FTIR compatibility study

Figure 9.3 (a and b) showcases the FT-IR spectra of Diltiazem HCl (DIL) and its mixtures with polymers. In Figure 9.3a, the distinct IR absorption bands corresponding to Diltiazem HCl were observed at specific wave numbers: 3397.57 cm^{-1} (N—H stretch in amine groups) [31], 3034.09, 3002.50, 2939.66 cm^{-1} (C—H stretch), 2385.42, 1738.34 cm^{-1} (C=O stretch), 1675.32 cm^{-1} (C=C stretch), and 1604.70, 1579.76 cm^{-1} for C=C stretch vibrations.[32] Additionally, bands at 1508.67, 1472.10, 1443.94, 1410.37, 1375.21, 1319.68, 1213.06, 1055.08 cm^{-1} (C—N stretch), and 1022.84 cm^{-1} (C—N stretch) were identified. In close similarity, Figure 9.3b portrays the IR absorption bands of DIL combined with polymer mixtures, exhibiting bands at 3328.91, 3055.78, 3003.55, 2916.26, 2382.93, 1742.46, 1679.58, 1606.61, 1582.14, 1538.51, 1510.19, 1473.58, 1444.51, 1412.89, 1400.34, 1217.27, 1058.08, and 1026.47 cm^{-1} .

The consistency of the characteristic peaks of Diltiazem HCl in the mixed spectra suggests the absence of significant alterations in the drug-polymer interactions [Krishan et al., 2020]. These findings indicate a harmonious compatibility between DIL and the respective polymers, signifying a lack of substantial chemical or molecular modifications induced by the presence of the polymer matrices. The retention of the specific peaks at their respective wavelengths suggests a stable and non-disruptive association between the drug and the polymer components, further confirming the suitability of the polymers as potential carriers or excipients in Diltiazem HCl formulations.

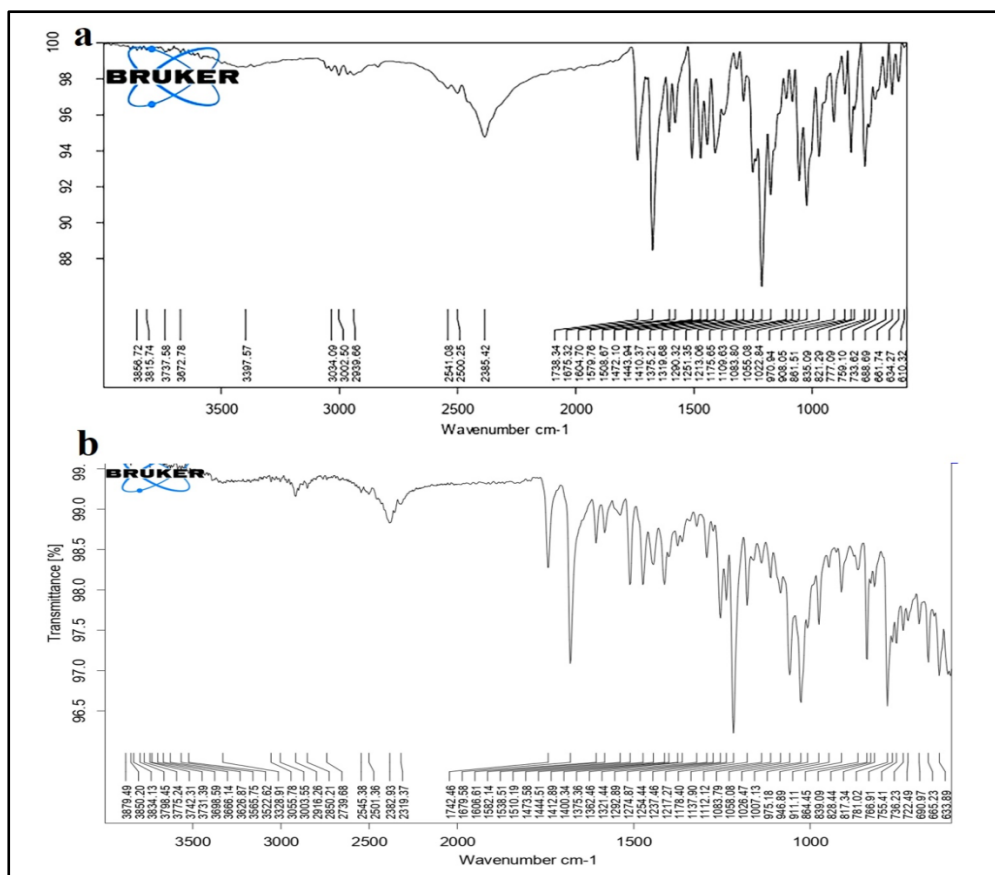


Figure 9.3: FT-IR spectrum of (a) DIL and (b) DIL with polymer mixtures

9.1.4. DIL-polymer thermal compatibility study

The examination of differential scanning calorimetry (DSC) curves for pure Diltiazem HCl (DIL) and DIL combined with polymer mixtures offers valuable insights into the thermal behavior of the drug in the presence of various polymers. Figure 9.4a and b depict the endothermic peaks observed in both cases, highlighting the melting behavior of DIL and the potential influence of polymers on its thermal properties.

In Figure 9.4a, the endothermic peak observed at approximately 216.7 °C is indicative of the melting point of pure DIL. This characteristic peak reflects the temperature at which DIL transitions from a solid to a liquid state, representing a well-defined and intrinsic property of the drug. However, when DIL is introduced to polymer mixtures, as illustrated in Figure 9.4b, a similar endothermic peak emerges at a slightly lower temperature, around 215.89 °C. This shift in the

melting point indicates the physical impact of the presence of polymers on the thermal behavior of DIL. However, the proximity of the peak in the DIL-polymer mixture to the melting point of pure DIL suggests that these interactions do not significantly alter the fundamental melting behavior of DIL [Patil & Jat 2019]. Consequently, this finding underscores the compatibility of the polymers with DIL, suggesting their potential suitability as carriers or excipients for Diltiazem HCl formulations, with minimal impact on the drug's thermal properties.

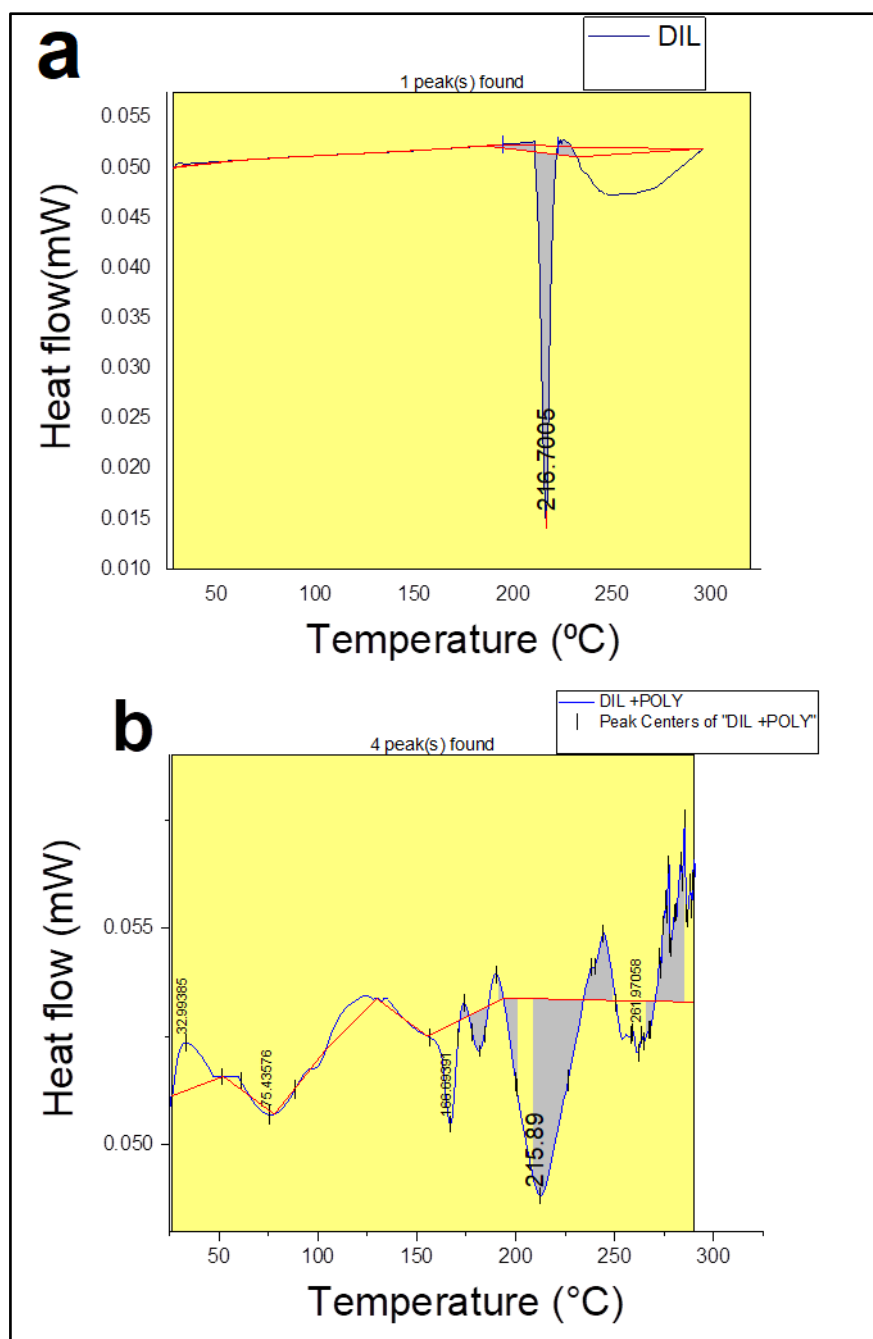


Figure 9.4: DSC thermogram of (a) DIL and (b) DIL with polymer mixtures

9.2. Evaluation of Micromeritic properties of polymeric granules

The maintenance of appropriate physical properties of granules is crucial for ensuring the efficacy and stability of pharmaceutical formulations. To assess the quality of the granules, various parameters were evaluated. The moisture content of the granules was maintained at 3-5%, ensuring favorable flowability by preventing adhesion. Additionally, the determination of bulk density, tapped density, Carr's index, and Hausner ratio aided in understanding the granules' compressibility and flow properties, as outlined in Table 9.1.

Evaluation of the angle of repose, a key parameter for understanding granular flow properties, revealed values less than 30° for all polymers, indicating favorable flow characteristics [Wells & Aulton 1988]. Further support was provided by the low compressibility index values, depicted in the table. The Carr's index values, which fell within the range of up to 15%, further affirmed the satisfactory flow properties of the granules [Wells & Aulton 1988]. These findings collectively suggest that the granules possessed favorable flow properties and compressibility, crucial for their successful processing and manufacturing as pharmaceutical formulations.

The tabulated results in Table 9.1 provide a comprehensive overview of the micromeritic properties of the granules for various polymers, including NAP, CMAP, and CCMAP. The data serves as a valuable reference for evaluating the quality and suitability of the granules for potential use in pharmaceutical formulations, indicating their favorable characteristics for processing and manufacturing applications.

Table: 9.1: Micromeritic properties of granules

<i>Polymers</i>	<i>Angle of Repose (θ) (Degree)*</i>	<i>Bulk Density (gm/ml)*</i>	<i>Tapped Density (gm/ml)*</i>	<i>Carr's Index (%)*</i>	<i>Hausner Ratio*</i>
NAP	26.26 \pm 0.5	0.53 \pm 0.08	0.62 \pm 0.08	14.51 \pm 1.35	1.169 \pm 0.061
NAP+MET	27.44 \pm 0.06	0.49 \pm 0.07	0.58 \pm 0.04	15.51 \pm 1.21	1.183 \pm 0.04
NAP+DIL	28.09 \pm 0.04	0.59 \pm 0.08	0.69 \pm 0.08	14.49 \pm 1.60	1.169 \pm 0.032
CMAp	25.77 \pm 0.06	0.46 \pm 0.03	0.57 \pm 0.04	19.29 \pm 1.35	1.239 \pm 0.029
CMAp+MET	28.55 \pm 0.07	0.45 \pm 0.08	0.56 \pm 0.07	19.64 \pm 1.21	1.244 \pm 0.025
CMAp+DIL	25.63 \pm 0.08	0.47 \pm 0.04	0.58 \pm 0.05	18.96 \pm 2.21	1.234 \pm 0.023
CCMAp	28.73 \pm 0.04	0.51 \pm 0.02	0.63 \pm 0.05	19.04 \pm 1.87	1.235 \pm 0.027
CCMAp+MET	29.88 \pm 0.03	0.55 \pm 0.03	0.65 \pm 0.03	15.38 \pm 1.62	1.181 \pm 0.035
CCMAp+DIL	29.57 \pm 0.03	0.58 \pm 0.04	0.68 \pm 0.05	14.70 \pm 2.05	1.172 \pm 0.041

*n=3

The micromeritic properties, as revealed by the data in the table, provide crucial insights into the flow properties and compressibility of the granules for various polymer formulations including NAP, CMAp, and CCMAp in combination with Metformin (MET) and Diltiazem HCl (DIL).

NAP granules exhibited an angle of repose of 26.26°, indicating favorable flow properties. The bulk density of NAP granules was 0.53 gm/ml, while the tapped density was 0.62 gm/ml, resulting in a Carr's index of 14.51% and a Hausner ratio of 1.169. These values suggest good flow properties and compressibility, making NAP a promising candidate for further pharmaceutical applications.

In the case of CMAp, the angle of repose was slightly lower at 25.77°, implying relatively better flow properties than NAP. However, CMAp exhibited a slightly lower bulk density of 0.46 gm/ml and a tapped density of 0.57 gm/ml, resulting in a higher Carr's index of 19.29% and a Hausner ratio of 1.239. These values

suggest that CMAP granules might have slightly reduced flow properties and increased compressibility compared to NAP.

For CCMAP, the angle of repose was found to be 28.73° , indicating somewhat poorer flow properties compared to NAP and CMAP. The bulk density for CCMAP was 0.51 gm/ml, and the tapped density was 0.63 gm/ml, resulting in a Carr's index of 19.04% and a Hausner ratio of 1.235. These values suggest that CCMAP granules might have slightly compromised flow properties and increased compressibility relative to both NAP and CMAP.

Moreover, the addition of MET and DIL to the polymer matrices resulted in some variations in the micromeritic properties, indicating potential influences of the drug formulations on the overall flow properties and compressibility of the granules.

9.3. Evaluation of placebo matrix tablets

9.3.1. Physical characteristics of tablet

The physical attributes of the tablets fell within acceptable parameters. A comprehensive comparison of these physical characteristics for each formulation is provided in Table 9.2.

Table 9.2: Physical characteristics of placebo tablets

<i>Placebo tablets containing polymer</i>	<i>Average weight (mg) (N=20)</i>	<i>Hardness (Newton/cm²) (N=10)</i>	<i>Average thickness (mm) (N=10)</i>	<i>Average length (mm) (N=10)*</i>	<i>Average breadth (mm) (N=10)*</i>	<i>Friability (%) (N=20) *</i>
		*	*			
NAP (X1)	1115.8-1117.03 ± 1.98%	64.14-66.37 ± 0.054	5.86 - 6.13 ± 0.03	19.44 - 19.49 ± 0.017	8.98 - 9.01 ± 0.016	0.52- 0.62 ±0.024
CMAp (X2)	1113.8 - 1116.14 ± 2.47%	60.43-61.27 ± 0.022	5.96 - 6.14 ± 0.02	19.43 - 19.49 ± 0.013	8.99- 9.03 ± 0.018	0.55- 0.67 ±0.032
CCMAp (X3)	1116.03 - 1119.24 ± 2.17%	66.27-68.74 ± 0.045	5.89 - 6.0 ± 0.02	19.46 - 19.49 ± 0.011	9.01- 9.03 ± 0.013	0.45- 0.59 ±0.05

*n=3

9.4. Swelling and erosion study

9.4.1. Swelling study

The swelling characteristics of blank matrix tablets containing NAP (X1), CMAP (X2), and CCMAP (X3) were investigated in acidic (pH 1.2) and buffer (pH 6.8) environments, as demonstrated in Figure 9.5 (a and b). The data indicates distinct variations in the degree of swelling for these matrices under different pH conditions [Maity & Sa 2014].

In addition, the visualization provided in Figure 9.6 (a to f) offers a comprehensive representation of the dissolution characteristics and structural integrity of NAP, CMAP, and CCMAP tablets following exposure to dissolution media over varying time intervals (120 minute and 600-minute of dissolution period) . The images vividly illustrate the impact of dissolution on the physical appearance, formation of swollen layer and morphology of the tablets.

NAP tablets exhibited a moderate degree of swelling, lower than that of CMAP but higher than CCMAP in both acidic and buffer environments. This difference can be attributed to the varying degrees of crosslinking and entanglement within the matrices. Notably, the CCMAP tablets displayed the least swelling, which can be linked to the presence of calcium crosslinking, impeding rapid water penetration and limiting the degree of disentanglement within the CCMAP matrices.

Interestingly, CMAP tablets demonstrated a more rapid and significant degree of swelling in both acidic and buffer media. This behavior can be ascribed to the formation of a disentangled and less viscous gel layer in the presence of the aqueous environment, allowing for a higher rate of water influx. The Coulombic repulsion among the chain segments in CMAP further facilitated the increased disentanglement, contributing to its pronounced swelling behavior. Moreover, the rapid swelling exhibited by CMAP tablets, particularly in both acidic and buffer media, highlights the potential of CMAP for immediate drug release formulations.

The order of swelling, as observed from highest to lowest, was CMAP, NAP, and CCMAP, emphasizing the profound impact of crosslinking and entanglement on the swelling properties of these matrices. The slower rate of water uptake in

CCMAP matrices can be advantageous in specific drug delivery applications where controlled or sustained release is desirable. The ability to modulate swelling properties is vital in designing drug delivery formulations tailored to specific physiological conditions.

Taking these findings into consideration, future drug delivery formulation design could leverage the distinctive swelling behaviors of NAP, CMAP, and CCMAP matrices to create tailored drug release profiles based on the specific therapeutic requirements. The potential applications range from sustained release systems utilizing the slower swelling characteristics of CCMAP to immediate release systems benefitting from the rapid and pronounced swelling exhibited by CMAP. These insights pave the way for the development of advanced and versatile drug delivery systems serving to diverse medical needs.

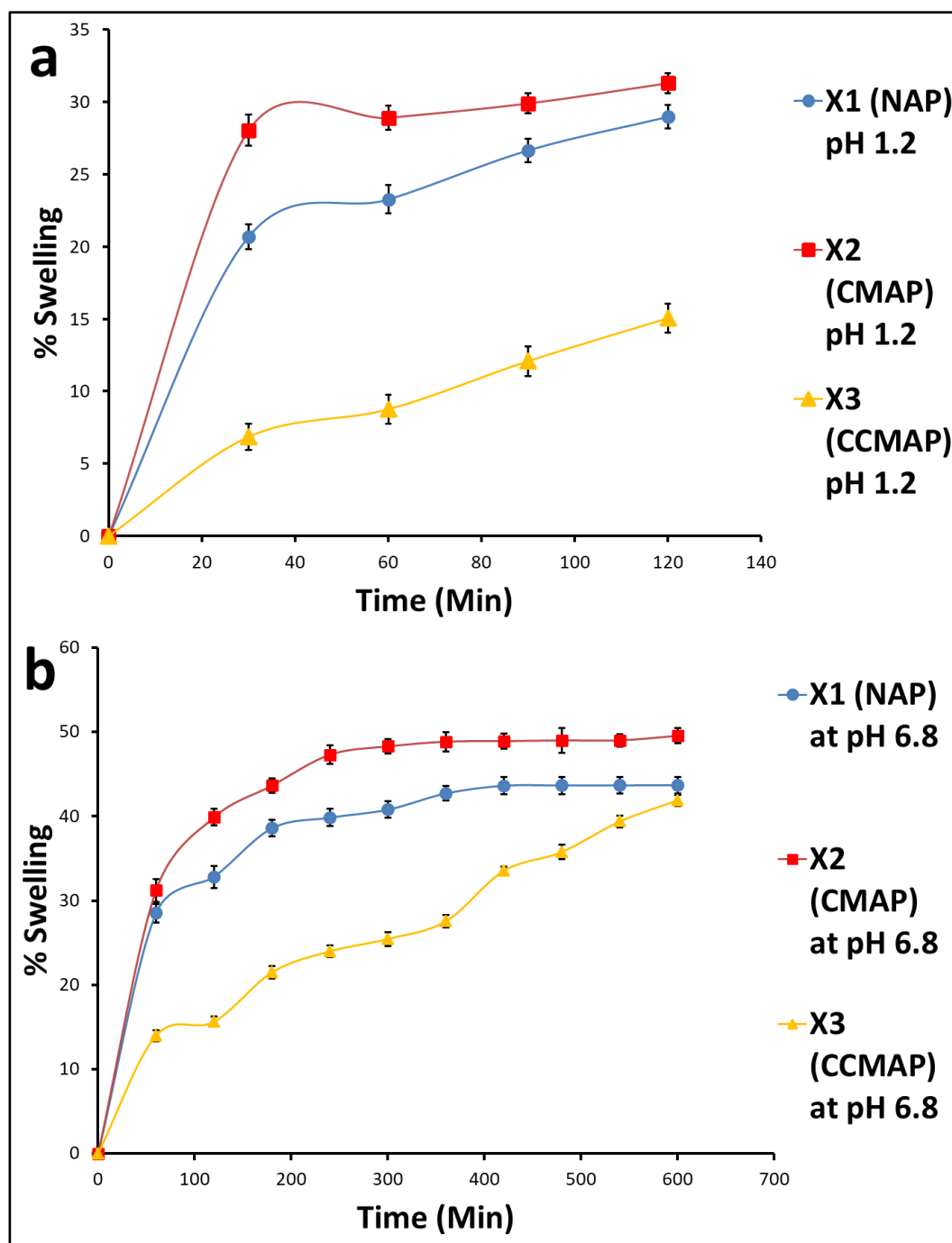


Figure 9.5: Swelling (%) of NAP, CMAP and CCMAP: (a) at pH 1.2, (b) at pH 6.8

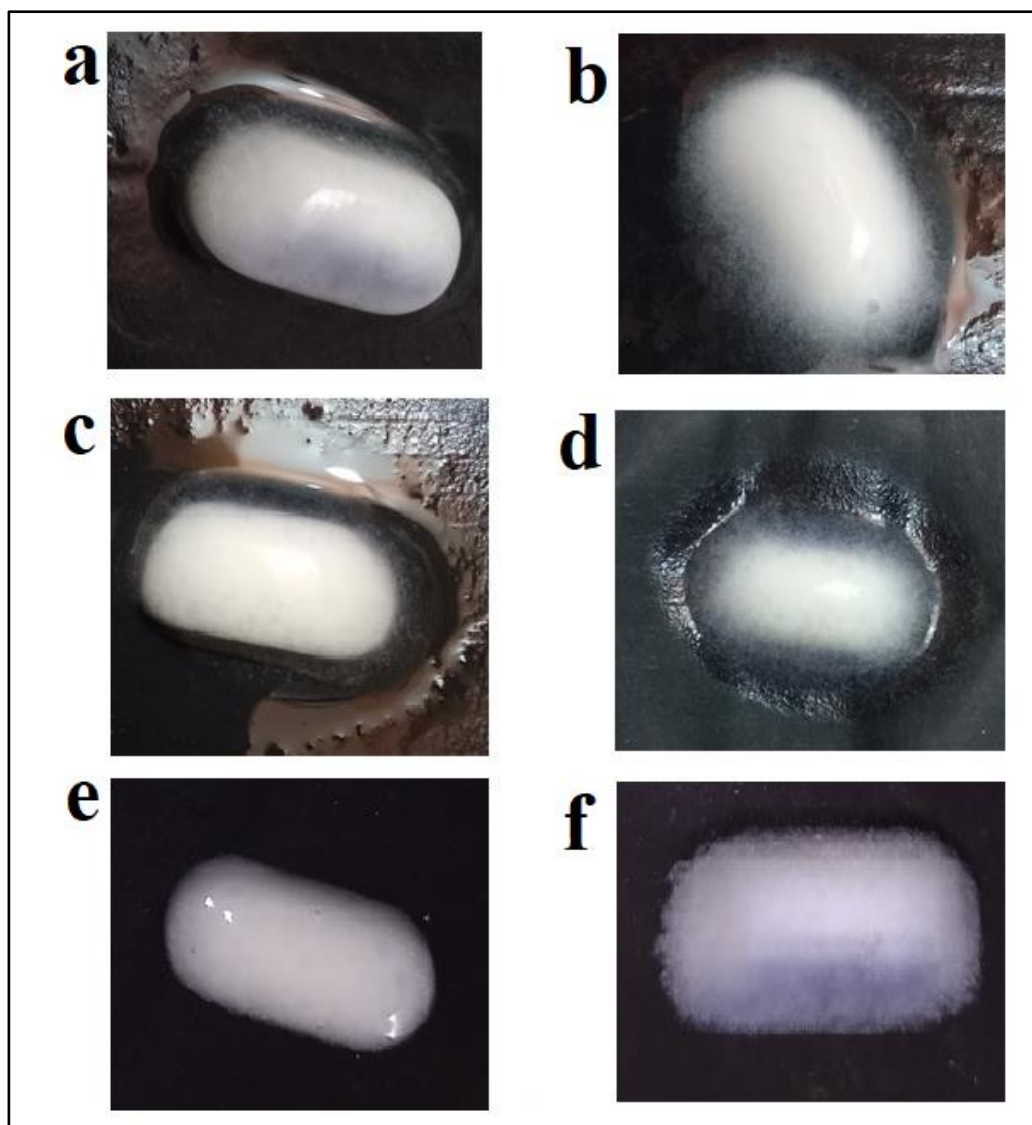


Figure 9.6: Comprehensive representation of the dissolution of (a) NAP after 2 hrs., (b) NAP after 10 hrs., (c) CMAP after 2 hrs., (d) CMAP after 10 hrs., (e) CCMAP after 2 hrs., (f) CCMAP after 10 hrs.

9.4.2. Water penetration velocity of placebo matrix tablets

The water penetration velocity data in Table 9.3, examining the behavior of NAP, CMAP, and CCMAP matrices in different pH environments, provides crucial insights into the intricacies of water uptake and swelling dynamics in these matrix systems. The distinct responses of these matrices to the surrounding aqueous conditions underscore the profound influence of their structural characteristics on water penetration and subsequent swelling behaviors [Quintana et al. in 1999].

As indicated in the table, blank NAP tablets exhibited relatively slower water uptake compared to CMAP in both acidic (pH 1.2) and buffer (pH 6.8) solutions. Conversely, the degree of swelling was found to be higher for blank NAP tablets than for blank CCMAP tablets. This disparity in water penetration and swelling tendencies is attributed to the unique crosslinking process, particularly evident in the CCMAP matrices, resulting in restricted water penetration due to enhanced entanglement within the CCMAP structure.

The characteristic behavior of the CMAP matrix in aqueous environments, characterized by disentangled and less viscous gel layers, allows for a rapid rate of water influx due to Coulombic repulsion among the chain segments. This distinctive behavior elucidates the underlying mechanisms driving the observed differences in water penetration velocities across the three matrix types.

The water penetration rate through CMAP matrix tablets was determined to be greater than that of CCMAP matrix tablets. Additionally, it was observed that the water penetration rate exhibited the following sequence: water penetration in a phosphate buffer (PB) solution > water penetration in an acidic solution. Furthermore, considering the water penetration velocity trend: PB solution > acidic solution, it follows that the rate of swelling also mirrored this sequence: swelling in PB solution > swelling in acidic solution. This higher degree of swelling and increased water penetration rate facilitated the dissolution of drugs within the matrix and their subsequent diffusion out.[20] As a result, it can be anticipated that the release of the drugs would adhere to the order: release in PB solution > release in acidic solution. This is primarily due to the fact that the velocity of water penetration and the consequent swelling of a hydrophilic matrix depend on the characteristics of the gel layer that forms around the matrix tablet upon contact with water [Maity & Sa 2014].

The observed order of water penetration velocity, with CMAP demonstrating the highest rate, followed by NAP and then CCMAP, emphasizes the distinctive nature of these matrices and their potential utility in diverse pharmaceutical formulations. These findings carry significant implications for the development of advanced drug delivery systems tailored to specific therapeutic requirements, thereby enabling the precise control of swelling behaviors for targeted and controlled release applications.

Table 9.3: Water penetration velocity of placebo matrix tablets

Placebo matrix tablet	Water penetration velocity (cm/s)	
	In acid solution (pH 1.2)	In PB solution (pH 6.8)
NAP	1.34×10^{-3}	1.21×10^{-3}
CMAp	1.5×10^{-3}	1.38×10^{-3}
CCMAp	7×10^{-4}	9×10^{-4}

9.4.3. Erosion study of placebo matrix tablets

The erosion behavior of NAP, CMAp, and CCMAp matrices in varying pH environments is effectively captured in the data presented in Figures 9.7a and 9.7b. The erosion characteristics play a pivotal role in understanding the stability and degradation dynamics of these matrices, providing key insights into their sustained release properties and potential applicability in drug delivery systems.

As depicted in the figures, NAP tablets (X1) exhibited a moderate degree of erosion, falling between the erosion levels of CMAp (X2) and CCMAp (X3) tablets. Notably, in the acidic medium, the erosion observed in blank CMAp tablets was notably lower than that observed in the phosphate buffer medium. However, it is essential to underscore that CMAp tablets exhibited a higher degree of erosion in both acidic and buffer media when compared to NAP and CCMAp tablets. This heightened erosion behavior can be attributed to the specific structural characteristics of the CMAp matrices, which are influenced by the presence of specific functional groups and the consequent interactions with the surrounding environment [Singh R et al., 2014].

The presence of Ca^{2+} ions is identified as a key contributing factor in constraining the erosion of CCMAp matrix tablets. This critical phenomenon not only elucidates the underlying mechanisms governing the erosion behavior of CCMAp matrices but also underscores their potential for sustained release applications.

The crosslinking facilitated by the Ca^{2+} ions contributes to the enhanced stability and prolonged erosion kinetics, which are highly desirable in drug delivery systems requiring sustained and controlled drug release profiles.

The comprehensive understanding of the erosion behaviors, in conjunction with the insights derived from the swelling and water penetration dynamics, serves as a critical foundation for the strategic design and development of advanced drug delivery systems. Leveraging the distinct erosion characteristics of NAP, CMAP, and CCMAP matrices it can significantly yield the tailored formulation of drug release profiles, facilitating precise control over drug delivery kinetics and enhancing therapeutic efficacy.

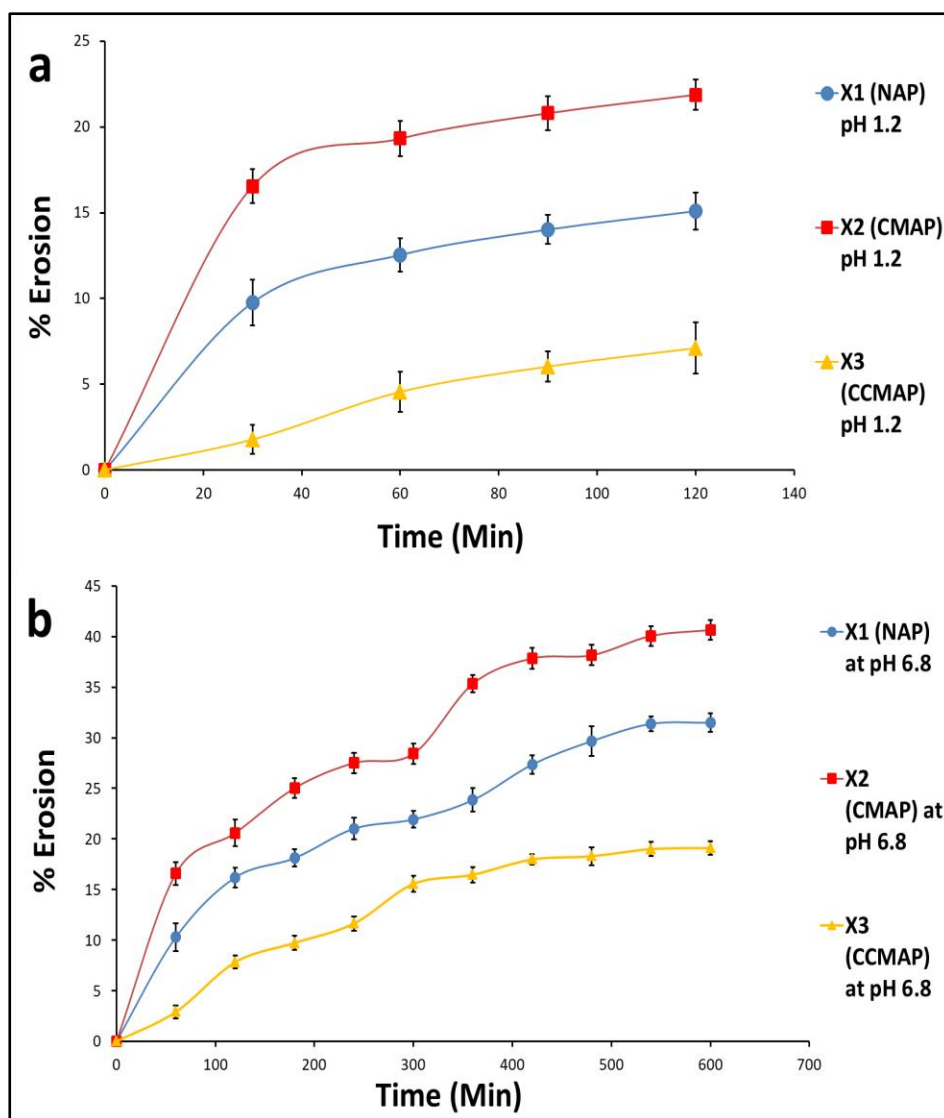


Figure 9.7: Erosion (%) of NAP, CMAP, and CCMAP at (a) pH 1.2, (b) pH 6.8

9.5. Topography of tablets by SEM studies

The SEM images presented in Figure 9.8 offer crucial insights into the surface morphology and dissolution behavior of the NAP, CMAP, and CCMAP tablets at different time intervals during the dissolution process. The visual analysis underscores the distinctive erosion patterns and dissolution kinetics exhibited by these formulations, providing valuable information on their drug release mechanisms and performance.

The findings extracted from Figure 9.8(a, b, and c) highlight the varying erosion levels among the three tablet types. The NAP tablets demonstrate moderate erosion, indicative of their susceptibility to dissolution, albeit to a lesser extent compared to the CMAP tablets. Conversely, the CCMAP tablets exhibit minimal erosion, emphasizing their enhanced stability and controlled dissolution characteristics. These observations align with the earlier data on dissolution profiles, further reinforcing the sustained release behavior of the CCMAP formulation.

In contrast, the SEM images captured in Figure 9.8(d, e, and f) illustrate the pronounced erosion observed on the surface of the CMAP tablets following 6 hours of dissolution. The visible breakdown and disintegration of the tablet surface emphasizes the rapid dissolution and drug release kinetics associated with the CMAP formulation, indicative of its immediate release properties.

In stark contrast, the SEM images presented in Figure 9.8(g, h, and i) portray a distinctly different dissolution behavior for the CCMAP tablets. Here, the formation of a gel-like structure on the tablet surface signifies the controlled and sustained release characteristics of the CCMAP formulation. The limited erosion observed in the CCMAP tablets further accentuates their robust structural integrity and prolonged drug release capabilities, attributed to the crosslinking facilitated by the presence of Ca^{2+} ions.

These microscopic observations serve to validate and augment the earlier findings related to the dissolution and erosion behaviors of the NAP, CMAP, and CCMAP matrices. The SEM images effectively corroborate the data on drug release profiles, offering a comprehensive understanding of the underlying dissolution mechanisms and surface dynamics. Imposing these insights can suggest the

rational design and optimization of drug delivery systems, enabling the development of tailored formulations catering to specific therapeutic needs and desired release profiles [Murphy et al., 2012].

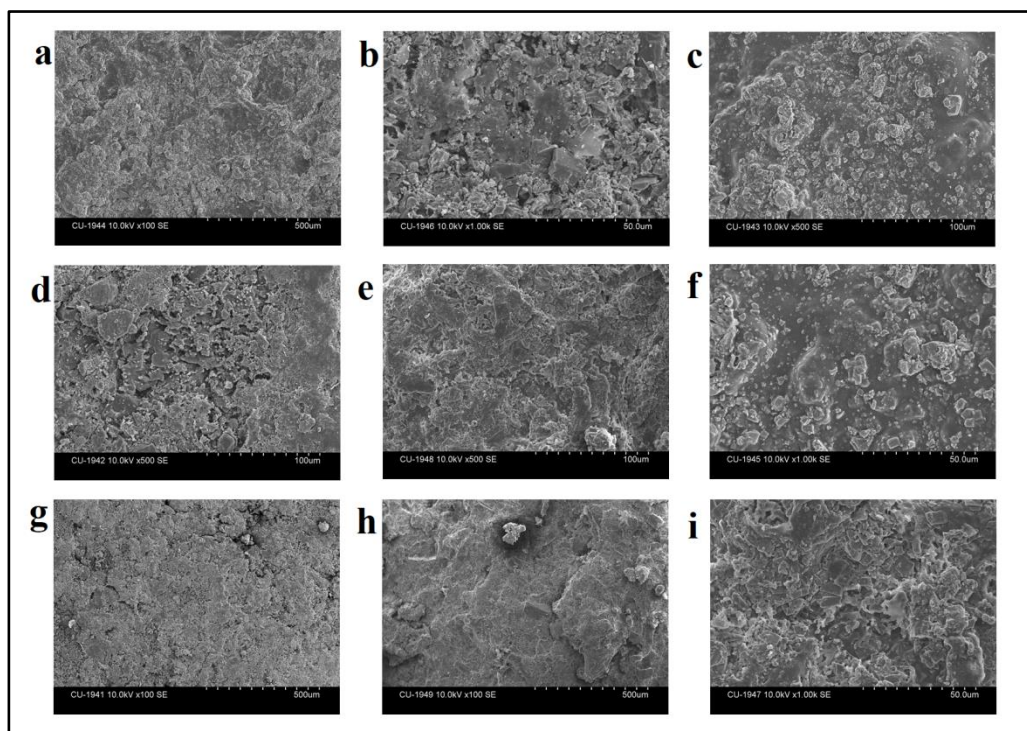


Figure 9.8: SEM images of (a) NAP at 0 hr., (b) NAP at 2 hrs., (c) NAP at 6 hrs.; (d) CMAP at 0 hr., (e) CMAP at 2 hrs., (f) CMAP at 6 hrs.; (g) CCMAP at 0 hr., (h) CCMAP at 2 hrs., (i) CCMAP at 6 hrs.

CHAPTER 10

EVALUATION OF MATRIX TABLETS FORMULATIONS AND DRUG RELEASE CHARACTERISTICS

EVALUATION OF MATRIX TABLETS FORMULATIONS AND DRUG RELEASE CHARACTERISTICS

In the field of pharmaceutical research and development, the quest for effective drug delivery systems has led to the exploration of novel polysaccharide-based materials as promising matrix-forming agents. Native Albizia Procera (NAP) gum, characterized by its galactopyranose and arabinofuranose monomeric units, emerged as a compelling candidate owing to its matrix-forming capabilities and versatile chemical modifiability. This natural resource polysaccharide presented an intriguing opportunity for sustained-release matrix tablet formulations, prompting its integration as a key polymer in drug delivery studies [Raina et al., 2022].

Metformin hydrochloride (MET) and Diltiazem hydrochloride (DIL), widely recognized as pivotal model drugs, were strategically employed in conjunction with NAP to develop matrix tablets. The introduction of NAP as the primary matrix-forming agent and its subsequent chemical modification through carboxymethylation (CMAP) brought forth significant alterations in the polymer's structural integrity and viscoelastic properties. The substitution of hydroxyl groups with carboxymethyl groups induced distinct rheological and physicochemical changes, rendering CMAP a dynamic entity susceptible to coulombic repulsion and diminished mechanical strength.

Building upon the insights derived from the analysis of CMAP, the tailored $-\text{COO}^-$ groups underwent further modification through ionic crosslinking with calcium ions, culminating in the creation of calcium crosslinked carboxymethylated albizia procera gum (CCMAP). The resulting CCMAP exhibited enhanced viscoelasticity, structural stability, and rheological robustness, positioning it as a strong and resilient matrix polymer for sustained-release formulations. Harnessing the unique attributes of NAP, CMAP, and CCMAP, this chapter delves into the comprehensive evaluation and discussion of the

formulated matrix tablets, with a key emphasis on delineating the impact of carboxymethylation and crosslinking on drug release kinetics and polymer behavior.

Through meticulous scrutiny of swelling and erosion studies and water penetration velocity determinations, the distinct water uptake and erosion patterns among NAP, CMAP, and CCMAP emerged, illuminating the transformative influence of chemical modification and crosslinking on the polymers' performance. This chapter serves as a comprehensive exploration of the effects of tailored *Albizia procera* gum polymers on drug delivery systems, underscoring the promising potential for their future applications in pharmaceutical formulations.

10.1. Physical characterization and drug release from MET-loaded matrix tablet formulations

10.1.1. Characterization of NAP matrix tablets containing MET

Table 10.1 presents a detailed analysis of the physical attributes of MET-loaded matrix tablets, encompassing crucial parameters such as average weight, hardness, physical dimensions, friability, and drug content. The findings from this comprehensive assessment underscore the robustness and consistency of the tablet formulations, confirming their adherence to the stringent quality standards and regulatory requirements set forth for pharmaceutical products.

In terms of average weight, the tablets exhibited uniformity and standardization, ensuring a consistent dosage profile across all formulations [Won DH et al., 2021].

Comparable outcomes were observed for the MET-loaded CMAP and CCMAP tablet formulations, as detailed in Table 10.4 (section 10.1.3) and 10.7 (section 10.1.5).

Table 10.1: Characteristics and active ingredient content of MET-loaded NAP matrix tablets

<i>Formulation code</i>	<i>Average weight</i>	<i>Hardness (Newton/cm²)</i>	<i>Average thickness (mm)</i>	<i>Average length (mm)</i>	<i>Average breadth (mm)</i>	<i>Friability (%)</i>	<i>Drug content (%)</i>
	(mg) (N=20)	*	(N=10) *	(N=10)*	(N=10)*	(N=20) *	(N=20)
F1	1117.2 ± 2.25%	56.87 ± 0.06	6.10 ± 0.02	19.49 ±0.011	9.00 ± 0.013	0.67 ±0.026	99.08 ±0.16
F2	1114.6 ± 1.23%	59.82 ± 0.021	5.89 ± 0.01	19.49 ±0.009	8.99 ± 0.021	0.63 ±0.047	99.13 ±0.21
F3	1108.2 ± 2.06%	61.58 ± 0.028	5.92 ± 0.012	19.42 ±0.014	9.01 ± 0.017	0.53 ±0.016	101.03 ±0.18
F4	1113.04 ± 4.02%	60.11 ± 0.047	5.96 ± 0.023	19.45 ±0.011	9.02 ± 0.012	0.57 ±0.031	98.98 ±0.24
F5	1119.20 ± 2.08%	67.27 ± 0.032	5.99 ± 0.011	19.50 ±0.01	9.02 ± 0.01	0.48 ±0.018	99.01 ±0.19
F6	1122.03 ± 1.04%	64.13 ± 0.016	6.20 ± 0.014	19.49 ±0.017	8.99 ± 0.023	0.51 ±0.033	100.05 ±0.23
F7	1119.25 ± 2.15%	69.13 ± 0.023	5.98 ± 0.022	19.46 ±0.013	9.01 ± 0.016	0.35 ±0.023	99.69 ±0.22
F8	1121.03 ± 1.29%	68.05 ± 0.051	5.99 ± 0.09	19.48 ±0.018	9.00 ± 0.023	0.39 ±0.014	99.16 ±0.20
F9	1121.16 ± 1.47%	70.31 ± 0.043	6.10 ± 0.023	19.48 ±0.012	9.03 ± 0.013	0.23 ±0.021	99.33 ±0.16
F10	1123.05 ± 1.07%	70.01 ± 0.049	5.99 ± 0.013	19.49 ±0.011	9.00 ± 0.020	0.26 ±0.03	99.43 ±0.22

* N= number of tablets tested; Mean ± SD (n=3)

10.1.2. *In-vitro* drug release study from MET-loaded NAP matrix tablet formulations

The investigation into the in-vitro drug release from various MET-loaded NAP matrix tablet formulations provides insightful findings, as illustrated in Figure 10.1. The linearity of the standard calibration curve of MET, featuring an impressive correlation coefficient (R^2) exceeding 0.998, facilitated the accurate determination of the dissolved drug amount in each sample. Notably, formulation F7 displayed the highest cumulative percentage (98.81%) of MET release within an 11-hour time frame, while formulation F10 exhibited a slightly superior release percentage of 99.28%.

However, it is essential to highlight that, among all the NAP formulations, only F10 demonstrated a sustained release profile, albeit restricted to 11 hours. This prolonged release behavior can be attributed to the higher quantity of NAP utilized in the formulation of F10, signifying the crucial role of polymer concentration in dictating the release kinetics of the drug.

Moreover, the evaluation of the area under the curve (AUC) using the linear trapezoidal rule provided crucial insights into the overall drug release profile from the various formulations, as depicted in Table 10.2. The AUC values (% mg hrs) shed light on the comprehensive drug release dynamics and offer a quantitative basis for comparing the overall release performances of different NAP formulations.

To further analyze the significance of the observed differences in drug release from NAP matrices, an analysis of variance (ANOVA) test was conducted. The results revealed a statistically significant variation in drug release among the NAP matrices ($p=0.05$), underscoring the influence of formulation parameters on the release behavior. The ANOVA table, provided in Table 10.3, furnishes detailed statistical information supporting the observed disparities in drug release and emphasizes the need for meticulous formulation optimization for achieving desired drug release profiles.

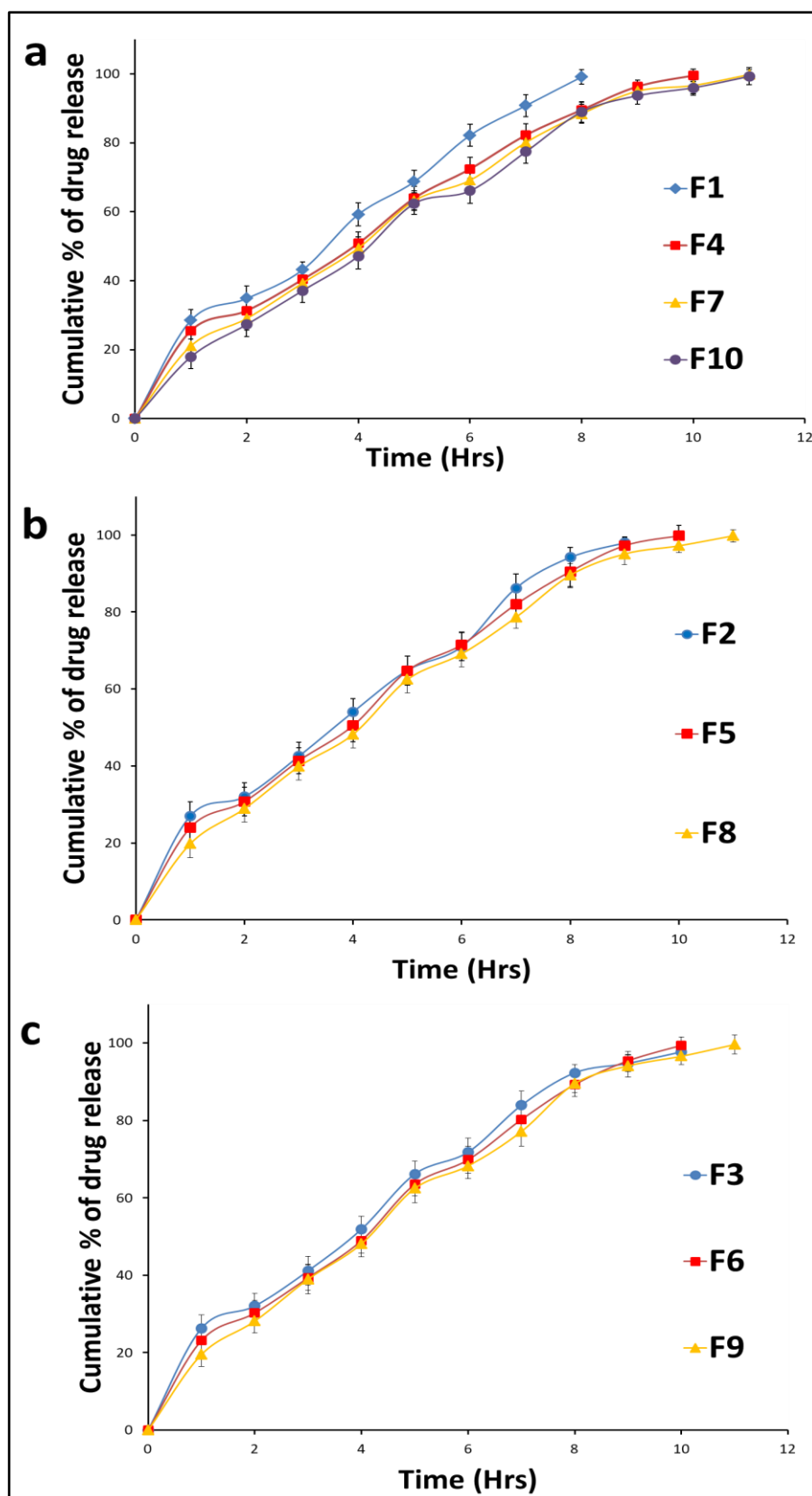


Figure 10.1: Drug release profiles of MET from NAP matrix tablet formulations

Table 10.2: AUC of MET release from NAP matrix

<i>Medi a</i>	<i>AUC of MET release from NAP matrix</i>									
	F1	F2	F3	F4	F5	F6	F7	F8	F9	F10
At pH 1.2	114.84 58	107.43 33	105.82 08	102.92 08	98.295 84	95.650 01	89.074 99	85.512 49	83.995 84	78.945 84
At pH 6.8	1142.3 67	1304.1 29	1525.3 75	1505.7 29	1505.7 21	1473.8 63	1703.3 87	1696.2 04	1681.2 42	1659.0 46

Table 10.3: ANOVA Table of cumulative release of MET from NAP matrix tablet formulations

<i>Table Analyzed</i>						
Two-way ANOVA Alpha	0.05					
Source of Variation	% of total variation	P value	P value summary	Significant?		
Row Factor	70.88	< 0.0001	****	Yes		
Column Factor	2.273	0.432	ns	No		
ANOVA table	SS	DF	MS	F (DFn, DFd)	P value	
Row Factor	117453	12	9788	F (12, 108) = 23.77	P < 0.0001	
Column Factor	3766	9	418.4	F (9, 108) = 1.016	P = 0.4320	
Residual	44479	108	411.8			
Number of missing values	0					

10.1.3. Characterization of CMAP matrix tablets containing MET

Table 10.4 provides an intricate examination of the physical characteristics of MET-loaded matrix tablets, encompassing vital parameters such as average weight, hardness, physical dimensions, friability, and drug content.

Table 10.4: Characteristics and active ingredient content of MET-loaded CMAP matrix tablets

Formulation code	Average weight (mg) (N=20)	Hardness (Newton/cm ²) (N=10) *	Average thickness (mm) (N=10) *	Average length (mm) (N=10)*	Average breadth (mm) (N=10)*	Friability (%) (N=20) *	Drug content (%) (N=20)
F1	1113.45 ± 1.17%	60.16 ± 0.04	5.99 ± 0.014	19.50 ± 0.024	9.02 ± 0.028	0.74 ±0.028	99.91 ±0.12
F2	1110.99 ± 2.08%	61.53 ± 0.033	5.99 ± 0.011	19.48 ± 0.018	9.01 ± 0.018	0.86 ±0.031	99.27 ±0.3
F3	1108.2 ± 2.06%	65.67 ± 0.065	5.92 ± 0.008	19.49 ± 0.021	9.02 ± 0.022	0.76 ±0.037	99.6 ±0.32
F4	1112.19 ± 2.74%	65.09 ± 0.047	5.98 ± 0.041	19.50 ± 0.014	9.01 ± 0.014	0.81 ±0.029	99.77 ±0.22
F5	1114.07 ± 3.01%	64.39 ± 0.017	5.99 ± 0.014	19.49 ± 0.033	8.98 ± 0.021	0.79 ±0.03 3	100.02 ±0.33
F6	1116.04 ± 2.13%	62.52 ± 0.011	5.98 ± 0.017	19.49 ± 0.029	9.01 ± 0.017	0.77 ±0.024	98.97 ±0.33
F7	1118.14 ± 3.07%	63.07 ± 0.021	5.99 ± 0.019	19.49 ± 0.024	9.00 ± 0.022	0.72 ±0.036	99.97 ±0.34
F8	1113.18 ± 2.11%	65.08 ± 0.044	5.98 ± 0.011	19.50 ± 0.031	9.01 ± 0.014	0.69 ±0.027	100.13 ±0.16
F9	1117.08 ± 4.01%	64.89 ± 0.013	5.98 ± 0.021	19.49 ± 0.023	9.02 ± 0.018	0.66 ±0.035	99.07 ±0.26
F10	1114.44 ± 1.48%	63.33 ± 0.031	5.98 ± 0.023	19.49 ± 0.011	9.01 ± 0.025	0.66 ±0.022	99.58 ±0.39

* N= number of tablets tested; Mean ± SD (n=3)

10.1.4. *In-vitro* drug release study from MET-loaded CMAP matrix tablet formulations:

The in-vitro drug release study of MET-loaded CMAP matrix tablet formulations revealed compelling insights into the release profiles and behavior of these formulations. All CMAP tablets exhibited maximum release before the 12-hour mark, suggesting a relatively fast drug release across the formulations.

Upon closer examination of the release profiles (Figure 10.2 a, b, and c), a consistent trend emerged, indicating that CMAP formulations generally demonstrated faster drug release compared to the corresponding NAP formulations. This observation was further supported by statistical analysis using an ANOVA test, which indicated a statistically significant difference in drug release from CMAP matrices ($p=0.05$).

To quantify the overall drug release dynamics, the area under the curve (AUC) was calculated using the linear trapezoidal rule, and the results are summarized in Table 10.5. The AUC values provide a numerical representation of the cumulative drug release over time for each formulation. It's noteworthy that the AUC values align with the observed trend, reinforcing the notion of faster drug release from CMAP matrices.

The hourly breakdown of drug release percentages for each formulation at pH 1.2 and pH 6.8 further elucidates the distinctive release patterns (Table 10.5). Notably, at both pH conditions, CMAP formulations consistently exhibited higher percentages of drug release compared to NAP formulations.

The two-way ANOVA analysis revealed a significant impact of the row factor (formulation type) on the total variation in drug release, further emphasizing the formulation-dependent variations (Table 10.6).

The detailed ANOVA table provided comprehensive statistical information, indicating highly significant differences in drug release among different formulations. The significance level ($p<0.0001$) for the row factor supports the conclusion that the choice of polymer (CMAP) significantly influences the drug release behavior.

In conclusion, the in-vitro drug release study highlights the robust and distinct drug release characteristics of MET-loaded CMAP matrix tablet formulations. The faster release kinetics observed in CMAP matrices compared to NAP matrices underscore the potential of carboxymethylated albizia procera gum as an effective matrix-forming agent for achieving desired drug release profiles.

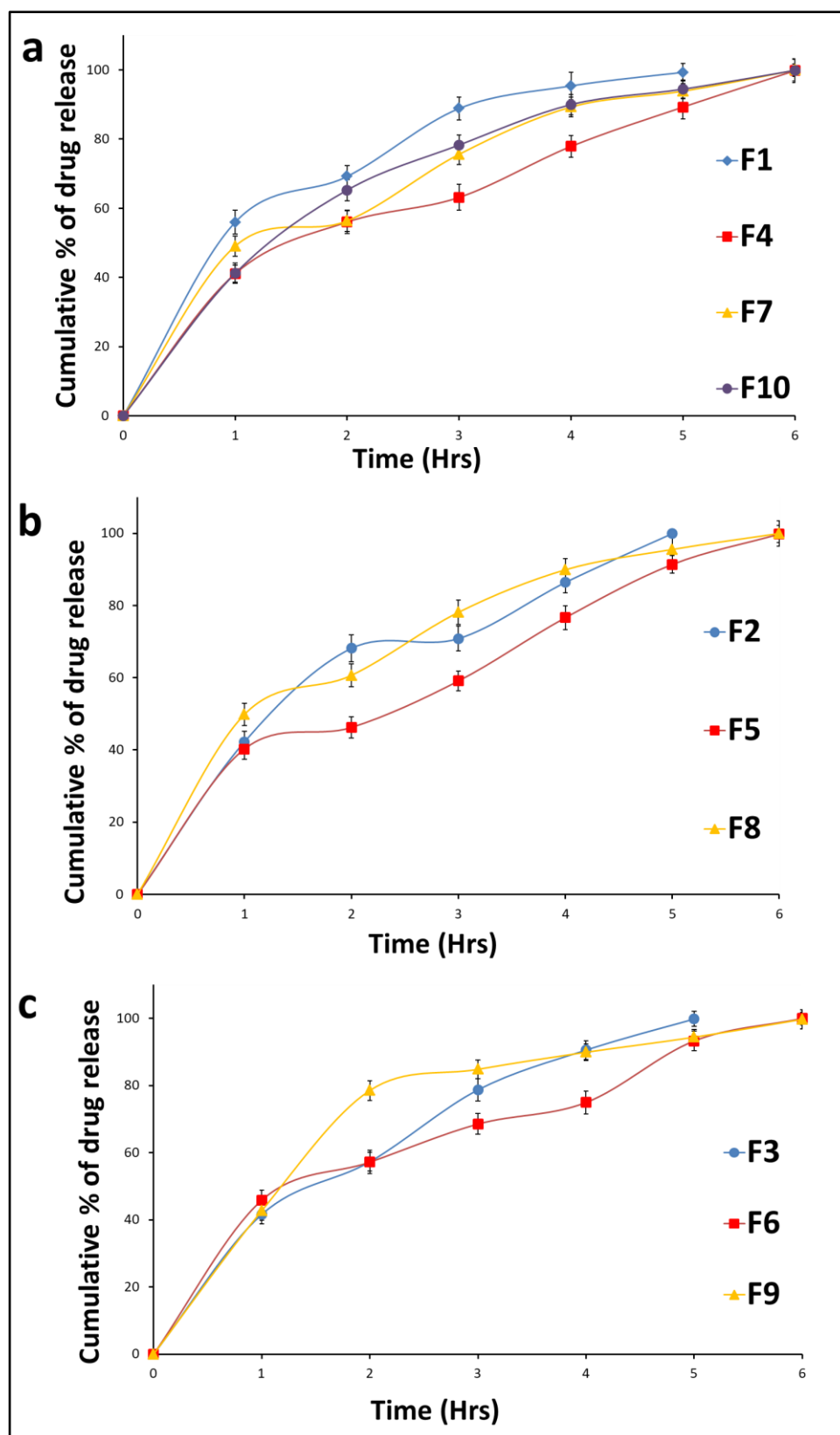


Figure 10.2: Drug release profiles of MET from CMAP matrix tablet formulations

Table 10.5: AUC of MET release from CMAP matrix

AUC of MET release from CMAP matrix										
Media	F1	F2	F3	F4	F5	F6	F7	F8	F9	F10
At pH 1.2	226.4 75	190.8 208	175.6 083	172.8 167	158.4 708	186.0 333	193.1 167	200.4 458	204.9 167	184.5 625
At pH 6.8	897.7 959	793.9	795.0 75	943.4 083	908.6 958	974.2 958	1035. 437	1060. 071	1100. 483	1047. 904

Table 10.6: ANOVA Table of cumulative release of MET from CMAP matrix tablet formulations

Formulations					
Two-way ANOVA					
Alpha	0.05				
Source of Variation	% of total variation	P value	P value summary	Significant?	
Row Factor	88.75	<0.0001	****	Yes	
Column Factor	0.6242	0.7029	ns	No	
ANOVA table	SS	DF	MS	F (DFn, DFd)	P value
Row Factor	183472	12	15289	F (12, 108) = 75.20	P < 0.0001
Column Factor	1290	9	143.4	F (9, 108) = 0.7052	P = 0.7029
Residual	21958	108	203.3		
Number of missing values	0				

10.1.5. Characterization of CCMAP matrix tablets containing MET

Table 10.7 provides an intricate examination of the physical characteristics of MET-loaded matrix tablets, encompassing vital parameters such as average weight, hardness, physical dimensions, friability, and drug content.

Table 10.7: Characteristics and active ingredient content of MET-loaded CCMAP matrix tablets

Formulation code	Average weight (mg) (N=20)	Hardness (Newton/cm ²) (N=10) *	Average thickness (mm) (N=10) *	Average length (mm) (N=10)*	Average breadth (mm) (N=10)*	Friability (%) (N=20) *	Drug content (%) (N=20)
F1	1119.6 ± 3.33%	64.67 ± 0.042	5.87 ± 0.014	19.50 ± 0.012	9.04 ± 0.025	0.69 ±0.017	99.69 ±0.14
F2	1118.53 ± 2.16%	66.22 ± 0.018	5.95 ± 0.011	19.48 ± 0.014	9.01 ± 0.017	0.66 ±0.037	99.83 ±0.29
F3	1116.24 ± 2.88%	63.79 ± 0.022	5.91 ± 0.022	19.48 ± 0.01	9.02 ± 0.013	0.57 ±0.027	98.99 ±0.21
F4	1121.04 ± 3.12%	66.27 ± 0.021	5.99 ± 0.013	19.49 ± 0.016	9.01 ± 0.011	0.51 ±0.018	99.47 ±0.17
F5	1120.08 ± 3.15%	64.77 ± 0.013	6.01 ± 0.024	19.51 ± 0.01	9.01 ± 0.01	0.46 ±0.024	99.96 ±0.24
F6	1121.13 ± 2.44%	65.72 ± 0.017	6.01 ± 0.017	19.48 ± 0.012	9.00 ± 0.014	0.47 ±0.029	99.19 ±0.13
F7	1114.07 ± 3.08%	70.06 ± 0.027	5.99 ± 0.015	19.48 ± 0.019	9.02 ± 0.011	0.44 ±0.034	99.37 ±0.34
F8	1116.48 ± 2.09%	70.74 ± 0.034	5.96 ± 0.013	19.49 ± 0.014	9.01 ± 0.013	0.41 ±0.022	98.59 ±0.16
F9	1121.86 ± 2.64%	72.03 ± 0.021	6.07 ± 0.017	19.49 ± 0.01	9.01 ± 0.016	0.37 ±0.016	100.08 ±0.25
F10	1120.18 ± 2.11%	72.14 ± 0.032	5.98 ± 0.027	19.49 ± 0.016	9.02 ± 0.013	0.30 ±0.023	99.37 ±0.13

* N= number of tablets tested; Mean ± SD (n=3)

10.1.6. *In-vitro* drug release study from MET-loaded CCMAP matrix tablet formulations

The in-vitro drug release study from MET-loaded CCMAP matrix tablet formulations provided crucial insights into the sustained-release behavior of these formulations. The drug release profiles, as illustrated in Figure 10.3 (a, b, and c), clearly depict the sustained and prolonged release characteristics of CCMAP matrices, with a notable correlation to increasing polymer concentrations.

Across the entire drug release profiles, it's evident that CCMAP formulations achieved a prolonged release, contrasting with the rapid and momentaneous drug release profile observed in CMAP formulations. The maximum amount of MET released from the CCMAP matrices was 246.6 mg (F6, 98.64%) within the first 12 hours, indicating a highly sustained release. F10, while exhibiting a lower cumulative percentage of drug release at 12 hours (64.17%), still demonstrated sustained release behavior, highlighting the influence of polymer concentration on the release kinetics.

The Ca^{++} crosslinking in CCMAP matrices played a pivotal role in restricting water influx, reducing swelling, and promoting the formation of a viscoelastic gel layer. These factors collectively contributed to a slower release of drugs, validating the sustained release behavior observed. In contrast, CMAP matrices, characterized by electrostatic repulsion between polymeric chains, exhibited higher mobility, de-coiled structures, and weak gel networks that lost their structural integrity, resulting in rapid deformation, increased water uptake, higher swelling, and accelerated drug release.

The AUC values for MET released from CCMAP tablets, presented in Table 10.8, further support the sustained release characteristics of these formulations. The significant difference in drug release between different formulations was confirmed through two-way ANOVA analysis (Table 10.9), with a highly significant p-value ($p < 0.0001$) for the row factor (formulation type).

In conclusion, the in-vitro drug release study establishes that CCMAP matrix tablet formulations, through the process of Ca^{++} crosslinking, achieve sustained and prolonged drug release, making them promising candidates for the development of controlled-release pharmaceutical formulations [Freitas et al., 2021]. The insights gained from this study contribute valuable information for the rational design of drug delivery systems, offering the potential for tailored and controlled drug release profiles.

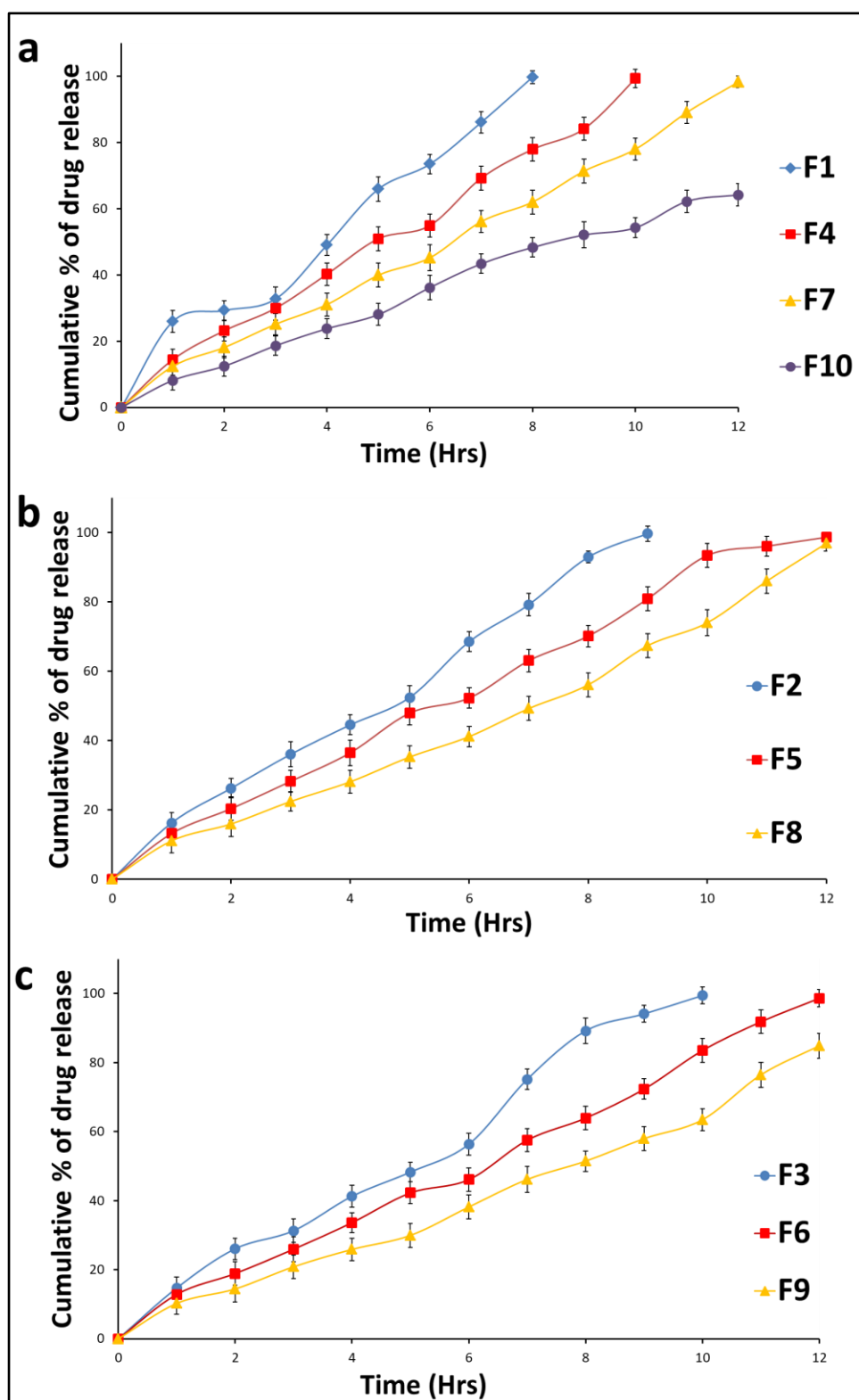


Figure 10.3: Drug release profiles of MET from CCMAP matrix tablet formulations

Table 10.8: AUC of MET release from CCMAP matrix

<i>AUC of MET release from CCMAP matrix</i>										
Media	F1	F2	F3	F4	F5	F6	F7	F8	F9	F10
At pH	101.3	73.42	69.4	64.93	58.41	55.80	53.59	47.62	43.72	35.93
1.2	958	918		334	251	418	166	499	501	333
At pH	1030.	1164.	1315.	1236.	1628.	1495.	1443.	1337.	1194.	1048.
6.8	654	783	771	063	088	604	454	525	083	558

Table 10.9: ANOVA Table of the cumulative release of MET from CCMAP matrix tablet formulations

Formulations					
Two-way ANOVA					
Alpha	0.05				
Source of Variation	% of total variation	P value	P value summary	Significant?	
Row Factor	47.57	<0.0001	****	Yes	
Column Factor	3.511	0.5621	ns	No	
ANOVA table	SS	DF	MS	F (DFn, DFd)	P value
Row Factor	60163	12	5014	F (12, 108) = 8.752	P < 0.0001
Column Factor	4441	9	493.4	F (9, 108) = 0.8613	P = 0.5621
Residual	61871	108	572.9		
Number of missing values	0				

10.1.7. Comparison of drug release

The comparison of drug release profiles of MET from NAP, CMAP, and CCMAP matrix tablet formulations, along with a marketed tablet (Figure 10.4), provides a comprehensive understanding of their release kinetics.

Examining the drug release profiles at various time points (1 to 12 hours), it is evident that NAP (F1) and CCMAP (F1) formulations exhibit a sustained release pattern, with a gradual increase in the cumulative percentage of drug release. Conversely, CMAP (F1) shows a comparatively faster release, reaching a higher percentage within the same timeframe. This trend is consistent across other formulations (F4, F7, and F10) for NAP, CMAP, and CCMAP. Notably, the marketed tablet demonstrates a controlled release pattern, aligning with pharmaceutical standards.

Analyzing the ANOVA results (Table 10.10), a statistically significant difference ($p < 0.0001$) in drug release is observed among different formulations (row factor). However, the column factor (time points) does not significantly influence the drug release ($p = 0.4962$).

This comparison underscores the formulation-dependent release kinetics of MET. The sustained release observed in CCMAP formulations can be attributed to the crosslinking process, which restricts water influx, reduces swelling, and promotes the formation of a viscoelastic gel layer. In contrast, CMAP formulations, with electrostatic repulsion between polymeric chains, exhibit rapid deformation, increased water uptake, higher swelling, and accelerated drug release. NAP formulations demonstrate an intermediate release pattern.

In conclusion, the comparison reveals the influence of polymer characteristics on drug release kinetics, emphasizing the potential of CCMAP matrices for achieving sustained release profiles. These findings are valuable for tailoring drug delivery systems based on specific therapeutic requirements and desired release kinetics.

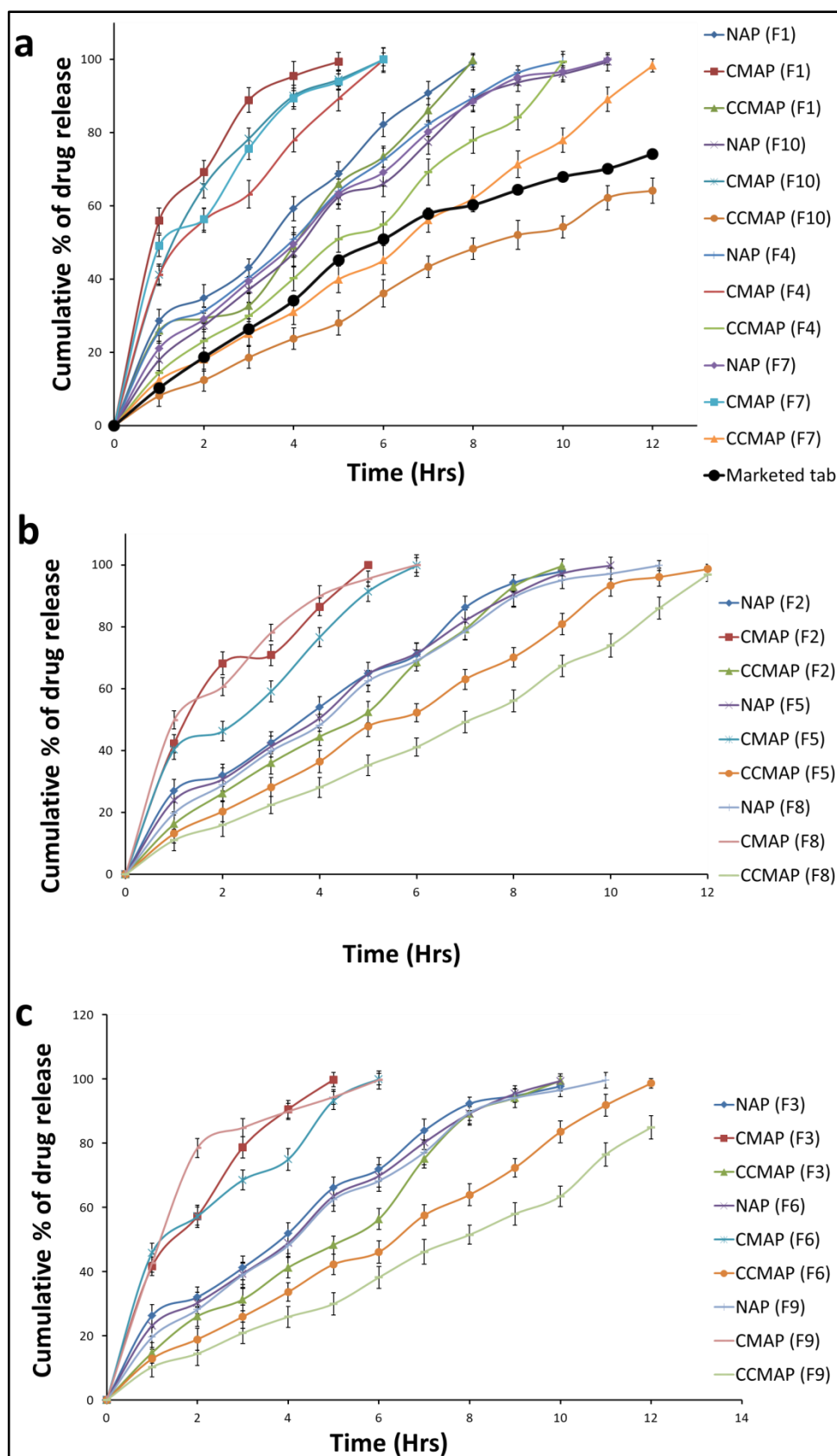


Figure 10.4: Drug release profiles of MET from NAP, CMAP and CCMAP matrix tablet formulations with marketed tablet

Table 10.10: ANOVA Table of cumulative release of MET from NAP, CMAP and CCMAP matrix tablet formulations

<i>Two-way ANOVA</i>					
Alpha	0.05				
Source of Variation	% of total variation	P value	P value summary	Significant?	
Row Factor	25.68	<0.0001	****	Yes	
Column Factor	5.62	0.4962	ns	No	
ANOVA table	SS	DF	MS	F (DFn, DFd)	P value
Row Factor	133098	12	11092	F (12, 348) = 10.84	P < 0.0001
Column Factor	29130	29	1004	F (29, 348) = 0.9816	P = 0.4962
Residual	356121	348	1023		
Number of missing values	0				

10.2. Physical characterization and drug release from DIL-loaded matrix tablet formulations

10.2.1. Characterization of NAP matrix tablets containing DIL

Table 10.11 provides an intricate examination of the physical attributes of DIL-loaded matrix tablets, encompassing vital parameters such as average weight, hardness, physical dimensions, friability, and drug content. The results from this thorough evaluation emphasize the strength and uniformity of the tablet formulations, affirming their compliance with the rigorous quality standards and regulatory requisites established for pharmaceutical products. Regarding average weight, the tablets displayed a consistent and standardized profile, ensuring uniform dosages across all formulations.

Similar outcomes were observed for the DIL-loaded CMAP and CCMAP tablet formulations, detailed in Table 10.14 (section 10.2.3) and 10.17 (section 10.2.5). These findings further validate the reliability and conformity of these formulations to specified quality benchmarks, essential for pharmaceutical products.

Table 10.11: Characteristics and active ingredient content of DIL-loaded NAP matrix tablets

Formulation code	Average weight (mg) (N=20)	Hardness (Newton/cm ²) (N=10) *	Average thickness (mm) (N=10) *	Average length (mm) (N=10)*	Average breadth (mm) (N=10)*	Friability (%) (N=20) *	Drug content (%) (N=20)
F1	1112.12 ± 3.14%	66.54 ± 0.048	5.47 ± 0.016	19.49 ± 0.010	9.01 ± 0.026	0.72 ±0.021	100.03 ±0.26
F2	1113.24 ± 2.33%	61.55 ± 0.021	5.35 ± 0.018	19.49 ± 0.016	9 ± 0.015	0.75 ±0.028	99.07 ±0.31
F3	1115.45 ± 1.56%	67.98 ± 0.035	5.71 ± 0.020	19.51 ± 0.02	9.01 ± 0.010	0.67 ±0.031	101.01 ±0.25
F4	1114.66 ± 1.49%	64.27 ± 0.017	5.89 ± 0.011	19.50 ± 0.015	9.02 ± 0.023	0.64 ±0.025	99.98 ±0.18
F5	1118.39 ± 3.28%	62.21 ± 0.032	6.11 ± 0.017	19.50 ± 0.019	9.00 ± 0.029	0.64 ±0.019	99.96 ±0.24
F6	1117.19 ± 1.99%	68.17 ± 0.026	6.08 ± 0.023	19.49 ± 0.010	9.01 ± 0.019	0.55 ±0.022	99.35 ±0.24
F7	1120.77 ± 2.31%	72.32 ± 0.039	5.82 ± 0.019	19.50 ± 0.012	9.02 ± 0.016	0.51 ±0.015	100.09 ±0.21
F8	1119.53 ± 1.39%	70.47 ± 0.043	5.99 ± 0.014	19.50 ± 0.010	8.99 ±0.0159	0.50 ±0.034	98.59 ±0.16
F9	1113.54 ± 1.74%	73.62 ± 0.011	6.02 ± 0.010	19.48 ± 0.011	± 0.023	0.46 ±0.011	98.87 ±0.11
F10	1116.25 ± 2.22%	69.34 ± 0.037	5.32 ± 0.015	19.49 ± 0.014	9.01 ± 0.015	0.42 ±0.027	99.67 ±0.15

* N= number of tablets tested; Mean ± SD (n=3)

10.2.2. *In-vitro* drug release study from DIL-loaded NAP matrix tablet formulations

The *in-vitro* drug release study of diltiazem hydrochloride (DIL)-loaded NAP matrix tablet formulations reveals distinctive release profiles and underscores the role of formulation factors in influencing drug release.

Analysis of drug release profiles at various time points (1 to 12 hours) illustrates that DIL release from NAP formulations (F1, F4, F7, and F10) is gradual, demonstrating sustained release characteristics. Notably, these formulations achieve almost 100% drug release within 8 hours, indicating their efficiency in delivering the drug steadily over time. The release profiles are visually depicted in Figure 10.5, providing a clear representation of the sustained drug release behavior.

Quantification of drug release using the area under the curve (AUC) values, detailed in Table 10.12, reveals the extent of drug release over time for each formulation under different pH conditions. The AUC values at pH 1.2 and pH 6.8 indicate substantial drug release for all formulations, with higher values observed at the more alkaline pH 6.8, signifying enhanced dissolution under physiological conditions mimicking the small intestine.

ANOVA results (Table 10.13) highlight a statistically significant difference in the cumulative release of DIL from NAP matrices ($p < 0.0001$). This emphasizes that different formulations significantly impact drug release. However, the column factor representing different time points does not exert a significant effect on drug release ($p = 0.3131$).

Contrary to a fully sustained release, a less sustained release behavior was observed in NAP formulations. This observation might indicate a controlled release pattern rather than a sustained one. The pH-dependent release indicates the formulations' responsiveness to the varying conditions of the gastrointestinal tract [Abbasi et al., 2019].

In conclusion, the study underscores the potential of NAP as a matrix-forming agent for achieving sustained drug release, a crucial aspect of the effective therapeutic action of DIL. The results contribute valuable insights into the formulation-dependent behavior of NAP matrices, advancing the development of controlled-release drug delivery systems.

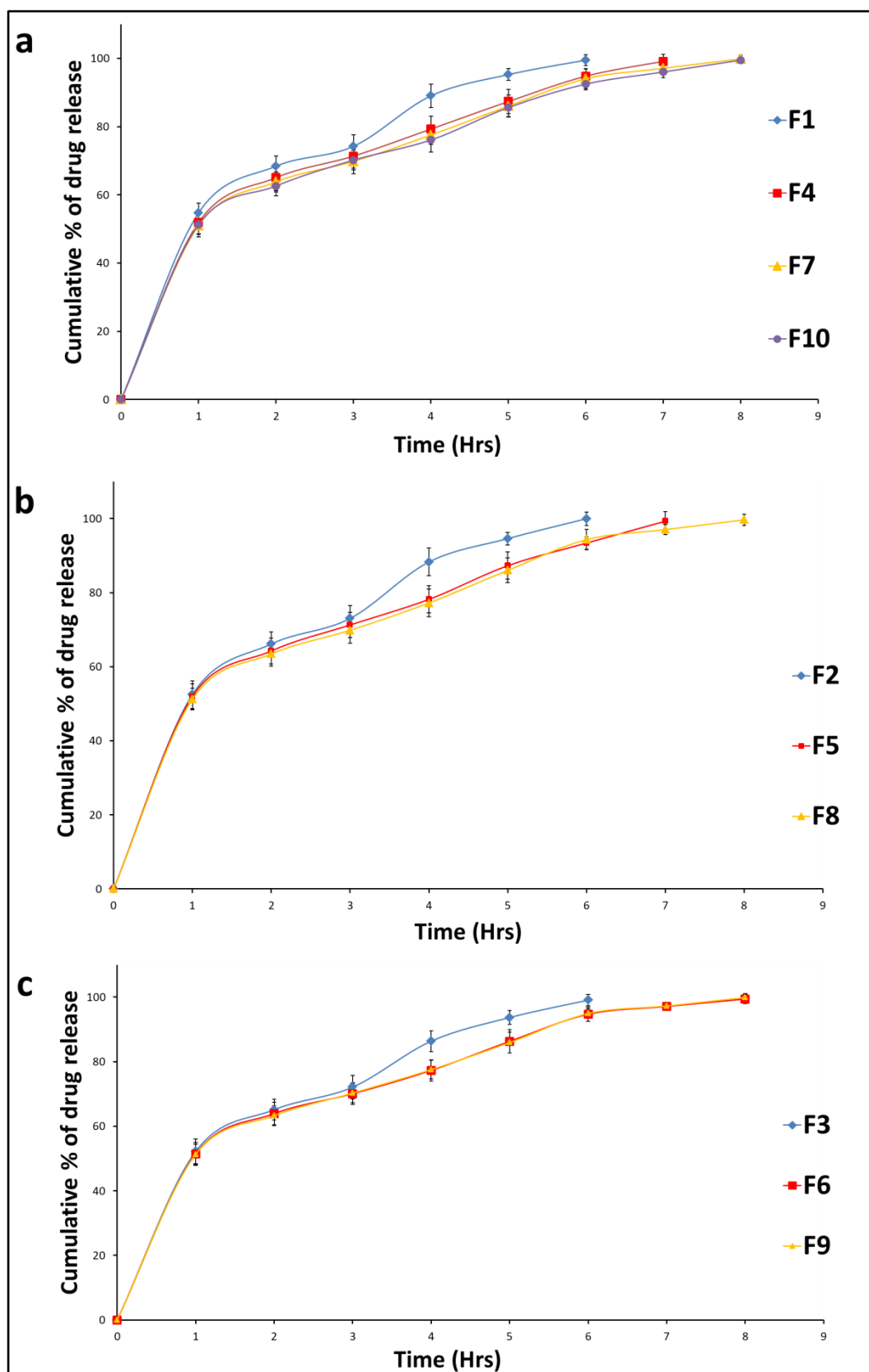


Figure 10.5: Drug release profiles of DIL from NAP matrix tablet formulations

Table 10.12: AUC of DIL release from NAP matrix tablets

<i>AUC of DIL release from NAP matrix</i>										
<i>Media</i>	<i>F1</i>	<i>F2</i>	<i>F3</i>	<i>F4</i>	<i>F5</i>	<i>F6</i>	<i>F7</i>	<i>F8</i>	<i>F9</i>	<i>F10</i>
At pH 1.2	222.4 208	213.7 958	211.8 083	211.2 458	210.1 583	208.4 542	207.4 292	207.4 208	207.3 125	206.5 917
At pH 6.8	1077. 65	1058. 508	1046. 033	1247. 579	1237. 217	1474. 842	1472. 454	1470. 85	1474. 512	1459. 246

Table 10.13: ANOVA Table of cumulative release of DIL from NAP

<i>Two-way ANOVA</i>					
Alpha	0.05				
Source of Variation	% of total variation	P value	P value summary	Significant?	
Row Factor	77.55	<0.0001	****	Yes	
Column Factor	2.183	0.3131	ns	No	
ANOVA table	SS	DF	MS	F (DFn, DFd)	P value
Row Factor	154171	11	14016	F (11, 99) = 34.44	P < 0.0001
Column Factor	4339	9	482.1	F (9, 99) = 1.185	P = 0.3131
Residual	40286	99	406.9		
Number of missing values	0				

10.2.3. Characterization of CMAP matrix tablets containing DIL

Table 10.14 provides an intricate examination of the physical characteristics of DIL-loaded matrix tablets, encompassing vital parameters such as average weight, hardness, physical dimensions, friability, and drug content.

Table 10.14: Characteristics and active ingredient content of DIL-loaded CMAP matrix tablets

Formulation code	Average weight (mg) (N=20)	Hardness (Newton/cm ²) (N=10)	Average thickness (mm) (N=10)	Average length (mm) (N=10)*	Average breadth (mm) (N=10)*	Friability (%) (N=20) *	Drug content (%) (N=20)
F1	1116.65 ± 2.35%	63.89 ± 0.024	5.35 ± 0.018	19.51 ± 0.02	9 ± 0.017	0.89 ±0.026	99.41 ±0.26
F2	1113.51 ± 1.21%	59.98 ± 0.023	5.58 ± 0.021	19.49 ± 0.013	9.02 ± 0.013	0.86 ±0.018	100.02 ±0.24
F3	1119.42 ± 3.82%	61.51 ± 0.035	5.96 ± 0.016	19.50 ± 0.017	9.03 ± 0.01	0.74 ±0.024	99.1 ±0.17
F4	1120.14 ± 2.42%	67.73 ± 0.040	5.98 ± 0.022	19.51 ± 0.013	9.01 ± 0.016	0.71 ±0.015	98.97 ±0.12
F5	1118.8 ± 3.75%	68.17 ± 0.027	6.11 ± 0.012	19.50 ± 0.015	9.01 ± 0.02	0.67 ±0.022	100.42 ±0.17
F6	1117.17 ± 1.44%	64.27 ± 0.011	6.09 ± 0.018	19.51 ± 0.016	9.01 ± 0.01	0.69 ±0.018	98.86 ±0.19
F7	1115.57 ± 2.48%	71.06 ± 0.019	5.68 ± 0.014	19.51 ± 0.013	9 ± 0.013	0.62 ±0.026	99.97 ±0.18
F8	1114.48 ± 3.09%	69.47 ± 0.039	5.94 ± 0.017	19.49 ± 0.017	9.02 ± 0.016	0.56 ±0.015	101.01 ±0.21
F9	1116.68 ± 1.37%	70.25 ± 0.022	6.37 ± 0.015	19.50 ± 0.011	9 ± 0.019	0.57 ±0.017	98.75 ±0.14
F10	1121.38 ± 3.14%	73.64 ± 0.042	5.76 ± 0.023	19.50 ± 0.013	9.01 ± 0.017	0.55 ±0.019	99.49 ±0.31

* N= number of tablets tested; Mean ± SD (n=3)

10.2.4. *In-vitro* drug release study from DIL-loaded CMAP matrix tablet formulations

In Figure 10.6 (a, b, and c), the in-vitro drug release profiles of DIL (120 mg) from tablets containing CMAP gum in each formulation were presented. The evaluation of the entire drug release profiles revealed a rapid momentary drug release profile demonstrated by the CMAP formulations. Notably, the maximum amount of DIL released from the CMAP matrices reached 120 mg (100%) within a 6-hour duration. This rapid release behavior was attributed to enhanced polymer chain mobility, a disentangled structure, and the loss of structural integrity in weak gel networks within CMAP matrices. These factors facilitated rapid deformation due to electrostatic repulsion between polymeric chains, promoting increased water uptake, higher swelling, and accelerated drug release.

The area under the curve (AUC) values for DIL released from CMAP tablets, presented in Table 10.15, demonstrated substantial drug release for all formulations at both pH 1.2 and pH 6.8. Higher AUC values at the more alkaline pH of 6.8 indicated enhanced dissolution under conditions mimicking the small intestine.

The drug release data underwent two-way ANOVA analysis to determine the significant difference in drug release between different formulations. The ANOVA table, as displayed in Table 10.16, confirmed that the differences in drug releases between the two matrices were statistically significant ($P < 0.0001$). This indicates that both the row factor (different formulations) and the column factor (time points) significantly impact drug release from CMAP matrices.

In conclusion, the study highlights the rapid and momentary drug release behavior of DIL from CMAP matrices, shedding light on the influential role of the formulation in drug release. The AUC values and ANOVA results underscore the substantial drug release from CMAP matrices and emphasize the significance of different formulations and time points in modulating drug release. This information holds value in the tailored design of drug delivery systems for optimal therapeutic outcomes.

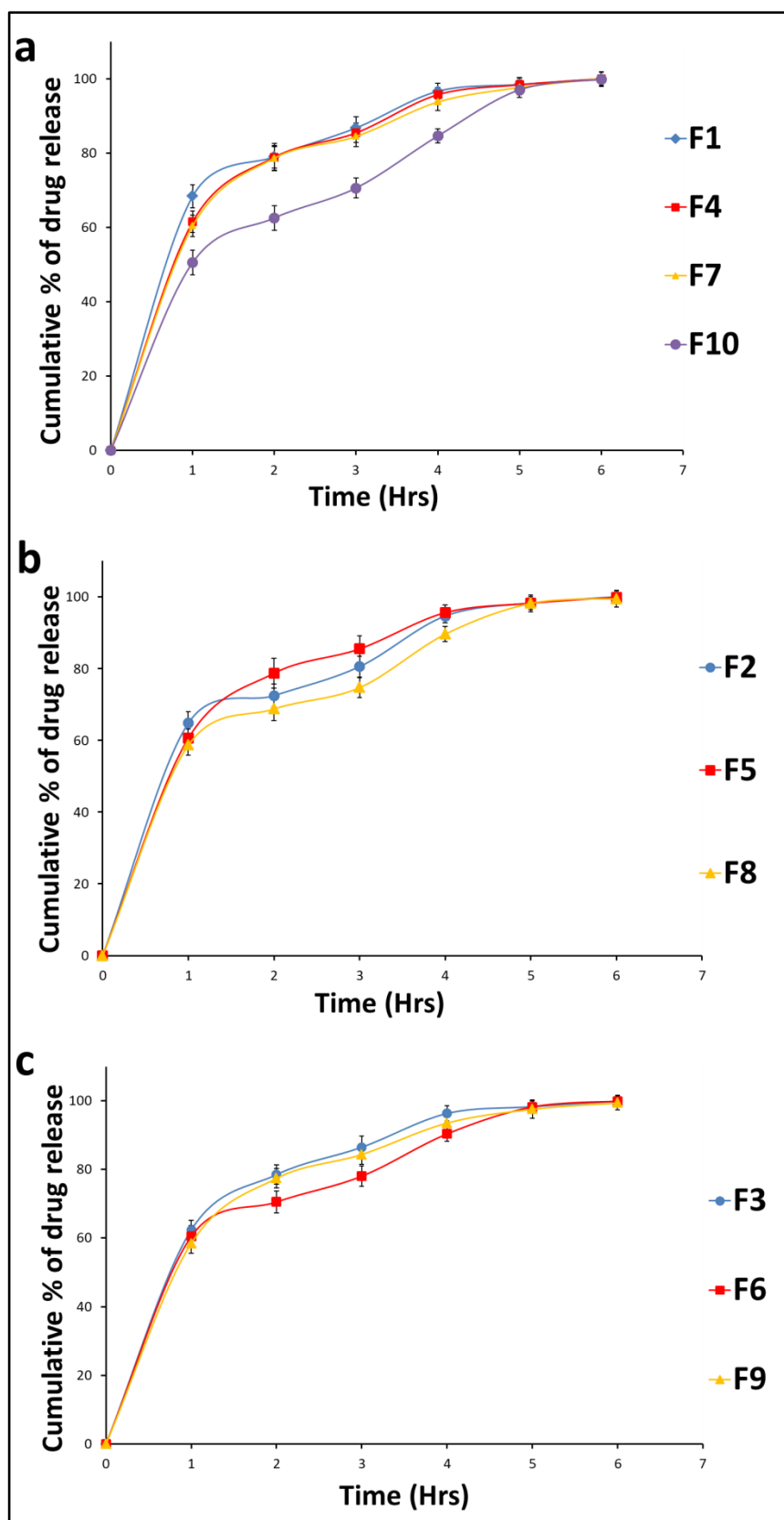


Figure 10.6: Drug release profiles of DIL from CMAP matrix tablet formulations

Table 10.15: AUC of DIL release from CMAP matrix tablets

<i>AUC of DIL release from CMAP matrix</i>										
<i>Media</i>	<i>F1</i>	<i>F2</i>	<i>F3</i>	<i>F4</i>	<i>F5</i>	<i>F6</i>	<i>F7</i>	<i>F8</i>	<i>F9</i>	<i>F10</i>
At pH 1.2	269.6 167	252.5 083	254.0 833	252.1 667	249.7 583	239.3 083	249.1 667	232.5 25	242.9 25	204.4 25
At pH 6.8	1197. 892	1151. 825	1179. 833	1174. 4	1171. 2	1118. 912	1161. 908	1098. 846	1152. 504	1037. 825

Table 10.16: ANOVA Table of cumulative release of DIL from CMAP

<i>Two-way ANOVA</i>					
Alpha	0.05				
Source of Variation	% of total variation	P value	P value summary	Significant?	
Row Factor	99.63	<0.0001	****	Yes	
Column Factor	0.1026	<0.0001	****	Yes	
ANOVA table	SS	DF	MS	F (DFn, DFd)	P value
Row Factor	243043	12	20254	F (12, 108) = 3375	P < 0.0001
Column Factor	250.3	9	27.81	F (9, 108) = 4.634	P < 0.0001
Residual	648.1	108	6.001		
Number of missing values		0			

10.2.5. Characterization of CCMAP matrix tablets containing DIL

Table 10.17 provides an intricate examination of the physical characteristics of DIL-loaded matrix tablets, encompassing vital parameters such as average weight, hardness, physical dimensions, friability, and drug content.

Table 10.17: Characteristics and active ingredient content of DIL-loaded CCMAP matrix tablets

Formulation code	Average weight (mg) (N=20)	Hardness (Newton/cm ²) (N=10) *	Average thickness (mm) (N=10) *	Average length (mm) (N=10)*	Average breadth (mm) (N=10)*	Friability (%) (N=20) *	Drug content (%) (N=20)
F1	1120.36 ± 2.38%	59.67 ± 0.028	5.97 ± 0.012	19.48 ± 0.016	9.01 ± 0.021	0.59 ±0.022	99.69 ±0.14
F2	1115.59 ± 1.29%	62.89 ± 0.031	5.65 ± 0.014	19.49 ± 0.013	9.03 ± 0.017	0.56 ±0.029	99.83 ±0.29
F3	1121.21 ± 3.07%	64.64 ± 0.042	5.93 ± 0.021	19.49 ± 0.011	9.01 ± 0.014	0.53 ±0.016	99.99 ±0.17
F4	1119.49 ± 2.12%	63.47 ± 0.040	5.61 ± 0.017	19.50 ± 0.015	9 ± 0.018	0.50 ±0.028	99.77 ±0.13
F5	1117.18 ± 1.15%	65.7 ± 0.024	6.08 ± 0.019	19.50 ± 0.014	9.02 ± 0.011	0.46 ±0.024	99.91 ±0.16
F6	1113.04 ± 1.21%	66.89 ± 0.019	6.11 ± 0.014	19.50 ± 0.019	9.01 ± 0.013	0.49 ±0.016	98.97 ±0.18
F7	1116.75 ± 2.84%	71.23 ± 0.012	5.82 ± 0.016	19.49 ± 0.013	9.01 ± 0.015	0.48 ±0.019	99.83 ±0.24
F8	1112.84 ± 2.69%	70.14 ± 0.027	5.92 ± 0.022	19.50 ± 0.016	9.01 ± 0.016	0.43 ±0.026	98.63 ±0.16
F9	1118.68 ± 1.64%	71.33 ± 0.015	6.05 ± 0.015	19.48 ± 0.013	9 ± 0.010	0.39 ±0.02	100.4±0.18
F10	1121.38 ± 3.01%	63.18 ± 0.026	5.81 ± 0.025	19.48 ± 0.017	9.01 ± 0.015	0.35 ±0.016	101.06 ±0.13

* N= number of tablets tested; Mean ± SD (n=3)

10.2.6. *In-vitro* drug release study from DIL-loaded CCMAP matrix tablet formulations

The in-vitro drug release profiles of DIL (120 mg) from tablets containing CCMAP in each formulation are visually presented in Figure 10.7 (a, b, and c). An overall assessment of these drug release profiles reveals distinctive characteristics based on the polymer concentration within CCMAP formulations.

Upon scrutinizing the complete drug release profiles, a notable trend emerges where CCMAP formulations with higher polymer concentrations exhibit prolonged and increasingly sustained release characteristics. In contrast, CMAP formulations demonstrate a rapid and momentary drug release profile. Specifically, within the first 12 hours, CCMAP matrices, such as F3, released 99.97% of DIL (119.964 mg), while the most sustained release of 97.81% within the same timeframe was achieved by F10. This delay in drug release in CCMAP matrices is attributed to factors such as the restriction of water influx, reduced swelling, and the formation of a viscoelastic gel layer due to Ca^{+2} crosslinking, contributing to a slower drug release [Nadgorny & Ameli 2018].

The area under the curve (AUC) values for DIL released from CCMAP tablets are detailed in Table 10.18. This data underwent two-way ANOVA analysis to discern significant differences in drug release among different formulations. As depicted in the ANOVA table (Table 10.19), the differences in drug releases between the two matrices were statistically significant ($P < 0.0001$).

The AUC values under pH 1.2 and pH 6.8 conditions illustrate the impact of polymer concentration on drug release. Higher polymer concentrations in CCMAP formulations result in a considerable reduction in AUC values, indicating a controlled and sustained drug release pattern. The statistical analysis confirms the significance of the polymer concentration (row factor) in influencing drug release, further emphasizing the role of formulation parameters in modulating drug release kinetics.

In summary, the discussion underscores the nuanced relationship between polymer concentration in CCMAP formulations and the resulting drug release profiles. The

sustained release characteristics observed in higher polymer concentrations, attributed to the crosslinking process, demonstrate the potential of CCMAP matrices for controlled drug delivery applications [Nayak & Pal 2011].

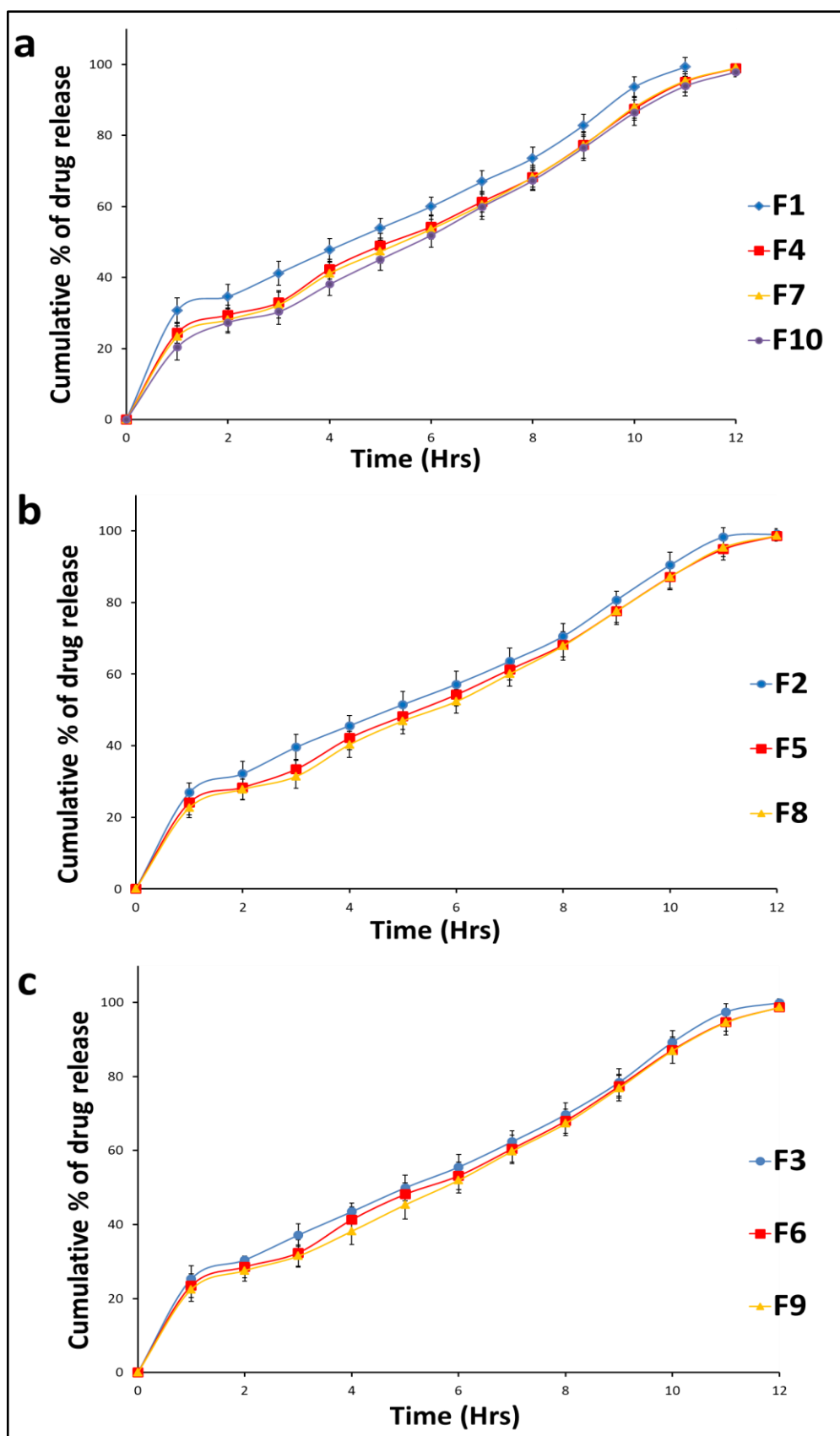


Figure 10.7: Drug release profiles of DIL from CCMAP matrix tablet formulations

Table 10.18: AUC of DIL release from CCMAP matrix tablets

<i>AUC of DIL release from CCMAP matrix</i>										
<i>Media</i>	<i>F1</i>	<i>F2</i>	<i>F3</i>	<i>F4</i>	<i>F5</i>	<i>F6</i>	<i>F7</i>	<i>F8</i>	<i>F9</i>	<i>F10</i>
At pH 1.2	119.8 633	107.4 383	101.2 634	97.78 751	95.57 5	94.30 833	93.23 334	91.27 499	90.55 416	85.05 418
At pH 6.8	1585. 831	1766. 301	1722. 65	1677. 754	1671. 354	1660. 325	1660. 242	1645. 729	1629. 392	1614. 329

Table 10.19: ANOVA Table of cumulative release of DIL from CCMAP

<i>Two-way ANOVA</i>					
Alpha	0.05				
Source of Variation	% of total variation	P value	P value summary	Significant?	
Row Factor	87.63	<0.0001	****	Yes	
Column Factor	0.436	0.9314	ns	No	
ANOVA table	SS	DF	MS	F (DFn, DFd)	P value
Row Factor	67080	11	6098	F (11, 99) = 66.09	P < 0.0001
Column Factor	333.8	9	37.08	F (9, 99) = 0.4019	P = 0.9314
Residual	9134	99	92.27		
Number of missing values	0				

10.2.7. Comparison of drug release

In Figure 10.8, the drug release profiles of diltiazem hydrochloride (DIL) from tablets containing NAP, CMAP, and CCMAP, along with those of the marketed tablets, were presented. The assessment of these profiles revealed distinct release patterns over a 12-hour period.

It was observed that NAP exhibited less sustained release behavior, CMAP demonstrated immediate release, and CCMAP displayed sustained release behavior. The drug release profiles depicted in the figures showcase the nuanced variations in release among the formulations.

In comparison with the marketed tablet, the NAP formulations demonstrated sustained release patterns, aligning with its design for prolonged drug release. Conversely, the CMAP formulations exhibited a more immediate release, suggesting potential applications for achieving rapid therapeutic effects. The CCMAP formulations, positioned between the extremes of NAP and CMAP, implied a balance suitable for controlled release scenarios. The cumulative release data presented in Table 10.20 were subjected to two-way ANOVA to discern the impact of different formulations on drug release. The row factor, representing various formulations, was found to be significantly influential, as indicated by the P value of less than 0.0001. This underscores that the distinctive release behaviors are attributed to the inherent characteristics of the formulations.

The ANOVA results also indicated that the column factor, representing different time points of measurement, did not significantly impact the drug release profiles ($P = 0.8564$). This implies that the observed differences in release behaviors among the formulations were predominantly due to formulation-specific factors rather than variations in the time points of assessment.

The formulation-specific release behaviors have substantial implications for drug delivery strategies. NAP, with its less sustained release, could find applications where a more immediate therapeutic effect is desired. CMAP, with its rapid release, might be suitable for scenarios requiring a quick onset of action. CCMAP, exhibiting a sustained release pattern, holds promise for controlled drug delivery applications. The pH-dependent release patterns, particularly notable at pH 6.8, suggest a responsiveness to the physiological conditions of the small intestine. This pH-dependent behavior is crucial for tailoring drug

release to specific regions of the gastrointestinal tract, enhancing the precision of drug delivery.

In conclusion, the comparative analysis of drug release profiles from NAP, CMAP, and CCMAP formulations provides valuable insights into their distinct release behaviors. The observed differences, supported by statistical analyses, emphasize the significance of formulation-specific factors in dictating drug release. These findings are instrumental in guiding the development of tailored drug delivery systems for optimized therapeutic outcomes.

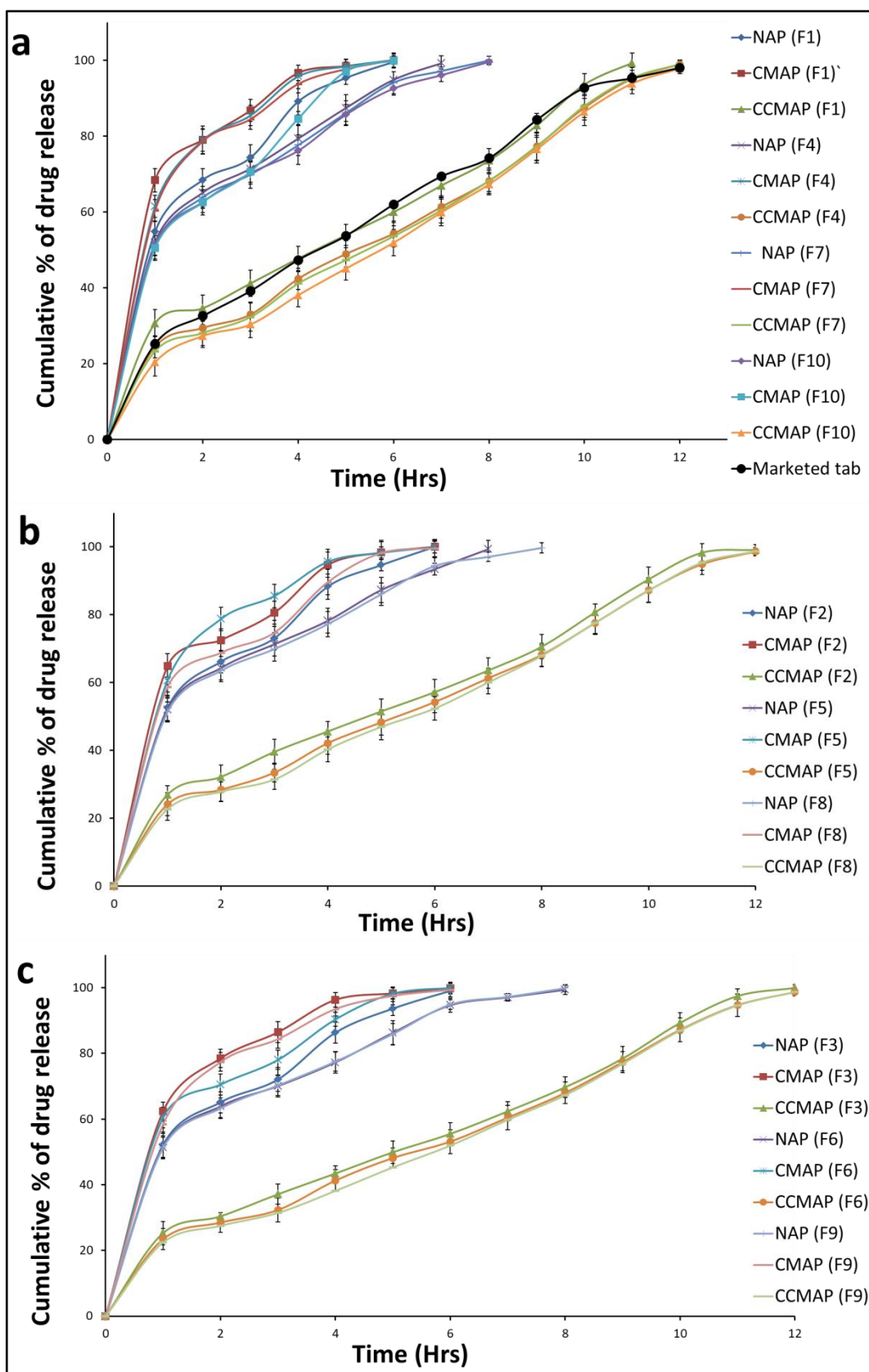


Figure 10.8: Drug release profiles of DIL from NAP, CMAP and CCMAP matrix tablet formulations with marketed tablets

Table 10.20: ANOVA Table of cumulative release of DIL from NAP, CMAP and CCMAP matrix tablet formulations

<i>Two-way ANOVA</i>					
Alpha	0.05				
Source of Variation	% of total variation	P value	P value summary	Significant?	
Row Factor	34.48	<0.0001	****	Yes	
Column Factor	3.712	0.8564	ns	No	
ANOVA table	SS	DF	MS	F (DFn, DFd)	P value
Row Factor	203455	12	16955	F (12, 348) = 16.18	P < 0.0001
Column Factor	21904	29	755.3	F (29, 348) = 0.7207	P = 0.8564
Residual	364700	348	1048		
Number of missing values	0				

10.3. Mechanism of drug release from MET-loaded matrix tablet formulations

In undertaking a thorough examination of data of drug release profiles from MET-loaded matrix tablet formulations were fitted to different kinetic model equations (Zero-order, first-order, Korsmeyer–Peppas, and Higuchi). Selective profiles of MET in the company of diverse matrices (NAP, CMAP, and CCMAP) were shown in Figure 10.9, 10.10 and 10.11 for F1, F5 and F10. Consistent graphical techniques were employed across various formulations (F2-F4, F6-F9) to gather data (R^2 , n). Graphically obtained data (R^2 , n) for different formulations (F1-F10) were tabulated in Table 10.21, 10.22, and 10.23.

MET-Loaded Matrix Tablets Containing NAP:

According to Table 10.21, amidst the MET-loaded matrix tablet formulations with NAP, only F1 ($R^2 = 0.9785$), F2 ($R^2 = 0.9801$), and F4 ($R^2 = 0.9749$) adhere to the zero-order kinetic model. In contrast, F3, F5-F10 conform to the Korsmeyer–Peppas model. The zero-order kinetic model, indicative of a robust correlation between time and drug release, sets the stage for a controlled release mechanism. The calculated diffusion exponent (n) values for all formulations (F1-F10) range from 0.6378 to 0.7616 ($0.45 < n < 0.89$), signifying anomalous (non-Fickian) diffusion for these formulations [Korsmeyer et al., 1983].

MET-Loaded CMAP Formulations:

Turning attention to MET-loaded CMAP formulations in Table 10.22, with the exception of F5, F1-F4, and F6-F10 fittingly align with Higuchi's model. F5, in contrast, adheres to first-order kinetics ($R^2 = 0.9815$). The observed models collectively suggest an immediate release scenario. Examining the diffusion exponent (n) values for formulations F2-F10, they uniformly reflect anomalous (non-Fickian) diffusion, while F1 distinctly demonstrates Fickian diffusion.

MET-Loaded CCMAP Formulations:

As delineated in Table 10.23, F1 to F9 among MET-loaded CCMAP formulations exhibit the best fit with the zero-order kinetics, implying sustained release characteristics. In contrast, F10 aligns more closely with the Korsmeyer–Peppas model. Analyzing the

diffusion exponent (n) values, F1 to F7 and F10 showcase anomalous (non-Fickian) diffusion patterns, while F8 presents a distinct case of Case-II transport.

Comparison of Formulations:

Comparative scrutiny reveals that MET-loaded matrix tablets with NAP generally manifest stronger correlations with the zero-order, first-order, and Higuchi models, indicating more predictable and controlled release patterns. In MET-loaded CMAP formulations, the Peppas model consistently yields high R^2 values, signaling the prevalence of non-Fickian diffusion.

For MET-loaded CCMAP formulations, the zero-order and Higuchi models exhibit steadfast correlations, implying a more predictable release mechanism. However, the Peppas model intimates some variability in release behaviors among the formulations.

Implications for Drug Delivery Design:

The gleaned insights into release kinetics assume critical importance in customizing drug delivery systems to cater to specific therapeutic requirements. The dominance of particular models within each formulation underscores the necessity for a nuanced approach in matrix selection for drug delivery. MET-loaded matrix tablets with NAP emerge as a potential choice for applications demanding precise and sustained release. Conversely, MET-loaded CCMAP formulations present a versatile option, apt for scenarios necessitating diverse release profiles.

In Conclusion:

The meticulous evaluation of drug release kinetics from MET-loaded matrix tablets stands as a cornerstone, offering valuable insights for the design and optimization of drug delivery systems. The observed variations in release behaviors among different formulations underscore the pivotal role played by the matrix in shaping drug release kinetics. This compendium of findings contributes significantly to the advancement of tailored drug delivery strategies, promising enhanced therapeutic outcomes.

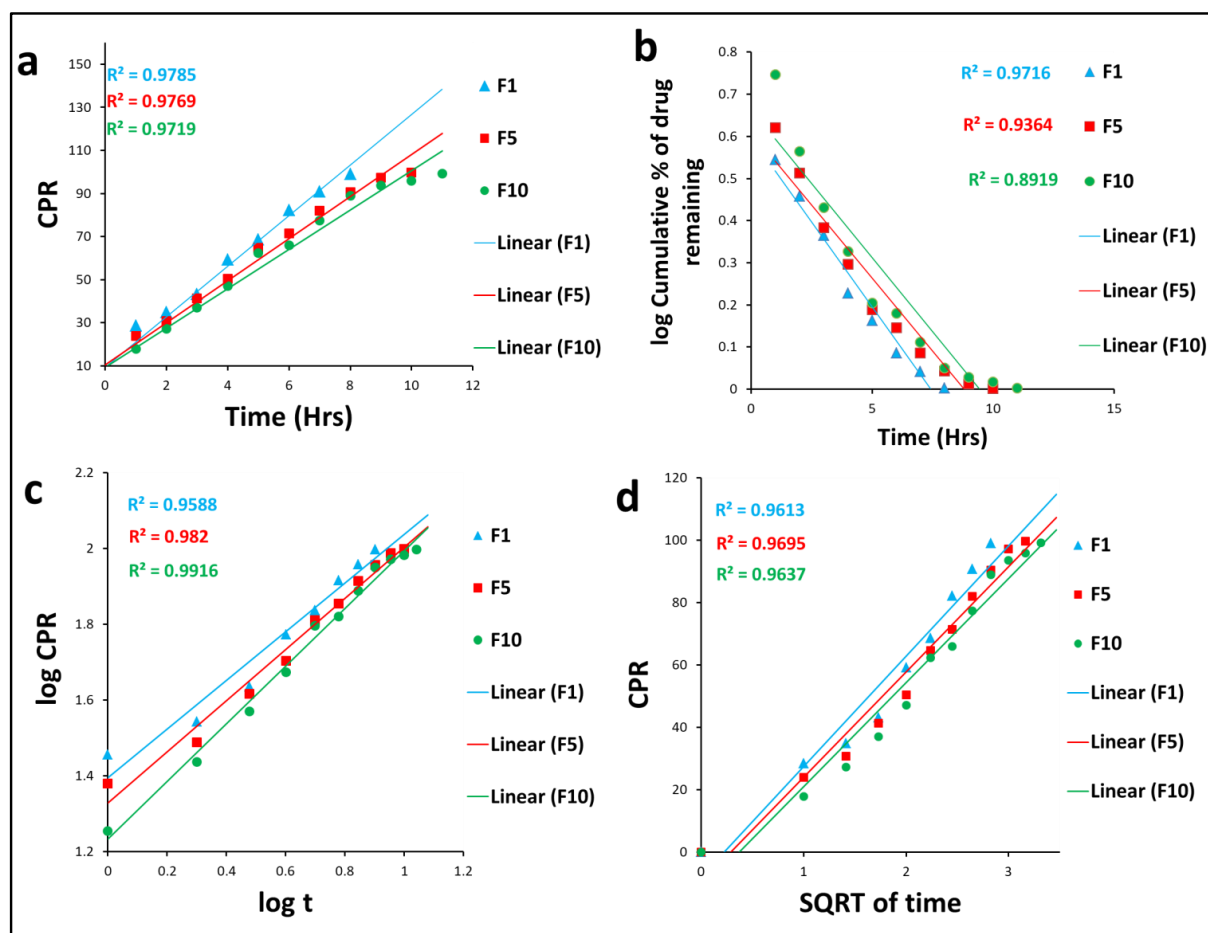


Figure 10.9: Release kinetics Models of MET-loaded NAP matrix tablet formulations (F1, F5, F10) (a) Zero-order, (b) 1st-order, (c) Korsmeyer–Peppas model, (d) Higuchi's model

Table 10.21: Coefficient of determination (R^2) from MET Release Kinetics Data of NAP matrix tablet formulations

Kinetic models	F1	F2	F3	F4	F5	F6	F7	F8	F9	F10
Zero-order	0.9785	0.9801	0.9688	0.9749	0.9769	0.9802	0.9673	0.9694	0.9705	0.9719
1 st -order	0.9716	0.9658	0.9377	0.9432	0.9364	0.9408	0.9011	0.8969	0.8975	0.8919
Korsmeyer–Peppas	0.9588	0.9654	0.972	0.9739	0.982	0.9813	0.9885	0.9919	0.9911	0.9916
Higuchi	0.9613	0.9623	0.9714	0.9702	0.9695	0.9662	0.9716	0.9695	0.9684	0.9637
<i>n</i>	0.6378	0.6448	0.6408	0.6529	0.6761	0.6859	0.7045	0.7246	0.7303	0.7616

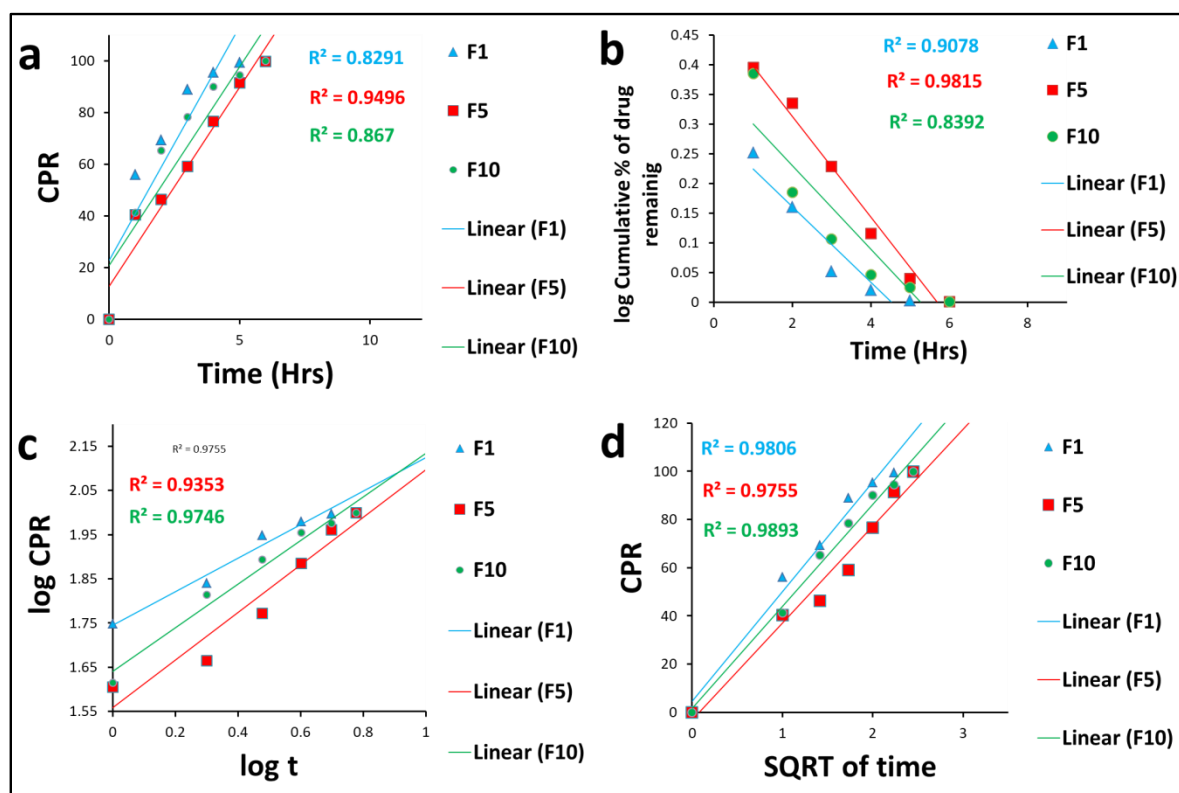


Figure 10.10: Release kinetics Models of MET-loaded CMAP matrix tablet formulations (F1, F5, F10) (a) Zero-order, (b) 1st-order, (c) Korsmeyer–Peppas model, (d) Higuchi's model

Table 10.22: Coefficient of determination (R^2) from MET Release Kinetics Data of CMAP matrix tablet formulations

Kinetic models	F1	F2	F3	F4	F5	F6	F7	F8	F9	F10
Zero-order	0.8291	0.7831	0.9351	0.9245	0.9496	0.9001	0.8729	0.857	0.7831	0.867
1st -order	0.9078	0.9002	0.9435	0.9731	0.9815	0.98	0.9279	0.9219	0.6912	0.8392
Korsmeyer–Peppas	0.9755	0.9632	0.9906	0.9831	0.9353	0.9684	0.9589	0.9806	0.8775	0.9746
Higuchi	0.9806	0.9888	0.9943	0.9939	0.9755	0.9892	0.9877	0.9885	0.9512	0.9893
<i>n</i>	0.3785	0.504	0.5629	0.4898	0.5386	0.4376	0.4308	0.4145	0.4408	0.4936

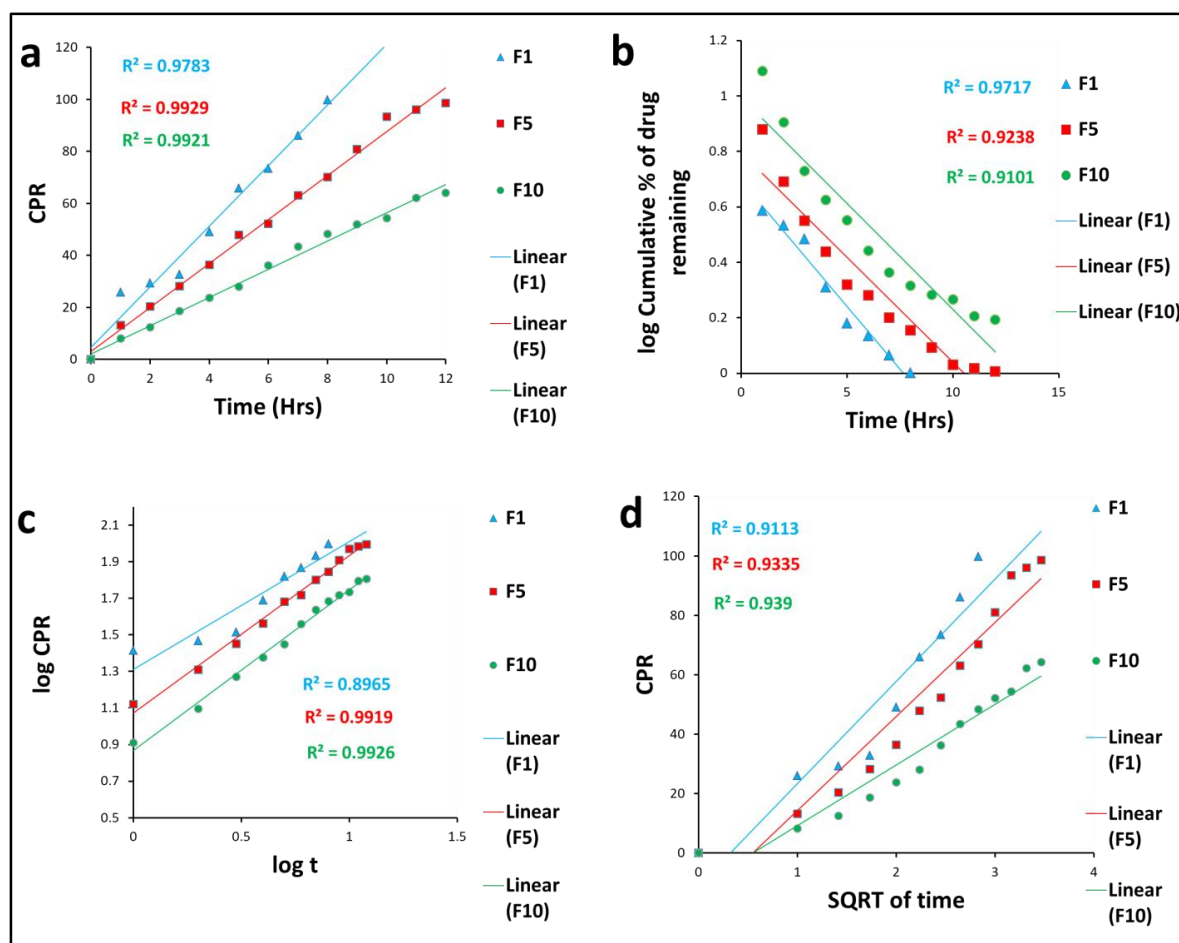


Figure 10.11: Release kinetics Models of MET-loaded CCMAP matrix tablet formulations (F1, F5, F10) (a) Zero-order, (b) 1st-order, (c) Korsmeyer–Peppas model, (d) Higuchi's model

Table 10.23: Coefficient of determination (R^2) from MET Release Kinetics Data of CCMAP matrix tablet formulations

Kinetic models	F1	F2	F3	F4	F5	F6	F7	F8	F9	F10
Zero-order	0.9783	0.9923	0.9864	0.9957	0.9929	0.9965	0.9961	0.9889	0.99	0.9921
1st –order	0.9717	0.9558	0.9469	0.9471	0.9238	0.9489	0.9535	0.9659	0.9614	0.9101
Korsmeyer–Peppas	0.8965	0.9884	0.9814	0.9896	0.9919	0.9865	0.9845	0.9777	0.978	0.9926
Higuchi	0.9113	0.9199	0.9109	0.9232	0.9335	0.9185	0.9129	0.8861	0.8954	0.939
<i>n</i>	0.6985	0.8424	0.8503	0.8417	0.8605	0.852	0.8601	0.8947	0.8726	0.8778

10.4. Mechanism of drug release from DIL-loaded matrix tablet formulations

In the thorough investigation of drug release kinetics from DIL-loaded matrix tablet formulations, employing a range of kinetic models, including zero-order, first-order, Korsmeyer–Peppas, and Higuchi, pivotal insights have been uncovered. Figures 10.12, 10.13, and 10.14 depict the specific release kinetics of DIL from various formulations using different matrices (NAP, CMAP, and CCMAP) for F1, F5, and F10. Similar graphical methods were utilized for all formulations to acquire data (R^2 , n) across different formulations (F2-F4, F6-F9). These findings, detailed in Tables 10.24, 10.25, and 10.26, serve as critical resources for comprehending the release patterns of DIL within a range of polymeric matrices (NAP, CMAP, and CCMAP).

Analyzing Table 10.24, for DIL-loaded matrix tablet formulations with NAP, only F1 ($R^2 = 0.9823$) and F2 ($R^2 = 0.9842$) adhered to the Korsmeyer–Peppas model. Conversely, F3 ($R^2 = 0.9875$), F4 ($R^2 = 0.9952$), F5 ($R^2 = 0.996$), and F10 ($R^2 = 0.9926$) followed the Higuchi model, while F6 to F9 aligned with the Korsmeyer–Peppas model. The diffusion exponents (n) of all formulations (F1-F10) in DIL-loaded NAP formulations ranged from 0.3255 to 0.3626 ($n < 0.45$), indicating a Fickian diffusion pattern.

For DIL-loaded CMAP formulations (Table 10.25), F1 ($R^2 = 0.9833$), F3 ($R^2 = 0.9779$), F4 ($R^2 = 0.9768$), F5 ($R^2 = 0.9742$), F7 ($R^2 = 0.9793$), and F9 ($R^2 = 0.9764$) followed the Korsmeyer–Peppas model. In contrast, F2 ($R^2 = 0.963$), F6 ($R^2 = 0.9813$), F8 ($R^2 = 0.9682$), and F10 ($R^2 = 0.9792$) adhered to the Higuchi model. The diffusion exponents (n) of all formulations (F1-F10) demonstrated Fickian diffusion ($n < 0.45$). These formulations exhibited both immediate release and diffusion-controlled behavior.

Concerning DIL-loaded CCMAP formulations (Table 10.26), F1 to F10 best fitted with zero-order kinetics, signifying sustained release. The diffusion exponents (n) for F1 to F10 formulations indicated anomalous (non-Fickian) diffusion.

These findings elucidate the nuanced release behaviors of DIL within different matrices, offering valuable insights for tailoring drug delivery systems. The Fickian diffusion observed in NAP formulations suggests a more predictable release mechanism, while the

anomalous diffusion in CMAP and sustained release in CCMAP formulations underline their potential for varied therapeutic applications. This meticulous evaluation contributes significantly to the optimization of drug delivery systems for enhanced therapeutic outcomes.

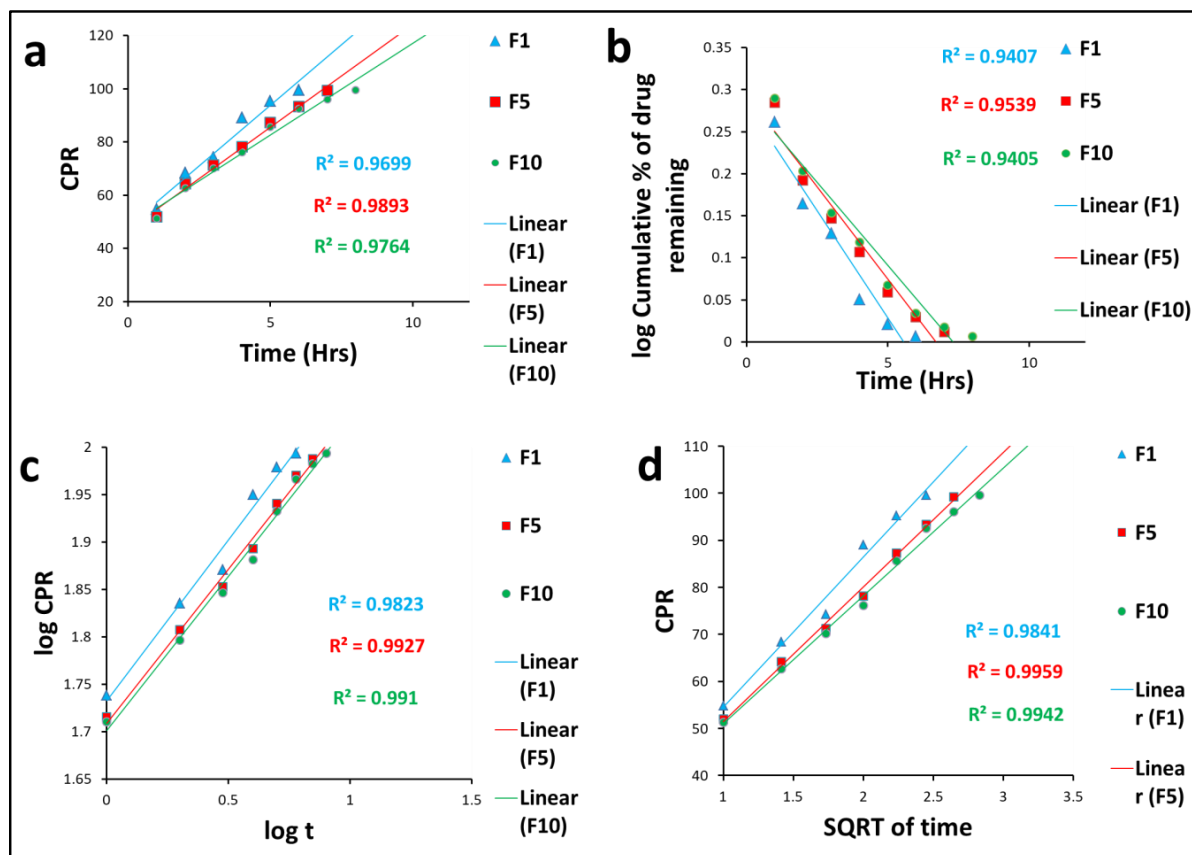


Figure 10.12: Release kinetics Models of DIL-loaded NAP matrix tablet formulations (F1, F5 and F10) (a) Zero-order, (b) 1st-order, (c) Korsmeyer–Peppas model, (d) Higuchi's model

Table 10.24: Coefficient of determination (R^2) from DIL Release Kinetics Data of NAP formulations

Kinetic models	F1	F2	F3	F4	F5	F6	F7	F8	F9	F10
Zero-order	0.9699	0.9651	0.9773	0.9818	0.9893	0.9606	0.9651	0.9647	0.9637	0.9764
1st-order	0.9407	0.9406	0.9548	0.9515	0.9539	0.9295	0.9317	0.9336	0.9326	0.9405
Korsmeyer–Peppas	0.9823	0.9842	0.985	0.9924	0.9927	0.988	0.9904	0.989	0.9894	0.991
Higuchi	0.9841	0.9828	0.9875	0.9952	0.9959	0.9859	0.9895	0.9882	0.988	0.9942
<i>n</i>	0.339	0.3618	0.3626	0.3295	0.3256	0.3268	0.3302	0.3293	0.3308	0.3255

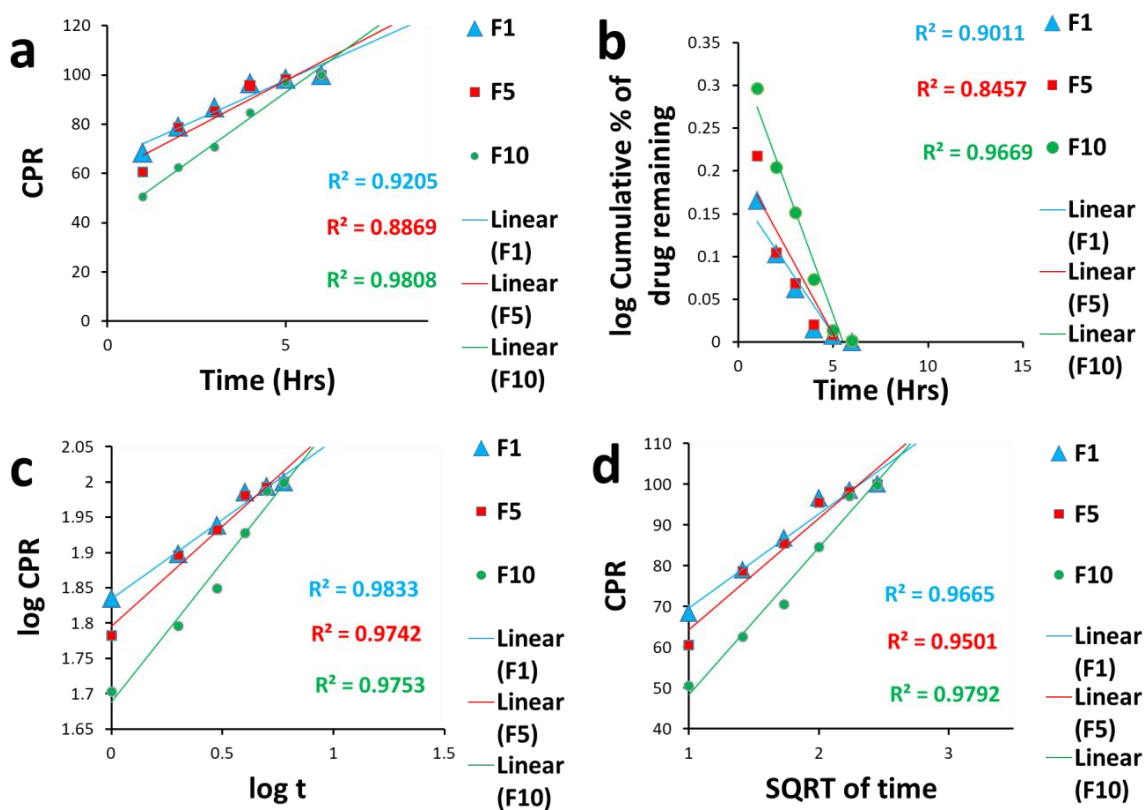


Figure 10.13: Figure 10.10: Release kinetics Models of DIL-loaded CMAP matrix tablet formulations (F1, F5 and F10) (a) Zero-order, (b) 1st-order, (c) Korsmeyer–Peppas model, (d) Higuchi's model

Table 10.25: Coefficient of determination (R^2) from DIL Release Kinetics Data of CMAP formulations

Kinetic models	F1	F2	F3	F4	F5	F6	F7	F8	F9	F10
Zero-order	0.9205	0.9473	0.8893	0.8929	0.8869	0.9709	0.9048	0.9653	0.8953	0.9808
1st -order	0.9011	0.9387	0.8541	0.8547	0.8457	0.9575	0.8612	0.9567	0.849	0.9669
Korsmeyer–Peppas	0.9833	0.9577	0.9779	0.9768	0.9742	0.9761	0.9793	0.9603	0.9764	0.9753
Higuchi	0.9665	0.963	0.9519	0.9535	0.9501	0.9813	0.9614	0.9682	0.9564	0.9792
<i>n</i>	0.2251	0.2646	0.2708	0.2771	0.2839	0.2973	0.282	0.3146	0.2983	0.3974

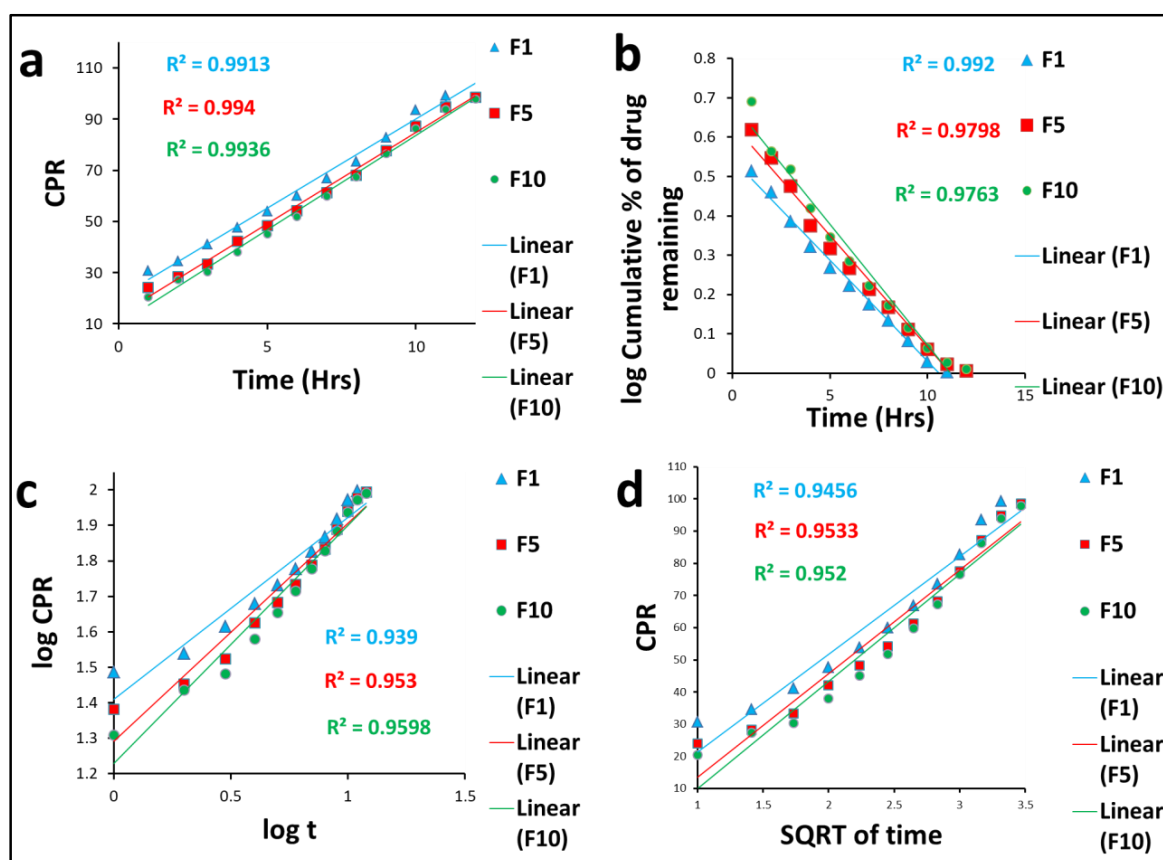


Figure 10.14: Figure 10.11: Release kinetics Models of DIL-loaded CCMAP matrix tablet formulations (F1, F5 and F10) (a) Zero-order, (b) 1st-order, (c) Korsmeyer–Peppas model, (d) Higuchi's model

Table 10.26: Coefficient of determination (R^2) from DIL Release Kinetics Data of CCMAP formulations

<i>Kinetic models</i>	F1	F2	F3	F4	F5	F6	F7	F8	F9	F10
Zero-order	0.9913	0.9923	0.9925	0.9929	0.994	0.9929	0.9925	0.9925	0.9911	0.9936
1st –order	0.992	0.9814	0.9816	0.9806	0.9798	0.9804	0.9809	0.9809	0.9848	0.9763
Korsmeyer–Peppas	0.939	0.9559	0.9561	0.9498	0.953	0.9515	0.9511	0.9503	0.9456	0.9598
Higuchi	0.9456	0.9527	0.9516	0.9509	0.9533	0.9505	0.9495	0.948	0.9438	0.952
<i>n</i>	0.5132	0.5644	0.5894	0.606	0.6136	0.6219	0.6293	0.6396	0.6429	0.6704

The investigation of MET-loaded and DIL-loaded matrix tablet formulations using NAP, CMAP, and CCMAP unveiled significant insights into their respective drug release behaviors.

Concerning the MET formulations, the combination with NAP exhibited a tendency towards sustained release but not in a fully sustained manner, indicating a moderate controlled release profile. In contrast, the CMAP matrices demonstrated faster and immediate release characteristics, signifying a rapid drug release from these formulations. Conversely, the CCMAP formulation showcased a completely sustained release behavior, indicative of a prolonged and consistent drug release over time. Similar trends were observed in the DIL-loaded formulations, reaffirming the robustness of the formulations and highlighting distinct behaviors among the polymer types.

Expanding the analysis to rheological data shed light on viscoelasticity, mechanical strength, rheological stability, and the consistency of viscoelastic gel across different polymer formulations. The superior attributes were exhibited by CCMAP, outperforming NAP and CMAP, which followed in a sequential order concerning their rheological properties.

Swelling data analysis further delineated differences in water penetration velocities among the various polymer matrices. CMAP displayed a higher water penetration velocity compared to NAP and CCMAP, indicating increased water absorption and subsequent swelling in CMAP.

Analysis of the release kinetics data revealed distinct drug release mechanisms among the formulations. NAP and CMAP adhered to the Korsmeyer–Peppas and Higuchi models, pointing to diffusion-controlled release mechanisms. On the contrary, all CCMAP formulations followed zero-order kinetics, indicating a consistent drug release rate independent of drug concentration over time.

Moreover, scrutinizing the diffusion exponent (n) values provided additional insights. All CMAP formulations exhibited diffusion-controlled drug release behavior. In contrast, NAP and CCMAP showcased Non-Fickian (anomalous) release patterns, implying a blend of diffusion and other contributing factors to the drug release mechanism.

In summary, these detailed analyses unveil distinctive behaviors among the three polymer matrices in drug-loaded formulations. CCMAP stands out for its sustained release profile and robust viscoelastic properties, while CMAP displays rapid release characteristics and higher water penetration. NAP showcases moderate sustained release behavior and presents anomalous drug release patterns, indicating complex release mechanisms. These findings underscore the pivotal role of polymer selection in shaping drug release kinetics and the rheological characteristics of matrix tablet formulations.

In conclusion, these findings revealed the intrinsic relationship between polymer tailoring, rheology, and drug release kinetics in matrix tablet formulations.

10.5. Correlation between polymer rheology and drug release

The correlation between polymer rheology and drug release presents a multifaceted relationship, intricately woven through the dynamics of polymer flow under diverse conditions and its consequential impact on drug release kinetics. The investigation, centered around matrices comprising NAP, CMAP, and CCMAP polymers, provides a nuanced perspective on this intricate correlation.

An initial focal point lies in the viscosity profiles of NAP, CMAP, and CCMAP matrices, revealing distinctive behaviors responsive to varying pH levels. Notably, NAP matrices exhibit non-Newtonian behavior, characterized by a pseudo-plastic flow pattern. The observed decline in viscosity with escalating shear rates, coupled with the pH-dependent variations, accentuates the environmental sensitivity of NAP matrices. This sensitivity, as

unveiled by the data, suggests potential applications where tailored rheological properties are paramount.

The exploration extends to the impact of crosslinking on rheological behavior, particularly pronounced in CCMAP matrices. The interplay between calcium ions and carboxylic groups induces crosslinking, resulting in a substantial increase in viscosity [Donati et al., 2021]. This modification in rheological behavior is attributed to the confinement and restriction of chain movement, spotlighting the governing role of chemical structure in polymer rheology [Madathinal Kunjappan et al., 2021]. The consequential increase in viscosity, especially in CCMAP matrices, underlines the potential for tailored rheological properties through controlled crosslinking processes.

The application of distinct models to describe the flow behavior of NAP and CMAP matrices further enriches the understanding of their distinctive rheological responses under different pH conditions. The varied model fittings underscore the complexity of NAP matrices, capturing their unique flow patterns in response to changes in pH. In contrast, the consistency of CMAP matrices, reflected by the prevalence of the Ellis model across pH levels, points to a more uniform rheological behavior.

Linear viscoelasticity studies contribute crucial insights into the mechanical strength and stability of NAP, CMAP, and CCMAP matrices. The shorter linear viscoelastic (LVE) range in CMAP, attributed to electrostatic repulsion, contrasts with the broader and more stable LVE observed in crosslinked CCMAP. These findings highlight the intricate balance between polymer structure, pH sensitivity, and crosslinking processes in governing the linear viscoelastic properties of these matrices.

The frequency sweep analysis delves into the viscoelastic nature of the matrices, with CCMAP consistently exhibiting higher G' values than NAP and CMAP. The absence of crossover points between G' and G'' in CCMAP matrices indicates heightened rheological stability, attributed to extensive entanglement resulting from the crosslinking process. This reinforces the pivotal role of crosslinking in tailoring the viscoelastic characteristics of polymers.

Transitioning to the comparison of drug release profiles, a formulation-dependent kinetics pattern emerges. The sustained release observed in CCMAP formulations is linked to the crosslinking process, which hinders water influx, reduces swelling, and promotes the formation of a viscoelastic gel layer. In contrast, CMAP formulations, driven by electrostatic repulsion, exhibit faster release. These formulation-specific release behaviors carry implications for designing drug delivery systems aligned with distinct therapeutic requirements.

In conclusion, the amalgamation of these findings establishes a comprehensive understanding of the correlation between polymer rheology and drug release. The chemical structure of polymers, coupled with their pH sensitivity and the influence of crosslinking processes, emerges as pivotal in dictating rheological behavior and, by extension, drug release kinetics. These insights provide a robust foundation for the design and optimization of polymer-based drug delivery systems tailored to diverse therapeutic applications.

10.6. Accelerated stability study

The accelerated stability study conducted on MET and DIL-loaded tablets, specifically formulations F1, F4, F7, and F10 of NAP, CMAP, and CCMAP, aimed to assess the impact of stress conditions (40°C and 75±5% RH) over a six-month period. The formulations, chosen based on their desired drug release profiles, underwent a rigorous analysis to evaluate changes in drug content, drug release profiles, and physical characteristics.

The visual representation of release profiles in Figure 10.15 and Figure 10.16, comparing the initial and aged tablets, indicated a remarkable consistency in both MET and DIL formulations under stress conditions. To quantify this, Similarity Factors (f_2) were calculated and presented in Table 10.27. The f_2 values, consistently exceeding 50 (except MET-loaded NAP F1 formulation), signify a high level of similarity between the dissolution profiles of initial and aged tablets, affirming the stability of both the drug and the formulations [Costa & Lobo, 2001].

Additionally, stability analysis encompassing physical characteristics and assay values (Tables 10.28 and 10.29) revealed that the tablet formulations maintained their integrity throughout the storage period. It's noteworthy that CMAP formulations of both MET and DIL exhibited an increase in average weight due to the hygroscopic nature attributed to the presence of carboxymethyl groups.

Table 10.28 outlines the parameters for MET matrix tablet formulations. The average weight and assay values for F10 formulations of NAP, CMAP, and CCMAP remained consistent during the six-month storage period, reinforcing their stability under stress conditions.

Similarly, Table 10.29 details the parameters for DIL matrix tablet formulations. The physical description, average weight, and assay values for F7 formulations of NAP, CMAP, and CCMAP demonstrated a sustained stability over the six months of accelerated aging.

In conclusion, the accelerated stability study provides robust evidence that the selected formulations of NAP, CMAP, and CCMAP matrices, loaded with MET and DIL, maintain their structural and chemical integrity under stress conditions. The visual representation, similarity factors, and assay values collectively validate the stability of these formulations, crucial for ensuring the reliability and effectiveness of drug delivery systems over time.

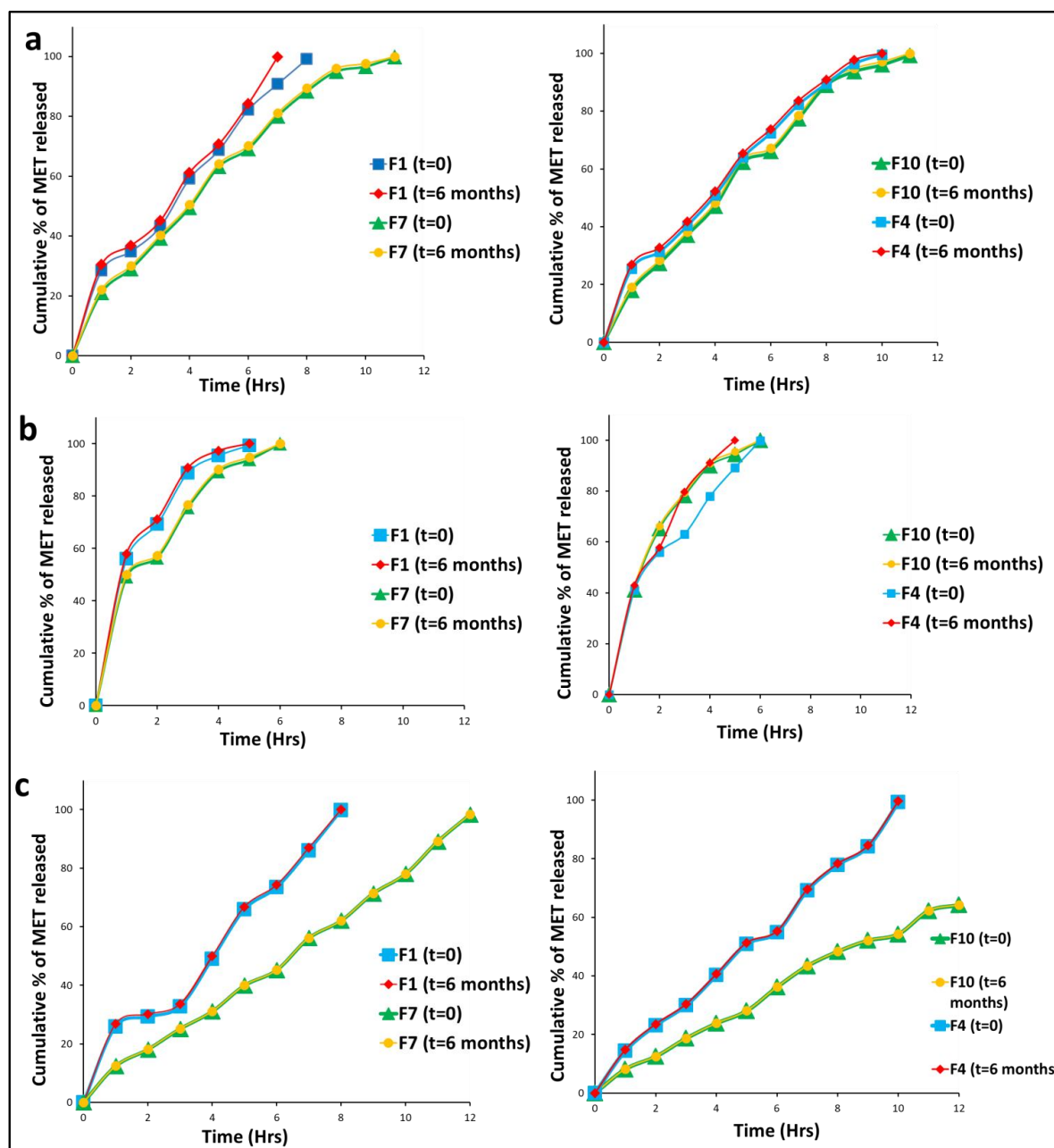


Figure 10.15: Effect of storage on the release of MET-loaded (a) NAP formulations, (b) CMAP formulations, (c) CCMAP formulations

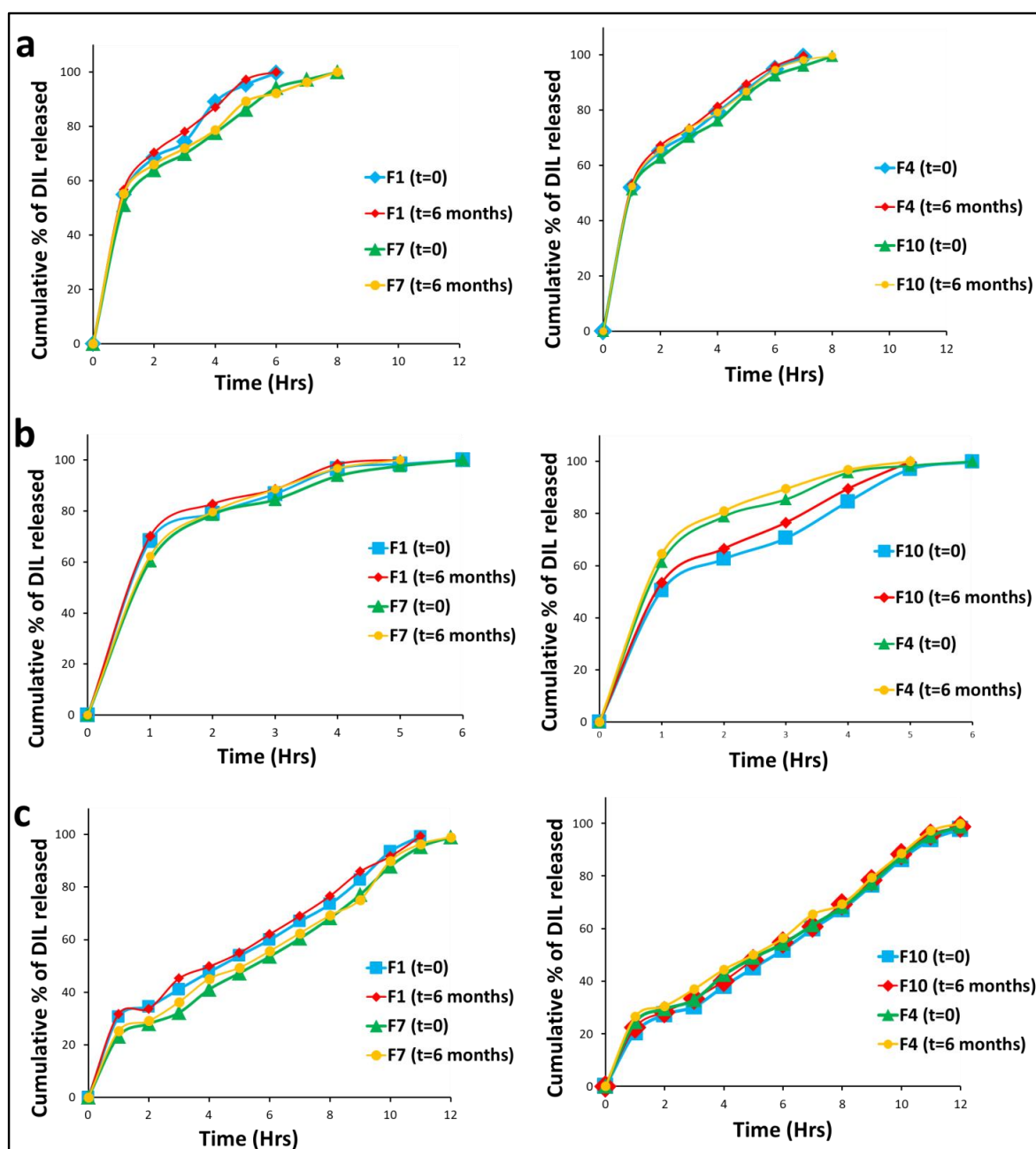


Figure 10.16: Effect of storage on the release of DIL-loaded (a) NAP formulations, (b) CMAP formulations, (c) CCMAP formulations

Table 10.27: Similarity factors (f_2) of corresponding to both MET and DIL formulations

MET Formulations	f_2	DIL Formulation	f_2
F1 MET+NAP	49.6995 ±1.87	F1 DIL+NAP	85.7321 ±2.04
F7 MET+NAP	92.2246 ±1.07	F7 DIL+NAP	81.327 ±1.43
F10 MET+NAP	92.4039 ±2.04	F10 DIL+NAP	83.405 ±2.15
F7 MET+NAP	88.3515 ±1.31	F4 DIL+NAP	84.9118 ±1.65
F1 MET+CMAP	82.9334 ±1.24	F1 DIL+CMAP	77.8785 ±1.08
F7 MET+CMAP	94.5578 ±1.08	F7 DIL+CMAP	80.031 ±1.99
F10 MET+CMAP	94.2133 ±2.16	F10 DIL+CMAP	68.8696 ±2.09
F4 MET+CMAP	77.6553 ±1.06	F4 DIL+CMAP	85.6625 ±1.38
F1 MET+CCMAP	95.1919 ±1.77	F1 DIL+CCMAP	89.0273 ±2.11
F7 MET+CCMAP	99.8947 ±1.29	F7 DIL+CCMAP	88.8442 ±1.27
F10 MET+CCMAP	99.8943 ±1.05	F10 DIL+CCMAP	83.1605 ±1.33
F4 MET+CCMAP	98.1422 ±1.63	F4 DIL+CCMAP	87.4816 ±1.48

Mean ± SD (n=3)

Table 10.28: Accelerated stability study profile of MET-loaded formulations

MET matrix tablet formulations						
SL NO.	Parameters	Standards	Initial	40°C and 75±5% % RH		
1	Description	Oval, Convex	complies	1st Month complies	3rd Months complies	6th Months complies
2	Average wt. (mg)	F10 (NAP)	1117.08 ±1.26%	1117.13 ±1.09	1117.56 ±1.51	1118.09 ±1.28
		F10 (CMAP)	1115.18 ±2.35	1115.68 ±1.43	1116.04 ±1.39	1119.23 ±1.06
		F10 (CCMAP)	1121.06 ±2.14	1121.24 ±1.74	1121.62 ±2.19	1121.79 ±1.61
3	Assay	F10 (NAP)	99.82% ±0.11	99.80% ±0.17	99.79% ±0.15	99.79% ±0.13
		F10 (CMAP)	98.77% ±0.2	98.71% ±0.25	98.67% ±0.23	98.63% ±0.28
		F10 (CCMAP)	100.09% ±0.26	100.05% ±0.17	99.98% ±0.16	99.95% ±0.14
Mean ± SD (n=3)						

Table 10.29: Accelerated stability study profile of DIL-loaded formulations

DIL matrix tablet formulations						
SL NO.	Parameters	Standards	Initial	40°C and 75±5% % RH		
1	Description	Oval convex,	complies	1st Month complies	3rd Month complies	6th Month complies
2	Average wt. (mg)	F7 NAP	1113.16	1113.15	1114.06	1114.18
			±1.26	±1.11	±1.31	±1.22
		F7 CMAP	1111.24	1111.97	1112.13	1113.03
			±1.07	±1.61	±1.04	±1.19
		F7 CCMAP	1115.43	1115.79	1116.02	1116.12
			±2.04	±1.08	±2.12	±1.12
3	Assay	F7 NAP	100.09%	100.07%	99.99%	99.98%
			±0.21	±0.13	±0.16	±0.17
		F7 CMAP	99.97%	99.91%	99.81%	98.96%
			±0.18	±0.1	±0.28	±0.25
		F7 CCMAP	99.83%	99.82%	99.78%	99.06%
			±0.24	±0.18	±0.26	±0.11
Mean ± SD (n=3)						

Conclusion

In conclusion, the investigation into MET and DIL-loaded matrix tablet formulations utilizing NAP, CMAP, and CCMAP provided comprehensive insights into drug release behaviors. The distinct behaviors observed—moderate sustained release for NAP, rapid release for CMAP, and fully sustained release for CCMAP—underscore the critical role of polymer selection in shaping drug release kinetics. Rheological analysis highlighted CCMAP's superior viscoelastic properties, establishing a clear correlation between polymer tailoring and rheology. Swelling data emphasized differences in water penetration among polymers, particularly CMAP's higher water absorption. Release kinetics revealed unique mechanisms, with NAP and CMAP following diffusion-controlled models, while CCMAP adhered to zero-order kinetics, showcasing varied release behaviors among the polymers. Additionally, the accelerated stability study confirmed the stability of select formulations of NAP, CMAP, and CCMAP under stress conditions over a six-month period. The consistency observed in visual representations, similarity factors, and assay values reinforces the reliability and integrity crucial for effective and consistent drug delivery systems.

CHAPTER 11

SUMMARY AND CONCLUSION

SUMMARY AND CONCLUSION

The study delves into *Albizia procera*, a fast-growing species found across various tropical forests in India and Vietnam. It's known for its root suckering ability and adaptability to different forest types. This work explores the potential of *A. procera* gum in drug delivery systems by analyzing its galactose and arabinose components and their impact on rheological properties. Customizing these components through chemical modification and cross-linking could alter the gum's stability and affect drug diffusivity. Understanding its rheological behavior may help predict drug release patterns and assess polymer matrix strength, crucial for effective drug delivery systems.

The study aims to investigate the impact of carboxymethylation and ionic crosslinking on the rheological properties and drug release behavior of native *Albizia procera* gum (NAP). Carboxymethylation enhances water solubility and modifies rheological properties. Ionic crosslinking aims to manipulate gelation behavior. Phase 1 involved synthesizing carboxymethyl *Albizia procera* gum (CMAP) and formulating matrix tablets to explore drug release and rheology. Phase 2 investigates ionic crosslinking effects on the gum and matrix tablets. Phase 3 assesses stability and optimizes formulations for long-term drug release and stability, aiming to identify the most stable and efficient formulation among NAP, CMAP, and crosslinked CMAP. The study could contribute to developing novel drug delivery systems using natural polysaccharides with tunable properties for pharmaceutical applications.

- ❑ The purification process of Native Albizia procera gum (NAP) involved a meticulously devised protocol comprising several systematic steps. Initially, the crude gum powder underwent a controlled boiling treatment in 80% ethanol to inactivate enzymes and extract low molecular weight carbohydrates and extraneous colorants. Following this, the resulting gum powder was dispersed in deionized water and stirred overnight using a magnetic stirrer to ensure optimum dissolution and the separation of any undissolved particles. The refined gum solution was allowed to settle undisturbed for 12 hours, facilitating the separation of residual particles. This solution underwent filtration through Whatman No.1 filter paper to eliminate solid impurities. Next, threefold volumes of propanol were added to the filtered solution, inducing the formation of a distinct precipitate that captured the purified gum material. This precipitated gum material was air-dried, sieved through a No. 85 sieve to ensure uniform particle size, and stored within desiccators to preserve its integrity and quality.

- ❑ Moving on to the synthesis and characterization of carboxymethyl Albizia procera (CMAP), the carboxymethylation process of NAP involved a base-catalyzed reaction mechanism. Powdered NAP underwent sieving and precise weighing before being gradually introduced into an aqueous solution of sodium hydroxide within a temperature-regulated ice chamber. Mono chloroacetic acid (MCAA) was then added gradually, followed by continuous stirring and controlled reaction under specified temperature conditions. The reaction mass underwent subsequent stages involving filtration, air-drying, and multiple washes with aqueous methanol, adjusting the pH to neutral and drying in a hot oven. This process was systematically applied to six different CMAP batches, aiming to scrutinize the influence of varying temperature ranges and MCAA quantities on the carboxymethylation process.

- ❑ Characterization studies included the determination of the degree of substitution (DS), Fourier Transform Infrared (FTIR) analysis, X-ray Powder Diffraction (XRD) study, Solid State ^{13}C NMR Spectroscopy, elemental analysis, zeta potential comparison, comparative rheological studies, and a RBC lysis test.

The DS determination involved several steps, including the addition of HCl, filtration, dissolution, and titration. FTIR and XRD studies were conducted to analyze the spectra and diffraction patterns of NAP and CMAP. Solid State ^{13}C NMR Spectroscopy was performed using powdered samples to assess molecular structures. Elemental analysis was carried out using a CHNS/O Elemental Analyzer. Zeta potential comparison evaluated surface charge properties, while rheological studies analyzed flow behavior and viscoelastic properties.

The RBC lysis test involved the isolation of RBCs, suspension preparation, incubation with sample solutions, and optical density assessment to evaluate any alterations in RBC properties due to sample interactions.

- ❑ The preparation of crosslinked CMAP (CCMAP) involved a similar process to CMAP synthesis with the addition of CaCl_2 and subsequent characterization, including FTIR spectrum analysis, Differential Scanning Calorimetry (DSC) study, Zeta potential analysis and comparison, X-ray Powder Diffraction (XRD) study, and Comparative Rheological studies.
- ❑ The comprehensive characterization of NAP through various analytical techniques offers significant insights into its chemical composition, thermal behavior, structural properties, and surface characteristics. The FTIR analysis highlights the presence of distinct functional groups, particularly strong hydrogen bonding involving hydroxyl groups, providing crucial information about the substance's composition. The DSC study reveals thermal stability and distinct exothermic and melting events, suggesting defined phase transitions within NAP. Solid State ^{13}C NMR Spectroscopy delineates specific carbon signals, elucidating the galactose and arabinose components within the

compound's structure. X-ray Diffractometry confirms the amorphous nature of NAP, which can influence its solubility and dissolution kinetics. Zeta potential measurements showcase a negative charge, impacting its colloidal stability, surface interactions, and potential biomedical applications. These detailed analyses collectively offer fundamental insights into NAP's properties, laying the foundation for tailored applications, particularly in drug delivery systems and biomedical fields.

- ❑ The investigation into CMAP involved a profound analysis elucidating the chemical transformation from NAP to CMAP and its ensuing properties. The extent of carboxymethylation, as reflected by the degree of substitution (DS), evidenced significant modifications in the chemical composition and functionalization of NAP. The FT-IR spectra demonstrated distinctive absorption bands in CMAP, affirming successful carboxymethylation and structural alterations. The DSC analysis unveiled distinct melting peaks in CMAP, indicating pronounced modifications in thermal behavior post-carboxymethylation, while preserving overall thermal stability. Solid State ^{13}C NMR Spectroscopy provided conclusive evidence of carboxymethyl group introduction and structural modifications in CMAP, differentiating it from NAP. X-ray Diffractometry highlighted crystalline patterns within CMAP, underscoring structural alterations resulting from carboxymethylation. Zeta potential measurements revealed a notable negative surface charge in CMAP, signifying enhanced stability and dispersion potential. These comprehensive characterizations shed light on the intricate molecular modifications and structural changes induced by carboxymethylation, offering invaluable insights into the tailored applications of CMAP particularly in pharmaceutical formulations and diverse industrial sectors. Further exploration into the relationship between carboxymethylation extent and CMAP properties promises deeper insights and refined applications in various domains.
- ❑ The characterization of Crosslinked Carboxymethylated Albizia procera gum (CCMAP) highlighted the successful synthesis through a two-step process

involving carboxymethylation of the native gum followed by ionic crosslinking with calcium chloride. The FT-IR spectrum analysis revealed structural modifications in CCMAP, showcasing shifted O-H stretching bands and distinctive vibrations, elucidating the interplay between the polymer and calcium ions, crucial for understanding its behavior. DSC thermograms depicted altered thermal behavior in CCMAP, indicating enhanced thermal stability due to the ionic crosslinking process. X-ray Diffractometry unveiled heightened crystallinity in CCMAP compared to CMAP, emphasizing the role of calcium crosslinking in structurally enhancing the polymer. Zeta potential measurements showcased a shift towards less negativity in CCMAP due to the interactions between carboxymethyl groups and calcium ions, reflecting the intricate interplay between chemical functionalities and ionic crosslinking. These comprehensive analyses provide fundamental insights into the structural alterations and interactions within CCMAP, offering key information crucial for its potential applications across various domains, particularly in biomedicine and pharmaceuticals. Understanding the intermolecular interactions that influence its properties paves the way for tailored applications in diverse fields. In essence, the characterization of CCMAP provided comprehensive insights into its structural modifications induced by the crosslinking process, emphasizing the pivotal role of intermolecular interactions and ionic crosslinking in shaping its properties for potential diverse applications.

- ❑ The investigation into the impact of NAP, CMAP, and CCMAP on red blood cell (RBC) properties through optical density measurements at 29.8°C over 1 and 3 hours incubation revealed minimal fluctuations. Both NAP and CCMAP exhibited consistent optical densities, indicating negligible influence on RBC properties throughout the experimental duration. Similarly, CMAP demonstrated stable optical densities, suggesting it maintained a mild effect on RBCs. In contrast, the positive control (WFI) showed notably higher optical densities, indicating substantial effects, potentially due to osmotic influences. The mild impact of NAP, CMAP, and CCMAP on RBC properties compared to the potent effects of the positive control suggests their suitability for various

applications involving RBCs without significant disruption to these vital blood components.

- ❑ The comparative rheological assessment of NAP, CMAP, and CCMAP matrices offered significant insights into their flow behavior, viscosity profiles, and response to varying pH levels. The investigation through dynamic rotational studies revealed distinct rheological characteristics across these polymers.

NAP matrices demonstrated non-Newtonian behavior with declining viscosity at increasing shear rates, displaying a pseudo-plastic flow pattern. Notably, variations in pH significantly impacted the viscosity of NAP matrices, showcasing their sensitivity to acidic or alkaline environments. The varying viscosities at different pH levels lay the groundwork for potential applications in diverse industries.

Conversely, CMAP matrices exhibited shear-thinning behavior with significantly lower viscosities compared to NAP matrices. The presence of carboxymethyl groups impeded chain entanglement, resulting in reduced viscosity. Variations in pH further affected the viscosity, emphasizing the impact of electrostatic repulsion on disentanglement and viscosity reduction.

CCMAP matrices, attributed to the crosslinking process involving calcium ions and carboxylic groups, displayed heightened viscosity compared to both CMAP and NAP matrices. The crosslinking-induced confinement and restriction of chain movement resulted in increased viscosity, facilitating the formation of viscoelastic gels with tailored rheological properties.

Flow curve model analysis highlighted diverse model fittings for NAP matrices at different pH levels, elucidating their nuanced rheological behavior. Similarly, CMAP matrices consistently exhibited the Ellis model across pH values, showcasing the uniformity of their flow properties.

Dynamic oscillatory studies delved into linear viscoelasticity, establishing the critical strain and linear viscoelastic region (LVE) for these matrices. NAP matrices demonstrated higher LVE and mechanical strength compared to CMAP. Conversely, CCMAP exhibited superior mechanical strength attributed to crosslinking, presenting a broader and more stable LVE compared to CMAP.

Frequency sweep analysis reaffirmed NAP's stronger viscoelastic behavior compared to CMAP, while CCMAP matrices consistently displayed superior rheological stability and viscoelastic characteristics due to extensive entanglement from the crosslinking process.

The damping factor analysis revealed that all polymers exhibited elastic deformation at varying pH levels, with CCMAP and NAP displaying higher elasticity compared to CMAP, as reflected in their respective loss tangent values.

In essence, these comprehensive rheological assessments underscored the intricate rheological behaviors of NAP, CMAP, and CCMAP matrices. The sensitivity of these polymers to pH variations, coupled with the impact of crosslinking on their rheological properties, offers valuable insights for tailored applications in diverse industrial and scientific domains.

- ❑ The analysis encompassing pre-formulation studies like micromeritic properties, swelling, erosion behaviors, water penetration velocity, and SEM studies of placebo (blank) matrix tablets of NAP, CMAP, and CCMAP that provides essential insights into their applicability for pharmaceutical formulations.
- ❑ All granules maintained favorable flow properties and compressibility, crucial for pharmaceutical processing.

- NAP displayed excellent flow characteristics, positioning it as a promising option for pharmaceutical applications.
- CMAP exhibited better flow but increased compressibility compared to NAP.
- CCMAP showcased compromised flow and increased compressibility relative to NAP and CMAP.
- The addition of MET and DIL influenced micromeritic properties, hinting at potential impacts on overall flow characteristics.

□ NAP showed moderate swelling, positioned between CMAP and CCMAP in acidic and buffer environments.

- CMAP exhibited rapid and substantial swelling, ideal for immediate drug release.

CCMAP demonstrated minimal swelling due to calcium crosslinking, suggesting controlled or sustained release potential.

Swelling order: CMAP > NAP > CCMAP, emphasizing crosslinking and entanglement impacts.

- Water penetration and swelling dynamics influenced dissolution and drug release patterns significantly.

Water penetration sequence: CMAP > NAP > CCMAP, reflecting their distinctive matrix characteristics.

CMAP's rapid water uptake due to disentangled gel layers suited immediate drug release formulations.

CCMAP's restricted water penetration indicated controlled release potential from enhanced entanglement.

- Erosion behavior varied; CMAP exhibited higher erosion, while Ca²⁺ ions in CCMAP restricted erosion, suggesting sustained release applications.

□ SEM images validated dissolution behaviors, emphasizing controlled dissolution in CCMAP and rapid dissolution in CMAP.

CCMAP's gel-like structure and limited erosion supported sustained release due to Ca^{2+} crosslinking.

- Unique properties of NAP, CMAP, and CCMAP present avenues for tailored drug delivery systems.

CMAP's potential for immediate drug release contrasts with CCMAP's controlled or sustained release possibilities.

Leveraging these insights enables the creation of specific drug release profiles, catering to diverse medical needs.

Overall evaluations provide a critical foundation for advanced drug delivery system designs, ensuring precise control over drug release kinetics and bolstering therapeutic efficacy.

The pursuit of effective drug delivery systems in pharmaceutical research led to the exploration of novel polysaccharide-based materials. Native Albizia Procera (NAP) gum, with its matrix-forming capabilities and modifiability, emerged as a compelling candidate for sustained-release matrix tablet formulations.

- ❑ The pre-formulation studies evaluated drug-polymer interaction compatibility using FTIR spectra and thermal analyses of the drugs (MET and DIL) and their mixtures with polymers (NAP, CMAP, and CCMAP). These studies aimed to assess potential interactions between components, crucial for subsequent formulation processes.
- ❑ This study also clarified the spectral characteristics and solubility behaviors of Metformin (MET) and Diltiazem (DIL) in different solvent systems. These drugs were selected due to their crucial roles in matrix tablet formulations. Through meticulous exploration of their spectral properties, calibration curves,

and solubility behaviors in diverse solvents, this research substantially enhances the understanding of these compounds.

The investigation elucidated the spectral properties of MET and DIL across multiple solvent systems, highlighting well-defined spectra in the UV range. These findings supported the applicability of UV spectrophotometric methods for straightforward analysis of these model drugs. The creation of calibration curves for both drugs in different solvent environments exhibited exceptional linearity within specified concentration ranges, affirming the precision and reliability of the methods used.

Furthermore, the solubility assessment of MET and DIL in various solvent systems at different pH levels provided vital insights. Both drugs demonstrated pH-dependent solubility behaviors, indicating variations in solubility based on the pH of the solvent. MET showed increased solubility in a phosphate buffer solution with a pH of 7.4 compared to water and an acidic solution with a pH of 1.2, suggesting its behavior as a weak base. Similarly, DIL displayed varying solubility patterns across different solvents, with higher solubility in water compared to an acidic solution, and slight improvement in solubility in the phosphate buffer solution with a pH of 7.4.

- ❑ The exploration of drug-polymer interactions through FTIR spectroscopy and thermal compatibility studies provided crucial insights into the molecular dynamics and thermal behavior of Metformin (MET) and Diltiazem HCl (DIL) in the presence of various polymers.
 - For Metformin, the FTIR analysis showcased no significant changes in characteristic absorption bands in the presence of NAP, CMAP, and CCMAP, suggesting an absence of substantial chemical interactions or structural alterations. Similarly, the thermal compatibility study revealed consistent melting points for MET across polymer mixtures, affirming the inert nature of the chosen polymers and their compatibility with Metformin. These results indicate the suitability of

NAP, CMAP, and CCMAP as excipients for MET formulations without affecting its thermal stability.

- Regarding Diltiazem HCl, FTIR spectra displayed consistent peaks in the presence of polymers, indicating stable drug-polymer interactions without significant chemical modifications. The thermal compatibility analysis revealed a slightly lower endothermic peak for DIL in polymer mixtures, suggesting minimal impact on the drug's melting behavior. However, the proximity of the peaks between pure DIL and DIL-polymer mixtures implies negligible alterations in Diltiazem HCl's fundamental thermal properties in the presence of the examined polymers.

These findings collectively highlight the compatibility and lack of substantial interactions between the selected polymers (NAP, CMAP, and CCMAP) and both Metformin and Diltiazem HCl. The absence of significant chemical modifications or alterations in the drug's structural and thermal properties indicates the potential suitability of these polymers as carriers or excipients in formulations involving Metformin and Diltiazem HCl, ensuring stability and integrity of the active pharmaceutical ingredients.

- The fabrication process of matrix tablets involved meticulous steps, ensuring precise formulation and preparation. These included weighing, sieving, granulation, drying, and compression to produce tablets meeting defined hardness specifications. Both MET and DIL-loaded matrix tablets were systematically formulated and categorized across different polymer groups—NAP, CMAP, and CCMAP, each having ten distinct formulations. Characterization tests such as weight uniformity, hardness, dimensions, friability, and content uniformity ensured quality compliance. In-vitro drug release studies in acidic and buffer solutions for MET and DIL-loaded tablets, followed by kinetics analysis, revealed distinct drug release profiles and

mechanisms across various formulations and polymers, vital for tailored drug delivery designs.

❑ Physical Characterization and Drug Release from MET-Loaded Matrix Tablet Formulations:

Detailed physical attributes of MET-loaded matrix tablets exhibited uniformity and compliance with pharmaceutical standards across NAP, CMAP, and CCMAP formulations.

❑ In-vitro Drug Release Study from MET-Loaded Matrix Tablet Formulations:

- MET release varied across formulations with F7 displaying the highest cumulative percentage (98.81%) within 11 hours. Only F10 demonstrated sustained release due to higher NAP concentration, highlighting the polymer's role in release kinetics. Area under the curve (AUC) analysis provided quantitative insights into drug release dynamics. ANOVA revealed significant variations in drug release among NAP matrices, emphasizing formulation impacts.
- CMAP formulations showed faster drug release compared to corresponding NAP formulations. Statistical analysis confirmed significant differences in drug release among CMAP matrices.
- CCMAP formulations exhibited sustained release behaviors influenced by polymer concentrations and Ca^{++} crosslinking. AUC values and ANOVA analysis supported sustained release characteristics and significant differences in drug release from CCMAP formulations.

❑ Comparison of Drug Release:

Distinct release observed among NAP, CMAP, and CCMAP formulations.

Sustained release in CCMAP contrasted with faster release in CMAP and intermediate release in NAP. ANOVA results highlighted significant variation in formulation-dependent release.

- MET-loaded CCMAP matrix tablets demonstrated sustained release patterns, indicating potential for controlled-release pharmaceutical formulations.
- Insights derived from the study offer valuable information for designing tailored drug delivery systems based on specific therapeutic needs and desired release kinetics.
- The exploration of modified albizia procera gum polymers underlines their potential applications in pharmaceutical formulations, providing a comprehensive understanding of their influence on drug delivery systems.
- Moreover, physical characterization of MET-loaded matrix tablets across NAP, CMAP, and CCMAP formulations confirmed uniformity and adherence to quality standards. These findings collectively underscore the potential of modified albizia procera gum polymers for tailored drug delivery systems, offering insights into their effects on drug release kinetics and polymer behavior.

❑ Physical Characterization and Drug Release from DIL-Loaded Matrix Tablet Formulations:

Detailed physical attributes of DIL-loaded matrix tablets exhibited uniformity and compliance with pharmaceutical standards across NAP, CMAP, and CCMAP formulations.

❑ In-vitro Drug Release Study from DIL-Loaded Matrix Tablet Formulations:

- Gradual and sustained release of DIL observed in NAP formulations within 8 hours, indicating controlled release properties. AUC values showcased substantial drug release at both pH conditions, suggesting responsiveness to gastrointestinal tract variations. ANOVA results highlighted significant differences in cumulative DIL release from NAP matrices, emphasizing formulation impacts on drug release kinetics. Contrary to complete sustained release, the observed release behavior in NAP formulations indicated a controlled release pattern with pH-dependent variations.
- CMAP formulations exhibited rapid and momentary drug release, attributed to enhanced polymer chain mobility and weak gel networks. AUC values

supported substantial drug release for all formulations at both pH conditions, highlighting formulation responsiveness to gastrointestinal variations. ANOVA confirmed significant differences in drug releases between different CMAP matrices, emphasizing the formulation's impact on drug release.

- Higher polymer concentrations in CCMAP formulations exhibited prolonged and sustained release characteristics due to Ca^{+2} crosslinking. AUC values demonstrated sustained drug release patterns influenced by polymer concentration. Statistical analysis underscored significant differences in drug release among different CCMAP formulations.

❑ Comparison of Drug Release:

NAP showed less sustained release, CMAP exhibited immediate release, and CCMAP displayed sustained release behavior. Formulation-specific release behaviors have implications for tailored drug delivery strategies catering to varied therapeutic needs.

❑ Mechanism of Drug Release from MET-Loaded Matrix Tablet Formulations:

Drug release data were fitted into different kinetic models, revealing nuanced release behaviors.

NAP formulations suggested more predictable and controlled release patterns, CMAP exhibited non-Fickian diffusion, while CCMAP demonstrated variability in release behaviors.

❑ Mechanism of Drug Release from DIL-Loaded Matrix Tablet Formulations:

DIL release kinetics from various matrices unveiled specific release patterns.

NAP formulations indicated predictable release mechanisms, CMAP exhibited immediate release with diffusion-controlled behavior, and CCMAP showcased sustained release with variability among formulations.

In conclusion, the study provides detailed insights into the distinctive release behaviors of DIL-loaded matrix tablet formulations across NAP, CMAP, and CCMAP matrices. The observed variations underscore the pivotal role of the matrix in shaping

drug release kinetics, offering valuable information for tailored drug delivery strategies, and promising enhanced therapeutic outcomes.

□ The correlation between polymer rheology and drug release is complex and nuanced, as revealed by investigations into NAP, CMAP, and CCMAP matrices. Viscosity profiles, notably the non-Newtonian behavior of NAP and the crosslinking impact on CCMAP, underscore the sensitivity of polymers to environmental changes. Models describing flow behavior and viscoelastic studies further distinguish the unique rheological responses of these polymers. CCMAP's heightened rheological stability due to crosslinking significantly influences drug release, fostering sustained release through gel layer formation. In contrast, CMAP's electrostatic repulsion prompts faster drug release. Ultimately, these findings highlight the pivotal role of polymer structure, pH sensitivity, and crosslinking in governing rheology and subsequent drug release kinetics, offering crucial insights for tailored drug delivery systems.

□ The accelerated stability study conducted over six months on MET and DIL-loaded matrix tablets aimed to assess their enduring stability under stress conditions (40°C, 75±5% RH). Ten tablets from four batches of each formulation were subjected to rigorous analysis. Upon examination, the tablets demonstrated remarkable consistency in drug content, dissolution profiles, and physical characteristics when compared to freshly prepared tablets. The Similarity Factor (f_2) values consistently above 50 indicated a high similarity between the dissolution profiles of initial and aged tablets, confirming the stability of both the drugs and formulations.

The visual representation of release profiles showcased consistent behavior between the initial and aged tablets, particularly for MET formulations, except for one case in the MET-loaded NAP F1 formulation. Additionally, physical descriptions, average weight, and assay values revealed sustained stability across the formulations, affirming the structural and chemical integrity of the tablets under stress conditions. Notably,

formulations with CMAP displayed an increase in average weight due to the hygroscopic nature attributed to the presence of carboxymethyl groups.

In conclusion, the accelerated stability study provided robust evidence supporting the stability of NAP, CMAP, and CCMAP matrix formulations containing MET and DIL under stress conditions. The consistency observed in dissolution profiles, physical characteristics, and assay values reinforces their reliability and effectiveness in drug delivery systems over time.

The study of Albizia procera gum for drug delivery systems explored its potential through meticulous analysis of its galactose and arabinose components, shedding light on crucial modifications like carboxymethylation and ionic crosslinking. Understanding its rheological behavior became pivotal, providing predictive insights into drug release patterns and matrix strength—a cornerstone for effective drug delivery systems. The purification process ensured the integrity of Native Albizia procera gum (NAP), while characterizing carboxymethyl Albizia procera (CMAP) revealed its varied applications, especially in drug delivery and biomedical fields.

Moreover, the exploration into Crosslinked Carboxymethylated Albizia procera gum (CCMAP) illuminated structural modifications due to ionic crosslinking, with minimal impact on red blood cell properties. The comparative rheological assessment of NAP, CMAP, and CCMAP underscored their responsiveness to pH changes and the influence of crosslinking on their properties, offering insights into pharmaceutical formulations.

Delving deeper into drug-polymer interactions and release behaviors across NAP, CMAP, and CCMAP matrices, the study highlighted unique release mechanisms crucial for tailored drug delivery designs. The extensive stability study further

reinforced the reliability of these formulations under stress conditions, consolidating their potential for sustained pharmaceutical use.

In essence, this comprehensive study establishes a vital link between polymer rheology and drug release, unveiling the potential of modified *Albizia procera* gum in specialized drug delivery systems—an advancement promising enhanced therapeutic outcomes in diverse medical applications.

BIBLIOGRAPHY

Abbasi M, Sohail M, Minhas MU, Khan S, Hussain Z, Mahmood A, Shah SA, Kousar M. Novel biodegradable pH-sensitive hydrogels: An efficient controlled release system to manage ulcerative colitis. *International journal of biological macromolecules*. 2019 Sep 1;136:83-96.

Achi OK, Okolo NI. The chemical composition and some physical properties of a water-soluble gum from *Prosopis africana* seeds. *International journal of food science & technology*. 2004 Apr;39(4):431-6.

Agrawal PK, Jain DC, Gupta RK, Thakur RS. Carbon-13 NMR spectroscopy of steroidal sapogenins and steroidal saponins. *Phytochemistry*. 1985 Oct 29;24(11):2479-96.

Aguir C, M'Henni MF. Experimental study on carboxymethylation of cellulose extracted from *Posidonia oceanica*. *Journal of applied polymer science*. 2006 Feb 15;99(4):1808-16.

Al-Behadili A, Sellier M, Hewett JN, Nokes RI, Moyers-Gonzalez M. Identification of Ellis rheological law from free surface velocity. *Journal of Non-Newtonian Fluid Mechanics*. 2019 Jan 1;263:15-23.

Ali A, Ahmed S. Recent advances in edible polymer based hydrogels as a sustainable alternative to conventional polymers. *Journal of agricultural and food chemistry*. 2018 Jun 7;66(27):6940-67.

Al-Saidan SM, Krishnaiah YS, Patro S, Satyanaryana V. In vitro and in vivo evaluation of guar gum matrix tablets for oral controlled release of water-soluble diltiazem hydrochloride. *Aaps Pharmscitech*. 2005 Mar;6:E14-21.

Alvarez-Lorenzo C, Blanco-Fernandez B, Puga AM, Concheiro A. Crosslinked ionic polysaccharides for stimuli-sensitive drug delivery. *Advanced drug delivery reviews*. 2013 Aug 1;65(9):1148-71.

Ankit B, Rathore RP, Tanwar YS, Gupta S, Bhaduka G. Oral sustained release dosage form: an opportunity to prolong the release of drug. *IJARPB*. 2013 Jan 1;3(1):7-14.

Avachat AM, Dash RR, Shrotriya SN. Recent investigations of plant based natural gums, mucilages and resins in novel drug delivery systems. *Ind J Pharm Edu Res*. 2011 Jan;45(1):86-99.

Baccile N, Laurent G, Babonneau F, Fayon F, Titirici MM, Antonietti M. Structural characterization of hydrothermal carbon spheres by advanced solid-state MAS ¹³C NMR investigations. *The Journal of Physical Chemistry C*. 2009 Jun 4;113(22):9644-54.

Bajpai AK, Shukla SK, Bhanu S, Kankane S. Responsive polymers in controlled drug delivery. *Progress in Polymer Science*. 2008 Nov 1;33(11):1088-118.

Bandelin FJ. Compressed tablets by wet granulation. *Pharmaceutical dosage forms: tablets*. 1989 Jun 5;1:131-93.

Bao H, You S, Cao L, Zhou R, Wang Q, Cui SW. Chemical and rheological properties of polysaccharides from fruit body of *Auricularia auricular-judae*. *Food Hydrocolloids*. 2016 Jun 1;57:30-7.

Barai BK, Singhal RS, Kulkarni PR. Optimization of a process for preparing carboxymethyl cellulose from water hyacinth (*Eichornia crassipes*). *Carbohydrate Polymers*. 1997 Mar 1;32(3-4):229-31.

Barak S, Mudgil D. Locust bean gum: Processing, properties and food applications—A review. *International journal of biological macromolecules*. 2014 May 1;66:74-80.

Barakat NS, Elbagory IM, Almurshedi AS. Controlled-release carbamazepine matrix granules and tablets comprising lipophilic and hydrophilic components. *Drug delivery*. 2009 Jan 1;16(1):57-65.

Beines PW, Klosterkamp I, Menges B, Jonas U, Knoll W. Responsive thin hydrogel layers from photo-cross-linkable poly (N-isopropylacrylamide) terpolymers. *Langmuir*. 2007 Feb 13;23(4):2231-8.

Bhatia M, Ahuja M. Psyllium arabinoxylan: Carboxymethylation, characterization and evaluation for nanoparticulate drug delivery. *International Journal of Biological Macromolecules*. 2015 Jan 1;72:495-501.

Bhatia S. Natural polymer drug delivery systems: Nanoparticles, plants, and algae. Springer; 2016 Sep 23.

Borsagli FG, Mansur AA, Chagas P, Oliveira LC, Mansur HS. O-carboxymethyl functionalization of chitosan: Complexation and adsorption of Cd (II) and Cr (VI) as heavy metal pollutant ions. *Reactive and Functional Polymers*. 2015 Dec 1;97:37-47.

Brummer Y, Cui SW. Understanding carbohydrate analysis. *Food carbohydrates: chemistry, physical properties and applications*. 2005 May 23:1-38.

Bush MB, Phan-Thien N. Drag force on a sphere in creeping motion through a Carreau model fluid. *Journal of non-newtonian fluid mechanics*. 1984 Jan 1;16(3):303-13.

Carraher Jr CE, Seymour RB. Structure—property relationships in polymers. Springer Science & Business Media; 2012 Dec 6.

Chakravorty A, Barman G, Mukherjee S, Sa B. Effect of carboxymethylation on rheological and drug release characteristics of locust bean gum matrix tablets. Carbohydrate polymers. 2016 Jun 25;144:50-8.

Chang RK, Robinson JR. Sustained drug release from tablets and particles through coating. Pharmaceutical Dosage Forms. 1990 Jul 27;3:199-302.

Chauhan D, Chauhan JS. Flavonoid glycosides from *Pongamia pinnata*. Pharmaceutical biology. 2002 Jan 1;40(3):171-4.

Coluccia S, Marchese L, Lavagnino S, Anpo M. Hydroxyls on the surface of MgO powders. SpectrochimicaActa Part A: Molecular Spectroscopy. 1987 Jan 1;43(12):1573-6.

Cooper J, Gunn C. Powder flow and compaction. Tutorial Pharmacy. New Delhi, CBS Publishers and Distributors, India. 0. 1986;10:20-30.

Corti G, Cirri M, Maestrelli F, Mennini N, Mura P. Sustained-release matrix tablets of metformin hydrochloride in combination with triacetyl- β -cyclodextrin. European Journal of Pharmaceutics and Biopharmaceutics. 2008 Feb 1;68(2):303-9.

Costa P, Lobo JM. Modeling and comparison of dissolution profiles. European journal of pharmaceutical sciences. 2001 May 1;13(2):123-33.

Dagar, V., Pahwa, R. and Ahuja, M., 2022. Preparation and Characterization of Calcium Cross-Linked Carboxymethyl Tamarind Kernel Polysaccharide as Release Retardant Polymer in Matrix. Biointerface Res. Appl. Chem, 13, p.111.

Davis RM. Analysis of dilute solutions of (carboxymethyl) cellulose with the electrostatic wormlike chain theory. Macromolecules. 1991 Sep;24(5):1149-55.

De Paula RC, Santana SA, Rodrigues JF. Composition and rheological properties of Albizia lebbeck gum exudate. Carbohydrate polymers. 2001 Feb 1;44(2):133-9.

Derosa G, D'Angelo A, Romano D, Maffioli P. Effects of metformin extended release compared to immediate release formula on glycemic control and glycemic variability in patients with type 2 diabetes. Drug Design, Development and Therapy. 2017 May 16:1481-8.

Dhua M, Maiti S, Sen KK. Modified karaya gum colloidal particles for the management of systemic hypertension. International Journal of Biological Macromolecules. 2020 Dec 1;164:1889-97.

Dodi G, Hritcu D, Popa MI. Carboxymethylation of guar gum: synthesis and characterization. Cellulose chemistry and Technology. 2011 Mar 1;45(3):171.

Donati I, Benegas J, Paoletti S. On the molecular mechanism of the calcium-induced gelation of pectate. Different steps in the binding of calcium ions by pectate. Biomacromolecules. 2021 Nov 3;22(12):5000-19.

Elieh-Ali-Komi D, Hamblin MR. Chitin and chitosan: production and application of versatile biomedical nanomaterials. International journal of advanced research. 2016 Mar;4(3):411.

Emami J, TAJ AM, Ahmadi F. Preparation and in vitro evaluation of sustained-release matrix tablets of flutamide using synthetic and naturally occurring polymers.

Fischer D, Li Y, Ahlemeyer B, Krieglstein J, Kissel T. In vitro cytotoxicity testing of polycations: influence of polymer structure on cell viability and hemolysis. Biomaterials. 2003 Mar 1;24(7):1121-31.

Flieger J, Feder-Kubis J, Tatarczak-Michalewska M. Chiral ionic liquids: Structural diversity, properties and applications in selected separation techniques. *International journal of molecular sciences*. 2020 Jun 15;21(12):4253.

Ford JL, Rubinstein MH, McCaul F, Hogan JE, Edgar PJ. Importance of drug type, tablet shape and added diluents on drug release kinetics from hydroxypropylmethylcellulose matrix tablets. *International journal of pharmaceutics*. 1987 Dec 1;40(3):223-34.

Fortman DJ, Brutman JP, De Hoe GX, Snyder RL, Dichtel WR, Hillmyer MA. Approaches to sustainable and continually recyclable cross-linked polymers. *ACS Sustainable Chemistry & Engineering*. 2018 Aug 26;6(9):11145-59.

Freitas ED, Freitas VM, Rosa PC, da Silva MG, Vieira MG. Development and evaluation of naproxen-loaded sericin/alginate beads for delayed and extended drug release using different covalent crosslinking agents. *Materials Science and Engineering: C*. 2021 Jan 1;118:111412.

Frishman WH. A new extended-release formulation of diltiazem HCl for the treatment of mild-to-moderate hypertension. *The Journal of Clinical Pharmacology*. 1993 Jul;33(7):612-22.

Gafourian T, Safari A, Adibkia K, Parviz F, Nokhodchi A. A drug release study from hydroxypropylmethylcellulose (HPMC) matrices using QSPR modeling. *Journal of pharmaceutical sciences*. 2007 Dec 1;96(12):3334-51.

Gandhi KJ, Deshmane SV, Biyani KR. Polymers in pharmaceutical drug delivery system: A review. *Int J Pharm Sci Rev Res*. 2012 May;14(2):57-66.
García-González CA, Alnaief M, Smirnova I. Polysaccharide-based aerogels—Promising biodegradable carriers for drug delivery systems. *Carbohydrate Polymers*. 2011 Oct 15;86(4):1425-38.

Gong H, Liu M, Chen J, Han F, Gao C, Zhang B. Synthesis and characterization of carboxymethyl guar gum and rheological properties of its solutions. *Carbohydrate polymers*. 2012 Apr 15;88(3):1015-22.

Gübitz GM, Paulo AC. New substrates for reliable enzymes: enzymatic modification of polymers. *Current opinion in biotechnology*. 2003 Dec 1;14(6):577-82.

Hamdani AM, Wani IA, Bhat NA. Sources, structure, properties and health benefits of plant gums: A review. *International journal of biological macromolecules*. 2019 Aug 15;135:46-61.

Higuchi TJ. Mechanism of sustained-action medication. Theoretical analysis of rate of release of solid drugs dispersed in solid matrices. *Journal of pharmaceutical sciences*. 1963 Dec;52(12):1145-9.

Hong SR, Wereley NM, Choi YT, Choi SB. Analytical and experimental validation of a nondimensional Bingham model for mixed-mode magnetorheological dampers. *Journal of Sound and Vibration*. 2008 May 6;312(3):399-417.

Hongbo T, Yanping L, Min S, Xiguang W. Preparation and property of crosslinking guar gum. *Polymer journal*. 2012 Mar;44(3):211-6.

Huang X, Garcia MH. A Herschel–Bulkley model for mud flow down a slope. *Journal of fluid mechanics*. 1998 Nov;374:305-33.

Huang Y, Yu H, Xiao C. Effects of Ca²⁺ crosslinking on structure and properties of waterborne polyurethane-carboxymethylated guar gum films. *Carbohydrate Polymers*. 2006 Nov 23;66(4):500-13.

Isaac VL, Chiari-Andréo BG, Marto JM, Moraes JD, Leone BA, Corrêa MA, Ribeiro HM. Rheology as a tool to predict the release of alpha-lipoic acid from

emulsions used for the prevention of skin aging. *BioMed Research International*. 2015 Dec 16;2015.

Izydorczyk M, Cui SW, Wang Q. Polysaccharide gums: structures, functional properties, and applications. *Food carbohydrates: Chemistry, physical properties, and applications*. 2005 May 23;293:299.

Jana S, Maiti S, Sen KK, Jana S. Interpenetrating polysaccharide networks as oral drug delivery modalities. In *Polysaccharide Carriers for Drug Delivery* 2019 Jan 1 (pp. 319-338). Woodhead Publishing.

Jana S, Pramanik R, Nayak AK, Sen KK. Gellan gum (GG)-based IPN microbeads for sustained drug release. *Journal of Drug Delivery Science and Technology*. 2022 Mar 1;69:103034.

Jantzen GM, Robinson JR. Sustained and controlled-release drug delivery systems. *Modern pharmaceuticals*. 2002;4:501-2.

Jensterle Sever M, Kocjan T, Pfeifer M, Kravos NA, Janez A. Short-term combined treatment with liraglutide and metformin leads to significant weight loss in obese women with polycystic ovary syndrome and previous poor response to metformin. *European journal of endocrinology*. 2014 Mar;170(3):451-9.

Jiang H, Zhang W, Chen L, Liu J, Cao J, Jiang W. Recent advances in guar gum-based films or coatings: Diverse property enhancement strategies and applications in foods. *Food Hydrocolloids*. 2023 Mar 1;136:108278.

Kaboorani A, Blanchet P. Determining the linear viscoelastic region of sugar maple wood by dynamic mechanical analysis. *BioResources*. 2014 Jun 5;9(3):4392-409.

Kaity S, Ghosh A. Carboxymethylation of locust bean gum: application in interpenetrating polymer network microspheres for controlled drug delivery. *Industrial & engineering chemistry research*. 2013 Jul 31;52(30):10033-45.

Katzenberg F, Janlewing R, Petermann J. Surface diffusion of metal atoms on polymer substrates during physical vapour deposition. *Colloid and Polymer Science*. 2000 Mar;278:280-4.

Kaur G, Grewal J, Jyoti K, Jain UK, Chandra R, Madan J. Oral controlled and sustained drug delivery systems: Concepts, advances, preclinical, and clinical status. In *Drug targeting and stimuli sensitive drug delivery systems* 2018 Jan 1 (pp. 567-626). William Andrew Publishing.

Kazzaz AE, Feizi ZH, Fatehi P. Grafting strategies for hydroxy groups of lignin for producing materials. *Green Chemistry*. 2019;21(21):5714-52.

Khondkar P. Composition and partial structure characterization of Tremella polysaccharides. *Mycobiology*. 2009 Dec 1;37(4):286-94.

Korsmeyer RW, Gurny R, Doelker E, Buri P, Peppas NA. Mechanisms of solute release from porous hydrophilic polymers. *International journal of pharmaceutics*. 1983 May 1;15(1):25-35.

Krishan BV, Rao CH, Kishore VS. Design and Development of Pulsatile drug delivery of Diltiazem Hydrochloride. *Research journal of pharmacy and technology*. 2020;13(5):2315-20.

Kulawik-Pióro A, Ptaszek A, Kruk J. Effective tool for assessment of the quality of barrier creams-relationships between rheological, textural and sensory properties. *Regulatory Toxicology and Pharmacology*. 2019 Apr 1;103:113-23.

Kulkarni Vishakha S, Butte Kishor D, RathodSudha S. Natural polymers–A comprehensive review. *Int. J. Res. Pharm. Biomed. Sci.* 2012 Oct;3(4):1597-613.

Kumar PS, Nair PK. X-ray diffraction studies on the relative proportion and decomposition of amorphous phase in electroless Ni□ B deposits. *Nanostructured Materials*. 1994 Mar 1;4(2):183-98.

Layek B, Mandal S. Natural polysaccharides for controlled delivery of oral therapeutics: a recent update. *Carbohydrate polymers*. 2020 Feb 15;230:115617.

Li C, Liu C, Liu J, Fang L. Correlation between rheological properties, in vitro release, and percutaneous permeation of tetrahydropalmatine. *Aaps Pharmscitech*. 2011 Sep;12:1002-10.

Li WH, Chen G, Yeo SH. Viscoelastic properties of MR fluids. *Smart Materials and Structures*. 1999 Aug 1;8(4):460.

Lin Y, Bilotti E, Bastiaansen CW, Peijs T. Transparent semi-crystalline polymeric materials and their nanocomposites: A review. *Polymer Engineering & Science*. 2020 Oct;60(10):2351-76.

Liu Y, Lu K, Hu X, Jin Z, Miao M. Structure, properties and potential applications of phytoglycogen and waxy starch subjected to carboxymethylation. *Carbohydrate polymers*. 2020 Apr 15;234:115908.

Lu R, Gan W, Wu BH, Zhang Z, Guo Y, Wang HF. C–H stretching vibrations of methyl, methylene and methine groups at the vapor/alcohol (n= 1– 8) interfaces. *The Journal of Physical Chemistry B*. 2005 Jul 28;109(29):14118-29.

Madathinal Kunjappan A, Reghunadhan A, Ramachandran AA, Mathew L, Padmanabhan M, Laroze D, Thomas S. Discussion on degree of entanglement,

chain confinement, and reinforcement efficiency factor of PTT/PE blend nanocomposite embedded with MWCNTs. *Polymers for Advanced Technologies*. 2021 Aug;32(8):2916-28.

Maity S, Sa B. Ca-carboxymethyl xanthan gum mini-matrices: swelling, erosion and their impact on drug release mechanism. *International journal of biological macromolecules*. 2014 Jul 1;68:78-85.

McCrum NG, Buckley CP, Bucknall CB. *Principles of polymer engineering*. Oxford University Press; 1997.

McDonagh MS, Eden KB, Peterson K, Oregon Health & Science University. Evidence-based Practice Center. Drug class review on calcium channel blockers. Portland (OR): Oregon Health & Science University; 2005 Mar.

Medina-Torres L, Brito-De La Fuente E, Torrestiana-Sanchez B, Katthain R. Rheological properties of the mucilage gum (*Opuntia ficus indica*). *Food hydrocolloids*. 2000 Sep 1;14(5):417-24.

Meena VS, Gupta S. Wood anatomy of *Albizia procera* correlation between tropical and subtropical from Different geographical zones of Indian subcontinent. *Int. J. Sci. Tech. Res.* 2014;3(5):1-8.

Mikušová V, Ferková J, Žigayová D, Krchňák D, Mikuš P. Comparative study of polysaccharide-based hydrogels: Rheological and texture properties and ibuprofen release. *Gels*. 2022 Mar 7;8(3):168.

Mohammed AS, Naveed M, Jost N. Polysaccharides; classification, chemical properties, and future perspective applications in fields of pharmacology and biological medicine (a review of current applications and upcoming potentialities). *Journal of Polymers and the Environment*. 2021 Aug;29:2359-71.

Moin A, Shivakumar HG. Formulation of sustained-release diltiazem matrix tablets using hydrophilic gum blends. *Tropical journal of pharmaceutical research*. 2010;9(3).

Moradi M, Sohrabi MR, Mortazavinik S. Spectroscopy Determination of Metformin in Drinking Water, Tablet, Human Serum, and Urine Based on the Aggregation of Nanoparticles. *Journal of Applied Spectroscopy*. 2021 Mar;88:63-9.

Mourya VK, Inamdara N, Ashutosh Tiwari N. Carboxymethyl chitosan and its applications. *Advanced Materials Letters*. 2010 Jun 1;1(1):11-33.

Mudgil D, Barak S. Composition, properties and health benefits of indigestible carbohydrate polymers as dietary fiber: A review. *International journal of biological macromolecules*. 2013 Oct 1;61:1-6.

Murphy C, Pillay V, Choonara YE, du Toit LC, Ndesendo VM, Chirwa N, Kumar P. Optimization of a dual mechanism gastrofloatable and gastroadhesive delivery system for narrow absorption window drugs. *AAPS PharmSciTech*. 2012 Mar;13(1):1-5.

Nadgorny M, Ameli A. Functional polymers and nanocomposites for 3D printing of smart structures and devices. *ACS applied materials & interfaces*. 2018 May 9;10(21):17489-507.

Nahar K, Hossain MK, Khan TA. Alginate and its versatile application in drug delivery. *Journal of Pharmaceutical Sciences and Research*. 2017 May 1;9(5):606.

Narain R, editor. *Polymer science and nanotechnology: fundamentals and applications*. Elsevier; 2020 Jun 16.

Nayak AK, Pal D. Development of pH-sensitive tamarind seed polysaccharide–alginate composite beads for controlled diclofenac sodium delivery using response surface methodology. *International journal of biological macromolecules*. 2011 Nov 1;49(4):784-93.

Nerurkar J, Jun HW, Price JC, Park MO. Controlled-release matrix tablets of ibuprofen using cellulose ethers and carrageenans: effect of formulation factors on dissolution rates. *European journal of pharmaceutics and biopharmaceutics*. 2005 Sep 1;61(1-2):56-68.

Nguyễn NC. Vietnam forest trees. Vietnam forest trees.. 1996.

Ojogbo E, Ogunsona EO, Mekonnen TH. Chemical and physical modifications of starch for renewable polymeric materials. *Materials Today Sustainability*. 2020 Mar 1;7:100028.

Osswald T, Rudolph N. Polymer rheology. Carl Hanser, München. 2015.

Pachau L, Lahlénmawia H, Mazumder B. Characteristics and composition of *Albizia procera* (Roxb.) Benth gum. *Industrial Crops and Products*. 2012 Nov 1;40:90-5.

Pachau L, Mazumder B. *Albizia procera* gum as an excipient for oral controlled release matrix tablet. *Carbohydrate polymers*. 2012 Sep 1;90(1):289-95.

Palmer D, Levina M, Nokhodchi A, Douroumis D, Farrell T, Rajabi-Siahboomi A. The influence of sodium carboxymethylcellulose on drug release from polyethylene oxide extended release matrices. *AAPS PharmSciTech*. 2011 Sep;12:862-71.

Panzitta M, Ponti M, Bruno G, Cois G, D'Arpino A, Minghetti P, Mendicino FR, Perioli L, Ricci M. The strategic relevance of manufacturing technology: An overall quality concept to promote innovation preventing drug shortage. *International journal of pharmaceutics*. 2017 Jan 10;516(1-2):144-57.

Patel H, Panchal DR, Patel U, Brahmbhatt T, Suthar M. Matrix type drug delivery system: A review. *J Pharm Sci Biosci Res*. 2011 Nov;1(3):143-51.

Patil R, Jat RK. Formulation and evaluation of matrix tablets containing chitosan based polyelectrolyte complex with natural gum for prolonged release of diltiazem HCl. *Journal of Drug Delivery and Therapeutics*. 2019 Aug 15;9(4-s):22-31.

Pharmacopoeia I. Controller of Publication, Govt. of India. New Delhi, India: Ministry of Health and Family Welfare. 2010:185.

Pharmacopoeia I. Vol. II, The Controller Publication. Govt. of India, New Delhi. 2010:1199.

Phuong PT, Oliver S, He J, Wong EH, Mathers RT, Boyer C. Effect of hydrophobic groups on antimicrobial and hemolytic activity: Developing a predictive tool for ternary antimicrobial polymers. *Biomacromolecules*. 2020 Nov 13;21(12):5241-55.

Prasad N, Thombare N, Sharma SC, Kumar S. Gum arabic—A versatile natural gum: A review on production, processing, properties and applications. *Industrial Crops and Products*. 2022 Nov 1;187:115304.

Prathapan R, Thapa R, Garnier G, Tabor RF. Modulating the zeta potential of cellulose nanocrystals using salts and surfactants. *Colloids and Surfaces A: Physicochemical and Engineering Aspects*. 2016 Nov 20;509:11-8.

Quanquan Miao, Huaishi Jiang, Lei Gao, Yujie Cheng, Jiachao Xu, Xiaoting Fu, Xin Gao, Rheological Properties of Five Plant Gums, American Journal of Analytical Chemistry, 2018, 9, 210-223.

Quintana JR, Valderruten NE, Katime I. Synthesis and swelling kinetics of poly (dimethylaminoethyl acrylate methyl chloride quaternary-co-itaconic acid) hydrogels. Langmuir. 1999 Jul 6;15(14):4728-30.

Rafe A, Razavi SM, Khan S. Rheological and structural properties of β -lactoglobulin and basil seed gum mixture: Effect of heating rate. Food research international. 2012 Nov 1;49(1):32-8.

Raina N, Pahwa R, Bhattacharya J, Paul AK, Nissapatorn V, de Lourdes Pereira M, Oliveira SM, Dolma KG, Rahmatullah M, Wilairatana P, Gupta M. Drug Delivery Strategies and Biomedical Significance of Hydrogels: Translational Considerations. Pharmaceutics. 2022 Mar 5;14(3):574.

Randrianarivo HR, Razafindrakoto AR, Ratsimanohatra HC, Randriamampianina LJ, Rajemiarimoelisoa CF, Ramamonjisoa L, Ramanitrahasimbola D, Rakoto DA, Jeannoda VL. Toxic effects of seed methanolic extracts of endemic Albizia species (Fabaceae) from Madagascar on animals. Journal of life Sciences. 2014 Aug 1;8(8).

Ramli H, Zainal NF, Hess M, Chan CH. Basic principle and good practices of rheology for polymers for teachers and beginners. Chemistry Teacher International. 2022 Aug 29;4(4):307-26.

Rasid IM, Do C, Holten-Andersen N, Olsen BD. Effect of sticker clustering on the dynamics of associative networks. Soft Matter. 2021;17(39):8960-72.

Reddy KR, Mutalik S, Reddy S. Once-daily sustained-release matrix tablets of nicorandil: formulation and in vitro evaluation. *AAPS pharmscitech*. 2003 Dec;4:480-8.

Rolón-Garrido VH, Wagner MH. The damping function in rheology. *Rheologica Acta*. 2009 Apr;48:245-84.

Rostamkalaei SS, Akbari J, Saeedi M, Morteza-Semnani K, Nokhodchi A. Topical gel of Metformin solid lipid nanoparticles: A hopeful promise as a dermal delivery system. *Colloids and Surfaces B: Biointerfaces*. 2019 Mar 1;175:150-7.

Rouessac F, Rouessac A. *Chemical analysis: modern instrumentation methods and techniques*. John Wiley & Sons; 2022 Apr 4.

Sa B, Mukherjee S, Roy SK. Effect of polymer concentration and solution pH on viscosity affecting integrity of a polysaccharide coat of compression coated tablets. *International journal of biological macromolecules*. 2019 Mar 15;125:922-30.

Sadalage PS, Pawar KD. Production of microcrystalline cellulose and bacterial nanocellulose through biological valorization of lignocellulosic biomass wastes. *Journal of Cleaner Production*. 2021 Dec 10;327:129462.

Sam ST, Nuradibah MA, Ismail H, Noriman NZ, Ragunathan S. Recent advances in polyolefins/natural polymer blends used for packaging application. *Polymer-Plastics Technology and Engineering*. 2014 Apr 19;53(6):631-44.

Sara H, Yahoum MM, Lefnaoui S, Abdelkader H, Moulai-Mostefa N. New alkylated xanthan gum as amphiphilic derivatives: Synthesis, physicochemical and rheological studies. *Journal of Molecular Structure*. 2020 May 5;1207:127768.

Scholze B, Hanser C, & Meier D. Characterization of the water-insoluble fraction from fast pyrolysis liquids (pyrolytic lignin): Part II. GPC, carbonyl groups, and ^{13}C -NMR. *Journal of Analytical and Applied Pyrolysis*. 2001; 58: 387-400.

Sengupta A, Datta P. Chemical modifications of polysaccharides. In *Food, Medical, and Environmental Applications of Polysaccharides* 2021 Jan 1 (pp. 47-77). Elsevier.

Shah SN, Asghar S, Choudhry MA, Akash MS. ur Rehman N, Baksh S. Formulation and evaluation of natural gum-based sustained release matrix tablets of flurbiprofen using response surface methodology. *Drug Dev Ind Pharm*. 2009;35(12):1470-8.

Shapovalov VM. On the applicability of the Ostwald–de Waele model in solving applied problems. *Journal of Engineering Physics and Thermophysics*. 2017 Sep;90(5):1213-8.

Shirwaikar A, Shirwaikar A, Prabu SL, Kumar GA. Herbal excipients in novel drug delivery systems. *Indian journal of pharmaceutical sciences*. 2008 Jul;70(4):415.

Shokri J, Adibkia K. Application of cellulose and cellulose derivatives in pharmaceutical industries. In *Cellulose-medical, pharmaceutical and electronic applications* 2013 Aug 29. IntechOpen.

Singh R, Maity S, Sa B. Effect of ionic crosslink on the release of metronidazole from partially carboxymethylated guar gum tablet. *Carbohydrate polymers*. 2014 Jun 15;106:414-21.

Smaeel SA, Al-Bayati YK. Determination of trace metformin in pharmaceutical preparation using molecularly imprinted polymer based pvc-membrane. *Eurasian Chem. Commun.* 2021; 3:812-30.

Sochi T. Flow of non-Newtonian fluids in porous media. *Journal of Polymer Science Part B: Polymer Physics.* 2010 Dec 1;48(23):2437-767.

Tako M, Teruya T, Tamaki Y, Konishi T. Molecular origin for rheological characteristics of native gellan gum. *Colloid and Polymer Science.* 2009 Dec;287:1445-54.

Talens P, Castells ML, Verdú S, Barat JM, Grau R. Flow, viscoelastic and masticatory properties of tailor made thickened pea cream for people with swallowing problems. *Journal of Food Engineering.* 2021 Mar 1;292:110265.

Toğrul H, Arslan N. Production of carboxymethyl cellulose from sugar beet pulp cellulose and rheological behaviour of carboxymethyl cellulose. *Carbohydrate Polymers.* 2003 Oct 1;54(1):73-82.

Varma MV, Kaushal AM, Garg A, Garg S. Factors affecting mechanism and kinetics of drug release from matrix-based oral controlled drug delivery systems. *American Journal of drug delivery.* 2004 Mar;2:43-57.

Vinod VT, Sashidhar RB, Suresh KI, Rao BR, Saradhi UV, Rao TP. Morphological, physico-chemical and structural characterization of gum kondagogu (*Cochlospermum gossypium*): A tree gum from India. *Food Hydrocolloids.* 2008 Jul 1;22(5):899-915.

Wang CS, Virgilio N, Carreau PJ, Heuzey MC. Understanding the effect of conformational rigidity on rheological behavior and formation of polysaccharide-based hybrid hydrogels. *Biomacromolecules.* 2021 Aug 16;22(9):4016-26.

Wang CS, Virgilio N, Carreau PJ, Heuzey MC. Understanding the effect of conformational rigidity on rheological behavior and formation of polysaccharide-based hybrid hydrogels. *Biomacromolecules*. 2021 Aug 16;22(9):4016-26.

Wang H, Ke L, Ding Y, Rao P, Xu T, Han H, Zhou J, Ding W, Shang X. Effect of calcium ions on rheological properties and structure of *Lycium barbarum* L. polysaccharide and its gelation mechanism. *Food Hydrocolloids*. 2022 Jan 1;122:107079.

Wei X, Sun N, Wu B, Yin C, Wu W. Sigmoidal release of indomethacin from pectin matrix tablets: effect of in situ crosslinking by calcium cations. *International Journal of Pharmaceutics*. 2006 Aug 2;318(1-2):132-8.

Wells, J.I. and Aulton, M.E., Preformulation. In Aulton, M.E. (Ed.), *Pharmaceutics: The Science of Dosage Form Design*, Churchill Livingstone, Edinburgh, 1988, pp. 223-253.

Wilbon PA, Chu F, Tang C. Progress in renewable polymers from natural terpenes, terpenoids, and rosin. *Macromolecular rapid communications*. 2013 Jan 11;34(1):8-37.

Wilson B, Sitarambhai PH, Sajeev MS, Vinothapooshan G. Design and evaluation of sustained release matrix tablets of levofloxacin for effective treatment of microbial infections. *International Journal of Drug Delivery*. 2011 Apr 1;3(2):305.

Won DH, Park H, Ha ES, Kim HH, Jang SW, Kim MS. Optimization of bilayer tablet manufacturing process for fixed dose combination of sustained release high-dose drug and immediate release low-dose drug based on quality by design (QbD). *International Journal of Pharmaceutics*. 2021 Aug 10;605:120838.

Wong TW, Colombo G, Sonvico F. Pectin matrix as oral drug delivery vehicle for colon cancer treatment. *Aaps PharmSciTech*. 2011 Mar;12:201-14.

Wu B, Deng D, Lu Y, Wu W. Biphasic release of indomethacin from HPMC/pectin/calcium matrix tablet: II. Influencing variables, stability and pharmacokinetics in dogs. *European journal of pharmaceutics and biopharmaceutics*. 2008 May 1;69(1):294-302.

Xiao F, Chen M, Wu S, Amirkhanian SN. A long-term ultraviolet aging effect on rheology of WMA binders. *Int. J. Pavement Res. Technol*. 2013 Sep 1;6(5):496-504.

Xu X, Xue C, Chang Y, Chen F, Wang J. Conformational and physicochemical properties of fucosylated chondroitin sulfate from sea cucumber *Apostichopus japonicus*. *Carbohydrate polymers*. 2016 Nov 5;152:26-32.

Yahoum MM, Toumi S, Hentabli S, Tahraoui H, Lefnaoui S, Hadjsadok A, Amrane A, Kebir M, Moula N, Assadi AA, Zhang J. Experimental Analysis and Neural Network Modeling of the Rheological Behavior of Xanthan Gum and Its Derivatives. *Materials*. 2023 Mar 23;16(7):2565.

Yazdani P, Wang B, Rimaz S, Kawi S, Borgna A. Glucose hydrogenolysis over Cu-La₂O₃/Al₂O₃: mechanistic insights. *Molecular Catalysis*. 2019 Apr 1;466:138-45.

Ye F, Miao M, Lu K, Jiang B, Li X, Cui SW. Structure and physicochemical properties for modified starch-based nanoparticle from different maize varieties. *Food Hydrocolloids*. 2017 Jun 1;67:37-44.

Yuan M, Hu M, Dai F, Fan Y, Deng Z, Deng H, Cheng Y. Application of synthetic and natural polymers in surgical mesh for pelvic floor reconstruction. *Materials & Design*. 2021 Nov 1;209:109984.

Yuen SN, Choi SM, Phillips DL, Ma CY. Raman and FTIR spectroscopic study of carboxymethylated non-starch polysaccharides. *Food chemistry*. 2009 Jun 1;114(3):1091-8.

Zhang B, Gao Z, Gao G, Zhao W, Li J, Ren X. Highly Mechanical and Fatigue-Resistant Double Network Hydrogels by Dual Physically Hydrophobic Association and Ionic Crosslinking. *Macromolecular Materials and Engineering*. 2018 Jul;303(7):1800072.

Zhang J, Akihisa T, Kurita M, Kikuchi T, Zhu WF, Ye F, Dong ZH, Liu WY, Feng F, Xu J. Melanogenesis-inhibitory and cytotoxic activities of triterpene glycoside constituents from the bark of *Albizia procera*. *Journal of natural products*. 2018 Dec 6;81(12):2612-20.

Zhang S, Qamar SA, Junaid M, Munir B, Badar Q, Bilal M. Algal Polysaccharides-Based Nanoparticles for Targeted Drug Delivery Applications. *Starch-Stärke*. 2022 Jul;74(7-8):2200014.

Zhou W, Rahimnejad S, Tocher DR, Lu K, Zhang C, Sun Y. Metformin attenuates lipid accumulation in hepatocytes of blunt snout bream (*Megalobrama amblycephala*) via activation of AMP-activated protein kinase. *Aquaculture*. 2019 Jan 15;499:90-100.

APPENDIX

RESEARCH ARTICLE

Impact of Carboxymethylation of *Albizia procera* Gum on Rheological Changes and Drug Release from Matrix Tablets

Sudipta Mukherjee*, Biswanath SA, Jasmina Khanam, Sanmoy Karmakar,
Rudranil Bhowmik

Department of Pharmaceutical Technology, Division of Pharmaceutics, Jadavpur University, Kolkata, West Bengal, India.

Received: 05th August, 2022; Revised: 03rd September, 2022; Accepted: 21st January, 2023; Available Online: 25th June, 2023

ABSTRACT

The use of carbohydrate polymers in pharmaceutical formulations as drug delivery carriers has gained significant interest from many perspectives. As an exudate of the *Albizia* tree, *Albizia procera* (Mimosaceae), a carbohydrate polymer, is used as an excipient to develop sustained-release drug delivery systems, owing to its biocompatibility and biodegradability. This study was conducted to investigate the influence of carboxymethylation of *A. procera* gum on rheological properties and drug release from the matrix tablet formulations. The study also revealed the comparative characterization of the native form of *A. procera* (NAP) as well as the carboxymethylated *A. procera* (CMAP). The rheological assessments of both polymers under different pH divulged the flow behavior, linear viscoelasticity (LVE), structural deformation, and gel network formation. The drug release from NAP and CMAP matrices of various formulations were evaluated and established correlations with rheology.

Keywords: *Albizia procera*, Carboxymethylation, Rheology, Amplitude sweep, Frequency sweep, Damping factor

International Journal of Drug Delivery Technology (2023); DOI: 10.25258/ijddt.13.2.15

How to cite this article: Mukherjee S, Biswanath SA, Khanam J, Karmakar S, Bhowmik R. Impact of Carboxymethylation of *Albizia procera* Gum on Rheological Changes and Drug Release from Matrix Tablets. International Journal of Drug Delivery Technology. 2023;13(2):551-561.

Source of support: Nil.

Conflict of interest: None

INTRODUCTION

Natural polymers (hydrophilic and hydrophobic) have been extensively used to fabricate NDDS for the past several years, resulting in substantial growth in the applications of these polymers. There are several species of *Albizia procera*, and one of these is considered fast-growing, semi-deciduous, light-demanding, relatively drought-tolerant, and susceptible to roots sucking after damage. It is locally named safed siris, karanji, Dun-siris, and forest siris in India. Species in the *Albizia* genus belong to the Fabaceae family, subfamily Mimosoideae. *A. procera* is found in a variety of tropical types of forests, including tropical semi-evergreen forests, tropical moist deciduous forests, low alluvial Savannah woodlands, and northern subtropical broadleaved forests throughout its range.¹ In Vietnam, it is found in tropical rainforests, dry open forests, and savannas.² Many studies have found that *A. procera* gum contains β -(1 \rightarrow 3)-D-galactopyranose units with some β -(1 \rightarrow 6)-D-galactopyranose units³ and α -(1 \rightarrow 3)-L-arabinofuranose units.⁴⁻⁷ According to certain studies, the two primary monosaccharides of the hydrolyzed *A. procera* gum are galactose and arabinose.³ The linkage and monosaccharide components in a gum's structure can influence its rheological and functional properties.⁴⁻⁷ The customization

of the D-galactopyranose units by chemical modification⁸ and cross-linking⁹ may result in changes in the rheological stability of *Albizia* gum that may lead to variation in diffusivity for drug delivery systems.¹⁰ Rheological characterization is a potential measure to determine the mechanical strength¹¹ of a polymeric matrix that influences the drug release pattern from delivery systems.¹² The study and measurement of variable rheological moduli can predict drug diffusion from the entangled polymeric matrix.¹³ The approach is aimed at investigating and studying the stability of polymers under the linear visco-elastic regime that greatly impacts drug release from the systems.

MATERIALS AND METHOD

Materials

Pulverised native *A. procera* (NAP) gum was procured from the University of Mizoram (Mizoram, India). Sodium hydroxide, hydrochloric acid, monochloroacetic acid (99.0%), trisodium phosphate dodecahydrate (mol.wt 380.119 g/mol), and trisodium citrate were obtained from Loba Chemie Pvt. Ltd (Mumbai, India). Methanol of the analytical reagent grade (99% v/v) was purchased from Merck Specialty Pvt. Ltd. (Mumbai, India). All other analytical-grade chemicals

*Author for Correspondence: dipta07tech@gmail.com

and reagents were purchased from commercial sources. Metformin was provided as a drug sample by Stadmed Pvt. Ltd. Kolkata, India.

Carboxymethylation of *A. procera*

The base-catalyzed reaction was used for the carboxymethylation of NAP. The powdered NAP was sieved through 45 meshes and weighed. A creamy dispersion was prepared by slowly sprinkling powdered NAP (10 g) into an aqueous sodium hydroxide solution (45% w/v). The mixture was kept in a double-walled ice chamber (stainless steel) at a temperature of 0 to 8°C and stirred vigorously to achieve proper hydration. At a temperature between 15 to 18°C, a slow, steady addition of monochloroacetic acid (45% w/v) was made to the slurry. The mixture was stirred continuously and allowed to react for a while. In order to complete the reaction, the mixture was heated at 75°C in a water bath for one hour while being stirred regularly and kept at room temperature for 24 hours. Afterward, the resultant mass was precipitated with aqueous methanol (80% v/v) and filtered through 8 mm filters. After collecting the filtered cake, it was air-dried and washed several times with aqueous methanol (80% v/v). The pH of CMAP was adjusted to neutral using glacial acetic acid and then washed with pure methanol. The tiny semi-crystalline CMAP was air-dried and kept in a hot oven at 60°C for 24 hours.

Characterization of CMAP

Degree of substitution (D_s)

Approximately 500 mg of CMAP was added to 5 mL of aqueous methanol (80% v/v) and stirred to form a dispersion. To this dispersion, concentrated HCl was added and stirred for 3 hours. Afterward, the mixture was filtered and the residue was washed with aqueous methanol (80% v/v) until neutrality was achieved with litmus papers. After a final wash with pure methanol, the sample was dried. 200 mg of dried CMAP was weighed accurately and added to 1.5 mL of aqueous methanol (70% v/v). Within a few minutes, 20 mL of distilled water was added to the mixture, followed by the addition of 5 mL of 0.5 N NaOH solution. A shaker was used to shake the mixture for 3 hours in order to dissolve the sample. The solution was titrated with 0.4 N HCl using phenolphthalein as an indicator.¹⁴ The following equation was used to determine the O-carboxymethyl group's substitution degree.¹⁵

$$D_s = \left[\frac{0.162 A}{1 - 0.058 A} \right] \quad (1)$$

Where, A represents the milli-equivalents of NaOH required per gram of sample.

FTIR spectrum analysis

Finely powdered samples of NAP and CMAP were mixed individually with dried potassium bromide (1:100) in a mortar, followed by pelletization in a hydraulic press at a pressure of 400 kg cm⁻². The pellets were analyzed for FTIR spectra using FTIR spectrophotometer (Perkin Elmer, RX-1, UK), in the range from 4000–400 cm⁻¹.

Differential scanning calorimetry study

DSC thermograms for NAP and CMAP were obtained using a DSC-4000, Perkin-Elmer, United States. An aluminum pan was used to seal the samples, and the samples were heated between 30 and 300°C at a rate of 10°C/minute.

Solid-state ¹³C-NMR spectroscopy

The solid state ¹³C-NMR study was conducted using each 300 mg of powdered samples of NAP and CMAP on an NMR spectrometer (JEOL, Japan) at field strength of 400 MHz using a cross-polarization method.

X-ray diffractometer

The XRD of powdered samples of NAP and CMAP were recorded using an X-ray diffractometer (ULTIMAI, Rigaku, Japan). At a voltage of 40 kV and a current of 30 mA, an X-ray generator was operated, with the K-β filtered Cu radiation at 1.54056 Å as the source of radiation. The powdered specimens were scanned at a 3°/min speed from 5 to 80° diffraction angle (2θ).

Zeta potential measurements

The zeta potential measurements were carried out in a Zeta-sizer (Nano ZS90, Malvern Instruments Ltd., UK) using 1% (w/v) dispersion of NAP and CMAP at neutral pH. This study used deionized water as a dispersion medium and several disposable zeta cells (DTS 1070) for each sample at 25°C. The experiments were repeated three times, with the mean values reported in this study.

Rheological studies

Rheological experiments were conducted in the present study using a Modular Compact Rheometer (MCR 102, Anton Parr, Austria). In the experimental setup, a standard 1° cone geometry (CP - 40) with a diameter of 40 mm was used.

Rheological analyses were performed on the polymer solutions (5% w/v) of NAP and CMAP prepared in various media that slowly turned into matrix solutions. For each polymer, three types of matrices were prepared at different pH levels to investigate the effects of pH on viscosity. The matrices under the "Polymer-A" category (NAP-A, CMAP-A) were prepared by dissolving the required amount of polymer in an acidic solution with constant stirring at 60°C. The pH of the matrices was adjusted to 1.2 at room temperature using a 0.2 (M) HCl solution. Similarly, "polymer-B" matrices (NAP-B, CMAP-B) were prepared for each polymer in buffer solution and the pH was adjusted to 6.8 with a 0.2 (M) NaOH solution. For "Polymer-W" category matrices (NAP-W, CMAP-W), deionized water was used to maintain neutral pH (pH 7).

A dynamic rotation mode (flow curve) and an oscillatory mode were used to perform the tests. The dynamic rotational mode was used to study changes in viscosity caused by variable shear rates in the samples.

The oscillatory mode was employed for the polymers to study the amplitude sweep and frequency sweep against loss and storage moduli (G' and G''). The amplitude sweep was carried out at a fixed angular frequency ($\omega=6.2831853$ rad/sec)

Table 1: Tablet formulations

Sl no.	Ingredients	Quantity (mg) per tablet of each formulation									
		F1	F2	F3	F4	F5	F6	F7	F8	F9	F10
1	MET	250	250	250	250	250	250	250	250	250	250
2	NAP	250	450	550	650	750	-	-	-	-	-
3	CMAF	-	-	-	-	-	250	450	550	650	750
4	Lactose anhydrous	500	300	200	100	50	500	300	200	100	50
5	MCC	80	80	80	80	30	80	80	80	80	30
6	Purified water	Qs*	Qs	Qs	Qs	Qs	Qs	Qs	Qs	Qs	Qs
7	Magnesium stearate	20	20	20	20	20	20	20	20	20	20

*Qs denote sufficient quantity

where the strain ($\gamma=0.01-10\%$) was varied to produce structural deformation on the entangled polymer.

The frequency sweep was carried out to study the changes in G' and G'' against variable angular frequency ($\omega=0.1-10$ rad/sec) using the pre-determined strain (%) under the linear viscoelastic (LVE) regime from amplitude sweep.

Drug-polymer DSC Compatibility Study

A differential scanning calorimeter (DSC-4000, Perkin-Elmer, USA) was used to record the DSC thermograms of the physical mixtures of MET with NAP and CMAF. The samples were impenetrably sealed inside an aluminum pan and heated from 30 to 300°C under a nitrogen atmosphere (20 mL/min) at a scan rate of 10°C/min.

Preparation of Matrix Tablet

Metformin hydrochloride (MET) as the active ingredient, powdered NAP and lactose and microcrystalline cellulose (MCC) were separately passed through the sieve with mesh #40. In the weight ratio shown in Table 1, the drug was thoroughly mixed (dry mixing) with the polymer and other ingredients for 15 minutes. The powder mixture was then moistened with the appropriate amount of purified water to form a moist cohesive mass. The cohesive mass was screened through a sieve with mesh #16, and the resulting moist granules were dried in a tray dryer at 65°C until the moisture content reached 2% w/v. The dried granules were passed through the sieve with mesh size 20 of BS, lubricated with magnesium stearate (2% w/w). The lubricated granules were compressed into tablets on a tablet compression machine (RIMEK, Karanavati Engineering Ltd., Gujarat, India) using 19.5 mm of oval concave surface punch. The compression force was adjusted to obtain tablets with hardness in the range of 49.04 to 63.74 Newton. MET contains CMAF tablets were prepared in a similar manner.

Physical Characterization of Tablet

Uniformity of weight

The test was carried out in accordance with the official procedure.¹⁶ The weight variation of 20 tablets of each formulation was studied using an electronic balance (Precisa, XB600 M-C, Switzerland). The tablets were selected at random

and weighed individually. Individual weights (X_1, X_2, \dots, X_{20}) were compared to the average weight of the tablets.

$$\text{Average weight (X)} = \left[\frac{X_1 + X_2 + X_3 + \dots + X_{20}}{20} \right] \quad (2)$$

Crushing strength and friability

The crushing strength and friability of 20 tablets for each formulation were determined using the Monsanto hardness tester (Cadmach, Ahmedabad, India) and the Roche friability (Campbell Electronics, Mumbai, India), respectively. To determine the percentage of weight loss, the friability was rotated at 25 ± 1 rpm for 4 minutes, and then the tablets were de-dusted and weighed again.

Content uniformity test

A fine powder was prepared by weighing and grinding 20 tablets. The powder containing about 0.1 g of metformin hydrochloride was precisely weighed and shaken for 15 minutes with 70 mL of water then diluted with water to 100 mL and filtered. From the filtrate, 10 mL was diluted to 100 mL with water, and then 10 mL from that dilution was diluted to 100 mL with water. Using a double-beam spectrophotometer (Shimadzu, UV, 2450, Japan), the absorbance of the resulting solution (0.01 mg/mL) was determined at 232 nm. The content of $C_4H_{11}N_5$, HCl was calculated by using 798 as the specific absorbance at 232 nm.¹⁷

Drug Release Study

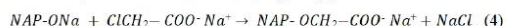
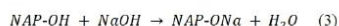
Using a USP II tablet dissolution tester (Electrolab, TDP-06P, India), matrix tablets were tested for in-vitro drug release in acidic (pH 1.2) and phosphate buffer solutions (pH 6.8). In a cylindrical dissolution vessel (1000 mL) with a stirring speed of 100 rpm, 750 mL of 0.1M hydrochloric acid solution was kept at $37 \pm 0.5^\circ\text{C}$. Then a randomly selected tablet from each formulation was placed inside it. During the experiment, aliquots were drawn every hour and promptly replaced with the same volume of fresh medium maintained at $37 \pm 0.5^\circ\text{C}$. After 2 hours of dissolution in acidic medium, 250 mL of 0.2M trisodium phosphate dodecahydrate solution (previously maintained at $37 \pm 0.5^\circ\text{C}$) was added. The medium was adjusted to a pH of 6.8 ± 0.05 with 2M sodium hydroxide solution.

The dissolution was carried out for 12 hours. The aliquots obtained by filtration and appropriate dilution were analyzed spectrophotometrically. The amount of drug released was measured at the wavelength of maximum absorbance (λ_{max}) in the relevant medium. MET exhibited maximum absorbances at 232 and 230 nm in acidic and buffer solutions, respectively.

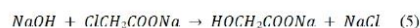
RESULTS AND DISCUSSION

Extent of Carboxymethylation

The native *A. procera* gum is primarily composed of galactose and arabinose.³ Structurally, NAP consists of a linear chain of - (1→3)- β -D-galactopyranose units with some - (1→6)- β -D-galactopyranose units and - (1→3)-L-arabinofuranose units.³ The substitution of numerous OH groups with carboxymethyl groups occurred during the conversion of NAP to CMAP. In the reaction, the hydroxyl groups in NAP were deprotonated by sodium hydroxide, forming alkoxides. Afterward, carboxymethyl groups were formed by reacting NAP-alkoxides with monochloroacetic acid.¹⁸ The overall reaction is given by:



At the bulk liquid phase, a side chain reaction occurred simultaneously with the formation of sodium-glycolate from monochloroacetic acid and sodium hydroxide.¹⁸



A degree of substitution (D_s) indicates the extent of carboxymethylation in a compound. D_s indicates the average number of substituted carboxymethyl groups per anhydroglucose unit.¹⁹ The values of D_s for different CMAP batches are shown in Table 2. The range of D_s was determined to be 0.38–0.51.

FTIR Spectrum Analysis

The conversion of NAP to CMAP was substantiated from FTIR, DSC, Solid-state ^{13}C -NMR, and XRD analysis. The FTIR spectra (4000–400 cm^{-1}) of NAP and CMAP are shown in (Figure 1) which exhibited the absorption in bands at 3449, 3420, 2927, 2925, 1620, 1615, and 1070 cm^{-1} , which are typical bands for carbohydrates.²⁰ Near 3449 cm^{-1} a strong O–H stretching band of the hydroxyl group²¹ was observed in NAP (Figure 1a) due to the involvement of hydrogen bonds of the hydroxyl groups. For CMAP, this O–H stretching

band was shifted with reduced intensity of the absorption (Figure 1b) which might indicate the breakage of hydrogen bonds in the carboxymethylation reaction.²² Figure 1b depicts the characteristic bands of CMAP, which appear at 1610 to 370 cm^{-1} , indicating carboxymethylation. The broad peak at 1420 cm^{-1} of CMAP was mainly attributed to C=O stretching of acid. The band at 2927 cm^{-1} is the indication of $-\text{CH}_2-$ groups. Although the bands at 1620, 1615 cm^{-1} are largely belong to C=O stretching. Many $-\text{C}-\text{O}-\text{C}-$ groups have peaks in the 950 to 1100 cm^{-1} range that may also indicate the presence of β - and α - linkages in the molecule, respectively.²³

Differential Scanning Calorimetry (DSC) study

DSC thermograms of NAP and CMAP have been depicted in Figure 2. The NAP exhibited an exothermic event at 73.99°C with a heat flow of 22.38 mW (Figure 2a) that was shifted for CMAP (55.31°C, 20.50 mW) (Figure 2b). In the NAP thermogram (Figure 2a), at around 239°C with a heat flow of 14.15968 mW a melting peak was seen to be intense, while CMAP occurred at 261.5°C with a heat flux of 9.899 mW (Figure 2b). It is likely that the substitution of hydroxyl group protons due to carboxymethylation triggered these variations in endothermic and exothermic behavior, along with heat flow alterations. The extent of carboxymethylation of polysaccharides results in the breaking of intermolecular and intra-molecular hydrogen bonds, as well as the vibrancy of chain segments leads to alteration in the thermal degradation of polymers.²⁴ However the DSC thermograms of NAP and CMAP indicated good thermal stability.

Solid State ^{13}C -NMR Spectroscopy

^{13}C -NMR spectra of NAP and CMAP are shown in Figure 3. The distinct signals appeared in the NMR spectrum of NAP (Figure 3a) at the respective chemical shifts (δ) 62.229, 72.740, and 103.760 ppm. The peak at 62.229 ppm is attributed to the galactose moiety's (sp^3 hybridization) C-6 carbon, which also indicates the presence of sugar ring carbon with hydroxyl group function. On the other side, the peak at δ = 72.740 ppm inflated at 82 ppm due to signals of C-2, C-3, and C-4 β -carbon atoms.²⁵ In addition, the peak at δ = 76.671 ppm indicates the presence of β -carbon at pyranose ring closure. The signal for the C-3 carbon atom of galactose has appeared as a small bulge at 82.738 ppm.²⁶ However, that peak at 82.738 ppm was also attributed to the presence of carbon at the furanose ring closure of α -anomers. A peak at δ = 99.316 ppm was detected

Table 2: Different batches of CMAP

Batch no.	Volume of 0.5N sodium Hydroxide (mL)	Volume of 0.4N hydrochloric acid (mL) consumed	A*	D_s **	SEM*** (statistical significance of 5%) (n = 3)
P1	5	6.2	3.5	0.41	± 0.0492
P2	5	6.1	3.5	0.51	± 0.0491
P3	5	6.3	3.22	0.38	± 0.0484
P4	5	6.2	3.225	0.41	± 0.0469
P5	5	6.2	3.225	0.41	± 0.0298
P6	5	6.3	3.22	0.38	± 0.0343

* Milliequivalents of NaOH required per gram of sample; ** Degree of substitution; *** Standard error of mean.

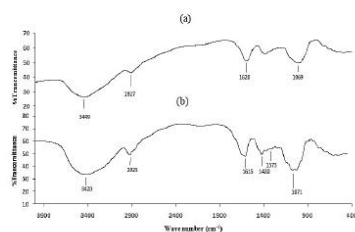


Figure 1: FTIR spectra (a) NAP, (b) CMAP

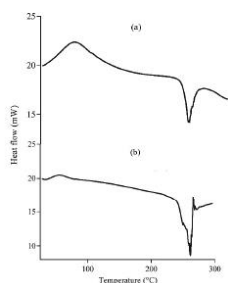


Figure 2: DSC thermogram (a) NAP (b) CMAP

due to the signal from β -anomeric carbon (C-1). Another intense peak observed at $\delta = 103.760$ ppm is due to arabinose's carbon (C-1).²⁷ In the case of CMAP, the spectra showed the appearance of an additional sharp peak at 177.252 ppm compared to NAP, explicitly the presence of carbonyl carbon of carboxymethyl group at 3-O- position (Figure 3b). Due to both sp^2 hybridizations for carbonyl carbon, the ^{13}C -NMR signal appears the utmost downfield (170–220 ppm).²⁸ The peak of absorption at 177.252 ppm also indicates the presence of exocyclic carboxyl groups. From the NMR data, the success of carboxymethylation on NAP could be assured. However, the spectral comparison (Figures 3 a and b) revealed the differentiation between NAP and CMAP

X-ray Diffractometry

An XRD of NAP is in Figure 4a, illustrating its amorphous nature. CMAP exhibits characteristic patterns in XRD at 2θ of 15.250 – 56.500° (Figure 4b). Moreover, the major sharp and intense patterns at about 2θ of 31.700° (369 cps) and 45.450° (134 cps) indicate the possible crystallinity of NAP on carboxymethylation.²⁹

Zeta Potential Measurements

The zeta potential is the electro-kinetic potential in the interfacial bilayer at the slip plane that separates the mobile fluid from the surface-clinging fluid.^{30, 31} The zeta potential of NAP and CMAP were -0.944 and -15.40 mV, respectively (Figure 5a and b). Because of the presence of anions on the carboxymethyl groups ($-OCH_2-COO^-$), CMAP had a lower zeta potential. (Figure 5b). The zeta potential decreased as the

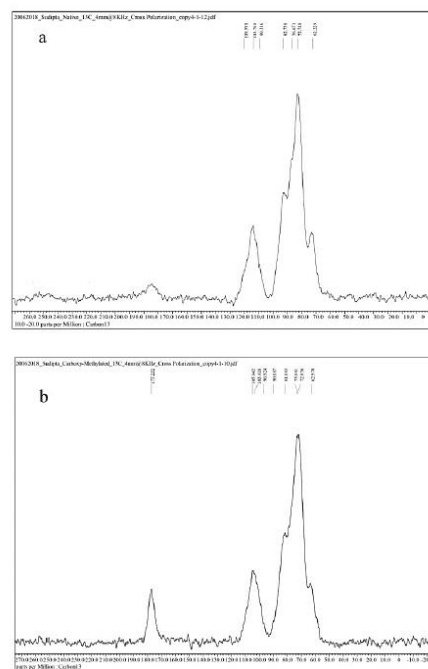


Figure 3: Solid state ^{13}C NMR spectrum of (a) NAP, (b) CMAP

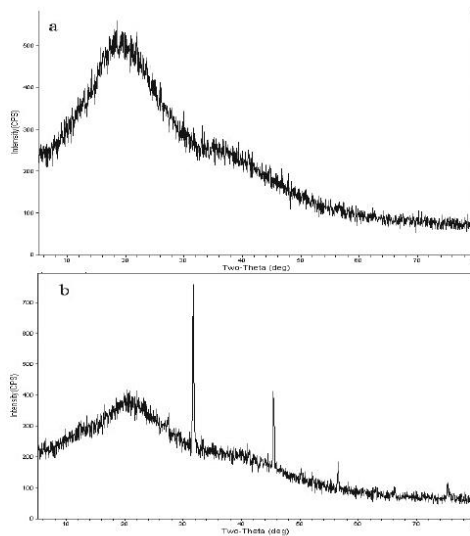


Figure 4: XRD patterns of (a) NAP and (b) CMAP

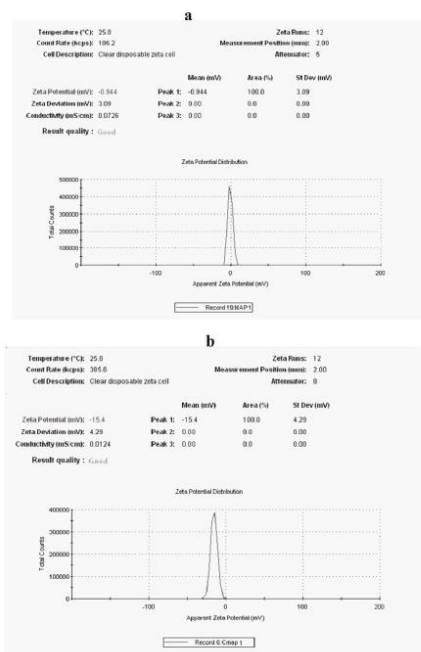


Figure 5: Zeta potential of (a) NAP, and (b) CMAP

D_S increased, showing that CMAP had more carboxymethyl groups and a stronger coulombic repulsion (Table 3). The zeta potential in the NAP samples did not exhibit any notable differences.

Rheological Characteristics

Rheology could be used as a method to evaluate parameters that aid in determining a material's mechanical strength, deformation, and flow properties.^{32, 33} The comparative study of the rheological parameters like flow curves, amplitude sweep, frequency sweep, and damping factor of NAP and CMAP (5% w/v) samples reflect the changes in structural integrity, flow behavior due to carboxymethylation.

Dynamic rotational study

The flow curves at variable shear rates are shown in Figure 6 (a-c). There is also a depiction of the viscosity profile of polymers at various pH levels in the Figures. 6d and e. In response to increases in shear rate, the viscosity of the NAP matrix was observed to decline. In addition, it was also found that the NAP matrices exhibited non-Newtonian behavior with the pseudo-plastic flow. In this case, the disentanglement of polymeric chains occurs at a faster rate than the new entanglement formation.³⁴ There was an observation in Figure 6(a) that, the NAP matrices exhibited higher viscosity (1420 Pa.s for NAP-W, 559 Pa.s for NAP-A, and 115 Pa.s for NAP-B) at a low shear rate (0.01290 S^{-1}). Additionally, the

Table 3: Zeta potential of different batches of CMAP

Batch no. of CMAP	D_S^*	Zeta potential of CMAP (mV)	Zeta potential of NAP (mV)
P1	0.41	-14.53	
P2	0.51	-15.40	
P3	0.38	-13.76	
P4	0.41	-14.91	
P5	0.41	-15.03	
P6	0.38	-12.17	-0.944

* Degree of substitution

rheogram demonstrated that NAP at neutral pH (NAP-W) displayed greater viscosity than NAP at pH 1.2 (NAP-A); however, the viscosity of NAP-A was higher than the NAP at pH 6.8 (NAP-B).

Flow curves of CMAP matrices also indicated shear-thinning behaviour however; they exhibited much lower viscosities than NAP matrices (Figure 6). There has been an explanation for the increased degree of molecular chain entanglement with concentration attributed to an increase in the viscosity of polymers.³⁵ Since carboxymethyl groups ($-OCH_2-COO^-$) in CMAP contain anions, the chain segments are electrostatically repellent, preventing entanglements. Due to lack of entanglement, the viscosity of CMAP became lower than NAP matrices. The viscosity of CMAP-A (at pH 1.2) matrix was found to be higher than CMAP-W (at pH 7) and significantly higher than CMAP-B (Figure 6e). The functional groups get ionized at pH 6.8, and the repulsive force becomes strong, which leads to disentanglement and a decrease in viscosity.^{36, 37} A shift in the molecular arrangements of the polysaccharide chains in buffer solution has been connected to the decreased viscosity of some ionic polymers with rising solution pH.^{38, 39}

According to the flow curve model analysis, the Carreau-Yasuda model best fitted to NAP-W as it displayed a short Newtonian plateau for low shear rates (0.022–0.045 S^{-1}). However, the cross model provided the best fit with NAP-A, and the Ellis model with NAP-B represented pseudo-plastic flow. As for CMAP, the Ellis model effectively fitted samples at all pH values, where the shear stress roughly coincides with half of the final asymptotic viscosity.⁴⁰

Dynamic Oscillatory Studies

Amplitude sweep

The linear viscoelastic region (LVE) is the region in which stress varies linearly with strain for the sample under study.⁴¹ The storage modulus (G') (Pa) is an elastic response of a viscoelastic material that stored the deformation energy subjected to measure during shear.⁴² While the loss modulus (G'') (Pa) evaluates the deformation energy used by a viscoelastic material during shear, it is the viscous part of the material.

During the amplitude sweep, the amplitude of the deformation is varied with strain (%) at a constant frequency (Rad/sec).⁴³

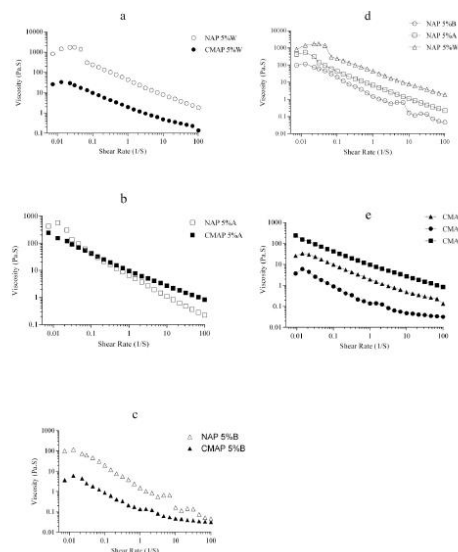


Figure 6: Flow curves (a) in water, (b) at pH 1.2 (c) at pH 6.8; viscosity profile of (d) NAP in water (Δ), at pH 1.2 (□), at pH 6.8 (○), (e) CMAP in water (▲), at pH 1.2 (■), at pH 6.8 (●)

An illustration of the strain sweep results for each matrix (NAP and CMAP) is presented in Figure 7 (a-c). G' and G'' in the amplitude curves were dependent on strain amplitude, and the LVE range was derived from these curves. Upon reaching a critical strain of 10%, LVE had been achieved, and G' values were found to be linear up to that point. Beyond the LVE the decline of G' indicated the occurrence of structural deformation. The critical strain refers to the mechanical strength of polymer and the amount of stress at which NAP and CMAP withstand before structural breakdown. IN ALL CASES, the LVE range and G' values of NAP were greater than CMAP (Figure 7 a-c). The overall critical strain of NAP (1–1.5%) was also found to be higher than CMAP (0.01–0.03%). The electrostatic repulsion between the chains of CMAP disrupted entanglements results in low mechanical strength and shorter LVE.

Frequency sweep

During the frequency sweep, the amplitude of the deformation is retained within the LVE, while the angular frequency (ω) is varied.⁴⁴ Variable oscillation frequencies make it possible to determine with greater precision the structural integrity, deformity, and rheological stability of a material. The higher values of G' over the G'' ($G' > G''$) indicate an elastic structure of material could be said to have a solid viscoelastic nature, while $G'' > G'$ impart the viscous behavior of the material could be said to have a viscoelastic.⁴² The crossover point refers to the transition point at which the value of G' and G'' remains the same. For material, if G' is higher than G'' before the crossover,

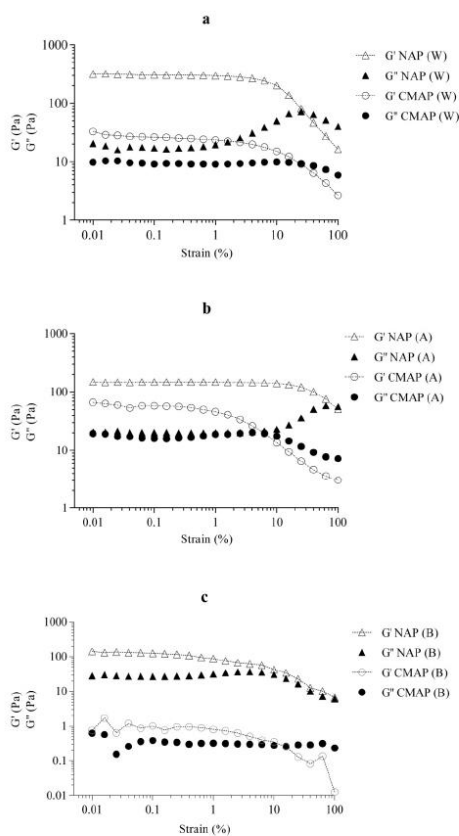


Figure 7: Amplitude sweep (a) in water, (b) at pH 1.2 (c) at pH 6.8

the crossover point could be considered a deformation point. On the other hand, $G'' > G'$ remains before the crossover then it corresponds to a gel point.⁴⁵ The higher differences between G' and G'' without crossing each other indicate the more rheological stability of a material.

The frequency sweep analysis was conducted on NAP and CMAP solutions as shown in Figure 8 a-c. Based on the frequency sweep curve, it was observed that G' for NAP is much higher than G'' ($G' > G''$) in water and is also rheologically stable (Figure 8a). The values of G' for CMAP in water were also higher than G'' but in comparison to NAP, it was much less. At pH 1.2, NAP and CMAP were found to be stable and remain gel-like consistency, although G' values of NAP-A were lower than NAP-W (Figure 8b). In case of CMAP at pH 1.2, the G' values were drastically higher than CMAP in water. However, both polymers were structurally deformed at pH 6.8 (Figure 8c), as they have shown crossover points (NAP at 15.8 Rad/sec, CMAP at 25 Rad/sec). The appearance of

any crossover region indicated the transformation of gel to sol. Moreover, the frequency sweep results indicated that NAP in water formed high entanglements and behaved as a strong viscoelastic gel than acidic pH. While at pH 6.8, the entanglements became weak. In contrast, CMAP at acidic pH has shown gel-like behavior, and ultimately, at pH 6.8, it lost its elastic energy and exhibited a weak gel with a disentangled structure. As the pH of the solution increased, there is a possibility that the functional groups (-COOH-) of CMAP would be ionized, leading to electrostatic repulsion and, thus an increase in molecular dimension and a decrease in entanglements.^{46, 47} However, there is also the possibility that the polymer chains would be de-polymerized as the pH rose.⁴⁸ Moreover, throughout the frequency sweep study, it has also been noted that in all cases, G' values of NAP were always higher than CMAP.

Damping factor

The inclusion of a damping function in the modeling of polymer melts is crucial to gaining an understanding of

nonlinear viscoelasticity.⁴⁹ The damping factor is the loss tangent ($\tan\delta = G''/G'$) that measures the internal frictions of materials. The value of loss tangent ($\tan\delta$) for different viscoelasticity functions⁵⁰ is as follows:

$\tan\delta=0$: The material is ideally elastic

$\tan\delta=100$: The material is ideally viscous

$\tan\delta>1$: material is more viscous than elastic

$\tan\delta<1$: material is more elastic than viscous

$\tan\delta=1$: material is viscoelastic

An investigation of the physical interpretation of the damping function based on experimental results for NAP and CMAP at different pH levels was conducted. From Figure 9, the loss tangents ($\tan\delta$) for NAP-W and CMAP-W were less than 1, but the mean $\tan\delta$ value for CMAP-W (0.56) was higher than NAP-W (0.16). Thus, NAP was more elastic in water than CMAP. Similarly, both polymers showed elastic deformation at pH 1.2. CMAP ($\tan\delta=0.45$) at this pH was a little more elastic than CMAP-W, while NAP at pH 1.2 ($\tan\delta=0.59$) remained less elastic than NAP-W. Moreover, both polymers were viscous at pH 6.8 as the loss tangents ($\tan\delta$) were more than 1.

Drug-polymer DSC compatibility study

DSC studies are useful tools for assessing the interaction between a drug and an excipient. The melting points of MET and the physical mixture with NAP and CMAP are presented in Table 4. It has been found that the melting point of MET in each of the polymer mixtures is similar to its reported values,⁵¹ despite some minor reductions in endothermic peak intensity. According to the results, there is no interaction between the excipients and the polymers.

Characterizations of matrix tablets

The average weight of randomly selected matrix tablets containing MET from each formulation of NAP was $1121.5 \text{ mg} \pm 0.04$. In contrast, the average weight of the matrix tablets from CMAP formulations containing MET was $1118.7 \text{ mg} \pm 0.05$.

The average hardness of all the tablets were about $53.94 \text{ Newton} \pm 0.02$ and friability was less than 1%.

A random sample of matrix tablets from each formulation of NAP containing MET was found to be uniform and ranged from $96.89\% \pm 0.04$ to $101.53\% \pm 0.03$. Similarly, the drug content of CMAP tablets was found to be $95.63\% \pm 0.12$ to $107.37\% \pm 0.06$.

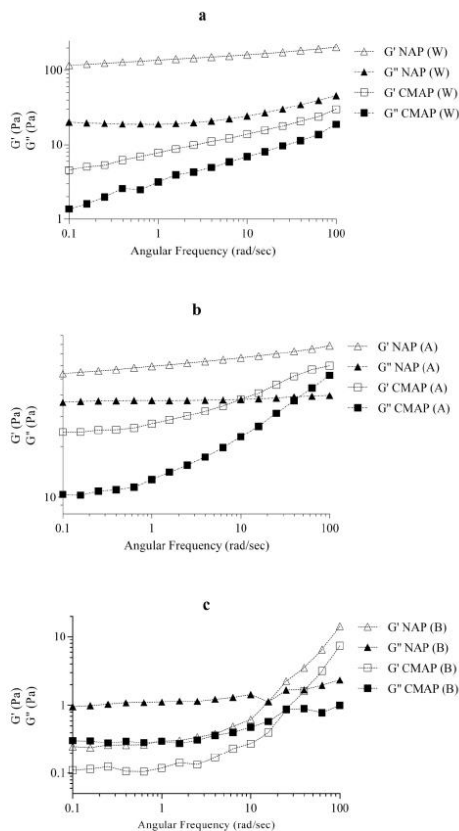


Figure 8: Frequency sweep (a) in water, (b) at pH 1.2, (c) at pH 6.8

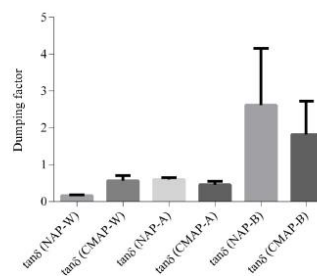
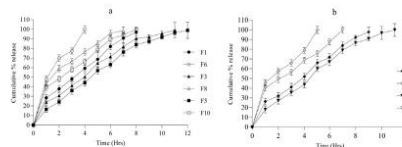


Figure 9: Damping factor of NAP and CMAP

Table 4: Melting point of MET in polymer mixtures from DSC endotherm data

Drug and mixtures	Melting point (°C)
MET	222.37°C
MET + Physical mixture of NAP	221.63°C
MET + Powdered tablet of NAP	221.63°C
MET + Physical mixture of CMAP	221.22°C
MET + Powdered tablet of CMAP	222.05°C

**Figure 10:** Drug release profiles of MET from NAP (—) and CMAP (---) matrix tablets. (a) NAP formulations: F1 (●), F3 (▲), F5 (■); CMAP formulations: F6 (○), F8 (Δ), F10 (□); (b) NAP formulations: F2 (◆), F4 (▼); CMAP formulations: F7 (◇), F9 (▽)**Table 5:** AUC of drug release

Medium	AUC of drug release from NAP matrix (% mg hrs.)					AUC of drug release from CMAP matrix (% mg hrs.)				
	F1	F2	F3	F4	F5	F6	F7	F8	F9	F10
In acid (pH 1.2)	47.44 ± 4.9	42.33 ± 4.7	39.32 ± 3.8	31.63 ± 4.1	28.59 ± 3.3	83.15 ± 2.4	74.24 ± 5.2	72.81 ± 4.3	64.82 ± 4.5	63.46 ± 4.2
In buffer (pH 6.8)	463.95 ± 3.9	514.4 ± 4.1	692.67 ± 3.8	653.44 ± 4.9	726.63 ± 4.6	245.57 ± 5.1	297.53 ± 4.2	476.01 ± 3.8	427.51 ± 4.6	524.88 ± 5.3

Comparison of drug release

The linearity of the standard calibration curve of MET was determined with a correlation coefficient (R^2) over 0.998 and then used to calculate the amount of drug dissolved in each sample. A comparison of the in vitro drug release from NAP and CMAP matrix tablets is presented in Figure. 10.

The highest amount of MET release in 12 hours from NAP formulation (F5) was 98.81%, while all CMAP tablets showed maximal release before 12 hours. From the entire release profiles of MET (Figure. 10 a and b), it was noted that NAP formulations showed prolonged release and became more sustained as the polymer concentration increased, while CMAP formulations, the release profile showed faster drug release. A "t"-test was used to analyze the data on drug releases from the two matrices. Thus, a statistically significant difference in drug release from NAP and CMAP matrices was observed ($p=0.05$).

Calculation of AUC was carried out using a linear trapezoidal rule. The calculated values of AUC of drug release (% mg hrs.) from formulations are shown in Table 5.

In CMAP tablets, predominantly drug was released from the gel-like structure owing to a lower viscosity and disentanglement than in NAP tablets. The weak gel networks in CMAP matrices are attributed to their low viscosity and loose entanglement structure. While, the strong gel-like structure of NAP and the high viscosity of the compound resulted in a higher degree of entanglement, which resulted in the prolonged release of the drug from tablets containing NAP. The carboxymethylation had changed the structural integrity of CMAP, making it more rheologically unstable than NAP and the rheological behaviors impacted on drug release.⁵²

CONCLUSION

An outgrowth of entanglements of the chains in NAP resulted in elastic nature, which imparted structural integrity and higher mechanical strength. Carboxymethylation of NAP significantly

altered its rheological properties. A coulombic repulsion between CMAP chains occurs due to the presence of anions within carboxymethyl groups. Therefore, the individual chains of CMAP were unrestricted in their movement, allowing the CMAP structure to disentangle rapidly. NAP and CMAP also exhibit significant differences in their rheological properties at variable pH. While NAP formed a highly entangled structure with higher viscosity at neutral pH, CMAP showed high viscosity at pH 1.2. Thus, such changes also had an impact on the significant change in drug release from matrix tablets. The lack of entanglements and weak gel structures in CMAP made it more prone to erosion.

ACKNOWLEDGMENT

We are grateful for the support the University Grants Commission, New Delhi (DSA Phase-III and UPE-II programs of the UGC) provided. We would also like to extend our gratitude to the Head of the Department of Pharmaceutical Technology at Jadavpur University.

REFERENCES

- Meena VS, Gupta S. Wood anatomy of *Albizia procera* correlation between tropical and subtropical from Different geographical zones of Indian subcontinent. *Int. J. Sci. Tech. Res.* 2014;3(5):1-8.
- Nguyễn NC. Vietnam forest trees. Vietnam forest trees.. 1996.
- Pachau L, Lalhlenmawia H, Mazumder B. Characteristics and composition of *Albizia procera* (Roxb.) Benth gum. *Industrial Crops and Products.* 2012 Nov 1;40:90-5.
- Zhang J, Akihisa T, Kurita M, Kikuchi T, Zhu WF, Ye F, Dong ZH, Liu WY, Feng F, Xu J. Melanogenesis-inhibitory and cytotoxic activities of triterpene glycoside constituents from the bark of *Albizia procera*. *Journal of natural products.* 2018 Dec 6;81(12):2612-20.
- Avachat AM, Dash RR, Shrotriya SN. Recent investigations of plant based natural gums, mucilages and resins in novel drug delivery systems. *Ind J Pharm Edu Res.* 2011 Jan;45(1):86-99.

6. De Paula RC, Santana SA, Rodrigues JF. Composition and rheological properties of *Albizia lebbek* gum exudate. *Carbohydrate polymers*. 2001 Feb 1;44(2):133-9.
7. De Pinto GL, Martínez M, Beltrán O, Rincón F, Clamens C, Igartuburu JM, Guerrero R, Vera A. Characterization of polysaccharides isolated from gums of two Venezuelan specimens of *Albizia niopoides* var. *colombiana*. *Ciencia*. 2002;19:382-7.
8. Gupta MN, Raghava S. Smart systems based on polysaccharides. In: *Natural-based polymers for biomedical applications* 2008 Jan 1 (pp. 129-161). Woodhead Publishing.
9. da Silva MA, Bierhalz AC, Kieckbusch TG. Alginate and pectin composite films crosslinked with Ca²⁺ ions: Effect of the plasticizer concentration. *Carbohydrate polymers*. 2009 Jul 19;77(4):736-42.
10. Zhang H, Lamnawar K, Maazouz A. Rheological modeling of the diffusion process and the interphase of symmetrical bilayers based on PVDF and PMMA with varying molecular weights. *Rheologica acta*. 2012 Aug;51(8):691-711.
11. Münstedt H, Schwarzl FR. Deformation and flow of polymeric materials. Heidelberg, Germany:: Springer; 2014 Nov 18.
12. Caramella C, Ferrari F, Bonferoni MC, Ronchi M, Colombo P. Rheological properties and diffusion dissolution behaviour of hydrophilic polymers. *Bollettino Chimico Farmaceutico*. 1989 Oct 1;128(10):298-302.
13. Michailova V, Titeva S, Kotsilkova R. Rheological characteristics and diffusion processes in mixed cellulose hydrogel matrices. *Journal of drug delivery science and technology*. 2005 Jan 1;15(6):443-9.
14. Toğrul H, Arslan N. Production of carboxymethyl cellulose from sugar beet pulp cellulose and rheological behaviour of carboxymethyl cellulose. *Carbohydrate Polymers*. 2003 Oct 1;54(1):73-82.
15. Barai BK, Singhal RS, Kulkarni PR. Optimization of a process for preparing carboxymethyl cellulose from water hyacinth (*Eichornia crassipes*). *Carbohydrate Polymers*. 1997 Mar 1;32(3-4):229-31.
16. Pharmacopoeia I. Vol. II, The Controller Publication. Govt. of India, New Delhi. 2010:1199.
17. Pharmacopoeia I, Volume II. Published by the controller of Publication. Vol. I, New Delhi. 2007:655.
18. Kaity S, Ghosh A. Carboxymethylation of locust bean gum: application in interpenetrating polymer network microspheres for controlled drug delivery. *Industrial & engineering chemistry research*. 2013 Jul 31;52(30):10033-45.
19. Chakravorty A, Barman G, Mukherjee S, Sa B. Effect of carboxymethylation on rheological and drug release characteristics of locust bean gum matrix tablets. *Carbohydrate polymers*. 2016 Jun 25;144:50-8.
20. Yuen SN, Choi SM, Phillips DL, Ma C.Y. Raman and FTIR spectroscopic study of carboxymethylated non-starch polysaccharides. *Food chemistry*. 2009 Jun 1;114(3):1091-8.
21. Sadalage PS, Pawar KD. Production of microcrystalline cellulose and bacterial nanocellulose through biological valorization of lignocellulosic biomass wastes. *Journal of Cleaner Production*. 2021 Dec 10;327:129462.
22. Aguir C, M'Henni MF. Experimental study on carboxymethylation of cellulose extracted from *Posidonia oceanica*. *Journal of applied polymer science*. 2006 Feb 15;99(4):1808-16.
23. Khondkar P. Composition and partial structure characterization of Tremella polysaccharides. *Mycobiology*. 2009 Dec 1;37(4):286-94.
24. Gong H, Liu M, Chen J, Han F, Gao C, Zhang B. Synthesis and characterization of carboxymethyl guar gum and rheological properties of its solutions. *Carbohydrate polymers*. 2012 Apr 15;88(3):1015-22.
25. Yazdani P, Wang B, Rimaz S, Kawi S, Borgna A. Glucose hydrogenolysis over Cu-La₂O₃/Al₂O₃: mechanistic insights. *Molecular Catalysis*. 2019 Apr 1;466:138-45.
26. Agrawal PK, Jain DC, Gupta RK, Thakur RS. Carbon-13 NMR spectroscopy of steroidal sapogenins and steroidal saponins. *Phytochemistry*. 1985 Oct 29;24(11):2479-96.
27. Chauhan D, Chauhan JS. Flavonoid glycosides from *Pongamia pinnata*. *Pharmaceutical biology*. 2002 Jan 1;40(3):171-4.
28. Scholze B, Hanser C, & Meier D. Characterization of the water-insoluble fraction from fast pyrolysis liquids (pyrolytic lignin): Part II. GPC, carbonyl groups, and 13C-NMR. *Journal of Analytical and Applied Pyrolysis*. 2001; 38: 387-400.
29. Bhatia M, Ahuja M. Psyllium arabinoxylan: Carboxymethylation, characterization and evaluation for nanoparticulate drug delivery. *International Journal of Biological Macromolecules*. 2015 Jan 1;72:495-501.
30. Liu Y, Lu K, Hu X, Jin Z, Miao M. Structure, properties and potential applications of phytoglycogen and waxy starch subjected to carboxymethylation. *Carbohydrate polymers*. 2020 Apr 15;234:115908.
31. Ye F, Miao M, Lu K, Jiang B, Li X, Cui SW. Structure and physicochemical properties for modified starch-based nanoparticle from different maize varieties. *Food Hydrocolloids*. 2017 Jun 1;67:37-44.
32. Isaac VL, Chiari-Andréo BG, Marto JM, Moraes JD, Leone BA, Corrêa MA, Ribeiro HM. Rheology as a tool to predict the release of alpha-lipoic acid from emulsions used for the prevention of skin aging. *BioMed Research International*. 2015 Dec 16:2015.
33. Kulawik-Piöro A, Ptasek A, Kruk J. Effective tool for assessment of the quality of barrier creams-relationships between rheological, textural and sensory properties. *Regulatory Toxicology and Pharmacology*. 2019 Apr 1;103:113-23.
34. Xu X, Xue C, Chang Y, Chen F, Wang J. Conformational and physicochemical properties of fucosylated chondroitin sulfate from sea cucumber *Apostichopus japonicus*. *Carbohydrate polymers*. 2016 Nov 5;152:26-32.
35. Mirtič J, Balažic H, Zupančič Š, Kristl J. Effect of solution composition variables on electrospun alginate nanofibers: Response surface analysis. *Polymers*. 2019 Apr 16;11(4):692.
36. Wang CS, Virgilio N, Carreau PJ, Heuzey MC. Understanding the effect of conformational rigidity on rheological behavior and formation of polysaccharide-based hybrid hydrogels. *Biomacromolecules*. 2021 Aug 16;22(9):4016-26.
37. Sa B, Mukherjee S, Roy SK. Effect of polymer concentration and solution pH on viscosity affecting integrity of a polysaccharide coat of compression coated tablets. *International journal of biological macromolecules*. 2019 Mar 15;125:922-30.
38. Boas M, Vasilyev G, Vilensky R, Cohen Y, Zussman E. Structure and rheology of polyelectrolyte complexes in the presence of a hydrogen-bonded co-solvent. *Polymers*. 2019 Jun 17;11(6):1053.
39. Chen TT, Zhang ZH, Wang ZW, Chen ZL, Ma H, Yan JK. Effects of ultrasound modification at different frequency modes on physicochemical, structural, functional, and biological properties of citrus pectin. *Food Hydrocolloids*. 2021 Apr 1;113:106484.

40. Al-Behadili A, Sellier M, Hewett JN, Nokes RI, Moyers-Gonzalez M. Identification of Ellis rheological law from free surface velocity. *Journal of Non-Newtonian Fluid Mechanics*. 2019 Jan 1;263:15-23.
41. Kaboorani A, Blanchet P. Determining the linear viscoelastic region of sugar maple wood by dynamic mechanical analysis. *BioResources*. 2014 Jan 1;9(3):4392-409.
42. Talens P, Castells ML, Verdú S, Barat JM, Grau R. Flow, viscoelastic and masticatory properties of tailor made thickened pea cream for people with swallowing problems. *Journal of Food Engineering*. 2021 Mar 1;292:110265.
43. Li C, Liu C, Liu J, Fang L. Correlation between rheological properties, in vitro release, and percutaneous permeation of tetrahydropalmatine. *Aaps Pharmscitech*. 2011 Sep;12:1002-10.
44. Xiao F, Chen M, Wu S, Amirkhanian SN. A long-term ultraviolet aging effect on rheology of WMA binders. *Int. J. Pavement Res. Technol*. 2013 Sep 1;6(5):496-504.
45. Rasid IM, Do C, Holten-Andersen N, Olsen BD. Effect of sticker clustering on the dynamics of associative networks. *Soft Matter*. 2021;17(39):8960-72.
46. Medina-Torres L, Brito-De La Fuente E, Torrestiana-Sanchez B, Katthain R. Rheological properties of the mucilage gum (*Opuntia ficus indica*). *Food hydrocolloids*. 2000 Sep 1;14(5):417-24.
47. Yan X, Xiao X, Au C, Mathur S, Huang L, Wang Y, Zhang Z, Zhu Z, Kipper MJ, Tang J, Chen J. Electrospinning nanofibers and nanomembranes for oil/water separation. *Journal of Materials Chemistry A*. 2021;9(38):21659-84.
48. Achi OK, Okolo NI. The chemical composition and some physical properties of a water-soluble gum from *Prosopis africana* seeds. *International journal of food science & technology*. 2004 Apr;39(4):431-6.
49. Rolón-Garrido VH, Wagner MH. The damping function in rheology. *Rheologica Acta*. 2009 Apr;48:245-84.
50. Wang H, Ke L, Ding Y, Rao P, Xu T, Han H, Zhou J, Ding W, Shang X. Effect of calcium ions on rheological properties and structure of *Lycium barbarum* L. polysaccharide and its gelation mechanism. *Food Hydrocolloids*. 2022 Jan 1;122:107079.
51. Gramaglia D, Conway BR, Kett VL, Malcolm RK, Batchelor HK. High speed DSC (hyper-DSC) as a tool to measure the solubility of a drug within a solid or semi-solid matrix. *International journal of pharmaceutics*. 2005 Sep 14;301(1-2):1-5.
52. Li C, Liu C, Liu J, Fang L. Correlation between rheological properties, in vitro release, and percutaneous permeation of tetrahydropalmatine. *Aaps Pharmscitech*. 2011 Sep;12:1002-10.

Ionic crosslinking of O-carboxymethylated *Albizia procera* gum and its effect on rheological changes and drug release from matrix tablets

Sudipta Mukherjee^{*1}, Jasmina Khanam², Sanmoy Karmakar³, Manas Bhowmik⁴, Rudranil Bhowmik⁵

^{1,2,3,4,5}Division of Pharmaceutics, Department of Pharmaceutical Technology, Jadavpur University, Kolkata 700032, West Bengal, India

Submitted: 10-07-2023

Accepted: 20-07-2023

ABSTRACT:

In this study, carboxymethylated *Albizia procera* gum (CMAP) was cross-linked by Ca^{2+} ions using concentrated calcium chloride solution as the cross-linking agent. The resulting cross-linked CMAP (CCMAP) was evaluated for its rheological properties and release of the drug from its matrix tablet formulation. The cross-linking of carboxymethylated polymer with Ca^{2+} ions restricts the water infiltration rate into the framework of the polymer matrices. As it brought about a decrease in electrostatic repulsion between the polymeric chains resulting in high entanglements with a strong gel network, an increase in the consistency of the gel layer affected the swelling rate and drug release. A dynamic rotational and oscillatory study was performed to analyze the rheological data and investigate the structural integrity of polymers (CMAP and CCMAP). Correlation coefficients (R^2) were used to evaluate the kinetic model for best fitting the drug release data. Based on instrumental analyses of drug-polymer compatibility, Metformin was used as a model drug in the formulations. This study aimed at achieving enhanced functional properties for improved drug release from the polymer core through cross-linking.

KEYWORDS: Carboxymethylated *Albizia procera*, Ca^{2+} ion cross-linking, Rheology, Swelling, Drug release kinetics

1. INTRODUCTION

There have been numerous studies that have explored the release behavior of drugs using polysaccharides such as guar gum, locust bean gum, xanthan gum and karaya gum as hydrophilic matrices [1-6]. Several efforts are being made to enrich the existing resources, including the search for new polysaccharides and the modification of existing ones. The diversity of chemical compositions and functional groups of native

polysaccharides makes them susceptible to modifying chemically [7] by using chemical derivatization, chemical crosslinking, or ionic crosslinking [8]. As a result, custom-built materials can be developed for modulating the release of drugs.

Carbohydrate polymers are proven in the field of pharmaceuticals industries received a lot of attention, especially as a site-specific or

sustained release drug delivery carrier. *Albizia procera* was considered for its biocompatibility and wide availability as a carbohydrate polymer. *A. procera* is an exudate gum obtained from *Albizia* tree belonging to Mimosaceae family. *A. procera* gum contains β -(1 \rightarrow 3)-D-galactopyranose units with some β -(1 \rightarrow 6)-D-galactopyranose units [9] and α -(1 \rightarrow 3)-L-arabinofuranose units [10-13]. A key aspect of this study was the conversion of carboxymethylated *A. procera* (CMAP) into its crosslinking structure (CCMAP) with calcium ions, which was investigated for rheological changes and effects on drug release. In this work, both CMAP and CCMAP matrix tablets were prepared by wet granulation method, and the effect of crosslinking was evaluated on drug release in a comparative manner.

Drug diffusion through entangled polymeric matrices is influenced by many factors, including the gel network size and gel strength [1], which have a direct impact on the viscosity of the polymer solution [2,3]. However, the polymeric entanglement depends on molecular domain of the polymer and the functional groups within it.

Since carboxymethylation affected the inherent rheological characteristics of native polymers due to coulombic repulsion between carboxyl groups, this was reflected in their significant change in drug release characteristics [14].

In addition, the ionic cross-linking with carboxyl groups attached to carboxymethylated polymer chains may have a significant effect on polymer entanglements, mechanical strength [15], and drug release from polymer matrices [16]. In addition to analyzing the drug release and kinetics, the drug-polymer compatibility was also assessed. The rheological properties of the polymer matrix can influence the drug release kinetics, duration, and mechanism. A polymer matrix with high viscosity can slow down the diffusion of drugs through the matrix, resulting in a slower drug release rate [17-19]. Similarly, a more elastic matrix can resist swelling, which can reduce the drug release rate. Therefore, understanding the rheological behavior of the polymer matrix is crucial for designing drug delivery systems with desired drug release profiles [20]. The results of such studies may be valuable for interpreting the behavior of crosslinked polymers that are essential to optimizing modified release tablets.

II. MATERIALS AND METHODS

Materials

The Metformin hydrochloride (MET) was provided as a gift sample by Stadmed Pvt. Ltd., Kolkata, India. The native *A. procera* (NAP) was procured from Mizoram University (Mizoram, India). Monochloroacetic acid (99.0%), sodium hydroxide, tri-sodium phosphate dodecahydrate (TSPD) Mol.Wt. 380.119 g/mole and Tri-sodium citrate (TSC) was purchased from Loba Chemie Pvt. Ltd. Mumbai, India. calcium chloride dehydrate, and methanol (99% v/v) analytical reagent grade were purchased from Merk Specialties Pvt. Ltd. Mumbai, India. All other chemicals and reagents used were of analytical grade.

1. Carboxymethylation of *Albizia procera*

The carboxymethylation of NAP was carried out by a base-catalyzed reaction [21]. Pulverized native *procera* gum was sieved through 45 meshes and weighed. The dispersion was prepared by slowly adding powdered NAP (10 g) to aqueous sodium hydroxide solution (45% w/v). To ensure complete hydration, the mixture was placed in a double-walled ice chamber (stainless steel) maintained at a temperature between 0-8°C and agitated vigorously. A solution of monochloro-acetic acid (45.05% in water) of 10 ml was gradually added to the slurry while stirring continuously at a temperature of 15-18°C. Afterward, the reaction

mixture was heated to 75°C in a water bath for one hour with regular stirring, and maintained at room temperature for 24 hours. After precipitating the resulting mass with methanol: water (80:20), it was filtered through 8mm filter paper and washed the filtered cake three to four times with aqueous methanol (80% by volume). To achieve the final pH of the CMAP samples, glacial acetic acid was used for pH adjustment and then methanol was used for washing. Air drying was carried out on the tiny semi-crystalline samples and they were then placed in a hot air oven at 60°C for 24 hours.

2. Degree of substitution (DS)

The amount of CMAP, at 5% w/v, was dispersed in 25 ml of 2M hydrochloric acid, and 2.5 ml of aqueous, 80% v/v methanol was gradually added while stirring for 2-3 hours. Then further 2 ml of aqueous 80% v/v methanol was added. The mixture was filtered and washed with methanol: water (80:20) until the wash showed neutrality on litmus paper. Finally, the residue was washed with pure methanol and air dried for 1-2 hours. Then it was dried in a hot air oven at 60°C until a constant mass was obtained. 200 mg of dried powdered CMAP was accurately weighed and the sample was added to aqueous 70% v/v methanol and allowed to stand for a few minutes. Then 20 ml of water and 5 ml of 0.5M NaOH solution were added. The mixture was shaken for 3-4 hours until the sample was completely dissolved. The solution was titrated with 0.4M HCl solution using phenolphthalein as an indicator [22]. The degree of substitution of the O-carboxymethyl group was determined according to the following equation [15].

$$Ds = \left[\frac{0.162 \times A_{NaOH}}{1 - 0.058 \times A_{NaOH}} \right] (1)$$

Where A_{NaOH} is the milliequivalents of NaOH required per gram of sample.

3. Preparation of crosslinked CMAP

Required quantity (approx. 10g) of dry basis semi-crystalline CMAP powder was weighed and passed through a BS screen #45. The powder was then slowly sprinkled into de-ionized water and stirred for 1 hour to form slurry. Afterwards, a freshly prepared NaOH solution (2% w/v, 10 ml) was slowly added to the slurry for complete solubilization. Then it was transferred into an aqueous $CaCl_2$ solution (5% w/w, 50 ml) and stirred. The mixture was kept overnight. The next day, the obtained mass was vacuum filtered, and the filtered cake was washed with methanol.

The resultant cake was dried in a hot air oven at 60°C for 4 hours. After obtaining the dried crosslinked CMAP (CCMAP), it was ground and screened [23-24].

4. FTIR spectrum analysis

CMAP and CCMAP powdered samples were analyzed using a FTIR spectrophotometer (PerkinElmer, RX-1, UK), using the potassium bromide disc technique, in the range of 4000 - 400 cm^{-1} . The disc was prepared using ground samples (2 mg) and KBr (45 mg) at 400 kg cm^{-2} pressure for 10 minutes.

5. Differential Scanning Calorimetry (DSC) study

The thermal analysis of CMAP and CCMAP was carried out on a differential scanning calorimeter (DSC-4000, Perkin-Elmer, USA). The samples were hermetically sealed in an aluminum pan and heated from 30 to 300°C with a nitrogen flow of 20 ml/min at a scan rate of 10°C/min.

6. Rheological studies

The rheological experiments were conducted in a Modular Compact Rheometer (Anton Parr MCR 102, Austria). Throughout the study, standard 1° cone geometry (CP-40) of 40 mm in diameter was used. Each experiment was conducted using 5% (w/v) matrices of CMAP and CCMAP at 25°C. Acidic solution (pH 1.2) and buffer solution (pH 6.7) were used to prepare the polymeric matrices for both polymers. At variable shear rates, the shear viscosity of samples was determined in the dynamic rotational mode. The oscillatory mode was used to study the amplitude sweep and frequency sweep of the polymers against their loss and storage moduli (G' and

G''). At a fixed angular frequency, the amplitude sweep was carried out with varying strains to induce structural deformation in the entangled polymer, while the frequency sweep was used to study the variation of G' and G'' with variable angular frequencies by using a predetermined strain (%) under linear viscoelastic (LVE) regime from the amplitude sweep.

7. Drug-polymer FTIR compatibility study

The FTIR spectra of MET, powdered tablet containing CMAP, and CCMAP were recorded using an FTIR spectrophotometer (Perkin Elmer, RX-1, UK) using the KBr pellet technique. The spectra were taken in the wave number region of 4000 - 400 cm^{-1} .

8. Preparation of matrix tablet

Several ingredients were passed through a #60 mesh BS screen, including powdered CMAP and lactose and microcrystalline cellulose (MCC). The drug was then thoroughly mixed with the polymer and the other ingredients in the weight proportions indicated in Table 1. It was then converted into a moist cohesive mass by adding a sufficient amount of water. After this, the cohesive mass was passed through a #16 mesh BS screen, and the resulting granules were dried in a tray dryer at 60°C until the moisture content reached 2-3% w/w. After passing the dried granules through the #20 mesh BS screen, magnesium stearate (2% w/w) was used to lubricate the blend, and the lubricated blend was then compressed into tablets on a single punch tablet machine using 19.5 mm concave-face oval-shaped tooling (RIMEK, Karanavati Engineering Ltd., Gujarat, India). In the same manner, MET containing CCMAP tablets were prepared.

Table 1: Matrix tablet Formulations

Sl no.	Ingredients per tablet (mg)	F1	F2	F3	F4	F5	F6	F7	F8	F9	F10
1	MET	250	250	250	250	250	250	250	250	250	250
2	CMAP	300	400	500	600	700	-	-	-	-	-
3	CCMAP	-	-	-	-	-	300	400	500	600	700
4	Lactose anhydrous	450	350	250	150	100	450	350	250	150	100
5	MCC	80	80	80	80	30	80	80	80	80	30
6	Purified water	qs	qs	qs	qs	qs	qs	qs	qs	qs	qs
7	Magnesium stearate	20	20	20	20	20	20	20	20	20	20

*qs indicate quantity sufficient

9. Swelling study

The swelling study of blank (placebo) CMAP and CCMAP matrix tablets was conducted in water, acid solution (pH 1.2) and buffer solution (pH 7.4) using USP II tablet dissolution test apparatus (model TDP-06P, Electrolab, India) at $37 \pm 0.5^\circ\text{C}$. As a buffer solution, 700 ml HCl solution with pH 1.2 was mixed with 200 ml 0.2 (M) trisodium orthophosphate dodecahydrate [25] as the media. In a stainless steel wire mesh basket, a matrix tablet was placed and weighed (Precisa, XB 600 M-C, Switzerland, readability 0.0001 g). Following that, the matrix basket was immersed in 900 ml of the test medium at $37 \pm 0.5^\circ\text{C}$ and stirred at 100 rpm. After a predetermined period of time, the basket containing the hydrated matrix tablet was carefully removed, excess water was blotted, and a new weight was taken. Percentage swelling of the tablets was determined using the following relationship [26]:

$$\% \text{ Swelling} = \left[\frac{(W_2 - W_1)}{W_1} \times 100 \right] (2)$$

Where, W_1 represents initial weight of the tablet at time 0 and W_2 is the weight of the tablet at time t after immersion in test medium.

10. Physical characteristics of tablet

A. Weight variation test

In order to determine the weight variation of each formulation, 20 tablets were weighed using an electronic balance (Precisa, XB600 M-C, Switzerland, readability 0.0001 g). According to official procedures, the individual weights of the tablets were compared with the average weights of the tablets [27].

B. Hardness, Thickness and Friability

In each formulation, 10 tablets were randomly taken to examine for hardness and dimension analysis.

The tablet hardness was determined using a pre-calibrated Monsanto hardness tester (Cadmach, Ahmedabad, India). A calibrated digital caliper was used to determine the physical dimensions of the tablets (length, breadth and thickness).

The Roche friabilator (Campbell Electronics, Mumbai, India) was used to test the friability of 20 tablets from each formulation. The friabilator was rotated at 25 rpm for 4 minutes; dedusted tablets were reweighed to determine percentage of weight loss.

C. Drug content of tablet

A total of 20 tablets were weighed and crushed into a fine powder. The powder containing about 0.1 grams of Metformin hydrochloride was accurately weighed and shaken with 70 ml of water for 15 minutes then diluted to 100 ml with water and filtered. The filtrate (10 ml) was diluted to 100 ml by adding water and then 10 ml from this dilution was further diluted to 100 ml by adding water. A double beam spectrophotometer (Shimadzu, UV, 2450, Japan) was used to measure the absorbance of the resulting solution (0.01 mg/ml). The content of $\text{C}_4\text{H}_{11}\text{N}_5$, HCl was calculated, taking 798 as the specific absorbance at 232 nm [28].

11. In-vitro drug release study

The matrix tablets were tested for drug release in acid solution (pH 1.2) and phosphate buffer solution (pH 6.8) using the USP II tablet dissolution rate test apparatus (Electrolab, TDP-06P, India). At $37 \pm 0.5^\circ\text{C}$ and 100 rpm, a tablet was immersed in 750 ml of 0.1M hydrochloric acid solution kept in a dissolution vessel. Each aliquot was removed and replenished with fresh medium, kept at $37 \pm 0.5^\circ\text{C}$, at predetermined intervals. Following the operation in the acid environment for two hours, 250 ml of 0.2M trisodium phosphate dodecahydrate solution (previously kept at $37 \pm 0.5^\circ\text{C}$) was added. After adjusting the pH (6.8 ± 0.05) of the medium with 2M sodium hydroxide solution, the dissolution process was conducted for 12 hours. After filtration and suitable dilution, the aliquots were spectrophotometrically analyzed. The measurement of drug release was made at the wavelength of the highest absorbance (λ_{max}) in the respective medium. Analysis of MET was performed at 232 nm and 230 nm in acid and buffer solutions, respectively.

III. RESULTS AND DISCUSSION

Extent of carboxymethylation

NAP is made up of a linear chain of - (1 \rightarrow 3)- β -D-galactopyranose units with some - (1 \rightarrow 6)- β -D-galactopyranose units, and some - (1 \rightarrow 3)-L-arabinofuranose units [9]. The conversion of NAP to CMAP involves the replacement of numerous hydroxyl groups (-OH) groups with O-carboxymethyl groups (-OCH₂-COO⁻H⁺). Sodium hydroxide dehydrates the hydroxyl groups in NAP by formation of alkoxides during the reaction. The average number of substituted

carboxymethyl groups per anhydro sugar unit is assigned by DS [14]. It was found that the degree of substitution for this reaction was 0.51.

Figure 1 illustrates the possible structures of CMAP and CCMAP.

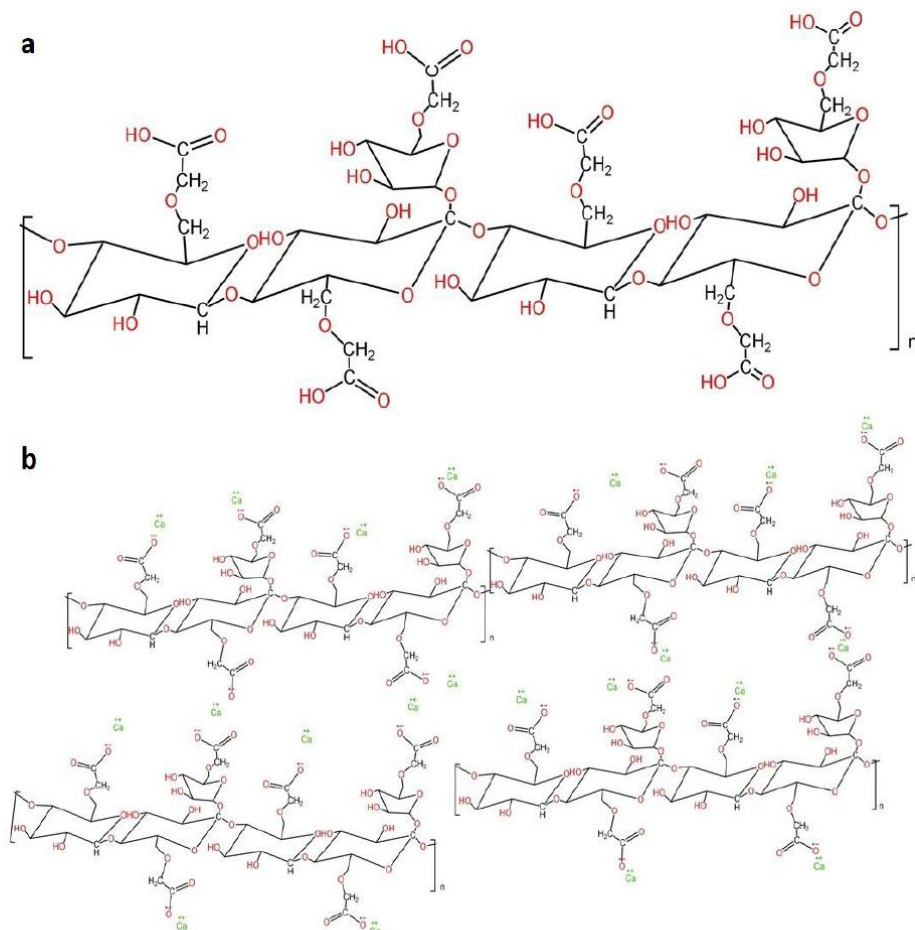


Figure 1: Structure of (a) CMAP, (b) CCMAP.

FTIR spectrum analysis of CMAP and CCMAP

A Fourier transform IR spectrum of CMAP and CCMAP is illustrated in Figure 2. According to Figure 2, The FT-IR spectra of CMAP and CCMAP did not exhibit significant differences in the positions of bands; however, the intensity was different. Based on Figure 2a, CMAP displayed bands of absorption at 2921, 2364.66, 1579.18, 1620, 1457.55, 1420.44, 1315.3 and 1028.74 cm⁻¹, which are representative bands for

carbohydrates [29] while the absorption bands of CCMAP, were found to be at 2888.3, 2356.41, 1577.12, 1457.56, 1418.38, 1319.42, 1018.43 cm⁻¹ (Figure 2b). Thus, other than the nominal shifts in the positions of the bands in both polymers, no significant changes were observed. Due to O—H stretching of the hydroxyl groups, a band appeared to be broadened between 3600-3200 cm⁻¹ for both polymers (Figure 2a and 2b) [30]. In the case of CCMAP, the band for O—H stretching (Figure

1b) was found to be more intense than CMAP due to crosslinked with Ca^{+2} ions [31]. The absorption bands at 2921 cm^{-1} and 2888.3 cm^{-1} were due to the vibrations of C—H stretching. The presence of carboxyl groups (—COO) is indicated by the appearance of the characteristic band around $1610\text{--}1370\text{ cm}^{-1}$ [32]. The bending vibration of the

hydroxyl group (O—H) was observed at 1457 cm^{-1} . The band around $1420\text{--}1418\text{ cm}^{-1}$ was attributed to C=O stretching of acid. Since the scissoring of methyl groups (—CH₂), bands were detected at 1315 and 1319 cm^{-1} . Several bands were detected at 1018 cm^{-1} and 1020 cm^{-1} as the stretching frequency of >CH—O—CH.

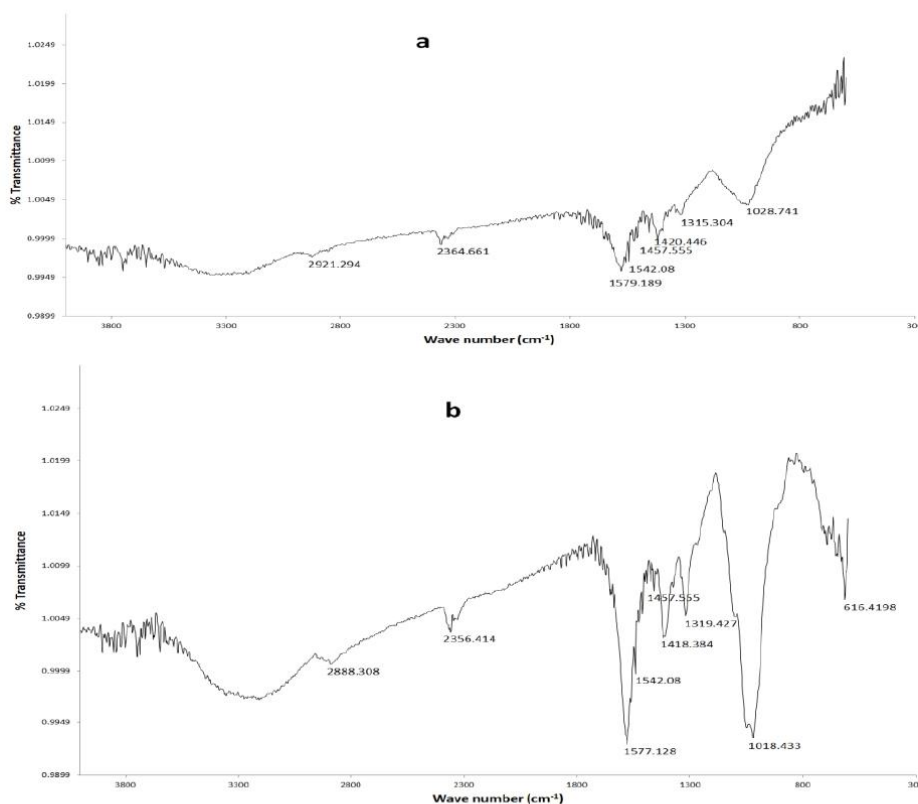


Figure 2: FTIR spectra (a) CMAP, (b) CCMAP.

Differential Scanning Calorimetry (DSC) study

Figure 3 depicts the superimposed plot of diversified DSC thermograms of CMAP and CCMAP. The results indicate that an exothermic event of CMAP occurred at 55.31°C with a heat flow of 20.50 mW . However, the exothermic event of CCMAP shifted at 57.98°C , 21.06 mW . Based on the DSC profiles of both polymers, each showed

an endothermic peak. While CMAP displayed a melting peak at around 261.39°C with a heat flow of 8.57 mW , CCMAP showed its melting peak at around 268.7°C with a heat flow of 8.76 mW . Therefore, there was a shift in the melting peak of CCMAP compared to CMAP. In this regard, CCMAP displayed greater thermal stability than CMAP due to the ionic crosslinking [33].

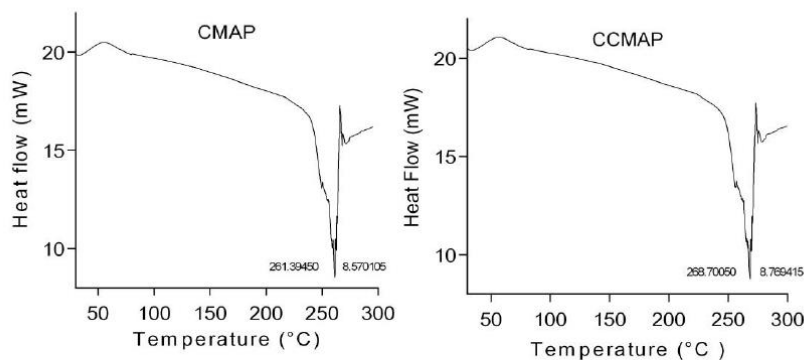


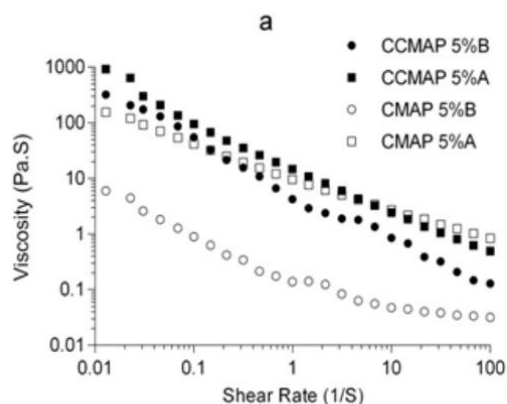
Figure 3: DSC thermograms (a) CMAP, (b) CCMAP.

Rheological studies

The flow curve of CMAP and CCMAP is shown in Figure 4a. The flow curves indicate that the viscosity of the CCMAP matrix at pH 1.2 is greater than the viscosity at neutral pH. Similarly, the viscosity of CMAP at pH 1.2 was higher than the viscosity at pH 6.8. However, when comparing the viscosity profiles of CCMAP and CMAP, it was found that CCMAP was always higher than CMAP. Additionally, both polymers displayed non-Newtonian behavior with the pseudo-plastic flow. The carboxymethyl groups in CMAP matrices are ionized and induce electrostatic

repulsion, resulting in polymer disentanglements and viscosity decline[34]. The ionization of carboxymethyl groups was more pronounced at pH 6.8 in comparison to acidic pH.

Due to the crosslinking, the Ca^{++} ions reacted with carboxylic groups and formed CCMAP ($-\text{OCH}_2\text{COO}^- \text{Ca}^{2+} \text{OCH}_2\text{CO}-$)[35]. Thus, Crosslinked polymer chains are prevented from moving and coulombic repulsion between them gets restricted. Therefore, CCMAP chains became highly disentangled and exhibited high viscosity, resulting in the formation of viscoelastic gels.



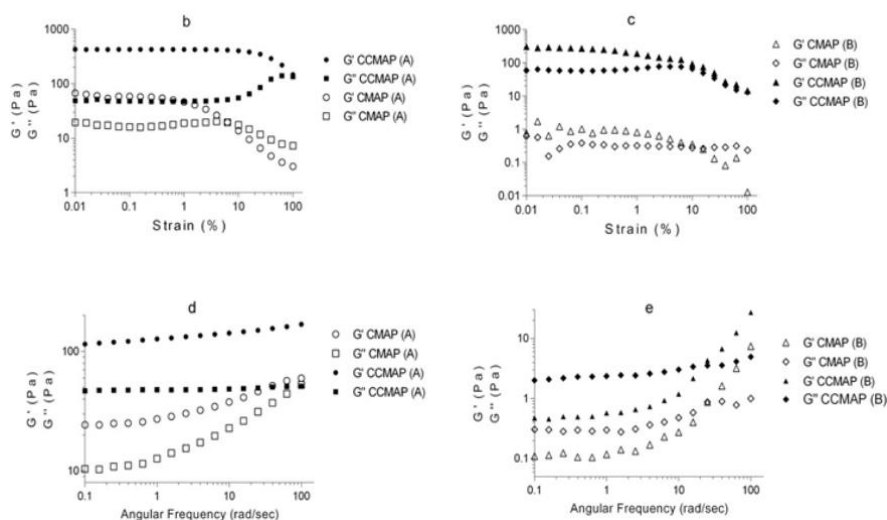


Figure 4:(a) Flow curves : CMAP at pH 1.2 (□), at pH 6.8 (○); CCMAP at pH 1.2 (■), at pH 6.8 (●); (b) Amplitude sweep at pH 1.2: CMAP G' (○), G'' (□); CCMAP G' (●), G'' (■); (c) Amplitude sweep at pH 6.8: CMAP G' (△), G'' (◇); CCMAP G' (▲), G'' (◆); (d) Frequency sweep at pH 1.2 : CMAP G' (○), G'' (□); CCMAP G' (●), G'' (■); (e) Frequency sweep at pH 6.8 : CMAP G' (△), G'' (◇); CCMAP G' (▲), G'' (◆).

Both polymers exhibit amplitude sweep curves illustrated in Figure 4b (at pH 1.2) and 4c (at pH 6.8). As a result of linear viscoelasticity, the linear viscoelastic region (LVE) corresponds to the stress varying linearly with strain for the sample under study [36]. The storage modulus G' (Pa) as an elastic response [37] and the loss modulus G'' (Pa) as a viscous response of both polymers were varied with variable strain (%) during the amplitude of the deformation. Initially, the polymers will maintain their structural integrity within the LVE, but after a critical strain (%) the structural deformations will begin as the declination of G' exceeds the LVE. Figure 4b indicates that in acidic pH, CCMAP had a critical strain of 2.5%, while CMAP had a critical strain of 0.3%. Crosslinking prevented CCMAP from being ionized, resulting in higher mechanical strength than CMAP. Additionally, CMAP had shorter LVE than CCMAP. However, the critical strain of CCMAP at pH 6.8 was found to be 0.4% while CMAP had 0.1%. It was also observed that the LVE in CCMAP at pH 6.8 became significantly shorter than at pH 1.2. In contrast, the LVE of CMAP at pH 6.8 became more unstable and showed irregular patterns.

As the frequency sweep was performed, the measured critical strain (%) was kept constant within the LVE while the angular frequency (rad/sec) was varied. According to the frequency sweep curves presented in Figure 4d and 4e, CCMAP had higher G' values than CMAP at pH 1.2 and 6.8. However, both polymers have a higher G' value than G'' ($G' > G''$). There was a larger difference between G' and G'' without crossing each other, indicating a higher degree of rheological stability for CCMAP matrices at pH 1.2 as compared to CCMAP matrices at pH 6.8 [38]. The higher values of G' over the G'' ($G' > G''$) indicate a visco-elastic structure of CCMAP [39]. The high degree of entanglement in CCMAP matrices resulted in a strong gel structure as a result of cross-linking. Conversely, CMAP matrices were found to have weak gel structures as compared to CCMAP matrices. At pH 6.8, both polymers showed crossover points (CMAP at 25.1 rad/sec, $G' = G'' = 0.873$, CCMAP at 25.1 rad/sec, $G' = G'' = 3.378$) that indicate structural deformation [40]. Additionally, the CMAP matrices at pH 1.2 exhibited a weak gel-like structure that lost their elastic energy at pH 6.8 and formed disentangled structure. It is the result of the ionization of

functional groups ($-\text{OCH}_2\text{COO}^- \text{H}^+$) of CMAP which leads to electrostatic repulsion, resulting in a decrease in entanglements[41, 42].

Drug-polymer FTIR compatibility study

The FTIR spectra of the drug and the drug-polymer mixture are shown in Figure 5a and b. As a fingerprint of Metformin, the FTIR spectrum (Figure 5a) showed characteristic absorption bands at 3371, 3392, 3176, 1622, 1568, 1167 and 1063 cm^{-1} wavenumbers[43]. The absorption bands of MET appeared at 3371, 3392 and 3176 cm^{-1} for the amine N—H stretching vibrations. As N—H bonds (in amines) are weaker

in polarity than O—H bonds, their absorption bands are less intense and less broad than O—H bands. MET exhibited characteristic bands at 1622 and 1568 cm^{-1} for C—N and C=N respectively. However, the absorption bands at 1620-1580 cm^{-1} are also responsible for N—H bending. In addition, the absorption bands at 1167 and 1063 cm^{-1} were due to C—N stretching. The band at 1475 cm^{-1} wavenumber was due to C—H bending. All of the characteristic bands of the drug were found almost at the same wavelength in the FTIR spectrum obtained from the MET-polymer mixtures (Figure 5b).

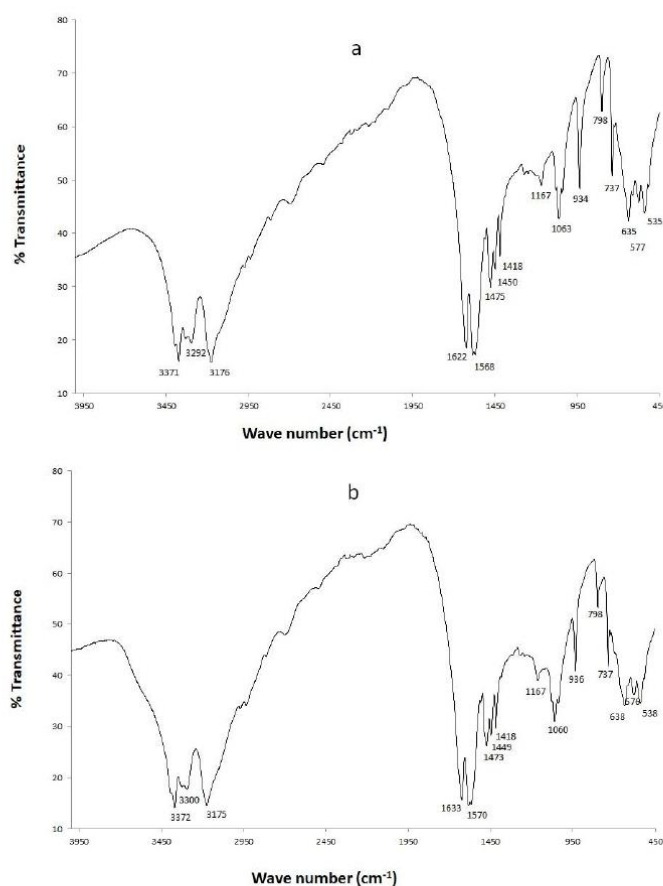


Figure 5: FTIR spectrum (a) Metformin, (b) Metformin-polymer mixture.

Swelling study

Figure 6a and b illustrate the swelling profiles of CMAP and CCMAP matrices in acidic (pH 1.2) and buffer (pH 6.4) media. In acid media, the % of swelling of blank CMAP tablets was considerably less than in buffer media.

However, CMAP tablets in both media exhibited a rapid and greater swelling than blank CCMAP tablets. The calcium crosslinking results in low water penetration velocity and high entanglement in CCMAP matrices, resulting in reduced swelling as compared to CMAP matrix.

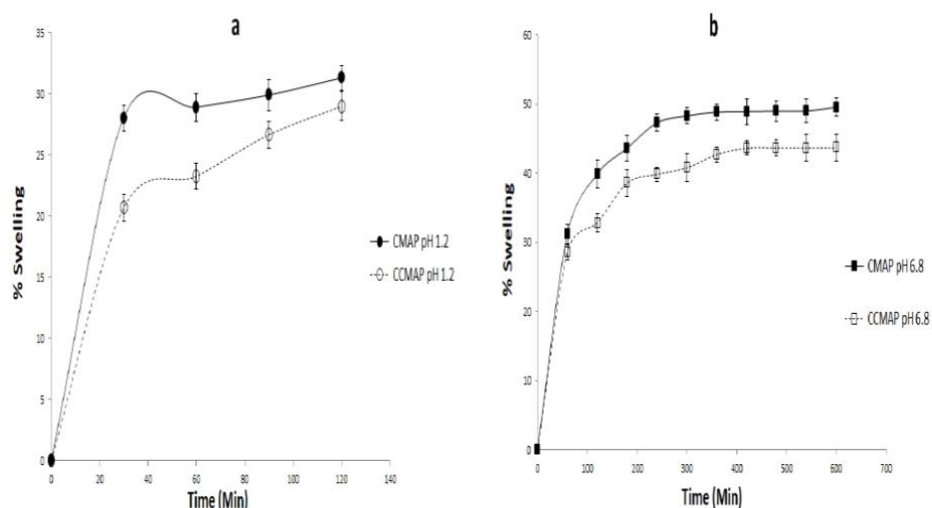


Figure 6: Swelling profiles (a) At pH 1.2: CMAP (●), CCMAP (○); (b) At pH 6.8: CMAP (■), CCMAP (◻).

Physical characteristics of tablet

The physical characteristics of the tablets were within acceptable limits. A comparison of all

the physical characteristics of the tablets of each formulation is presented in Table 2.

Table 2: Physical evaluation of formulated batches of matrix tablet

Formulation code	Average weight (mg) (N=20)	Hardness (Newton/cm ²) (N=10) *	Average thickness (mm) (N=10) *	Average length (mm) (N=10) *	Average breadth (mm) (N=10) *	Friability (%) (N=20) *	Drug content (%) (N=20)
F1	1117.2 ± 2.25%	56.87 ± 0.06	6.1 ± 0.02	19.49 ± 0.011	9.00 ± 0.013	0.67 ± 0.026	99.08 ± 0.16
F2	1114.6 ± 1.23%	59.82 ± 0.021	5.89 ± 0.01	19.49 ± 0.009	8.99 ± 0.021	0.63 ± 0.047	99.13 ± 0.21
F3	1108.2 ± 2.06%	61.58 ± 0.028	5.92 ± 0.012	19.42 ± 0.014	9.01 ± 0.017	0.53 ± 0.016	101.03 ± 0.18
F4	1113.04 ± 4.02%	60.11 ± 0.047	5.96 ± 0.023	19.45 ± 0.011	9.02 ± 0.012	0.57 ± 0.031	98.98 ± 0.24

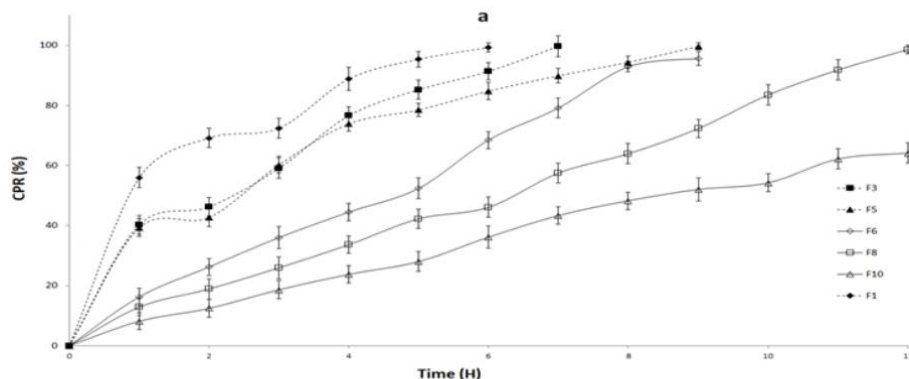
F5	1119.2 ± 2.08%	67.27 ± 0.032	5.99 ± 0.011	19.50 ± 0.01	9.02 ± 0.01	0.48 ± 0.018	99.01 ± 0.19
F6	1122.03 ± 1.04%	64.13 ± 0.016	6.2 ± 0.014	19.49 ± 0.017	8.99 ± 0.023	0.51 ± 0.033	100.05 ± 0.23
F7	1119.25 ± 2.15%	69.13 ± 0.023	5.98 ± 0.022	19.46 ± 0.013	9.01 ± 0.016	0.35 ± 0.023	99.69 ± 0.22
F8	1121.03 ± 1.29%	68.05 ± 0.051	5.99 ± 0.09	19.48 ± 0.018	9.00 ± 0.023	0.39 ± 0.014	99.16 ± 0.2
F9	1121.16 ± 1.47%	70.31 ± 0.043	6.1 ± 0.023	19.48 ± 0.012	9.03 ± 0.013	0.23 ± 0.021	99.33 ± 0.16
F10	1123.05 ± 1.07%	70.01 ± 0.049	5.99 ± 0.013	19.49 ± 0.011	9.00 ± 0.020	0.26 ± 0.03	99.43 ± 0.22

* N= number of tablets tested; Mean ± SD (n=3)

In-vitro drug release study

Based on the standard calibration curve of MET, the coefficient of correlation (R^2) was obtained and the amount of drug dissolved in each sample was determined. The in-vitro drug release profiles of MET (250 mg) from tablets containing CMAP and CCMAP in each formulation are presented in Figure 7a and b. Based on the entire drug release profiles, CCMAP formulations exhibited prolonged release and became more sustained with increasing polymer concentrations. Conversely, the CMAP formulations exhibited a rapid momentaneous drug release profile. The maximum amount of MET released from the CMAP matrices was 249.25 mg (99.7%) within 9 hours (F5), while CCMAP matrices released 246.6 mg (98.64%) upto 11 hours. The Ca^{++} crosslinking restricted the permeation of water influx into the

CCMAP matrices, reduced swelling and promoted the formation of the viscoelastic gel layer. Consequently, these factors contributed to a slower release of drugs. In CMAP matrices, the electrostatic repulsion between the polymeric chains enhanced the mobility, de-coiled structure and weak gel networks lost their structural integrity assisted rapid deformation. Consequently, they permeated water uptake, leading to higher swelling and accelerated drug release. For CMAP and CCMAP tablets, the AUC values for MET released are presented in Table 3. The drug release data were analyzed for two-way ANOVA to determine the significant difference in drug release between different formulations. According to the ANOVA table shown in Table 4 the differences between the drug releases from the two matrices were statistically significant ($P < 0.0001$).



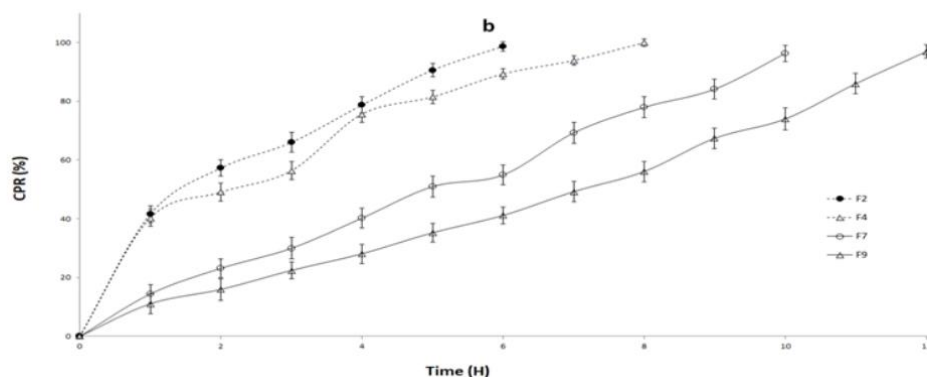


Figure 7: Drug release profiles of MET from CMAP (—) and CCMAP (□) matrix tablets. (a) CMAP formulations: F1 (♦), F3 (■), F5 (▲); CCMAP formulations: F6 (◇), F8 (□), F10 (Δ); (b) CMAP formulations: F2 (●), F4 (△); CCMAP formulations: F7 (○), F9 (Δ).

Table 3: AUC of drug release

Media	Formulations									
	AUC of drug release from CMAP matrix (% mg hrs)					AUC of drug release from CCMAP matrix (% mg hrs)				
	F1	F2	F3	F4	F5	F6	F7	F8	F9	F10
At pH 1.2	226.475 ± 3.6	175.6083 ± 2.6	158.4708 ± 4.2	162.0625 ± 3.6	151.4958 ± 4.8	73.42918 ± 3.2	64.93334 ± 4.2	55.80418 ± 2.9	47.62499 ± 3.5	35.93333 ± 3.7
At pH 6.8	1078.963 ± 4.1	958.5917 ± 4.7	1121.871 ± 3.2	1339.796± 2.9	1533.942 ± 4.4	1159.783 ± 4.2	1232.313 ± 3.7	1495.604± 2.4	1337.525 ± 4.6	1048.558 ± 4.4

* Mean ± SD, n=3

Table 4: Two-way ANOVA table

Two-way ANOVA						
Alpha	0.05					
Source of Variation	% of total variation	P value	P value summary	Significant?		
Row Factor	28.91	<0.0001	****	Yes		
Column Factor	2.679	0.892	ns	No		
ANOVA table	SS	DF	MS	F (DFn, DFd)	P value	
Row Factor	46569	12	3881	F (12, 108) = 3.803	P < 0.0001	
Column Factor	4315	9	479.4	F (9, 108) = 0.4699	P = 0.8920	
Residual	110194	108	1020			
Number of missing values	0					

The drug release data was analyzed using several kinetic models, including zero-order, first-order, Higuchi, and Korsmeyer-Peppas. In accordance with the obtained results, the release mechanism of different formulations has been determined based on the best fit in several models, as shown in Table 5. Based on the linear regression analysis, the coefficient of correlation coefficient (R^2) indicated that the drug release from CMAP

formulations was diffusion controlled and followed the Higuchi model. However, CMAP followed zero order kinetics (F6 to F9) except for F10 which followed Korsmeyer-Peppas model. As the formulation F10 showed a diffusion exponent of 0.877, it indicates the Anomalous (non-Fickian) diffusion, which implies that the drug was released by both diffusion-controlled and swelling-controlled mechanisms [44].

Table 5: Formulation-specific release kinetics data

Kinetic model	R ² of Formulations									
	F1	F2	F3	F4	F5	F6	F7	F8	F9	F10
zero order	0.965	0.993	0.974	0.968	0.946	0.991	0.996	0.996	0.986	0.991
1-st order	0.948	0.962	0.953	0.934	0.889	0.95	0.944	0.949	0.966	0.91
Korsmeyer-Peppas	0.965	0.993	0.958	0.97	0.96	0.989	0.991	0.987	0.978	0.993
Higuchi	0.97	0.993	0.978	0.978	0.975	0.964	0.968	0.958	0.932	0.979

IV. CONCLUSION

The study revealed a decrease in the magnitude of viscosity of CMAP matrices attributed to electrostatic repulsion between carboxymethyl groups caused by the ionization of CMAP. However, cross-linking of O-carboxymethylated procera gum by Ca²⁺ ions contributed to the formation of entangled structures and high viscoelasticity. The enhanced viscoelastic properties of the CMAP matrix counteracted the matrix deformation. Eventually, the high viscoelastic CMAP matrices formed a strong gel layer around the tablet surface which confined water ingress leading to less swelling. Thus the CMAP tablets provided sustained drug release by controlling the diffusion rate of the drug molecules. Therefore a chemically modified and ionically cross-linked polymer can affect the rheological parameters of the polymer matrix. It is also possible to achieve a specific drug release rate, duration, and mechanism from the flexibility of polymers.

CONFLICT OF INTEREST

In relation to this manuscript, all authors declare that there is no conflict of interest.

ACKNOWLEDGEMENTS

It is our pleasure to express our gratitude to the Head of the Department of Pharmaceutical Technology at Jadavpur University.

REFERENCES

- [1] Sujja-Areevath J, Munday DL, Cox PJ, Khan KA. Relationship between swelling, erosion and drug release in hydrophilic natural gum mini-matrix formulations. *European journal of pharmaceutical sciences*. 1998 Jul 1;6(3):207-17.
- [2] Roy DS, Rohera BD. Comparative evaluation of rate of hydration and matrix erosion of HEC and HPC and study of drug release from their matrices. *European Journal of Pharmaceutical Sciences*. 2002 Aug 1;16(3):193-9.
- [3] Zuleger S, Lippold BC. Polymer particle erosion controlling drug release. I. Factors influencing drug release and characterization of the release mechanism. *International Journal of Pharmaceutics*. 2001 Apr 17;217(1-2):139-52.
- [4] Mughal MA, Iqbal Z, Neau SH. Guar gum, xanthan gum, and HPMC can define release mechanisms and sustain release of propranolol hydrochloride. *AapsPharmSciTech*. 2011 Mar;12:77-87.
- [5] Munday DL, Cox PJ. Compressed xanthan and karaya gum matrices: hydration, erosion and drug release mechanisms. *International Journal of Pharmaceutics*. 2000 Aug 1;203(1-2):179-92.
- [6] Sriamornsak P, Thirawong N, Weerapol Y, Nunthanid J, Sungthongjeen S. Swelling and erosion of pectin matrix tablets and their impact on drug release behavior. *European*

- journal of pharmaceuticals and biopharmaceutics. 2007 Aug 1;67(1):211-9.
- [7] Vyas SP, Khar RK. Controlled drug delivery concepts and advances. vallabhprakashan. 2002;1:411-7.
- [8] Prajapati VD, Jani GK, Moradiya NG, Randeria NP. Pharmaceutical applications of various natural gums, mucilages and their modified forms. Carbohydrate polymers. 2013 Feb 15;92(2):1685-99.
- [9] Pachua L, Lahlennawia H, Mazumder B. Characteristics and composition of Albiziaprocera (Roxb.) Benth gum. Industrial Crops and Products. 2012 Nov 1;40:90-5.
- [10] Zhang J, Akihisa T, Kurita M, Kikuchi T, Zhu WF, Ye F, Dong ZH, Liu WY, Feng F, Xu J. Melanogenesis-inhibitory and cytotoxic activities of triterpene glycoside constituents from the bark of Albiziaprocera. Journal of natural products. 2018 Dec 6;81(12):2612-20.
- [11] Avachat AM, Dash RR, Shrotriya SN. Recent investigations of plant based natural gums, mucilages and resins in novel drug delivery systems. Ind J Pharm Edu Res. 2011 Jan;45(1):86-99.
- [12] De Paula RCM, Santana SA, Rodrigues JF. Composition and rheological properties of Albizialebeck gum exudates. Carbohydr. Polym. 2001; 44:133-139.
- [13] De Pinto, Leon G, Martinez M, Beltran O, Rincon F, Clamens C, Igartuburu JM, Guerrero R, Vera A. Characterization of polysaccharides isolated from gums of two Venezuelan specimens of Albizianiopoides var. colombiana. Ciencia. 2002;19: 382-387.
- [14] Chakravorty A, Barman G, Mukherjee S, Sa B. Effect of carboxymethylation on rheological and drug release characteristics of locust bean gum matrix tablets. Carbohydrate polymers. 2016 Jun 25;144:50-8..
- [15] Barai BK, Singhal RS, Kulkarni PR. Optimization of a process for preparing carboxymethyl cellulose from water hyacinth (Eichhorniacrassipes). Carbohydrate Polymers. 1997 Mar 1;32(3-4):229-31..
- [16] Singh R, Maity S, Sa B. Effect of ionic crosslink on the release of metronidazole from partially carboxymethylated guar gum tablet. Carbohydrate polymers. 2014 Jun 15;106:414-21.
- [17] Wang JZ, Ding ZQ, Zhang F, Ye WB. Recent development in cell encapsulations and their therapeutic applications. Materials Science and Engineering: C. 2017 Aug 1;77:1247-60.
- [18] Shilpa A, Agrawal SS, Ray AR. Controlled delivery of drugs from alginate matrix. Journal of Macromolecular Science, Part C: Polymer Reviews. 2003 Jan 6;43(2):187-221.
- [19] Gupta PK, Bhandari N, Shah H, Khanchandani V, Keerthana R, Nagarajan V, Hiremath L. An update on nanoemulsions using nanosized liquid in liquid colloidal systems. Nanoemulsions-Properties, Fabrications and Applications. 2019 Mar 29;1(1):1-4.
- [20] Shaker DS, Ishak RA, Ghoneim A, Elhuoni MA. Nanoemulsion: A review on mechanisms for the transdermal delivery of hydrophobic and hydrophilic drugs. Scientia Pharmaceutica. 2019;87(3):17.
- [21] Dodi G, Hritcu D, Popa MI. Carboxymethylation of guar gum: synthesis and characterization. Cellulose chemistry and Technology. 2011 Mar 1;45(3):171
- [22] Toğrul H, Arslan N. Production of carboxymethyl cellulose from sugar beet pulp cellulose and rheological behaviour of carboxymethyl cellulose. Carbohydrate Polymers. 2003 Oct 1;54(1):73-82.
- [23] Hongbo T, Yanping L, Min S, Xiguang W. Preparation and property of crosslinking guar gum. Polymer journal. 2012 Mar;44(3):211-6.
- [24] Huang Y, Yu H, Xiao C. Effects of Ca²⁺ crosslinking on structure and properties of waterborne polyurethane-carboxymethylated guar gum films. Carbohydrate Polymers. 2006 Nov 23;66(4):500-13.
- [25] Indian Pharmacopoeia, vol. I, The Indian Pharmacopoeia Commission, Government of India, Ghaziabad, 2010
- [26] Sriamornsak, P., Thirawong, N., Weerapol, Y., Nunthanid, J., & Sungthongjeen, S.(2007). Swelling and erosion of pectin matrix tablets and their impact on drug release behavior. European Journal of Pharmaceutics and Biopharmaceutics, 67,211-219.
- [27] Indian Pharmacopoeia, vol. II, controller of publications, Delhi (2018), pp. 1143-1144

- [28] Pharmacopoeia I, Volume II. Published by the controller of Publication. Vol. I, New Delhi. 2007;655.
- [29] Yuen SN, Choi SM, Phillips DL, Ma CY. Raman and FTIR spectroscopic study of carboxymethylated non-starch polysaccharides. Food chemistry. 2009 Jun 1;114(3):1091-8.
- [30] Sadalage PS, Pawar KD. Production of microcrystalline cellulose and bacterial nanocellulose through biological valorization of lignocellulosic biomass wastes. Journal of Cleaner Production. 2021 Dec 10;327:129462.
- [31] Dagar, V., Pahwa, R. and Ahuja, M., 2022. Preparation and Characterization of Calcium Cross-Linked Carboxymethyl Tamarind Kernel Polysaccharide as Release Retardant Polymer in Matrix. Biointerface Res. Appl. Chem, 13, p.111.
- [32] Aguir C, M'Henni MF. Experimental study on carboxymethylation of cellulose extracted from Posidonia oceanica. Journal of applied polymer science. 2006 Feb 15;99(4):1808-16.
- [33] Hongbo T, Yanping L, Min S, Xiguang W. Preparation and property of crosslinking guar gum. Polymer journal. 2012 Mar;44(3):211-6.
- [34] Maiti S, Ray S, Mandal B, Sarkar S, Sa B. Carboxymethyl xanthan microparticles as a carrier for protein delivery. Journal of microencapsulation. 2007 Jan 1;24(8):743-56.
- [35] Huang Y, Yu H, Xiao C. Effects of Ca²⁺ crosslinking on structure and properties of waterborne polyurethane-carboxymethylated guar gum films. Carbohydrate Polymers. 2006 Nov 23;66(4):500-13.
- [36] Kaboorani A, Blanchet P. Determining the linear viscoelastic region of sugar maple wood by dynamic mechanical analysis. BioResources. 2014 Jun 5;9(3):4392-409.
- [37] Talens P, Castells ML, Verdú S, Barat JM, Grau R. Flow, viscoelastic and masticatory properties of tailor made thickened pea cream for people with swallowing problems. Journal of Food Engineering. 2021 Mar 1;292:110265.
- [38] Xiao F, Chen M, Wu S, Amirkhani SN. A long-term ultraviolet aging effect on rheology of WMA binders. Int. J. Pavement Res. Technol. 2013 Sep 1;6(5):496-504.
- [39] Li C, Liu C, Liu J, Fang L. Correlation between rheological properties, in vitro release, and percutaneous permeation of tetrahydropalmatine. AapsPharmscitech. 2011 Sep;12:1002-10.
- [40] Rasid IM, Do C, Holten-Andersen N, Olsen BD. Effect of sticker clustering on the dynamics of associative networks. Soft Matter. 2021;17(39):8960-72.
- [41] Medina-Torres L, Brito-De La Fuente E, Torrestiana-Sanchez B, Katthain R. Rheological properties of the mucilage gum (Opuntia ficus indica). Food hydrocolloids. 2000 Sep 1;14(5):417-24.
- [42] Yan X, Xiao X, Au C, Mathur S, Huang L, Wang Y, Zhang Z, Zhu Z, Kipper MJ, Tang J, Chen J. Electrospinning nanofibers and nanomembranes for oil/water separation. Journal of Materials Chemistry A. 2021;9(38):21659-84.
- [43] Smaeel SA, Al-Bayati YK. Determination of trace metformin in pharmaceutical preparation using molecularly imprinted polymer based pvc-membrane. Eurasian Chem. Commun. 2021; 3:812-30.
- [44] Arora G, Malik K, Singh I, Arora S, Rana V. Formulation and evaluation of controlled release matrix mucoadhesive tablets of domperidone using Salvia plebeian gum. Journal of advanced pharmaceutical technology & research. 2011 Jul;2(3):163.

Regular Article

Exploring the Effectiveness of Carboxymethylated and Crosslinked *Albizia procera* Gum in Diltiazem Hydrochloride Matrix Tablets: A Comparative Analysis

Sudipta Mukherjee* and Jasmina Khanam

Department of Pharmaceutical Technology, Jadavpur University, Kolkata 700032, West Bengal, India.

Received September 21, 2023; accepted March 3, 2024; advance publication released online April 19, 2024

This study investigates the efficacy of modified *Albizia procera* gum as a release-retardant polymer in Diltiazem hydrochloride (DIL) matrix tablets. Carboxymethylated *Albizia procera* gum (CAP) and ionically crosslinked carboxymethylated *Albizia procera* gum (Ca-CAP) were utilized, with Ca-CAP synthesized via crosslinking CAP with calcium ions (Ca^{2+}) using calcium chloride (CaCl_2). Fourier Transform (FT) IR analysis affirmed polymer compatibility, while differential scanning calorimetry (DSC) and X-ray diffraction (XRD) assessed thermal behavior and crystallinity, respectively. Zeta potential analysis explored surface charge and electrostatic interactions, while rheology examined flow and viscoelastic properties. Swelling and erosion kinetics provided insights into water penetration and stability. CAP's carboxymethyl groups ($-\text{CH}_2-\text{COO}^-$) heightened divalent cation reactivity, and crosslinking with CaCl_2 produced Ca-CAP through $-\text{CH}_2-\text{COO}^-$ and Ca^{2+} interactions. Structural similarities between the polymers were revealed by FTIR, with slight differences. DSC indicated modified thermal behavior in Ca-CAP, while Zeta potential analysis showcased negative charges, with Ca-CAP exhibiting lower negativity. XRD highlighted increased crystallinity in Ca-CAP due to calcium crosslinking. Minimal impact on RBC properties was observed with both polymers compared to the positive control as water for injection (WFI). Ca-CAP exhibited improved viscosity, strength, controlled swelling, and erosion, allowing prolonged drug release compared to CAP. Stability studies confirmed consistent six-month drug release, emphasizing Ca-CAP's potential as a stable, sustained drug delivery system over CAP. Robustness and accelerated stability tests supported these findings, underscoring the promise of Ca-CAP in controlled drug release applications.

Key words calcium ion crosslinked carboxymethylated gum, carboxymethylated-*Albizia-procera*-gum, linear viscoelasticity, water penetration velocity, release kinetics, scanning electron microscopy

Introduction

The field of pharmaceutical research continually strives to develop innovative drug delivery systems that enhance therapeutic outcomes while minimizing adverse effects. Among these systems, matrix tablet formulations have emerged as a promising strategy for achieving controlled drug release.¹⁾ Such formulations provide a stable platform to regulate the release of therapeutic agents, optimizing their efficacy and patient compliance. *Albizia procera*, sourced as an exudate from the *Albizia* tree belonging to the Mimosaceae family, serves as a carbohydrate polymer. It can be employed as an excipient in the production of sustained-release drug delivery systems. This choice is attributed to its notable biocompatibility and biodegradability properties.²⁾ According to numerous research studies, it has been documented that *Albizia procera* gum (AP) is composed of β -(1 \rightarrow 3)-D-galactopyranose units, along with some β -(1 \rightarrow 6)-D-galactopyranose units, as well as α -(1 \rightarrow 3)-L-arabinofuranose units.²⁾ These monomeric units are characterized by the presence of hydroxyl groups on their side chains. These hydroxyl groups can be chemically modified to form carboxymethyl groups, resulting in the formation of carboxymethylated *Albizia procera* gum (CAP). In light of these advancements, the present study embarks on an extensive investigation into the fabrication and characterization of matrix tablet formulations, utilizing CAP³⁾ and Ca-CAP as matrix materials in conjunction with Diltiazem hydrochloride (DIL) as a model drug. The significance of controlled drug

delivery systems has been acknowledged in numerous studies. The potential of matrix tablets in prolonging drug release and maintaining therapeutic levels over an extended period, thereby enhancing patient compliance and reducing dosing frequency.⁴⁾ Natural polymers gain attention in pharmaceuticals due to biocompatibility and sustainability. Researchers use carboxymethylated plant gum for sustained drug release in plant-based polymers for controlled drug delivery.⁵⁾ This investigation systematically explores critical phases, revealing underlying mechanisms governing matrix tablet formulations. It extensively analyzes the polymer's rheological behavior, vital for processing and performance, using techniques like flow curves and amplitude sweep studies. This focus on rheological properties aligns with research highlighting the correlation between polymer rheology and drug release behavior.⁶⁾ Matrix tablet response to water affects drug release. Swelling, erosion, and water penetration studies reveal behavior in aqueous environments. Similar findings link polymer erosion to drug release in hydrophilic matrices.⁷⁾ Interactions between polymers and the model drug are meticulously explored through Fourier Transform (FT) IR spectrum and differential scanning calorimetry (DSC) thermogram analyses. Such in-depth investigations into polymer-drug interactions which underscore the importance of understanding these interactions to predict drug release behavior.⁸⁾ The study's core intention lies in establishment of controlled release activity of the tailored matrix tablet formulations, which is ascertained by

* To whom correspondence should be addressed. e-mail: sudipta07tech@gmail.com

comprehensive evaluation of drug release kinetics.⁹⁾ Further enriching the study, visualization of dynamic changes in tablet surface topography during dissolution using scanning electron microscopy (SEM) provides insights into dissolution kinetics, surface topography, and structural integrity of tablet.¹⁰⁾ To ensure practical feasibility, an accelerated stability study coupled with similarity studies emphasizes the formulation's robustness under challenging conditions.¹¹⁾ This investigation explores the design, development, and evaluation of controlled drug delivery systems. The objectives entail a comprehensive approach: initiating the preparation of Ca-CAP, conducting a meticulous characterization of polymers, ingredients, and the drug components, delving into the viscoelastic properties of the polymers, crafting tablets using modified polymers to analyze their unique attributes, establishing *in-vitro* release profiles, and scrutinizing accelerated stability for a holistic assessment of the formulations. A comprehensive *in-vitro* red blood cell (RBC) lysis test was conducted using CAP and Ca-CAP solutions to evaluate the substance's capacity to induce the breakdown or destruction of red blood cells, occurring outside of a living organism. This evaluation helps determine the substance's impact on cellular membranes and its hemolytic properties, often crucial in understanding the safety profile of various compounds or formulations. The meticulous characterization, analysis, and evaluation offered by the research contribute substantially to the field of pharmaceutical research and practice. This study's findings hold the promise of advancing drug delivery strategies, thereby fostering enhanced therapeutic outcomes and transforming the landscape of pharmaceutical formulations.

Experimental

Materials DIL, Colloidal anhydrous silicon dioxide (Aerosil), and Microcrystalline cellulose (MCC, PH 102) were provided by Stadmed Pvt. Ltd., Kolkata, India. The carboxymethylated CAP (with a degree of substitution of 0.51) was obtained from the native *Albizia procera* gum sourced from Mizoram (Mizoram, India). Sodium hydroxide, tri-sodium phosphate dodecahydrate (TSPD), and Tri-sodium citrate (TSC) were obtained from Loba Chemie Pvt. Ltd., Mumbai, India. Calcium chloride dihydrate and analytical reagent grade methanol (99% (v/v)) were sourced from Merk Specialties Pvt. Ltd., Mumbai, India. Lactose anhydrous was from Oxford Lab Fine Chem LLP, Mumbai. Magnesium stearate (MS) was purchased from Merck Specialties Private Limited, Mumbai, India. A 0.9% w/v sodium chloride (NaCl) solution was procured from Pharma Impex Laboratories Pvt. Ltd., Kolkata, India. Other chemicals and reagents used were of analytical grade, ensuring experimental accuracy and reliability.

Methods

Preparation of Ca⁺² Crosslinked CAP

A 10-g portion of semi-crystalline CAP with a degree of substitution of 0.51 was sieved through a BS screen #45 and mixed with de-ionized water under stirring for 1 h, forming a slurry. A 2% (w/v) sodium hydroxide (NaOH) solution (10 mL) was gradually added to dissolve the powder, followed by the introduction of this mixture into a 5% (w/w) calcium chloride (CaCl₂) aqueous solution (50 mL) with agitation. After overnight settling, the resulting mass was vacuum-filtered, the cake washed with methanol, and then dried at 60°C for 4 h to obtain dried Ca-CAP, which was further characterized.¹²⁾

FTIR Analysis of CAP, Ca-CAP, DIL, and Mixtures

Samples of finely powdered CAP, Ca-CAP, DIL, and DIL with polymer mixtures were individually subjected to FTIR spectroscopy using an ATR-FTIR (Attenuated Total Reflection Fourier Transform Infrared) spectrophotometer (Alpha II, Bruker, U.K.). ATR-FTIR eliminates the requirement for KBr (potassium bromide) sample pelletization. This technique was designed to overcome the need for pelletization,¹³⁾ a conventional preparation method in traditional transmission FTIR spectroscopy. To analyze solid samples, gently apply pressure to the sample against the crystal surface. The solid powdered samples underwent analysis at an optimized resolution of 4 cm⁻¹, with 16 integrations executed to enhance the signal-to-noise ratio in the resulting spectrum.

Thermal Compatibility Study

DSC thermographs of CAP, Ca-CAP, DIL, and DIL with polymer mixtures were acquired using a DSC-4000 instrument (Perkin-Elmer, U.S.A.). The samples were hermetically sealed in aluminum pans and subjected to heating from 30 to 300°C at a rate of 10°C/min under a nitrogen flow. At the time of the experiment, the weight of each polymer sample was taken at 4 mg, whereas each DIL sample was taken at 3 mg.

Comparative Assessment of Zeta Potential Measurements

Zeta potential measurements were conducted utilizing a Zeta-sizer Nano ZS90 instrument (Malvern Instruments Ltd., U.K.). A 1% (w/v) dispersion of polymers was prepared at a neutral pH for the analysis. Deionized water served as the dispersion medium, and disposable zeta cells (DTS 1070) were employed for each sample at a temperature of 25°C. The experiments were replicated thrice, and the average values were recorded. Data analysis was performed using the "Zetasizer" software version 7.03 PSS0012 - 34 EN-JP (Malvern Instruments Ltd.).

X-Ray Powder Diffraction Analysis

X-Ray diffraction (XRD) patterns were obtained for powdered polymer samples using an X-ray diffractometer (ULTIMAIII, Rigaku, Japan). The X-ray generator operated at a voltage of 40 kV and a current of 30 mA, utilizing K- β filtered Cu radiation at 1.54056 Å as the radiation source. The powdered samples were scanned over a diffraction angle (2 θ) range of 5 to 80° at a scanning speed of 3°/min.

In-Vitro RBC Lysis Test

The purpose of this study is to investigate the impact of different sample solutions, specifically CAP and Ca-CAP, on red blood cells (RBCs) and their properties. The study involves a series of procedures to prepare and analyze blood samples in the presence of these sample solutions. Fresh goat blood was procured from a slaughterhouse, and 80 mL of the blood underwent preservation using a 10% (w/v) Tri-sodium citrate solution within a 0.9% (w/v) NaCl solution. This preservation method effectively prevents blood clotting and preserves the blood sample's integrity. The preserved blood was then transferred to 1.5 mL Eppendorf tubes and subjected to centrifugation at 2000 rpm for 10 min, resulting in the separation of blood components. A dark red-colored pellet, primarily composed of RBCs, formed at the bottom, while the liquid supernatant containing plasma and other components was discarded.¹⁴⁾ The RBC pellets underwent triple washing with freshly prepared phosphate buffer (pH 7.4) to ensure purity and eliminate impurities. Subsequently, the washed RBC pel-

lets were suspended in phosphate buffer solution (PBS) to create a 1% RBC suspension, which was then used for the experiment. For the experiment, each well of a 96-well plate was loaded with 30 μ L of the 1% RBC suspension. To this, an additional 30 μ L of PB solution was added, followed by varying volumes of sample solutions to achieve a final well volume of 150–200 μ L. The plate was incubated at 37 °C for 1 and 3 h, allowing the samples to interact with the RBCs. Post-incubation; the optical density of the samples was measured at 540 nm using a Multimode plate spectrophotometer. This measurement provided insights into changes in RBC properties, as indicated by alterations in optical density. To validate results, two control samples were employed: marketed water for injection as the positive control (for comparison with expected RBC behavior) and a 0.9% (w/v) NaCl solution as the negative control (to assess background effects). This experimental setup facilitated the assessment of the impact of different sample solutions on RBCs by analyzing changes in optical density, thus revealing potential effects on cellular properties.¹⁵⁾

Comparative Rheological Analysis

Rheological analyses were performed on the polymer matrices (5% (w/v)) of both CAP and Ca-CAP, which were prepared using deionized water as the dispersion medium. The rheological experiments were conducted using a Modular Compact Rheometer (Anton Parr, MCR 102, Austria) equipped with a standard 1° cone geometry (CP-40) having a diameter of 40 mm. Each experiment was conducted at different pH levels using 5% (w/v) polymer matrices at a temperature of 25 °C. The air pressure was maintained at 6.8646 bar using a compressor unit. Two test methods were employed: dynamic rotational mode (flow curve) and oscillatory mode. For the flow curve study, the dynamic rotational mode was utilized to investigate the shear viscosity of the samples at varying shear rates. Additionally, the impact of pH on the shear viscosity of the polymeric matrices was assessed. In the amplitude sweep study, the oscillatory mode was employed to explore amplitude sweep and frequency sweep experiments. This aimed to analyze the storage and loss moduli (G' and G'') of the polymers. The amplitude sweep was conducted at a fixed angular frequency¹⁶⁾ ($\omega = 6.2831853$ rad/s), where the strain ($\gamma = 0.01$ –10%) was adjusted to induce structural deformation within the entangled polymer. Furthermore, the frequency sweep study was carried out to examine changes in G' and G'' against a range of variable angular frequencies ($\omega = 0.1$ –10 rad/s). This was accomplished by utilizing the critical strain (0.3% for CAP, 2% for Ca-CAP) obtained from the amplitude sweep conducted within the linear viscoelastic (LVE) regime.¹⁷⁾

Preparation of Matrix Tablets: Placebo and DIL-Loaded

Matrix tablets were formulated using the wet-granulation method. Ingredients were accurately weighed as per batch size. Drug, polymer, lactose, and MCC were sieved through mesh #40. Drug was mixed with polymer and other ingredients for 15 min. Dry mixture was moistened, forming cohesive mass, screened through mesh #16 for moist granules. Granules were dried at 65 °C until moisture content reached 2% (w/v). Dried granules were sieved through #20, lubricated with 0.25 to 5% (w/w) magnesium stearate and 0.1 to 0.5% (w/w) aerosol. Lubricated granules were compressed into tablets using tablet compression machine. Compression force was adjusted for tablets with 49.05 to 68.67 Newton hardness.¹⁸⁾ To explore

the swelling and erosion characteristics of the matrix, inert ingredients were used to formulate placebo matrix tablets, omitting the drug component. Both formulations, X1 and X2, were prepared with a consistent amount of polymer, with X1 containing CAP and X2 containing Ca-CAP.

For the DIL-loaded matrix tablets, the active ingredient DIL was incorporated along with CAP and Ca-CAP as polymers. The weight ratios specified in Tables 1, 2 were maintained for both placebo and DIL-loaded formulations.

Swelling Study

The swelling analysis of placebo matrix tablets (X1, X2) was conducted in acid solution of pH 1.2, and Phosphate buffer solution of pH 6.8 using a USP II tablet dissolution test apparatus (model TDP-06P, Electrolab, India) at 37 ± 0.5 °C. Each tablet was weighed, placed in a stainless steel wire mesh basket, and immersed in 900 mL of test medium. The basket was stirred at 75 rpm. After a predetermined time, the hydrated tablet was removed, excess water was blotted, and the new weight was measured. The percentage swelling was calculated using the formula:

$$\%Swelling = \left[\frac{(W_2 - W_1)}{W_1} \times 100 \right] \quad (1)$$

Where W_1 represents the initial weight of the tablet at time 0 and W_2 is the weight of the tablet at time t after immersion in the test medium.

Erosion Study

The erosion study was conducted following a methodology similar to the swelling study, with the only difference being the removal of the basket containing the placebo matrix tablet from the test medium (acid solution of pH 1.2, and Phosphate buffer solution of pH 6.8) at specific time intervals. The basket was then dried in a hot air oven at 70 °C until it achieved complete dryness. The percentage erosion at different time points was calculated using Equation:

$$\%Erosion = \left[\frac{(W_1 - W_3)}{W_1} \times 100 \right] \quad (2)$$

W_1 denotes the initial weight of the tablet at the starting time (time 0), while W_3 signifies the tablet's weight at time t following its immersion in the test medium and subsequent drying.

Water Penetration Velocity in Matrix Tablets

The determination of water penetration velocity in a tablet through a swelling study provides insights into the rate at which water permeates the tablet structure, which can have

Table 1. Formulation of Placebo Matrix Tablets

Sl No.	Ingredients per tablet (mg)	Formulation code	
		X1	X2
1.	CAP	600	—
2.	Ca-CAP	—	600
3.	Lactose anhydrous	380	380
4.	MCC	100	100
5.	Purified water	Qs*	Qs*
6.	Magnesium stearate	18	18
7.	Aerosil	2	2

*Qs indicates quantity sufficient.

Table 2. Formulation of DIL Matrix Tablets

Sl No.	Ingredients per tablet (mg)	Formulation code									
		F1	F2	F3	F4	F5	F6	F7	F8	F9	F10
1	DIL	120	120	120	120	120	120	120	120	120	120
2	CAP	120	360	540	600	780	—	—	—	—	—
3	Ca-CAP	—	—	—	—	—	120	360	540	600	780
4	Lactose anhydrous	680	450	300	260	100	680	450	300	260	100
5	MCC	160	150	120	100	80	160	150	120	100	80
6	Purified water	Qs*	Qs*	Qs*	Qs*	Qs*	Qs*	Qs*	Qs*	Qs*	Qs*
7	Magnesium stearate	18	18	18	18	18	18	18	18	18	18
8	Aerosil	2	2	2	2	2	2	2	2	2	2

*Qs indicates quantity sufficient.

implications for the tablet's disintegration, dissolution, drug release, and overall performance. Water penetration velocity data can be used in mathematical models to predict drug release behavior under different conditions, aiding in formulation design.¹⁹⁾

Water penetration velocities were ascertained utilizing the following equation

$$V = \left(\frac{1}{2\rho A} \right) \times \frac{ds}{dt} \quad (3)$$

Here, V stands for the velocity of water penetration, ds/dt denotes the gradient of the curve illustrating the relationship between percentage swelling and the square root of time ($\sqrt{\text{Time}}$), ρ symbolizes the density of the water, acid solution, and PB solution at a temperature of 310 K, and A represents the tablet's surface area.

The surface area of the caplet-shaped convex tablet can be calculated by considering its curved top surface, bottom surface, and the lateral surface connecting them.²⁰⁾ The determination of the surface area was accomplished using the subsequent formula:

$$A = 2\pi r(h + 2r) \quad (4)$$

In this context, h signifies the thickness of the tablet, while r represents its radius, both of which were ascertained through the utilization of calipers. The radius (r) of the cylindrical shape was calculated as half of the length (length/2).

Tablet Characterization and Drug Content Determination Weight Uniformity Assessment

The weight uniformity test followed the established procedure.²¹⁾ From each formulation, 20 tablets were subjected to analysis using a precision electronic balance (Precisa, XB600 M-C, Switzerland). The tablets were selected randomly and weighed individually. The individual weights (m_1, m_2, \dots, m_{20}) were compared to the average weight of the tablets.

$$\text{Average weight (m)} = \left[\frac{m_1 + m_2 + m_3 + \dots + m_{20}}{20} \right] \quad (5)$$

Tablet Hardness Test

The crushing strength evaluation involved testing 10 tablets from each formulation utilizing a pre-calibrated Monsanto hardness tester (Cadmach, Ahmedabad, India). The tablet to be assessed was positioned between the spindle and anvil. The

required pressure for maintaining the tablet's position was applied by turning the screw knob clockwise.²²⁾ The scale was adjusted to set the indicator at zero, and then pressure was steadily increased until the tablet fractured.

Tablet Physical Dimensions Measurement

The physical dimensions of the tablets, including length, breadth, and thickness, were determined using a calibrated digital caliper. Measurements were taken for ten tablets from each formulation.

Friability Assessment

The friability of 20 tablets from each formulation was evaluated utilizing the Roche friabilator, provided by Campbell Electronics, Mumbai, India. To ascertain the weight loss percentage, the friabilator was set to rotate at a speed of 25 ± 1 rpm for 4 min (equivalent to 100 revolutions). Following the process, the tablets were de-dusted and reweighed. The friability percentage was computed using the subsequent equation:

$$\text{Friability (\%)} = \left[\frac{(W_1 - W_2)}{W_1} \times 100 \right] \quad (6)$$

Where W_1 represents the initial weight of the tablets before tumbling and W_2 is the weight of the matrix tablets after tumbling.

Content Uniformity for Tablets Containing DIL

Ten tablets were weighed and crushed with a pestle in a mortar. The resulting fine powder was weighed to obtain 100 mg (equivalent to 120 mg of Diltiazem HCl) and transferred to a 250 mL conical flask containing 100 mL of a 6.8 pH phosphate buffer. The mixture was stirred for 45 min using an ultrasonic bath (sonicator). Afterward, the solution was filtered through Whatman filter paper (pore diameter 11 μm), and the drug content was determined by analyzing it using UV spectrophotometry at a wavelength (λ_{max}) of 236 nm. The content of $\text{C}_{22}\text{H}_{26}\text{N}_2\text{O}_4\text{S}$, HCl (diltiazem hydrochloride) was determined by calculating the specific absorbance at 236 nm of the reference solution (RS) containing 0.0012% (w/v) of diltiazem hydrochloride in PB solution of pH 6.8.²³⁾

In-Vitro Drug Release Study from DIL-Loaded Matrix Tablets

To examine the *in-vitro* drug release from matrix tablets containing DIL, a USP II tablet dissolution tester (Electrolab, TDP-06P, India) was employed with acidic (pH 1.2) and phosphate buffer (pH 6.8) solutions. The experiment was conducted in a cylindrical dissolution vessel (1000 mL) under stirring at 100 rpm. The temperature was maintained at $37 \pm 0.5^\circ\text{C}$ with

750 mL of 0.1 M hydrochloric acid solution. A tablet from each formulation was randomly placed in the vessel. Throughout the experiment, hourly aliquots were drawn and replaced with an equal volume of fresh medium at the same temperature. After 2 h of dissolution in an acidic medium, 250 mL of 0.2 M tri-sodium phosphate dodecahydrate solution (previously held at $37 \pm 0.5^\circ\text{C}$) was introduced. The medium's pH was adjusted to 6.8 ± 0.05 using a 2 M sodium hydroxide solution. The dissolution process was sustained for 12 h. The collected aliquots were filtered, appropriately diluted, and subjected to spectrophotometric analysis. Drug release quantification was performed at the wavelength of maximum absorbance (λ_{max}), found to be 236 nm for DIL in both acidic and buffer solutions.

Analysis of Drug Release Kinetics and Mechanism in *in-Vitro* Release Profile

The drug release profiles were subjected to analysis using various kinetic models, including zero-order, first-order, Higuchi, and Korsmeyer–Peppas models. By comparing the obtained results, the release mechanisms of different formulations were elucidated based on the best fit to these models. The drug transport mechanism was further explored through linear regression analysis, considering the coefficient of determination values and diffusion exponent values.

To understand the drug release mechanism, the release data were fitted to exponential equations as follows:

Zero-Order Release Kinetics:

$$\frac{dq}{dt} = K_0 \quad (7)$$

Where q represents cumulative % release, K_0 is the zero-order release rate constant, and t stands for time. A graph was plotted to illustrate the relationship between cumulative % drug release (Q) and time (t), and the coefficient of determination (R^2) was calculated.

First-Order Release Kinetics:

$$\ln Q_t = \ln Q_0 + K_1 t \quad (8)$$

Here, Q_t denotes the amount of drug released per unit surface area after time t , K_1 is the first-order release rate constant, and Q_0 is the initial amount. Another graph was plotted, depicting the relationship between the logarithm of cumulative percentage release and time. The coefficient of determination (R^2) was computed to assess the fit.

Higuchi Square Root Equation:

$$\frac{M_t}{M_\infty} = K_{HG} t^{1/2} \quad (9)$$

In this equation, M_t and M_∞ represent cumulative amounts of drug release at time t and infinite time, respectively, while K_{HG} signifies the Higuchi release rate constant. A plot was generated to visualize the cumulative percentage release against the square root of time, representing Higuchi release kinetics. The coefficient of determination (R^2) was calculated for this representation.²⁴⁾

Korsmeyer–Peppas Model:

$$\log [M_t/M_\infty] = \log K + n \log t \quad (10)$$

Here, M_t and M_∞ represent cumulative amounts of drug release at time t and infinite time. K is a constant, and n is a diffusional release exponent that signifies the mechanism of drug release during dissolution. A graph was plotted with $\log [M_t/M_\infty]$ on the y -axis and $\log t$ on the x -axis. The slope of the graph was used to calculate the “ n ” value.²⁵⁾

Scanning Electron Microscopic (SEM) Study

The matrix tablets were collected from the dissolution chamber to study the morphological changes during the dissolution study. The surface morphology of the polymer layer was examined under SEM. Each sample was coated with gold-palladium-alloy using a fine coat ion-sputter (Hitachi, E-1010) and examined at $10.0\text{ Kv} \times 100\text{ SE}$ and $10.0\text{ Kv} \times 1.00\text{ k SE}$ and $10.0\text{ Kv} \times 500\text{ SE}$ with tilt edge of 45° . The coated samples were subsequently analyzed under a field emission Scanning Electron Microscope (Hitachi, S-3400N).

Accelerated Stability Study

Accelerated stability studies were conducted on DIL-loaded matrix tablets from each formulation of CAP, and Ca-CAP for a duration of 6 months. The objective was to assess the stability of DIL in the respective formulations. Ten tablets from each of the formulation were placed in glass vials separately with bakelite caps, marked, and stored in a stability chamber at a temperature of 40°C and a relative humidity of $75 \pm 5\%$ for the duration of 6 months. Upon completion of the specified duration, the samples were compared to fresh tablets in terms of drug content and dissolution profile. The similarity factor (f_2) was calculated to assess the similarity between the dissolution rates of the fresh and stored tablets, utilizing the following Equation²⁶⁾:

$$f_2 = 50 \log \left\{ \left[1 + \left(\frac{1}{n} \right) \sum_{i=1}^n (R_i - T_i)^2 \right]^{-0.5} \times 100 \right\} \quad (11)$$

Where n is the number of dissolution time points, R_i is the mean percentage drug released at each time point of the reference at time t , and T_i is the mean percentage drug released at each time point of the test product at time t . The f_2 comparison is widely utilized in various FDA and EMEA guidelines as a criterion to assess the similarity of *in vitro* dissolution profiles (Costa, 2001). An f_2 value of 100 indicates identical profiles, and an average variation of 10% at all time points results in an f_2 value of 50. The FDA and EMEA have set a standard range of f_2 values between 50 and 100 to ensure equivalence of the two dissolution profiles.²⁶⁾

Statistical Data Treatment

The impact of different formulation parameters on drug release was assessed using ANOVA (Two-way ANOVA) at a significance level of $p < 0.05$.

Results

Formation of Ca-CAP Carboxymethylated CAP with a degree of substitution of 0.51 was successfully synthesized from the native Albizia procera gum. The carboxymethylation process introduced COO^- groups onto the gum's chains³⁾ rendering them reactive with divalent cations. This property was exploited in the subsequent crosslinking step using CaCl_2 to create crosslinked carboxymethylated Albizia procera gum (Ca-CAP). The successful conversion of Ca-CAP through the cross-linking of carboxymethylated gum with calcium chlo-

ride was achieved. The interaction between COO^- groups on CAP chains and divalent calcium ions resulted in the formation of Ca-CAP (Fig. 1).

Characterization and Comparative Study

FT-IR Spectrum Analysis

Figures 2a and b present the Fourier transform IR (FT-IR) spectra of CAP and Ca-CAP, respectively. Despite minor variations in intensity, the positions of bands in both spectra remained largely consistent, indicating structural similarities. CAP exhibited significant absorption bands at 3292.383, 2880.317, 2360.537, 1585.374, 1459.616, 1416.322, 1321.489, and 1020.494 cm^{-1} , which correspond to characteristic carbohydrate bands.²⁷⁾ Similarly, Ca-CAP displayed absorption bands at 3296.307, 2880.062, 2364.661, 1586.066, 1457.555, 1414.261, 1321.489, and 1020.371 cm^{-1} (Fig. 2b).

Figures 2c and d showcase the FT-IR spectra of Diltiazem HCl (DIL) and its mixtures with polymers.

DSC Thermogram Analysis

Figures 3a and b provide a comprehensive view of DSC thermograms for CAP and Ca-CAP. The data highlights distinctive thermal behavior in these polymers. CAP exhibited an exothermic event at 54.65 $^{\circ}\text{C}$, characterized by a heat flow

of 20.49 mW. In contrast, Ca-CAP displayed a slightly shifted exothermic event at 55.15 $^{\circ}\text{C}$, accompanied by a heat flow of 21.08 mW. Both polymers exhibited endothermic peaks, with CAP showing a melting point at approximately 261.54 $^{\circ}\text{C}$ and a heat flow of 8.54 mW, while Ca-CAP demonstrated a melting peak at around 263.97 $^{\circ}\text{C}$ with a heat flow of 8.84 mW.

Figures 3c and d provide the DSC curves of the pure DIL and DIL with polymer mixtures. The endothermic peak observed at approximately 216.7 $^{\circ}\text{C}$ in both curves signifies the melting of pure DIL. This peak represents the temperature at which DIL undergoes a phase transition from a solid to a liquid state, which is a well-defined characteristic of DIL.

Zeta Potential Analysis

The zeta potential analysis is depicted in Figs. 4A and B, yielded insightful results regarding the surface charge properties of both CAP and Ca-CAP samples. The zeta potential assessment revealed that CAP samples possessed a zeta potential value of -13.8 mV . This negative value signifies a predominance of negatively charged sites on the CAP particles' surfaces.

XRD Pattern Analysis

The X-ray diffractograms of CAP and Ca-CAP, as presented

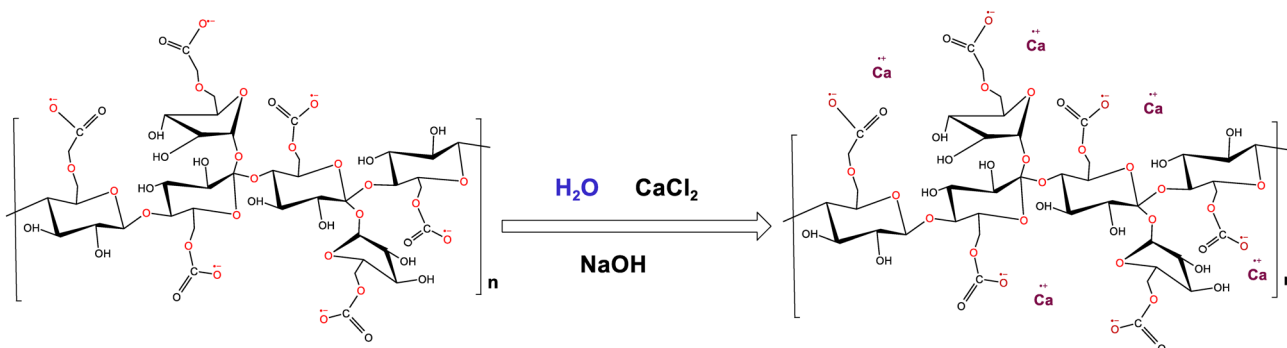


Fig. 1. Conversion of CAP to Ca-CAP

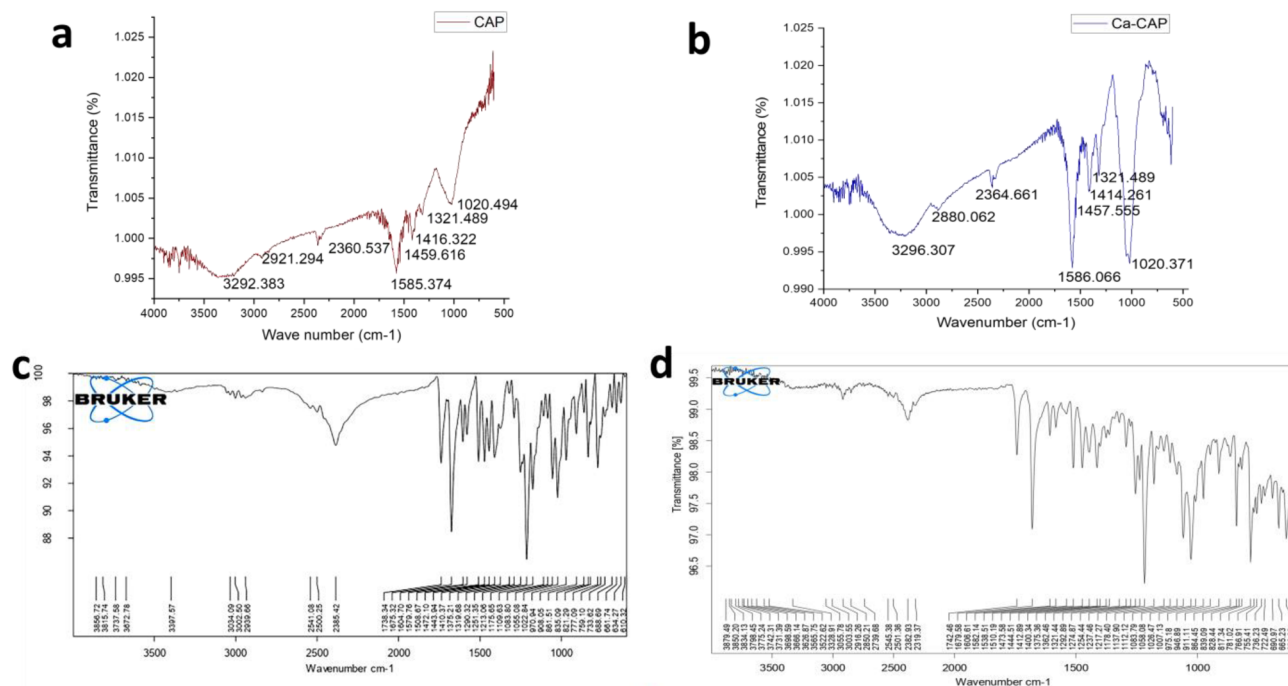


Fig. 2. FT-IR Spectrum (a) CAP, (b) Ca-CAP, (c) DIL and (d) DIL with Polymer Mixtures

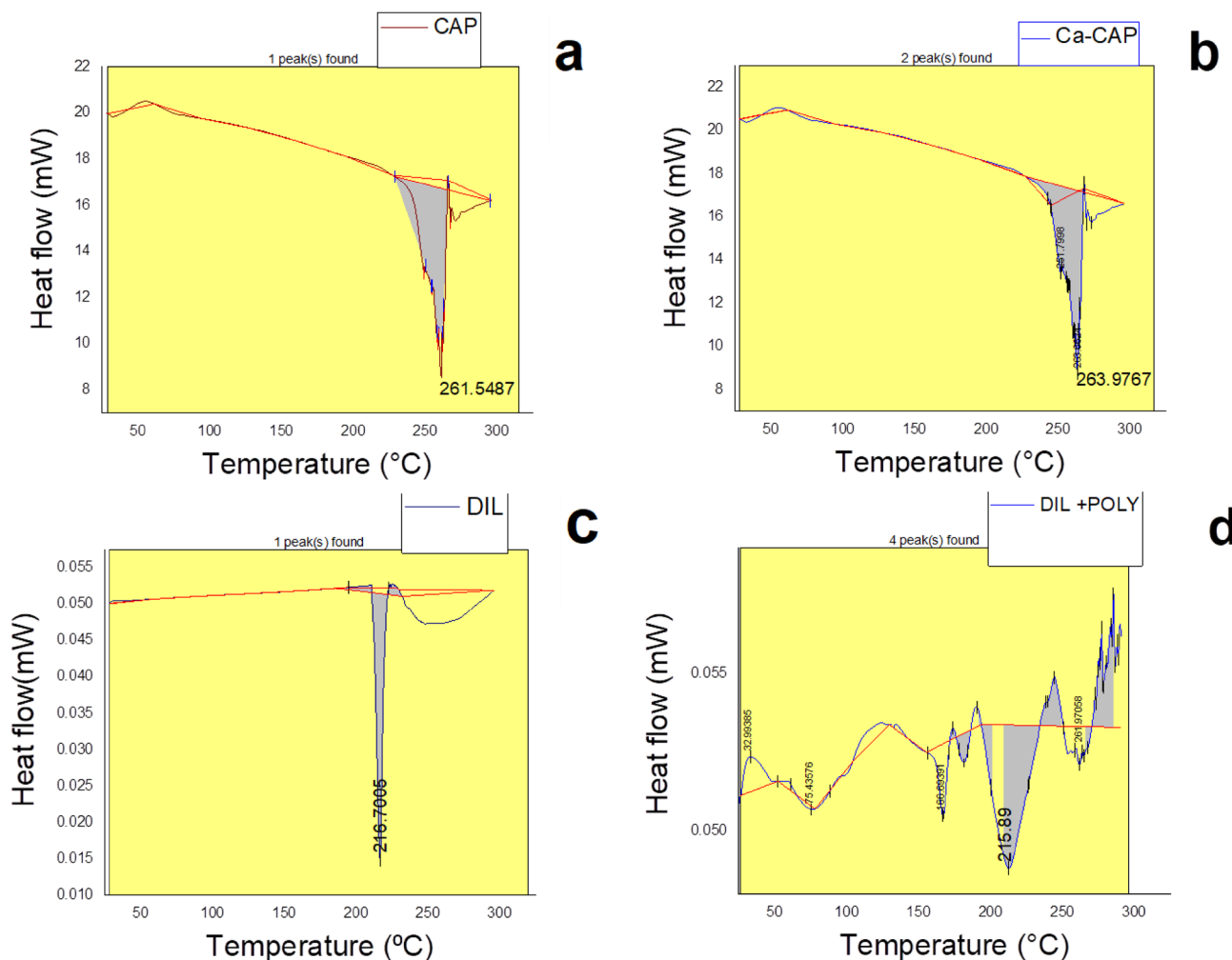


Fig. 3. DSC Thermogram (a) CAP, (b) Ca-CAP, (c) DIL and (d) DIL with Polymer Mixtures

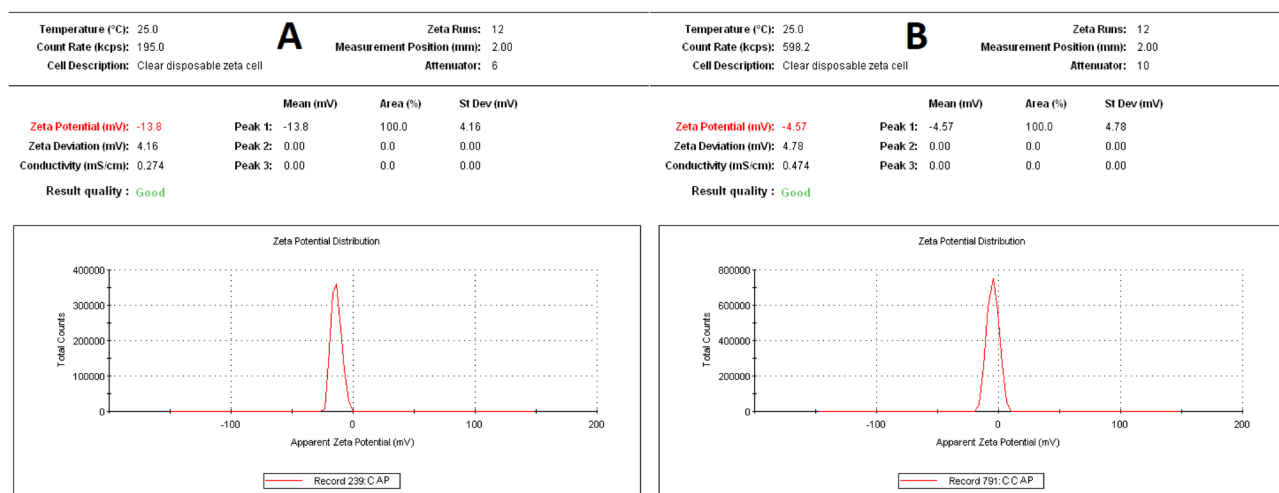


Fig. 4. Zeta Potential of (A) CAP, (B) Ca-CAP

in Figs. 5A and B, provide valuable insights into the crystalline nature of these materials. The X-ray diffractogram of CAP reveals characteristic patterns occurring at 2θ values ranging from 15.250 to 56.500°. Significantly, the major, sharp, and intense patterns were detected at approximately 2θ values of 31.700° (756 cps), 45.450° (409 cps), and 56.5° (182 cps).

In contrast, the X-ray diffractogram of Ca-CAP exhibits

characteristic patterns within a 2θ range of 17.35 to 47.1°. Notably, the major, sharp, and intense patterns observed at specific 2θ values, including 17.35° (354 cps), 18.25° (350 cps), 19.55° (391 cps), 24.7° (383 cps), 25.5° (539 cps), 28.1° (585 cps), 27.5° (503 cps), 29.4° (348 cps), 29.85° (322 cps), 33.45° (342 cps), and 47.1° (183 cps).

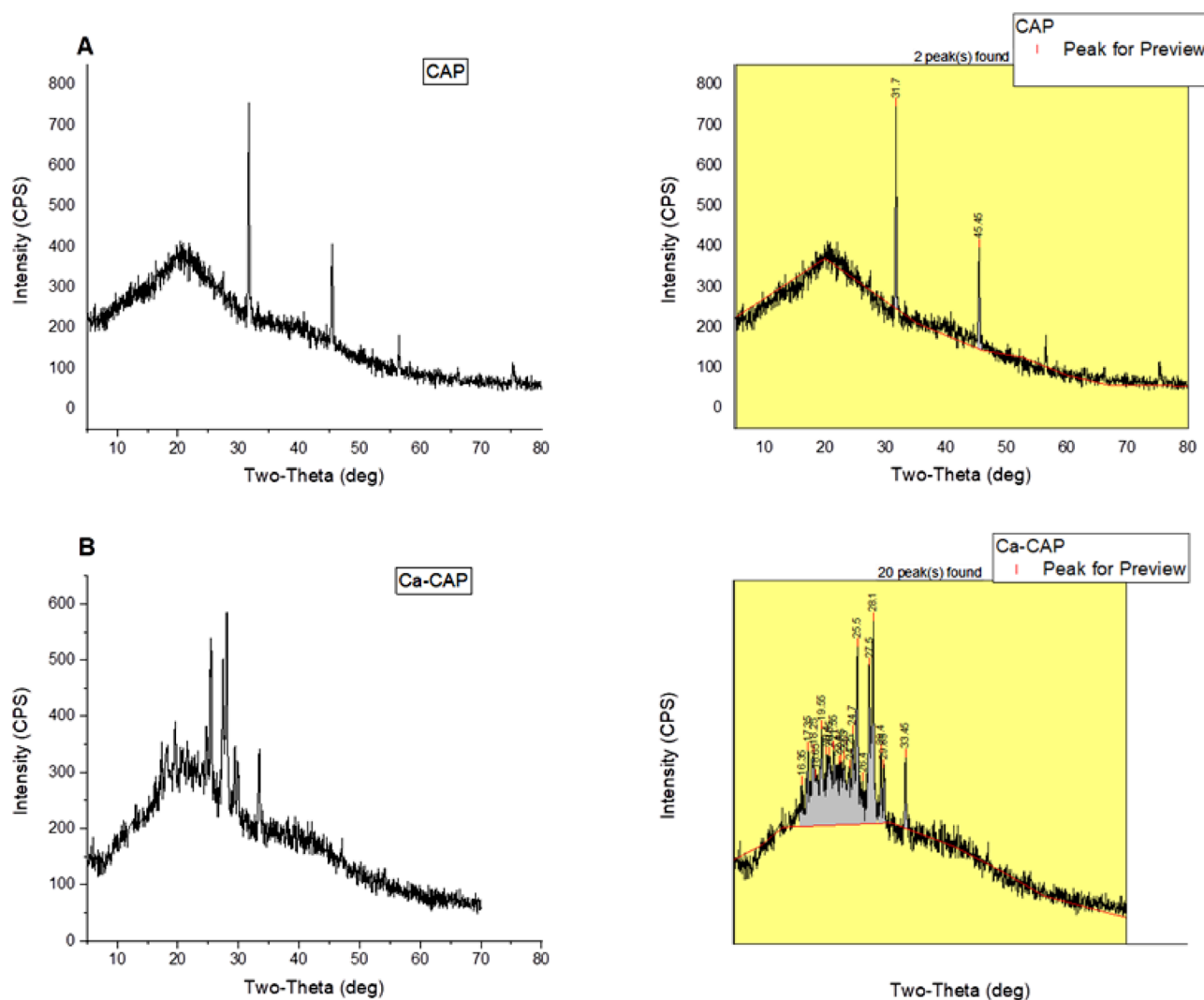


Fig. 5. XRD Patterns of (A) CAP, (B) Ca-CAP

Table 3. RBC Lysis Evaluation at 540nm: 1 and 3h Incubation

Samples	Optical density at 540nm									
	1 h					3 h				
CAP + RBC + PBS	0.0728	0.0751	0.0731	0.0751	0.0714	0.0734	0.0753	0.0763	0.0756	0.0716
Ca-CAP + RBC + PBS	0.0719	0.0763	0.0733	0.0755	0.0758	0.0723	0.0765	0.0738	0.0758	0.0762
WFI (positive control)	0.787	0.892	0.726			0.791	0.897	0.743		
Normal saline (negative control)	0.0752	0.0769	0.0755			0.0752	0.0769	0.0755		
RBC suspension			0.1687					0.1687		

In-Vitro RBC Lysis Test

The study delved into the effects of CAP and Ca-CAP on RBC properties, employing optical density (OD) measurements after 1 and 3h of incubation at 29.8°C. The OD data, summarized in Table 3, paints a revealing picture.

For CAP-treated samples after 1h, the optical density exhibited minimal variation, signaling no discernible impact on RBC properties. This trend persisted after 3h, indicating that CAP maintained a steady influence, effectively leaving RBCs unaffected. In the case of Ca-CAP-treated samples, the optical densities remained consistently stable, further corroborating the absence of any substantial impact on RBC properties throughout the experimental duration. However, the positive

control, represented by WFI, displayed markedly higher optical densities. This discrepancy implies a substantial influence, potentially attributable to osmotic effects. Summing up, both CAP and Ca-CAP demonstrated relatively negligible effects on RBC properties when compared to the potent impact of the positive control. This suggests that these sample solutions are apt for applications related to RBCs, as they do not significantly disrupt their inherent properties.

Comparative Rheological Analysis

The flow behavior of CAP and Ca-CAP is visually represented in Fig. 6A. These flow curves provide crucial insights into the viscosity characteristics of the two materials. Upon examining the flow curves, a notable trend becomes evident:

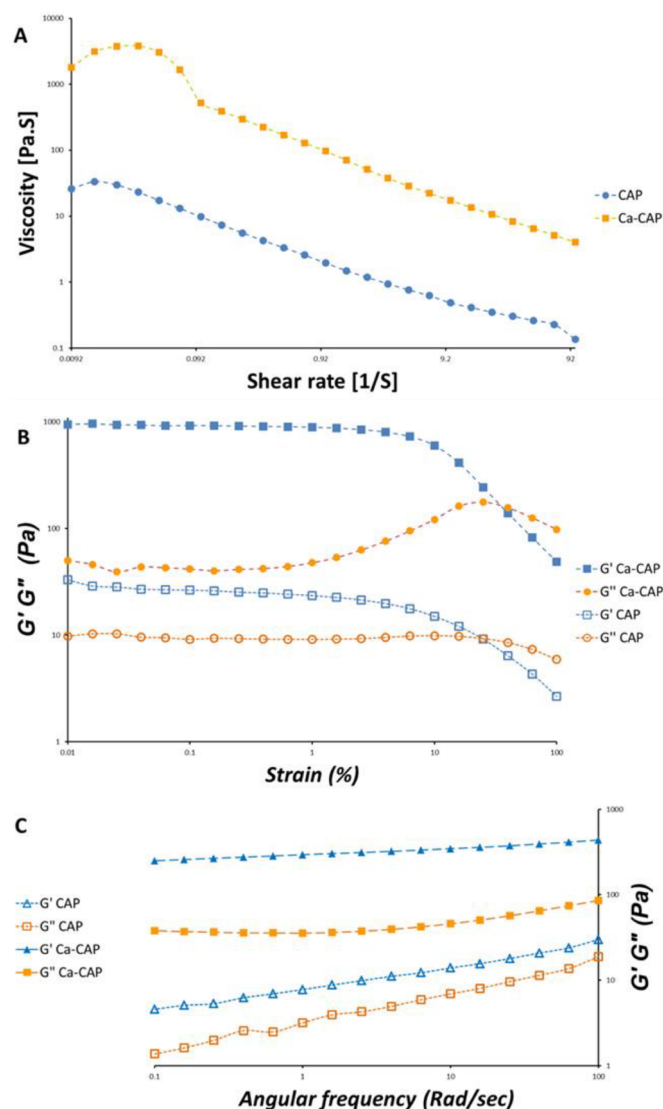


Fig. 6. (A) Flow Curves: CAP and Ca-CAP; (B) Amplitude Sweep: CAP and Ca-CAP; (C) Frequency Sweep: CAP and Ca-CAP

the viscosity of the Ca-CAP matrix consistently surpasses that of CAP. This difference in viscosity profiles emphasizes the distinctive rheological behaviors exhibited by Ca-CAP and CAP. Both polymers exhibit non-Newtonian behavior characterized by pseudo-plastic flow.

Both polymers have been subjected to amplitude sweep tests, and the outcomes are presented in Fig. 6B. These parameters are observed as strain (%) is systematically varied during the course of amplitude deformation. The Ca-CAP matrix displayed a critical strain of 2%, whereas CAP showed a significantly lower critical strain of 0.3%.

During the frequency sweep analysis, the critical strain (0.3% for CAP and 2% for Ca-CAP) was maintained at a constant level within the Linear Viscoelastic (LVE) region while the angular frequency (rad/s) was systematically varied. Figure 6C illustrates the frequency sweep curves, revealing that Ca-CAP exhibited notably higher G' values in comparison to CAP.

Figures 7a and b depict the relationship between G' and G'' concerning angular frequency for CAP and Ca-CAP matrices. This visualization aims to comprehend the viscoelastic prop-

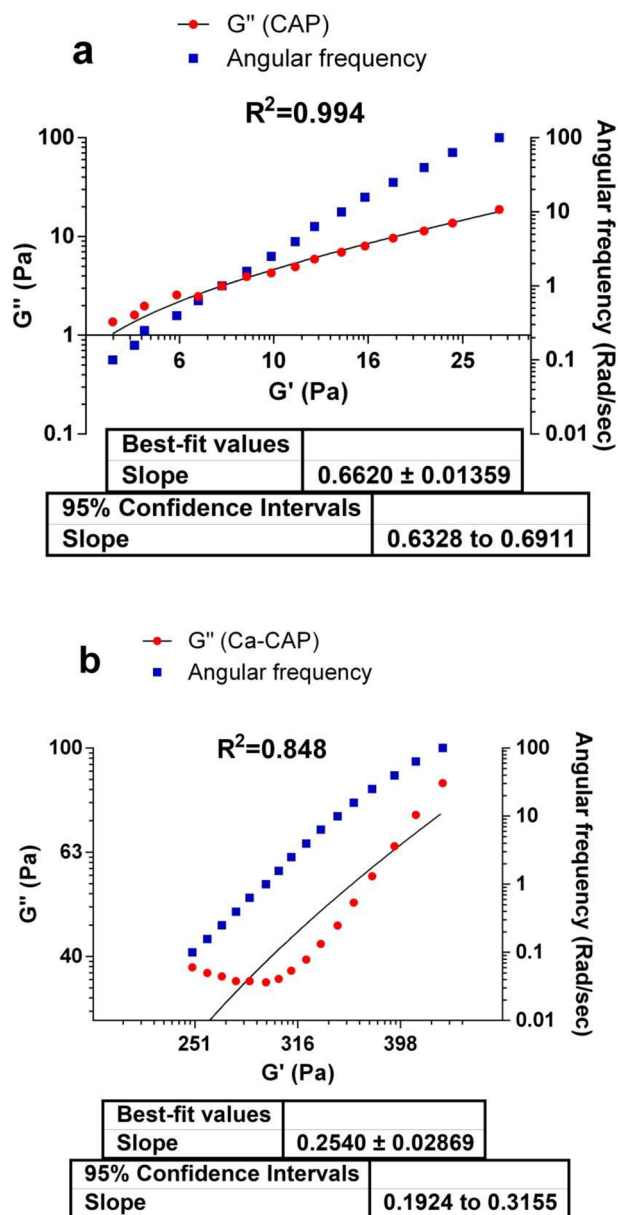


Fig. 7. Angular Frequency-Dependent Relationship between G' and G'' in (a) CAP Matrices (b) Ca-CAP Matrices

erties of the polymers through frequency sweep data. Comparison of R^2 values (0.994 for CAP, 0.848 for Ca-CAP) and best-fit slope values (0.662 ± 0.013 for CAP, 0.254 ± 0.028 for Ca-CAP) was conducted to gain insights into the viscoelastic behavior of these polymers based on the frequency sweep data.

Table 4 displays the Trends in phase-angle (δ) for CAP and Ca-CAP matrices across various angular frequencies. Both CAP and Ca-CAP exhibit decreasing phase angles as angular frequency increases. These trends offer insights into the viscoelastic behavior of CAP and Ca-CAP matrices, with potential implications for their mechanical properties and applications. CAP generally shows higher phase angles than Ca-CAP, The rate of phase angle decrease varies between CAP and Ca-CAP, indicating differences in their viscoelastic properties.

Figures 8a and b showcase the swelling behavior observed in X1 and X2 placebo tablets, each containing CAP and Ca-CAP matrices, correspondingly, within acidic (pH 1.2) and

buffer (pH 6.8) environments. In contrast, Figs. 8c and d present the erosion patterns evident in the CAP and Ca-CAP matrices under both acidic (pH 1.2) and buffer (pH 6.8) conditions.

Table 5 indicates that the water penetration velocity through X1 matrix tablets surpassed that of X2 matrix tablets. In addition, the visualization provided in Fig. 9 offers a comprehensive

representation of the dissolution characteristics and structural integrity of X1 and X2 tablets following exposure to dissolution media after 6 h.

Physical Characteristics of Tablet The physical attributes of the tablets fell within acceptable parameters. A comprehensive comparison of these physical characteristics for each formulation is provided in Table 6.

In Table 6, it was observed that the hardness of the Ca-CAP tablet is higher than that of the CAP tablet, and the friability of the Ca-CAP tablet is lesser than that of the CAP tablet. As Ca-CAP tablet is found harder and more robust its friability is found less. This is attributed to the cross-linking of gum with calcium ions in which polymeric chains are entangled.

In-Vitro Drug Release Study The coefficient of correlation (R^2) was obtained, and the quantity of drug dissolved in each sample was determined based on the standard calibration curve of DIL. In Figs. 10a and b, the *in-vitro* drug release profiles of DIL (120mg) from tablets containing CAP and Ca-CAP in each formulation were presented. The *AUC* values for DIL released from CAP and Ca-CAP tablets are presented in Table 7. The drug release data were subjected to two-way ANOVA analysis to determine the significant difference in drug release between different formulations (Table 8).

In acidic pH, *AUC* DIL-loaded CAP formulations (F1–F5) is higher than that of Ca-CAP formulations (F6–F10) and in pH 6.8 it shows the opposite effect.

The mechanism of drug release from hydrophilic matrix tablets is based on diffusion of the drug through, and erosion of the surrounding hydrated polymeric gel layer on the surface of the matrix. In the case of a highly soluble drug,

Table 4. Phase Angle (δ) Trends of CAP and Ca-CAP Matrices across Varying Angular Frequencies

Angular frequency (rad/sec)	Phase angle δ	
	CAP	Ca-CAP
100	0.62666667	0.195859
63.1	0.573221757	0.180663
39.8	0.548076923	0.165095
25.1	0.537430168	0.15195
15.8	0.514102564	0.140986
10	0.497841727	0.132076
6.31	0.483606557	0.126432
3.98	0.445045045	0.121871
2.51	0.432186235	0.120014
1.58	0.448630137	0.119054
1	0.406692407	0.120591
0.631	0.358381503	0.125787
0.398	0.412520064	0.129687
0.251	0.372180451	0.136655
0.158	0.317554241	0.143355
0.1	0.300438596	0.152019

Swelling and erosion study.

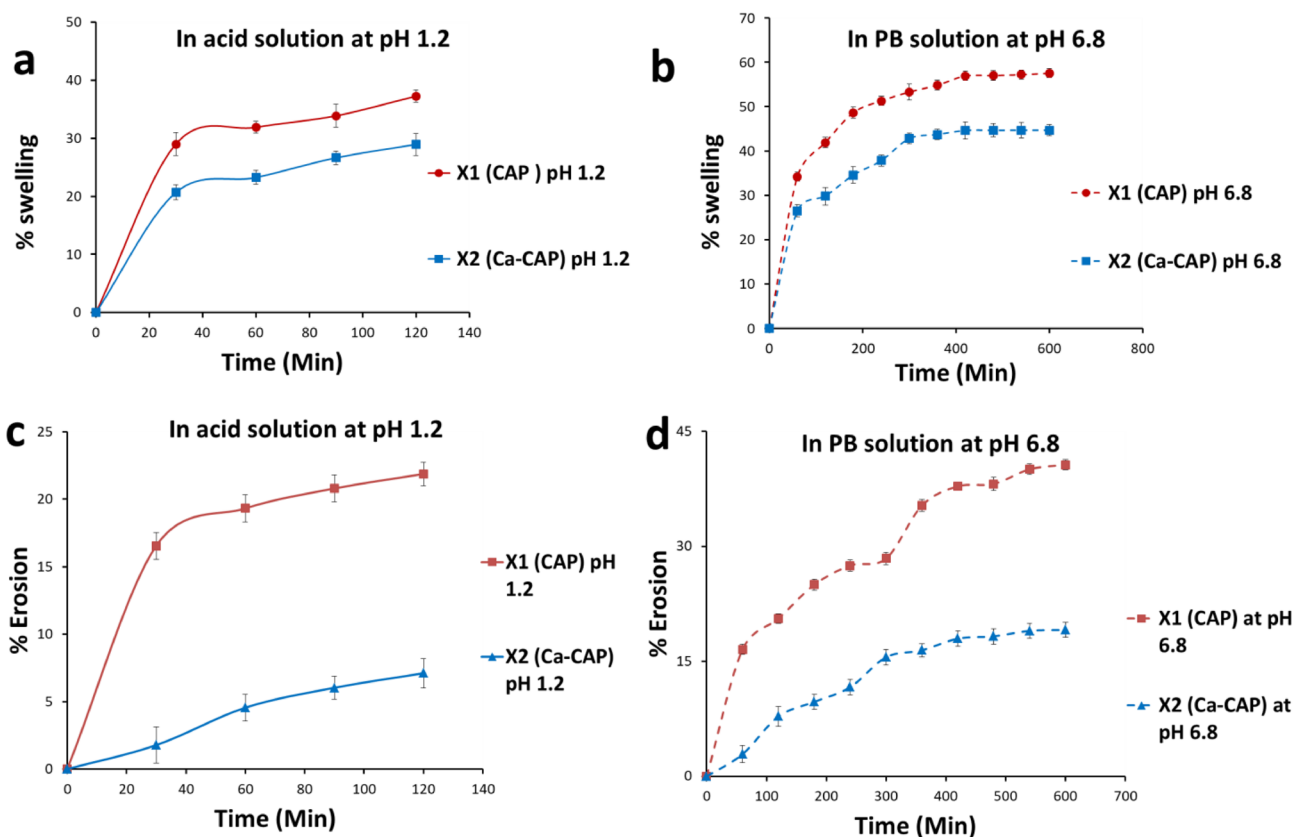


Fig. 8. % Swelling of X1 (CAP) and X2 (Ca-CAP) Tablets: (a) at pH 1.2, (b) at pH 6.8; % Erosion of X1(CAP) and X2 (Ca-CAP) Tablets: (c) at pH 1.2, (d) at pH 6.8

this phenomenon may lead to an initial burst release due to the presence of the drug on the surface of the matrix tablet. In the case of the DIL-CAP tablet, it was observed that a huge amount of the drug (58–68%) was released within 1 h of dissolution and 100% of the drug was released in the 6-h experiment. The gel layer (rubbery state) grows gradually as more water permeates into the core of the matrix, thereby increasing the thickness of the gel layer and providing a diffusion barrier to drug release. Water continues to penetrate towards the core of the tablet, through the gel layer, until it has been completely eroded. The release data were evaluated by applying the equation of zero order, first order, Higuchi and Korsmeyer equation. The regression coefficient values of difference release kinetic equations evaluated from the dissolution profiles of developed formulations are compared in Table 9.

Topography of Tablets by SEM Studies Figures 11A and B reveal CAP tablet surface morphology changes during dissolution over 0–6 h, while Figs. 11C and D depict Ca-CAP tablet surface alterations at the same time points, observed *via* SEM.

Accelerated Stability Study of Tablets For the stability study, the DIL-loaded tablet formulations, specifically F1, F5, F6, and F10, which exhibited the desired drug release profiles, were selected. These formulations underwent storage for a duration of six months under stress conditions, and upon thorough analysis, no significant differences in drug content or dissolution profiles were discernible ($p < 0.05$).

Figure 12 provides a visual representation of the release profiles for both the freshly prepared tablets and those subjected to the aging process under stressed conditions. To further assess the similarity between these two sets of data, Similarity Factors (f_2) were calculated.²⁶⁾ Specifically, for DIL-loaded CAP tablets (F1 and F5) and Ca-CAP tablets (F6 and F10), the f_2 values were determined as follows: 85.17 ± 2.64 ($n = 3$), 81.94 ± 2.13 ($n = 3$), 85.06 ± 1.83 ($n = 3$), and 94.30 ± 2.07 ($n = 3$), respectively.

Discussion

FT-IR Spectrum Analysis While subtle shifts in band positions were observed, they did not signify significant structural changes between the polymers. Both CAP and Ca-CAP exhibited a broadened band between $3600\text{--}3200\text{ cm}^{-1}$,

attributed to the O–H stretching of hydroxyl groups.²⁷⁾ The alteration appears in the FT-IR spectrum, usually as a shift in peak intensity or position within the O–H stretching region, around $3600\text{--}3200\text{ cm}^{-1}$. However, it is crucial to acknowledge that the exact nature of this shift may differ based on the particular polymer and the interaction characteristics with calcium ions. Therefore, changes in the O–H stretching band can provide an indication of calcium ion binding.²⁸⁾ Notably, the band for O–H stretching in Ca-CAP (Fig. 2b) exhibited heightened intensity due to crosslinking with Ca^{+2} ions.²⁸⁾ The spectra showed characteristic vibrations of C–H stretching at 2880.317 and 2880.062 cm^{-1} .²⁹⁾ The appearance of bands within the $1610\text{--}1370\text{ cm}^{-1}$ range indicated the presence of carboxyl groups ($-\text{COO}$).³⁰⁾ The bending vibration of hydroxyl groups (O–H) was evident around $1459\text{--}1457\text{ cm}^{-1}$. The C=O stretching of acids was represented by the band at $1420\text{--}1418\text{ cm}^{-1}$. Furthermore, bands at 1318 and 1322 cm^{-1} corresponded to the scissoring of methyl groups ($-\text{CH}_2$). The stretching frequency of $>\text{CH-O-CH}$ was reflected by bands at 1020.49 and 1020.37 cm^{-1} .³⁰⁾ The overlapping bands and consistent positions underscored the structural affinity between the two polymers.

In Fig. 2c, the distinct IR absorption bands corresponding to Diltiazem HCl were observed at specific wave numbers: 3397.57 cm^{-1} (N–H stretch in amine groups),³¹⁾ 3034.09 , 3002.50 , 2939.66 cm^{-1} (C–H stretch), 2385.42 , 1738.34 cm^{-1} (C=O stretch), 1675.32 cm^{-1} (C=C stretch), and 1604.70 , 1579.76 cm^{-1} for C=C stretch vibrations.³²⁾ Additionally, bands at 1508.67 , 1472.10 , 1443.94 , 1410.37 , 1375.21 , 1319.68 , 1213.06 , 1055.08 cm^{-1} (C–N stretch), and 1022.84 cm^{-1} (C–N stretch) were identified. In contrast, Fig. 2d portrays the IR absorption bands of DIL combined with polymer mixtures, exhibiting bands at 3328.91 , 3055.78 , 3003.55 , 2916.26 , 2382.93 , 1742.46 , 1679.58 , 1606.61 , 1582.14 , 1538.51 , 1510.19 , 1473.58 , 1444.51 , 1412.89 , 1400.34 , 1217.27 , 1058.08 , and 1026.47 cm^{-1} .

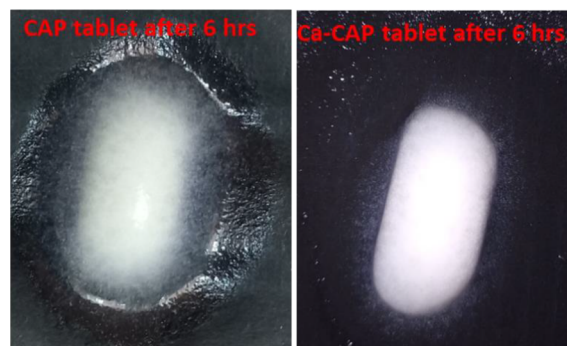


Fig. 9. Comprehensive Representation of the Dissolution of X1 (CAP) and X2 (Ca-CAP) Tablets after 6 h

Table 5. Water Penetration Velocity of Placebo Matrix Tablets

Placebo matrix tablet	Water penetration velocity (cm/s)	
	In acid solution (pH 1.2)	In PB solution (pH 6.8)
X1 (CAP)	1.5×10^{-3}	1.38×10^{-3}
X2 (Ca-CAP)	7×10^{-4}	9×10^{-4}

Table 6. Physical Characteristics of Tablet

DIL-loaded tablets containing polymer	Average weight (mg) ($N = 20$)	Hardness (Newton/cm ²) ($N = 10$)*	Average thickness (mm) ($N = 10$) *	Average length (mm) ($N = 10$)*	Average breadth (mm) ($N = 10$)*	Friability (%) ($N = 20$) *	Drug content (%) ($N = 20$)
CAP(F1–F10)	1117.2–	56.87–	5.96–	19.45–	8.99–	0.62–	99.08–
	1113.04	61.58	6.1	19.49	9.00	0.67	98.98
	$\pm 2.25\%$	± 0.06	± 0.02	± 0.011	± 0.013	± 0.026	± 0.21
Ca-CAP(F1–F10)	1114.6–	67.27–	5.89–	19.42–	9.01–	0.56–	99.13–
	1122.03	68.74	6.2	19.49	9.02	0.61	100.05
	$\pm 2.06\%$	± 0.032	± 0.01	± 0.009	± 0.021	± 0.047	± 0.19

* N = number of tablets tested; Mean \pm standard deviation (S.D.) ($n = 3$).

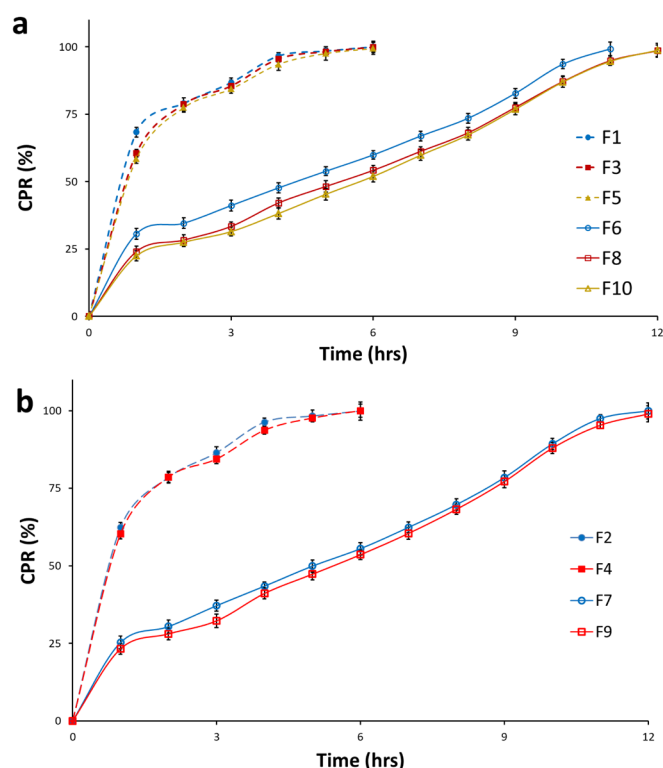


Fig. 10. Drug Release Profiles of DIL from CAP (-----) and Ca-CAP (————) Matrix Tablets, (a) F1, F3, F5, F6, F8, and F10; (b) F2, F4, F7, and F9

Table 7. AUC of DIL Release from Matrix Tablets

Media	DIL + CAP formulations						DIL + Ca-CAP formulations			
	F1	F2	F3	F4	F5	F6	F7	F8	F9	F10
At pH 1.2	269.62	254.08	249.7583	249.17	242.93	119.86	101.26	95.575	93.233	90.554
At pH 6.8	1197.9	1179.8	1171.2	1161.9	1152.5	1585.8	1722.7	1671.354	1660.2	1629.4

Table 8. ANOVA Table of Cumulative Drug Release from Two Matrices

Table analyzed					
Two-way ANOVA	Ordinary				
Alpha	0.05				
Source of variation	% of total variation	p-Value	p-Value summary	Significant?	
Row factor	26.93	0.0002	***	Yes	
Column factor	3.841	0.738	ns	No	
ANOVA table	SS	DF	MS	F (DFn, DFd)	p-Value
Row factor	50774	12	4231	F (12, 108) = 3.501	p = 0.0002
Column factor	7242	9	804.7	F (9, 108) = 0.6658	p = 0.7380
Residual	130517	108	1208		
Number of missing values	0				

Table 9. Formulation-Tailored Drug Release Kinetics Data

Release kinetic equations	DIL-loaded CAP formulations					DIL-loaded Ca-CAP formulations				
	F1	F2	F3	F4	F5	F6	F7	F8	F9	F10
Zero order, (R^2)	0.682	0.718	0.727	0.731	0.741	0.872	0.908	0.922	0.926	0.923
1st order, (R^2)	0.45	0.464	0.467	0.468	0.472	0.584	0.575	0.580	0.585	0.584
Higuchi (R^2)	0.911	0.933	0.938	0.911	0.946	0.985	0.993	0.985	0.984	0.983
Korsmeyer–Peppas, (R^2)	0.983	0.978	0.973	0.979	0.976	0.949	0.971	0.945	0.945	0.947
n	0.224	0.271	0.283	0.282	0.291	0.381	0.445	0.464	0.471	0.463

These findings indicate a lack of significant alteration in the drug–polymer interaction.

In addition, all characteristic peaks of DIL were retained in the spectra at their respective wavenumbers, suggesting harmonious compatibility between the drug and polymer components.

DSC Thermogram Analysis This alteration in melting peaks suggests a modified thermal behavior in Ca-CAP. Notably, Ca-CAP exhibited a higher melting point compared to CAP, a feature attributed to the ionic crosslinking process.³³⁾

Additionally, when DIL is combined with polymers, as shown in Fig. 3d, a similar endothermic peak emerges at a slightly lower temperature, around 215.89°C. This shift in the melting point indicates that the presence of polymers influences the thermal behavior of DIL. It suggests that the DIL–polymer interactions may affect the energy required for DIL to transition from a solid to a liquid state. The proximity of this peak to the pure DIL melting point implies that these interactions are not significantly altering the fundamental melting behavior of DIL.³⁴⁾

Zeta Potential Analysis In stark contrast, the zeta potential measurement for Ca-CAP samples displayed a value of -4.57 mV. The negative zeta potential of -13.8 mV for CAP is attributed to the presence of anions on the carboxymethyl groups ($-\text{OCH}_2\text{COO}^-$) along CAP's polymer chains. These anions contribute to the overall negative charge on CAP's surface. A higher negative zeta potential suggests stronger electrostatic repulsion among CAP particles, contributing to

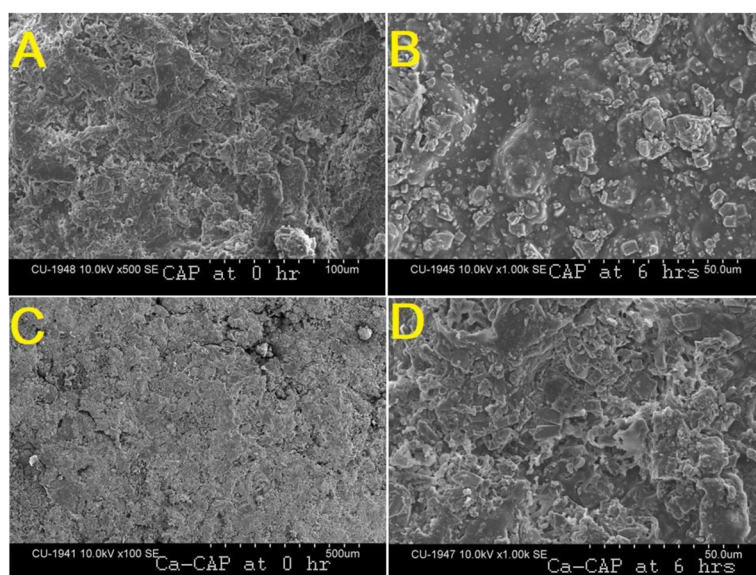


Fig. 11. SEM Images of (A) CAP at 0h., (B) CAP at 6h., (C) Ca-CAP at 0h., (D) Ca-CAP at 6h

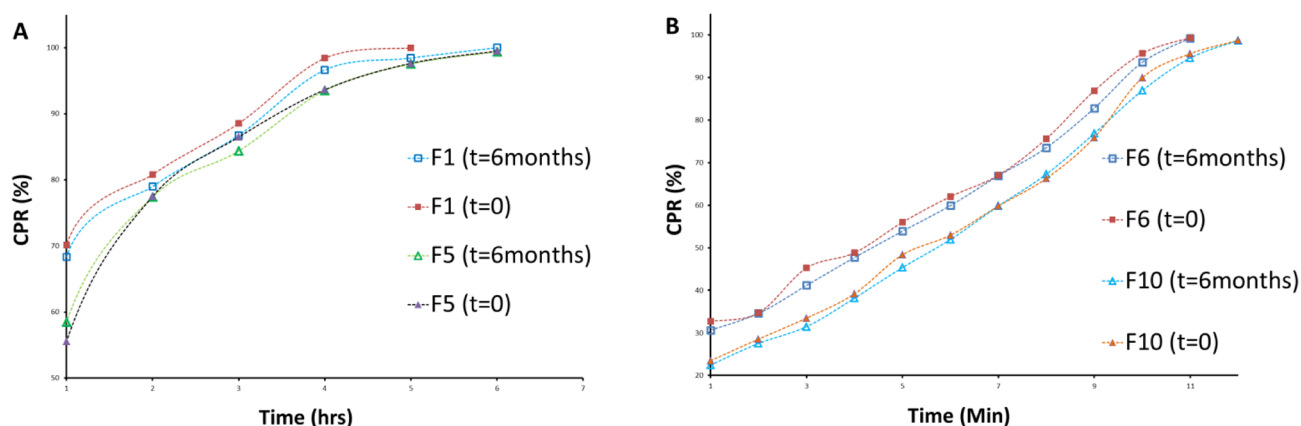


Fig. 12. Effect of Storage on the Release of (A) DIL-Loaded CAP Formulations and (B) DIL-Loaded Ca-CAP Formulations

improved dispersion and stability.³⁵⁾ In the case of Ca-CAP, despite the inherent negative charge due to carboxymethyl groups, the interactions between positively charged calcium ions (Ca^{2+}) and carboxymethyl groups ($-\text{OCH}_2\text{COO}^-$) on CAP's chains led to a less negative zeta potential of -4.57 mV. The presence of calcium ions altered the zeta potential towards the positive side. However, the overall charge remained negative.

XRD Pattern Analysis The X-ray diffractogram analysis confirms the influence of chemical modifications (carboxymethylation and calcium crosslinking) on the crystalline properties of the polymers.³⁶⁾ The characteristic patterns within CAP strongly suggest the presence of crystallinity. This crystallinity is attributed to the process of carboxymethylation, which introduces structural modifications to the polymer, leading to the formation of crystalline regions. Ca-CAP demonstrates a notably higher degree of crystallinity than CAP. This increased crystallinity is attributed to the presence of calcium crosslinking, which induces more ordered and structured regions within the polymer. These differences in crystalline characteristics can have significant implications for the physical and chemical properties of CAP and Ca-CAP.

RBC Lysis Test For CAP-treated samples after 1h, the

optical density exhibited minimal variation, signaling no discernible impact on RBC properties. This trend persisted after 3h, indicating that CAP maintained a steady influence, effectively leaving RBCs unaffected. In the case of Ca-CAP-treated samples, the optical densities remained consistently stable, further corroborating the absence of any substantial impact on RBC properties throughout the experimental duration. However, the positive control, represented by Water for Injection (WFI), displayed markedly higher optical densities. This discrepancy implies a substantial influence, potentially attributable to osmotic effects. Summing up, both CAP and Ca-CAP demonstrated relatively negligible effects on RBC properties when compared to the potent impact of the positive control (WFI). This suggests that these sample solutions are apt for applications related to RBCs, as they do not significantly disrupt their inherent properties.

Comparative Rheological Analysis

Flow Curves

The observed contrast in viscosity can be attributed to the unique properties of these polymers. In the case of CAP, the presence of carboxymethyl groups induces ionization, giving rise to electrostatic repulsion forces. These repulsion forces act to disentangle the polymer chains, resulting in a reduction

in viscosity.³⁷⁾

Conversely, the formation of Ca-CAP involves the reaction of calcium ions (Ca^{+2}) with carboxylic groups, leading to the creation of a crosslinked structure ($-\text{OCH}_2\text{COOSUP}^-\text{Ca}^{2+}-\text{OOCH}_2\text{CO}-$).³⁸⁾ This crosslinking has a profound effect on the mobility of polymer chains. Specifically, it restricts their movement and significantly limits coulombic repulsion forces between them. Consequently, the chains within the Ca-CAP matrix become highly entangled, leading to a substantial increase in viscosity. This heightened viscosity, in turn, facilitates the formation of viscoelastic gels.

Amplitude Sweep

Initially, within the LVE, both polymers maintain their structural integrity. However, beyond a specific critical strain (%), structural deformations commence, marked by a decline in G' that surpasses the confines of the LVE. The data are presented in Fig. 6B sheds light on these phenomena. In the context of linear viscoelasticity, it is crucial to establish the linear viscoelastic region (LVE), which denotes the range where stress exhibits a linear relationship with strain for the material under examination.³⁹⁾ In this regard, two critical parameters are monitored: the storage modulus G' (Pa), which signifies the elastic response^{39,40)} and the loss modulus G'' (Pa), which represents the viscous response. The amplitude sweep analysis conducted in this study revealed noteworthy differences in the mechanical behavior between Ca-CAP and CAP. Notably, Ca-CAP exhibited a critical strain of 2%, representing the threshold at which this polymer can withstand stress before initiating deformation. In contrast, CAP displayed a markedly lower critical strain of 0.3%, denoting its limited capacity to endure stress before deformation begins. The critical strain signifies the maximum stress threshold a material can endure without undergoing significant deformation. Beyond this point, the material experiences structural changes, initiating deformation or irreversible alterations in its form.⁴¹⁾ This parameter serves as a crucial indicator of a material's mechanical limits and its ability to withstand external forces before exhibiting deformation or failure. This divergence can be attributed to the effect of crosslinking, which effectively prevents Ca-CAP from undergoing ionization. Consequently, Ca-CAP manifests superior mechanical strength compared to CAP. Furthermore, a noteworthy observation is the difference in the linear viscoelastic region (LVE) between the two polymers. CAP experiences a relatively shorter LVE, indicating a more limited range where its linear viscoelastic properties hold. In contrast, Ca-CAP exhibits a broader and more stable LVE. It's also worth mentioning that CAP's LVE shows irregular patterns and increased instability, further highlighting the impact of crosslinking on the rheological behavior of these polymers.

Frequency Sweep

In the Frequency sweep analysis conducted on CAP and Ca-CAP polymers, their G' values consistently surpassed G'' ($G' > G''$), highlighting a prevalence of elastic behavior over viscosity. Within the Ca-CAP analysis, the frequency sweep plots distinctly showcased a substantial gap between G' and G'' without any crossover, indicating the presence of a robust viscoelastic gel structure. This absence of crossover signifies enhanced stability for the Ca-CAP matrices owing to their distinct structural integrity.

In contrast, during the evaluation of the CAP matrix, a nar-

rower margin between G' and G'' was observed without any intersection, signifying a smaller difference between these parameters. This narrower gap implies a less pronounced viscoelastic structure and consequently denotes lower stability for the CAP matrix compared to Ca-CAP.⁴²⁾ This structural strength is attributed to the extensive entanglement in Ca-CAP matrices as a result of cross-linking. In contrast, CAP matrices were found to possess weaker gel structures when compared to their Ca-CAP counterparts. This phenomenon is attributed to the ionization of functional groups ($-\text{OCH}_2\text{COO}^- \text{H}^+$) present in CAP, which induces electrostatic repulsion, consequently leading to a reduction in entanglement within the matrix.^{43,44)}

According to Fig. 7a, the R^2 value of 0.994 for CAP suggests a highly linear relationship between G' and G'' , indicating that the change and differences between the storage (G') and loss (G'') moduli were minimal.⁴⁵⁾ This strong linear correlation implies that CAP exhibited less disparity between its elastic and viscous properties across the tested angular frequencies, resulting in a more balanced and less viscoelastic behavior.

On the other hand, the lower R^2 value for Ca-CAP (0.848) indicates a less perfect linear relationship between G' and G'' (Fig. 7b), signifying a larger disparity between its storage and loss moduli. This suggests that Ca-CAP showcased more significant differences between its elastic and viscous properties at various angular frequencies, demonstrating higher viscoelasticity.

The high R^2 value for CAP implies a more uniform and balanced response between its elastic and viscous properties, resulting in a less viscoelastic behavior. Conversely, the lower R^2 value for Ca-CAP indicates a more substantial difference between its storage and loss moduli, representing a higher degree of viscoelasticity with more pronounced differences between its elastic and viscous characteristics.

Furthermore, the best-fit slope values represent the rate of change of G'' with respect to G' . A higher slope value indicates a more pronounced viscous behavior relative to the elastic behavior. In this comparison, CAP demonstrated a substantially higher best-fit slope value of 0.662 ± 0.013 compared to Ca-CAP's value of 0.254 ± 0.028 . This indicates that CAP exhibits a steeper increase in G'' relative to G' , implying a more dominant viscous behavior compared to Ca-CAP.⁴⁵⁾

The slope of the G'' vs. G' plot was typically calculated as the change in G'' divided by the change in G' . It characterizes the relationship between the G' and the G'' with respect to frequency, providing information about the viscoelastic behavior of the material. On the other hand, the loss tangent or phase angle ($\tan\delta$) was calculated separately as the ratio of G'' to G' . It represents the phase difference between the G' and G'' responses of the polymers and provides insights into its viscoelastic properties.⁴⁶⁾

Therefore, while both the slope value and the loss tangent are related to the viscoelastic behavior of the material, they are distinct measures and are calculated differently. The slope value characterizes the linear relationship between G'' and G' , while the loss tangent represents the phase difference between them.

In conclusion, based on the frequency sweep data analysis, it can be inferred that CAP exhibits stronger viscoelastic properties with a more prominent viscous behavior compared

to Ca-CAP. This suggests that CAP is less elastic and more viscous than Ca-CAP under the conditions tested.

According to Table 4, the phase angle, represented as δ or the loss tangent ($\tan\delta$), crucially outlines a material's viscoelasticity by comparing its loss and storage moduli (G'' and G'). This ratio unveils the balance between the elastic and viscous elements in a substance.^{40,47)} Specifically, certain values of $\tan\delta$ hold specific implications: when $\tan\delta = 0$, the material is ideally elastic; when $\tan\delta = 100$, the material is ideally viscous; when $\tan\delta > 1$, the material is more viscous than elastic; when $\tan\delta < 1$, the material is more elastic than viscous; and when $\tan\delta = 1$, the material is considered viscoelastic.⁴⁸⁾

In particular, a higher phase angle suggests that the loss modulus (G'') dominates over the storage modulus (G'). This implies that the material dissipates more energy (associated with G'') than it stores (associated with G'). Therefore, a higher phase angle indicates a material that exhibits more pronounced viscous behavior, where energy is dissipated and stored energy is less readily recovered. This behavior contrasts with materials with lower phase angles, which tend to exhibit more elastic behavior, where energy is stored and recovered more efficiently.

In this dataset, studying CAP and Ca-CAP matrices phase angles across diverse angular frequencies reveals intriguing patterns. Both show lower phase angles at higher frequencies, indicating a stronger elastic response. As frequency drops, both matrices exhibit an upward trend in phase angle, hinting at a shift toward increased viscous behavior.⁴⁷⁾

At 100 Rad/s, CAP sits around 0.63 in phase angle, while Ca-CAP is at 0.20. These lower values imply a robust elastic response in both polymers at higher frequencies. However, as frequency decreases, the phase angle ascends for both, showing a rising influence of the viscous component. At near-zero angular frequencies, CAP reaches roughly 0.30, whereas Ca-CAP is around 0.15. These higher phase angles at lower frequencies indicate a predominant viscous nature in both materials.^{40,47)} These trends illustrate the viscoelastic changes in CAP and Ca-CAP concerning angular frequency. Their behavior leans elastic at higher frequencies and more viscous at lower frequencies. This shift in phase angles highlights the intricate interplay between their elastic and viscous properties, providing insights into their behavior across varying conditions.

Swelling and Erosion Study In the acidic medium, the degree of swelling observed in blank CAP tablets was notably lower than that observed in the buffer medium. Nevertheless, it is important to note that CAP tablets exhibited a rapid and more pronounced swelling in both acidic and buffer media when compared to Ca-CAP tablets. This disparity in swelling behavior is attributed to the calcium crosslinking process, which results in a reduced rate of water penetration (as indicated in Table 5) and a higher degree of entanglement within the Ca-CAP matrices. Consequently, this leads to decreased swelling in comparison to CAP matrices.²⁰⁾ In addition, Fig. 9 displays images of the CAP and Ca-CAP tablets retrieved after undergoing a 10-h (600-min) dissolution period.

Additionally, it was observed that the water penetration rate exhibited the following sequence: water penetration in a phosphate buffer (PB) solution > water penetration in an acidic solution. Furthermore, considering the water penetration velocity trend: PB solution > acidic solution, it follows that the

rate of swelling also mirrored this sequence: swelling in PB solution > swelling in acidic solution. This higher degree of swelling and increased water penetration rate facilitated the dissolution of drugs within the matrix and their subsequent diffusion out.²⁰⁾ As a result, it can be anticipated that the release of the drugs would adhere to the order: release in PB solution > release in acidic solution. This is primarily due to the fact that the velocity of water penetration and the consequent swelling of a hydrophilic matrix depend on the characteristics of the gel layer that forms around the matrix tablet upon contact with water.

In the acidic medium, the extent of erosion observed in blank CAP tablets was significantly lower than that observed in the buffer medium. However, it is important to highlight that CAP tablets exhibited a higher degree of swelling in both acidic and buffer media when compared to Ca-CAP tablets. The presence of Ca^{2+} ions plays a crucial role in constraining the erosion of Ca-CAP matrix tablets.⁴⁹⁾ This phenomenon contributes to the sustained release characteristics of Ca-CAP matrices.

In-Vitro Drug Release Study Upon the evaluation of the entire drug release profiles, it was observed that prolonged and increasingly sustained release characteristics were exhibited by Ca-CAP formulations with higher polymer concentrations. Conversely, a rapid momentary drug release profile was demonstrated by the CAP formulations. Notably, the maximum amount of DIL released from the CAP matrices was 120 mg (100%) within a 9-hour duration, while 119.964 mg (99.97%) of DIL was released from Ca-CAP matrices within 12 h (F7). This delay in drug release in Ca-CAP matrices was attributed to the restriction of water influx, reduced swelling, and the promotion of a viscoelastic gel layer formation due to Ca^{+2} crosslinking, contributing to a slower drug release. In CAP matrices, enhanced mobility, a disentangled structure, and the loss of structural integrity in weak gel networks facilitated rapid deformation due to electrostatic repulsion between the polymeric chains.⁵⁰⁾ Consequently, they exhibited increased water uptake, resulting in higher swelling and accelerated drug release.

The ANOVA table, as displayed in Table 8, confirmed that the differences in drug releases between the two matrices were statistically significant ($p < 0.0001$).⁵¹⁾ The two-way ANOVA table examines the influence of two factors on the observed variation. In this analysis, the Row Factor contributes significantly, explaining about 26.93% of the total variation with a very low p -value ($p = 0.0002$), denoted by three asterisks (***), indicating its statistical significance. On the other hand, the Column Factor demonstrates a much smaller impact, accounting for 3.841% of the total variation, and possesses a non-significant p -value ($p = 0.738$), labeled as 'ns' (not significant). Overall, the Row Factor significantly affects the observed variation, whereas the Column Factor does not demonstrate a substantial impact, as indicated by the ANOVA results.

The results suggest that *in vitro* release profiles of all the matrix formulations of DIL-CAP conform better to the Korsmeyer Peppas model as the profiles showed better linearity when compared with other release kinetic equations. Release of drug from the matrix tablet generally follows the diffusion mechanism for water-soluble drugs. Fickian diffusion refers to the solute transport process in which the polymer relaxation

time is much greater than the characteristic solvent diffusion time. In the case of the DIL-CAP tablet, values of exponent ' n ' are found as 0.224–0.283 which indicates Case I Fickian diffusion. After burst release, the drug was released by diffusion through the gel layer formed around the tablet and initially huge burst release happened as polymer chains are not entangled much as the DIL-Ca-CAP tablet and diffusional resistance is less for the DIL-CAP tablet. Drug release characteristics of DIL-Ca-CAP tablets are somewhat different from that of DIL-CAP tablets. These profiles showed conformity with the Higuchi model and Korsmeyer–Peppas model (Table 9) as suggested by the regression coefficients. As water penetrates through the tablet a gel layer is formed on the surface of the tablet which acts like a thin film, and the drug is diffused from this thin layer. The exponent n values are closer to 0.45 except the n (0.381) value of F6. In the case of $n > 0.45$, the drug is released involving more than one mechanism (swelling/erosion) in addition to diffusion then it is categorized as anomalous diffusion, and when $n \leq 0.45$, it is termed as Fickian diffusion.⁵²⁾ The formulation with a lesser amount of polymer (Ca-CAP) and a higher amount of disintegrant might have caused Fickian-type drug diffusion. There is the possibility of higher erosion when the amount of polymer is increased. Drug release rate is retarded successfully when ionically crosslinked carboxymethyl gum was used as the cumulative release is in the range of 52–60% during 6 h experiment.

Topography of Tablets by SEM Studies In Fig. 11B, the surface of the CAP tablet sample after 6 h of dissolution clearly shows significant erosion. Erosion here refers to the gradual breakdown of the tablet's surface due to the dissolution process. Conversely, Fig. 11D presents a contrasting image. The Ca-CAP tablet sample, at the same 0 to 6-h dissolution point, exhibits a notably different surface morphology (Figs. 11C, D). In this case, there is considerably less erosion, and instead, a gel-like structure has formed on the tablet's surface. This gel formation indicates that the Ca-CAP tablet is undergoing a different dissolution behavior compared to the CAP tablet, resulting in a more controlled and sustained release of the drug. These SEM images provide visual evidence of the distinct dissolution characteristics between the two tablet formulations, further corroborating the findings related to drug release profiles and mechanisms.^{53,54)}

Accelerated Stability Study of Tablets Notably, f_2 values exceeding 50 signified that the dissolution profiles of the fresh and aged tablets remained highly consistent, indicating the stability of the drug and the formulations.^{55,56)} Moreover, the stability analysis underscored that the characteristics of the Ca-CAP tablets remained unchanged throughout the storage period.

Conclusion

The comprehensive exploration into CAP and Ca-CAP polymers in drug delivery formulations has yielded valuable insights. FT-IR spectra revealed structural similarities with minor changes due to calcium ions. Enhanced O–H stretching in Ca-CAP suggests calcium crosslinking. DSC showed Ca-CAP's thermal stability without any effect on the drug. Zeta potential analysis highlighted surface charge differences, and X-ray diffractograms confirmed higher crystallinity in Ca-CAP. Rheological studies unveiled distinct viscosities and mechanical behaviors attributed to cross-linking. Ca-CAP

exhibited sustained drug release, while CAP showed rapid release following Fickian diffusion. SEM images illustrated the effect of dissolution on the surface texture of tablets. Stability studies affirmed the durability of drug-loaded tablets. In conclusion, calcium ion crosslinking significantly influences and culminates the properties and performance of Ca-CAP in sustained drug release behavior and heightened formulation stability, offering promising prospects for pharmaceutical applications.

Acknowledgments We would also like to extend our gratitude to the Head of the Department of Pharmaceutical Technology at Jadavpur University.

Conflict of Interest The authors declare no conflict of interest.

References

- 1) Muruganantham S., Krishnaswami V., AnithaManikandan D., Aravindaraj N., Suresh J., Murugesan M., Kandasamy R. Gums as Pharmaceutical Excipients: An Overview. "Gums, Resins and Latexes of Plant Origin: Chemistry, Biological Activities and Uses," Springer, Cham, 2022, pp. 145–189.
- 2) Pachuau L., Lahlhenmawia H., Mazumder B., *Ind. Crops Prod.*, **40**, 90–95 (2012).
- 3) Mukherjee S., Biswanath S. A., Khanam J., Karmakar S., Bhowmik R., *International Journal of Drug Delivery Technology*, **13**, 551–561 (2023).
- 4) Jain A. K., Kumar N., Jain A., Garg R., Jain A., *J. Drug Deliv. Ther.*, **8**, 246–255 (2018).
- 5) Patel D. K., Purohit B. M., Joshi J. R., Natural polysaccharides in drug delivery and biomedical applications, ed. by Nasrain M. S., Nayak A. K., "Natural Polymers for Drug Delivery," Academic Press, MA, 2019, pp. 1–33.
- 6) Kumar R., Rath M., Yadav R., Sharma D., *J. Drug Deliv. Sci. Technol.*, **54**, 101348 (2019).
- 7) Yin X., Li H., Guo Z., Wu L., Chen F., de Matas M., Shao Q., Xiao T., York P., He Y., Zhang J., *AAPS J.*, **15**, 1025–1034 (2013).
- 8) Singh S., Srivastava M., Singh R., *J. Pharm. Bioallied Sci.*, **13**, 393–404 (2021).
- 9) Sharma R., Panda S. K., Devi S. M., Choudhury P. K., *Int. J. Pharm. Investig.*, **8**, 135–142 (2018).
- 10) Rajasekaran A., Sekar R., Duraipandian V., Ignacimuthu S., *J. Young Pharm.*, **11**, 342–346 (2019).
- 11) Mishra S. K., Patra S., Sahoo S. K., *Saudi Pharm. J.*, **25**, 398–405 (2017).
- 12) Huang Y., Yu H., Xiao C., *Carbohydr. Polym.*, **66**, 500–513 (2006).
- 13) Al-Hadeethi Y., Umar A., Ibrahim A. A., Al-Heniti S. H., Kumar R., Baskoutas S., Raffah B. M., *Ceram. Int.*, **43**, 6765–6770 (2017).
- 14) Phuong P. T., Oliver S., He J., Wong E. H., Mathers R. T., Boyer C., *Biomacromolecules*, **21**, 5241–5255 (2020).
- 15) Fischer D., Li Y., Ahlemeyer B., Krieglstein J., Kissel T., *Biomaterials*, **24**, 1121–1131 (2003).
- 16) Zhang X. Z., Li W. H., Gong X. L., *Smart Mater. Struct.*, **17**, 035027 (2008).
- 17) Shaayegan V., "Linear viscoelastic behaviour and relaxation phenomena of immiscible blends: the application of creep," Doctoral dissertation, Concordia University, 2010.
- 18) Chaturvedi H., Garg A., Rathore U. S., *Eur. J. Pharm. Med. Res.*, **4**, 526–530 (2017), Internet.
- 19) Singh R., Maity S., Sa B., *Carbohydr. Polym.*, **106**, 414–421 (2014).
- 20) Ford J. L., Rubinstein M. H., McCaul F., Hogan J. E., Edgar P. J., *Int. J. Pharm.*, **40**, 223–234 (1987).
- 21) "Pharmacopoeia I," Vol. II, The Controller Publication, Govt. of India, New Delhi, 2010, p. 1199.

- 22) Gubbi S. R., Jarag R., *Asian J. Pharm. Sci.*, **5**, 50–60 (2010).
- 23) Rao P. R., Diwan P. V., *Drug Dev. Ind. Pharm.*, **24**, 327–336 (1998).
- 24) Higuchi T. J., *J. Pharm. Sci.*, **52**, 1145–1149 (1963).
- 25) Korsmeyer R. W., Gurny R., Doelker E., Buri P., Peppas N. A., *Int. J. Pharm.*, **15**, 25–35 (1983).
- 26) Huang H., Wu Z., Qi X., Zhang H., Chen Q., Xing J., Chen H., Rui Y., *Int. J. Pharm.*, **446**, 211–218 (2013).
- 27) Coluccia S., Marchese L., Lavagnino S., Anpo M., *Spectrochim. Acta A*, **43**, 1573–1576 (1987).
- 28) Dagar V., Pahwa R., Ahuja M., *Biointerface Res. Appl. Chem.*, **13**, 111 (2022).
- 29) Lu R., Gan W., Wu B. H., Zhang Z., Guo Y., Wang H. F., *J. Phys. Chem. B*, **109**, 14118–14129 (2005).
- 30) Aguir C., M'Henni M. F., *J. Appl. Polym. Sci.*, **99**, 1808–1816 (2006).
- 31) Sumalatha B., Reddy D. V., Reddy D. S., *Pharma Sci. Monitor*, **6** (2015).
- 32) Krishan B. V., Rao C. H., Kishore V. S., *Research Journal of Pharmacy and Technology*, **13**, 2315–2320 (2020).
- 33) Hongbo T., Yanping L., Min S., Xiguang W., *Polym. J.*, **44**, 211–216 (2012).
- 34) Vijayasankar GR, Bhargava A. *Asian Journal of Pharmaceutical Science & Technology*, **6**, 19–26 (2016).
- 35) Liu Y., Lu K., Hu X., Jin Z., Miao M., *Carbohydr. Polym.*, **234**, 115908 (2020).
- 36) Bhatia M., Ahuja M., *Int. J. Biol. Macromol.*, **72**, 495–501 (2015).
- 37) Maiti S., Ray S., Mandal B., Sarkar S., Sa B., *J. Microencapsul.*, **24**, 743–756 (2007).
- 38) Huang Y., Yu H., Xiao C., *Carbohydr. Polym.*, **66**, 500–513 (2006).
- 39) Kaboorani A., Blanchet P., *BioResources*, **9**, 4392–4409 (2014).
- 40) Ishikawa S., Kobayashi M., Samejima M., *Chem. Pharm. Bull.*, **36**, 2118–2127 (1988).
- 41) Chakravorty A., Barman G., Mukherjee S., Sa B., *Carbohydr. Polym.*, **144**, 50–58 (2016).
- 42) Talens P., Castells M. L., Verdú S., Barat J. M., Grau R., *J. Food Eng.*, **292**, 110265 (2021).
- 43) Medina-Torres L., Brito-De La Fuente E., Torrestiana-Sanchez B., Katthain R., *Food Hydrocoll.*, **14**, 417–424 (2000).
- 44) Yan X., Xiao X., Au C., Mathur S., Huang L., Wang Y., Zhang Z., Zhu Z., Kipper M. J., Tang J., Chen J., *J. Mater. Chem. A Mater. Energy Sustain.*, **9**, 21659–21684 (2021).
- 45) Lee J. H., Um C. M., Lee I. B., *Dent. Mater.*, **22**, 515–526 (2006).
- 46) Gao T., Gillispie G. J., Copus J. S., Pr A. K., Seol Y. J., Atala A., Yoo J. J., Lee S. J., *Biofabrication*, **10**, 034106 (2018).
- 47) Ramli H., Zainal N. F., Hess M., Chan C. H., *Chem. Teach. Int.*, **4**, 307–326 (2022).
- 48) Wang H., Ke L., Ding Y., Rao P., Xu T., Han H., Zhou J., Ding W., Shang X., *Food Hydrocoll.*, **122**, 107079 (2022).
- 49) Wei X., Sun N., Wu B., Yin C., Wu W., *Int. J. Pharm.*, **318**, 132–138 (2006).
- 50) Nadgorny M., Ameli A., *ACS Appl. Mater. Interfaces*, **10**, 17489–17507 (2018).
- 51) Nayak A. K., Pal D., *Int. J. Biol. Macromol.*, **49**, 784–793 (2011).
- 52) Korsmeyer R. W., Peppas N. A., *J. Membr. Sci.*, **9**, 211–227 (1981).
- 53) Murphy C., Pillay V., Choonara Y. E., du Toit L. C., Ndesendo V. M., Chirwa N., Kumar P., *AAPS PharmSciTech*, **13**, 1–5 (2012).
- 54) Abe T., Yanagihara Y., Uchino T., Oriyama T., Komatsu M., Nakajima K., Suzuki H., *Chem. Pharm. Bull.*, **62**, 617–626 (2014).
- 55) Alshetaili A., Almutairy B. K., Alshehri S. M., Repka M. A., *Pharmaceutics*, **13**, 213 (2021).
- 56) Aggarwal A. K., Jain S., *Chem. Pharm. Bull.*, **59**, 629–638 (2011).

CERTIFICATE

OF ACHIEVEMENT



BRAINWARE
UNIVERSITY



THIS IS TO CERTIFY THAT

Dr./Mr./Ms./Mrs

Sudipta Mukherjee

of

Tadavpur University

has presented a paper entitled

"

and secured

1st

Position in the Oral/Poster Presentation in the National Conference on the theme of

"Transforming Pharmacy Education as per the National Education Policy (NEP) 2020 for Holistic Development"

held on August 25 & 26, 2023, organised by the Department of Pharmaceutical Technology, Brainware University in collaboration with Association of Pharmaceutical Teachers of India (APTI, West Bengal State Branch).

Sankar Gangopadhyay

Prof. Sankar Gangopadhyay
Patron & Honorable Vice Chancellor
Brainware University

mmondal

Prof. Nityananda Mondal
Chairman of the Conference
President, APTI
West Bengal State Branch

Barik

Prof. (Dr) B. B. Barik
Organizing Secretary
HOD, Dept. of Pharm. Tech.
Brainware University

Prasenjit Mondal

Prof. (Dr) Prasenjit Mondal
Convener
Prof. Dept. of Pharm. Tech.
Brainware University



Scanned with OKEN Scanner

Two Days online National Seminar
on
Pharmaceutical Product Management
Organized by
Gupta College of Technological Sciences, Asansol
28th & 29th May 2020

Poster Presentation

Certified that
Sudipta Mukherjee
presented poster
in the scientific session of the seminar.

Kalyan K Sen

Dr. Kalyan Kumar Sen
Principal
Gupta College of Technological Sciences



Susmita Chakraborty

Mrs. Susmita Chakraborty
Chairman, Trinity Trust
Gupta College of Technological Sciences

Two days Online National Seminar
on
Pharmaceutical Product Management
Organized By
Gupta College of Technological Sciences
28th & 29th May 2020

Certificate of Participation

To
Sudipta Mukherjee
For attending the seminar

Kalyan K Sen

Dr. Kalyan Kumar Sen
Principal
Gupta College of Technological Sciences



Susmita Chakraborty

Mrs. Susmita Chakraborty
Chairman, Trinity Trust
Gupta College of Technological Sciences



Sudipta Mukherjee

Jadavpur University, Kolkata

attended the online seminar on

Tribology: Friction and Wear Characterization

Date: May 19, 2020

Time: 11:30 to 12:30 hours

Contents

The training provided the essential knowledge for:

- ▶ Mapping tribological characteristics in static and extreme boundary regimes through "Extended" Stribeck curves
- ▶ Studying the effect of additives and contaminants on engine oils
- ▶ Extreme low-temperature testing of greases – upto -80°C
- ▶ Developing correlation between friction and sensory data for cosmetics, and food and beverages

Date of issue: June 01, 2020

A handwritten signature in black ink, appearing to read "Kartik", with a stylized flourish underneath.

Dr. Kartik Pondicherry
Technical Manager - Rheology
Anton Paar India Pvt. Ltd.



Sudipta Mukherjee

Jadavpur University, Kolkata

attended the seminar on

Face Your Surface with Solid Surface Zeta Potential

Date: May 13, 2020

Time: 11:30 – 12:30 hours

Contents

The training provided the essential knowledge for:

- ▶ Concept of streaming potential and streaming current
- ▶ Instrumentation for solid surface zeta potential measurement
- ▶ Surface Charge Analysis: Membrane and Biomaterials, Fibers and Textiles
- ▶ Surface Adsorption: Liquid-on-solid surface adsorption kinetics

Date of issue: June 02, 2020

A handwritten signature in black ink that reads "Prasad Gosavi".

Prasad Gosavi
Technical Manager - Surface Area and Porosity
Anton Paar India Pvt. Ltd.

COLLOQUIUM-2020



This is to certify that

Sudipta Mukherjee

has participated in Three Days Online International Conference, *"Colloquium-2020"* on the theme *Innovations in Pharmacy & Green Chemistry in Post Covid-19 Era* from 11th June to 13th June 2020

Organized by

Dept. of Pharmaceutical Technology, Dept. of Biotechnology & Dept. of Chemistry
JIS UNIVERSITY, KOLKATA, 700109, INDIA

Prof. Dr. B. C. Mal
Vice Chancellor
(Patron, Colloquium-2020)

Prof. Dr. T. K. Chatterjee
Dean
(Chairman, Colloquium-2020)

Prof. Dr. H. S. Maji
Head, Pharmacy
(Convener, Colloquium-2020)

COLLOQUIUM-2020





This is to certify that

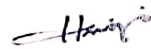
Sudipta Mukherjee

has participated in Three Days Online International Conference, "Colloquium-2020" on the theme
Innovations in Pharmacy & Green Chemistry in Post Covid-19 Era from 11th June to 13th June 2020

Organized by
Dept. of Pharmaceutical Technology, Dept. of Biotechnology & Dept. of Chemistry
JIS UNIVERSITY, KOLKATA, 700109, INDIA


Prof. Dr. B. C. Mal
Vice Chancellor
(Patron, Colloquium-2020)


Prof. Dr. T. K. Chatterjee
Dean
(Chairman, Colloquium-2020)


Prof. Dr. H. S. Maji
Head, Pharmacy
(Convener, Colloquium-2020)

Sudipta Mukherjee
14.12.2023

Signature of guide
Jasmina Khanam
14.12.2023

PROF. JASMINA KHANAM
PROFESSOR
PHARMACEUTICAL TECHNOLOGY
JADAVPUR UNIVERSITY

